Author:
Buckner, Nikki R

Title:
Investigating the role of RNA Binding Proteins and Modulators of Mitochondrial Function in Neurodegenerative Disease

Investigating the role of RNA Binding Proteins and Modulators of Mitochondrial Function in Neurodegenerative Disease

Nicola Rose Buckner

A dissertation submitted to the University of Bristol in accordance with the requirements for award of the degree of Doctor of Philosophy in the Faculty of Health Sciences, Bristol Medical School.

March 2020

Word count (main text only): 53,224

Abstract

Neurodegenerative diseases have a devastating impact on patients, and they are becoming more prevalent due to the increasing age of the global population. However, despite intensive research there are no disease-modifying therapies for any neurodegenerative conditions. Dysregulation of RNA binding protein (RBP) and mitochondrial function are key hallmarks of the molecular pathology of neurodegenerative diseases such as amyotrophic lateral sclerosis, polyglutamine (polyQ) disorders and Parkinson's disease. This thesis aims to contribute to the understanding of how RBPs mediate neurodegenerative pathology, and to investigate pharmacological modulation of mitochondrial function as a neuroprotective strategy. The expression of the RBP scaffold attachment factor 1 (SAFB1) was investigated in degenerating human brains. These studies revealed a novel, abnormal SAFB1 cytoplasmic expression pattern associated specifically with polyQ disease including spinocerebellar ataxias and Huntington's disease. Spinocerebellar ataxia type 1 is caused by an expansion of the polyQ tract in the *ATXN1* gene. The interaction between SAFB1 protein and pathological expanded tandem repeat RNA (xtrRNA) was therefore investigated. RNA immunoprecipitation confirmed SAFB1 interacted with *ATXN1* transcripts and demonstrated that a pathological CAG expansion confers a relative increase in the level of *ATXN1* associated with SAFB1. This result suggests that an interaction between SAFB1 and expanded polyQ tracts may result in the mislocalisation of SAFB1 to the cytoplasm in degenerating polyQ neurons. Furthermore, these findings support the hypothesis that it is RBP dysfunction that leads to neurodegenerative pathology. Drugs that promote mitochondrial function may be effective in treating neurodegenerative conditions such as Parkinson's disease. Using an *in-vitro* phenotypic screen, kenpaullone, a GSK-3 beta/CDK5 inhibitor, was identified as a novel modulator of parkin recruitment. Kenpaullone was also found to increase mitochondrial length, protect against mitochondrial toxins and alter respiratory function. Based on these findings, further investigations are recommended to explore the potential neuroprotective actions of kenpaullone like drugs.

Dedication

This thesis is dedicated to my Mum and Dad, Gillian and Stephen.

Thank you for your unconditional love and support, I am so very lucky to have you as my parents.

Acknowledgements

This work was supported by grant MR/N0137941/1 for the GW4 BioMed DTP, awarded to the Universities of Bath, Bristol, Cardiff and Exeter from the Medical Research Council (MRC)/UKRI.

I would like to thank Professor James Uney for supervising my PhD. I am sincerely grateful for the opportunity to have worked within your research group. I thank Dr. Liang-Fong Wong and Professor Nick Allen for their supervision and support. I wish to extend a special thank you to Dr. Helen Scott for your ongoing support and for being a brilliant role model. Thank you also for proofreading and offering valuable suggestions. Thank you to Dr. Oscar Cordero-Llana for your continued guidance and support. I would like to thank Dr. Alastair Wilkins and Dr. Kevin Kemp for providing cerebellar sections, and for guidance on immunofluorescent staining and confocal imaging. Thank you to Professor Craig McArdle and group for provision of high-content imaging and analysis.

I would like to acknowledge the MRC London Neurodegenerative Diseases Brain Bank for supplying patient tissue used in this study, and I wish to express gratitude to the patients who generously agreed to donate their tissue for research, and to their families.

Thank you also to the Biomedical Science Building B and C floor technical team, especially Mr. Doug Owen, for providing laboratory technical assistance. I also thank the technical team in the Dorothy Hodgkin Building. I am grateful to my fellow PhD students within the GW4 BioMed DTP for creating a positive and supportive training environment, and to the DTP staff for arranging training opportunities throughout my PhD.

I have been lucky to work with a wonderful group of colleagues within both the UWOC research lab and in the Biomed building C floor office. I would like to thank my colleagues and friends Ms. Andriana Gialeli, Dr. Sian Baker, Ms Renata Raele, Dr. Mamdouh Allahyani, Mr. Gongyu Shi and Mr. Ben Exley. Thank you to Ben for kindly proofreading many of these pages. Andriana, thank you for your expert help culturing hfNPCs and for working so hard in the lab, you are a star. Sian, thank you for being someone to turn to, and for your valued words of PhD advice. Renata, thank you for your continued friendship and support, especially during the writing process; our coffee breaks were invaluable! Thank you to Gongyu for your collaboration on the parkin recruitment project work and to Mr. Ben Clennell for your valuable contribution to previous RNA IP experiments.

Thank you to my wonderful parents and to my sister Hattie and brother Matt for being there always, I am so grateful to have you all. I also thank Hattie for your kind help with proofreading. I must also acknowledge my rescue greyhounds, Jax and Della. Their company has been invaluable in helping me through the harder days! Finally, I wish to thank my partner Alex for your unwavering love, patience and support. I could not have done this without you.

Author's declaration

I declare that the work in this dissertation was carried out in accordance with the requirements of the University's *Regulations and Code of Practice for Research Degree Programmes* and that it has not been submitted for any other academic award. Except where indicated by specific reference in the text, the work is the candidate's own work. Work done in collaboration with, or with the assistance of, others, is indicated as such. Any views expressed in the dissertation are those of the author.

SIGNED: .....Nikki Buckner..... DATE: 16th March 2020

Publication statement

Some of the data presented in Chapter 5 has been published in the Journal of Biological Chemistry (295 (10): 3285-3300), “A dual druggable genome-wide siRNA and compound library screening approach identifies modulators of parkin recruitment to mitochondria” by Scott et al. 2020.

The work in this thesis directly contributed to Figure 5, Figure 6, Supplementary Figure 8 and Supplementary Figure 9 in the above publication.

Signed by Dr. Helen Scott (first author of Scott et al. 2020):

Signature……Helen Scot…….. Date…16th March 2020…..

Signed by Professor James Uney (last author of Scott et al. 2020):

Signature…..…James Uney…….. Date…16th March 2020…..

Some of the data presented in Chapters 3 and 4 has been included in a publication in Brain Pathology, “Abnormal Scaffold Attachment Factor 1 Expression and Localisation in Spinocerebellar Ataxias and Huntington’s Chorea” by Buckner et al. 2020, In Press.

The work in this thesis directly contributed to all the main and supplementary figures in the above publication, with the exception of data from iCLIP experiments in Figure 7 (A and B) which were carried out by Dr. Caroline Rivers.

Signed by Ms. Nicola Buckner (first author of Buckner et al. 2020):

Signature……Nikki Buckner…….. Date…10th June 2020…..

Signed by Professor James Uney (last author of Buckner et al. 2020):

Signature…..…James Uney…….. Date…16th March 2020…..

Table of Contents

List of Figures

List of Tables

List of Abbreviations

ΔΨm	Mitochondrial membrane potential
µl	Microliter
µm	Micrometer
µM	Micromole
A.D.	Autosomal dominant
ABC	Avidin-biotin complex
AD	Alzheimer's disease
ADAR	Double-stranded RNA-specific adenosine deaminase
ADP	Adenosine diphosphate
ALS	Amyotrophic lateral sclerosis
ANOVA	Analysis of variance
ASO	Antisense oligonucleotide
ATP	Adenosine triphosphate
ATXN	Ataxin gene/ataxin RNA
AU	Arbitrary units
BBB	Blood brain barrier
BCA	Bicinchoninic acid
BLAST	Basic Local Alignment Search Tool
CCCP	Carbonyl cyanide m-chlorophenyl hydrazone
CDK	Cyclin-dependent kinase
cDNA	Complementary DNA
CIC	Capicua
CNS	Central nervous system
Ctl	Control
CRISPR	Clustered regularly interspaced short palindromic repeats
crRNA	CRISPR RNA (used interchangeably with gRNA)
CT	Threshold cycle number
DA	Dopamine / dopaminergic
DAB	3,3′-Diaminobenzidine
DJ-1	Parkinsonism associated deglycase
DMEM	Dulbecco's Modified Eagle's Medium
DMPK	Myotonic dystrophy associated protein kinase
DMSO	Dimethyl sulfoxide
DN	Dentate nucleus
DNA	Deoxyribonucleic acid
DRBP	DNA/RNA binding protein
Drp1	Dynamin-related protein 1
DRPLA	Dentatorubral-pallidoluysian atrophy
ECAR	Extracellular acidification rate
EDTA	Ethylenediaminetetraacetic acid
eGFP	Enhanced green fluorescent protein
ELISA	Enzyme linked immunosorbent assay
E.R.	Endoplasmic reticulum
ER	Estrogen receptor
ERH	Enhancer of rudimentary homologue
ETC	Electron transport chain
EWSR1	Ewing sarcoma breakpoint region 1
F	Female
FA	Friedreich's ataxia
FACS	Fluorescence activated cell sorting
FCCP	Trifluoromethoxy carbonyl cyanide phenylhydrazone
FET	FUS/EWS/TAF15 protein family
FFPE	Formalin fixed paraffin embedded

FTD	Fronto-temporal dementia
FTLD	Fronto-temporal lobar degeneration
FUS	Fused in sarcoma
g/mol	Grams per mole
GABA	Gamma-aminobutyric acid
GDAP1	Ganglioside-induced differentiation-associated protein 1
gDNA	Genomic DNA
GFAP	Glial fibrillary acidic protein
GFP	Green fluorescent protein
GL	Granule cell layer
GPe	External globus pallidus
GPi	Internal globus pallidus
gRNA	Guide RNA (used interchangeably with crRNA)
GSK-3 beta	Glycogen synthase kinase-3 beta
GWAS	Genome-wide association study
H&E	Haematoxylin and eosin
HD	Huntington's disease
HeLa	Henrietta Lacks
hfNPC	Human foetal neuroprogenitor
HipSci	Human induced pluripotent stem cell initiative
hnRNP	Heterogenous ribonucleoprotein particle
HRP	Horseradish peroxidase
HS	High similarity
HSF	Heat shock factor
HSP	Heat shock protein
I.P.	Inheritance pattern
IC_{50}	Half maximal inhibitory concentration
iCLIP	Individual crosslinking and immunoprecipitation
IF	Immunofluorescence
IgG	Immunoglobulin G
IHC	Immunohistochemistry
IMM	Inner mitochondrial membrane
IP	Immunoprecipitation
iPSC	Induced pluripotent stem cell
kDA	Kilodalton
LAMP	Lysosomal membrane associated protein
LB	Luria-Bertani
LC3	Microtubule-associated proteins 1A/1B light chain 3B
LC3-II	Microtubule-associated protein 1A/1B-light chain 3 (phosphatidylethanolamine conjugated)
M	Male
mA	Milliamp
MAM	Mitochondria-associated membranes
MDV	Mitochondria-derived vesicles
Mfn	Mitofusin
ml	Milliliter
MND	Motor neuron disease
MPP+	1-methyl-4-phenylpyridinium
mPTP	Mitochondrial permeability transition pore
MPTP	1-methyl-4-phenyl-1,2,3,6-tetrahydropyridine
mRNA	Messenger RNA
MS	Multiple sclerosis
MSA	Multiple systems atrophy
MSN	Medium spiny neuron
MTA	Multi-target analysis

mtDNA	Mitochondrial DNA
MBNL1	Musclebind-like 1
MW	Molecular weight
ncRNA	Non-coding RNA
NES	Nuclear export signal
ng	Nanogram
NHS	National Health Service
NLS	Nuclear localisation signal
nm	Nanometer
nSB	Nuclear stress body
OCR	Oxygen consumption rate
OMM	Outer mitochondrial membrane
OPA1	Optic atrophy 1
PARL	Presenilins-associated rhomboid-like protein
PBS	Phosphate-buffered saline
PC	Purkinje cell
PCR	Polymerase chain reaction
PD	Parkinson's disease
PFA	Paraformaldehyde
PI3K	Phosphoinositide 3-kinase
PINK1	PTEN-induced kinase 1
PMD	Post-mortem delay
PolyQ	Polyglutamine
PVDF	Polyvinylidene difluoride
Q	Glutamine
qPCR	Quantitative polymerase chain reaction
R/E	Arginine/glutamic acid-rich motif
RA	Reactive astrocytosis
RAN	Repeat-associated non-AUG
RBD	RNA binding domain
RBP	RNA binding protein
RBR	RING-between-RING
REST	RE1 silencing transcription factor
RGG	Arginine-glycine rich motif (used interchangeably with R/G)
RNA	Ribonucleic acid
RNAi	RNA interference
RNP	Ribonucleoprotein
ROCK	Rho-associated protein kinase inhibitor (Y-27632)
ROS	Reactive oxygen species
RPM	Revolutions per minute
RRM	RNA recognition motif
SAFB	Scaffold attachment factor B
SAP	SAF-A/B, Acinus and PIAS
SatIII	Satellite 3
SBMA	Spinal and bulbar muscular atrophy
SCA	Spinocerebellar ataxia
SDS	Sodium dodecyl sulfate
SEM	Standard error of the mean
Ser	Serine
SHF	Src homology 2 domain containing F
siRNA	Small interfering RNA
SMN2	Survival of motor neuron 2
SNP	Single nucleotide polymorphism
SNpc	Substantia nigra pars compacta
SOD	Superoxide dismutase

SR	Serine and arginine-rich proteins
SRSF1	Serine and arginine rich splicing factor 1
STAR	Steroidogenic acute regulatory protein
STN	Subthalmic nucleus
TAE	Tris-acetate EDTA
TAF15	TATA-binding protein-associated factor 2N
TDP-43	Transactive response DNA binding protein (43 kDa)
TE	Tris EDTA
TET	Ten-eleven translocation proteins
TIA1	T-cell-restricted intracellular antigen 1
TIM	Translocase of the inner membrane
TOM	Translocase of the outer membrane
Ub	Ubiquitin
UBL	Ubiquitin-like
UTR	Untranslated region
VMAT2	Vesicular monoamine transporter 2
xtrRNA	Expanded tandem repeat RNA
ZFP	Zinc finger protein

1. Chapter 1

General Introduction

1.1 Neurodegenerative disease

1.1.1 The impact of neurodegenerative disease

Human neurodegenerative diseases are characterised by the deterioration and loss of cell populations within the brain or spinal cord over time, which ultimately causes permanently debilitating clinical symptoms. Neurodegenerative disease represents a major public health concern worldwide, especially within the older population. The World Health Organisation reports that in 2015 the global financial cost of dementia, the most common syndrome associated with neurodegenerative diseases, was 818 billion US dollars (World Health Organisation, accessed March 2019). With ongoing advances in medicine and healthcare across the planet, life expectancy is increasing. A global increase of 5.5 years between 2000-2015 was recorded by the World Health Organisation (accessed February 2020). The United Nations reports that the global population aged over 60 is growing faster than all age groups, whilst the number of people aged over 80 is predicted to triple by 2050 (accessed February 2020). As increasing age is the greatest risk factor for neurodegenerative disease (Hou et al. 2019) a rise in incidence of these disorders will occur, further increasing the global impact.

In the UK there are over two million people living with a progressive neurological illness (The Neurological Alliance, Table 1.1) and they suffer the lowest health-related quality of life of any long-term condition (NHS England). Patients with neurodegenerative disorders are diagnosed with the knowledge that they have a condition which will severely worsen with time, and for which there is no curative treatment. With high quality person-centred care regimens many patients are able to maintain a good quality of life for a number of years after diagnosis, but the effects of worsening

physical and cognitive deterioration on the individual and their family should not be understated.

The clinical presentation of neurodegenerative diseases varies widely. Patients experience physical, cognitive and psychological symptoms. Main symptoms are usually related to cognition, and movement or coordination problems. Patients also frequently experience a wide range of other symptoms which have a huge impact on their quality of life. These include sleep disturbances, gastrointestinal dysfunctions and psychiatric manifestations (Martinez-Martin et al. 2007). Family members and friends who assume caregiver roles are also likely to experience a reduction in their quality of life (Caga et al. 2019, Sturm et al. 2019, Yu et al. 2019).

Neurodegenerative disease	**Approximate number of patients living with condition (UK)**	**Reference**
Dementia (including AD)	850,000	Alzheimer's Research UK
PD	137,000	Parkinson's UK
MS	100,000	MS Society
FTD	17,000	Alzheimer's Society
Progressive ataxias	10,500	Ataxia UK
HD	6,700	Huntington's Disease Association
ALS	5,000	Motor Neuron Disease Association

Table 1.1 Approximate number of patients living with selected neurodegenerative diseases in the UK. AD Alzheimer's disease, PD Parkinson's disease, MS multiple sclerosis, FTD fronto-temporal dementia, HD Huntington's disease, ALS amyotrophic lateral sclerosis.

Despite decades of research and medical innovation, there are currently no approved disease-modifying or neuroprotective treatments available for any neurodegenerative disease (Cummings 2017). Current treatment regimens aim to provide symptomatic relief and eventually palliative care (Braga Neto et al. 2016, Dickey and La Spada 2018). The challenge of delivering curative or disease-modifying therapies is further complicated by the fact that a significant proportion of irreversible degenerative loss has already occurred

by the time of clinical presentation in most sporadic neurodegenerative conditions (Cheng et al. 2010).

The road to developing disease-modifying therapies highlights key research challenges; first, the need to gain greater depth of understanding of the molecular mechanisms driving neurodegenerative pathology, and second, the ability to detect disease early, for instance using novel biomarkers or diagnostic technologies. The research presented in this thesis focuses on the first of these challenges and aims to make a contribution of knowledge towards our understanding of the molecular pathology of neurodegeneration, with the hope that ongoing research will make it possible to offer disease-modifying therapies to patients in the future.

1.1.2 Molecular hallmarks of neurodegeneration

Classification of this highly complex and diverse group of diseases can be based upon clinical presentation or anatomical location of pathological changes, but this does not necessarily correlate to the underlying molecular pathology. The human brain is necessarily comprised of extreme anatomical complexity, containing approximately 170 billion cells in a 1:1 ratio of neuronal to non-neuronal types (Azevedo et al. 2009). There are hundreds of identified sub-types of neuron in the brain, alongside macroglia (including astrocytes and oligodedrocytes) and microglial cells. The importance of non-neuronal brain cells in the molecular pathology of neurodegenerative disorders is now widely recognised and has been extensively reviewed (Singh and Joshi 2017, Luca et al. 2018, Peteri et al. 2019). Although further discussion is beyond the scope of this project, it is important to consider the context of neurons within this highly complex *in-vivo* environment.

It is recognised that an intricate combination of genetic and environmental factors are usually involved in the aetiology of neurodegenerative disease. Environmental triggers most recently associated with disease pathology include inflammation and immune activation caused by infectious agents triggering Parkinson's disease (PD) (Caggiu et al. 2019). It has long been

established that mutations in specific genes can directly cause inherited forms of many neurodegenerative diseases. Examples include PARK2 (encoding the E3 ubiquitin ligase parkin), mutations in which cause familial PD (Bras et al. 2015), and mutations in the RNA binding protein (RBP) TDP-43 which cause forms of amyotrophic lateral sclerosis (ALS) (Mackenzie and Rademakers 2010). In other cases, specific neurodegenerative disease can be exclusively caused by a genetic mutation. This is exemplified by the polyglutamine (polyQ) disorders which include Huntington's disease (HD) and forms of autosomal dominant spinocerebellar ataxia (SCA), which are caused by a CAG trinucleotide expansion repeat within an exon of the affected gene. More recently, genetic risk loci are being identified using genome-wide association studies (GWAS) to identify novel genetic risk factors in the development of conditions such as Alzheimer's disease (AD) (Jansen et al. 2019) and PD (Singleton and Hardy 2019).

Despite diverse aetiology, the cellular pathology of neurodegenerative diseases can be classified into characteristic hallmark features which are common across numerous diseases (Tofaris and Buckley 2018). The combination and relative contribution of these features varies with disease and is likely to differ between individual patients and with disease stage. Many of these features are extremely well-established, and some are only more recently becoming well understood. A selection of these key mechanisms are summarised in Figure 1.1.

As non-dividing cells, neurons are unable to dilute damaged cell contents through cell division, leaving them vulnerable to accumulation of cellular deficits at the RNA, protein and organelle level over time. One of the earliest discovered cellular hallmarks of neurodegeneration is the accumulation of intracellular protein inclusions which are often formed from misfolded, aggregated or mislocalised proteins (Dziewulska and Rafalowska 2005). Protein inclusions may be nuclear and/or cytoplasmic, with key examples summarised in Table 1.2.

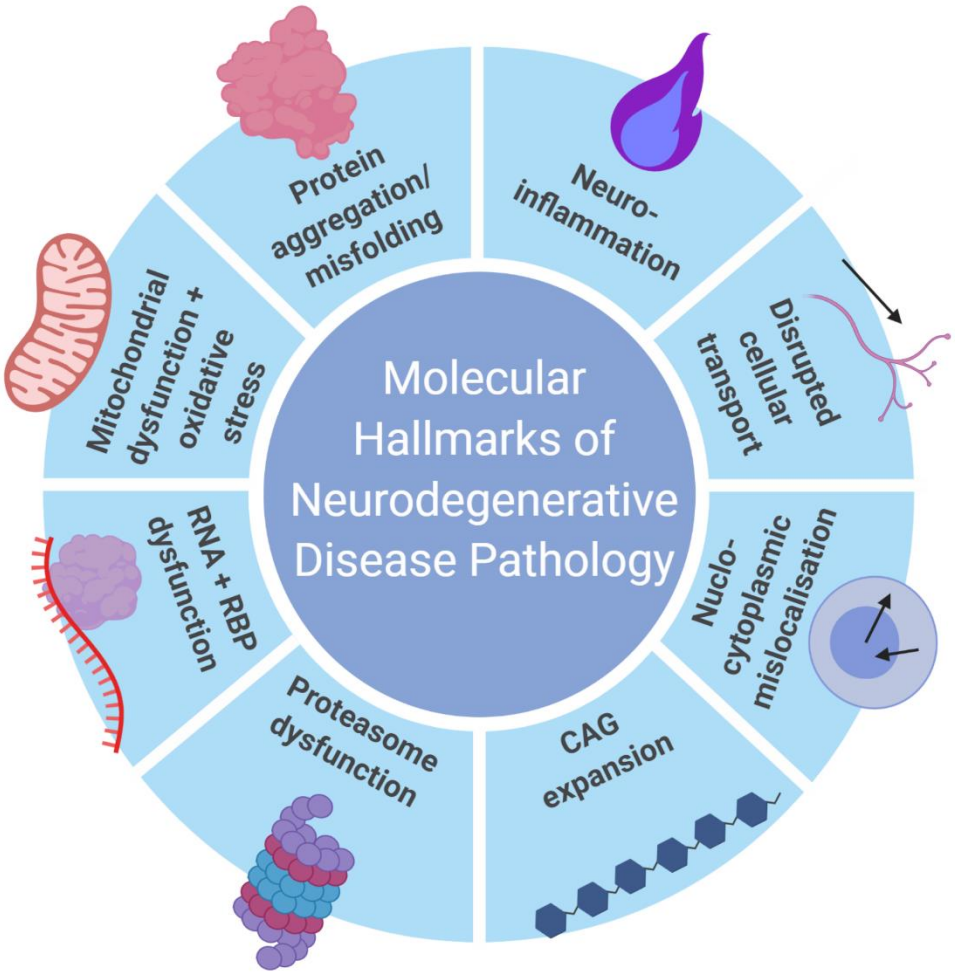

Figure 1.1 Molecular hallmarks of neurodegenerative disease pathology

Toxic loss or gain of function may arise directly or indirectly from protein inclusions. Proteinopathies are associated with alterations in protein processing and dysfunction of the ubiquitin-proteasome system, which are also common features of many neurodegenerative diseases (Zheng et al. 2016). Dysregulation of the ubiquitin system is exemplified in PD through the critical role of parkin, which is involved in mitochondrial quality control. Indeed, mitochondrial dysfunction is one of the most important pathological processes underlying neuronal loss in PD. Mitochondrial dysfunction also contributes to the molecular pathology of AD, HD and ALS (Filosto et al. 2011), representing a key target for potential therapeutic intervention (Gao et al. 2017). The role of mitochondria in neurodegenerative disease is discussed in detail in sections 1.7-1.9, and is investigated in Chapter 5.

Neurodegenerative disease	Intraneuronal protein inclusions
AD	Cytoplasmic neurofibrillary tangles containing phosphorylated tau
ALS	Varies with genetic type. Inclusions may contain SOD1, TDP-43, FUS, ubiquitin or C9ORF72.
FTD	Varies with genetic type. Cytoplasmic inclusions may contain TDP-43, FUS and ubiquitin. Some types feature tau-positive neurofibrillary tangles.
HD	Nuclear and cytoplasmic inclusions containing polyQ expanded huntingtin
PD, Lewy body dementia	Cytoplasmic Lewy bodies composed of alpha-synuclein, parkin and ubiquitin
PolyQ SCA	Nuclear and/or cytoplasmic inclusions containing disease-specific polyQ expanded ataxin proteins
Spongiform encephalopathies	Intracellular prion protein inclusions

Table 1.2 Pathological intracellular protein inclusions in various neurodegenerative conditions

In addition to cellular hallmarks which manifest at the organelle and protein level, RNA level pathology has now been established as a driver of neuronal degeneration (De Conti et al. 2017). The transcription of RNA from DNA and translation of RNA into peptides is exquisitely highly regulated. mRNA processing confers the diversity of protein expression necessary for the functioning of highly complex, differentiated cells such as neurons. Post-transcriptional regulation occurs through many mechanisms including 3' polyadenylation, splicing, and post-transcriptional silencing.

RBPs are trans-acting effectors of RNA processing, interacting with RNA transcripts and other proteins in complex functional networks of ribonucleoproteins (RNPs) to regulate gene expression. Dysfunction of the RBPs TDP-43 and FUS cause forms of ALS and FTD, and recent research has implicated RBPs in the pathogenesis of many other neurodegenerative conditions including SCAs, AD and HD (Conlon and Manley 2017). The role of RNA level pathology and RBPs in neurodegenerative conditions is

discussed further in sections 1.3-1.4, and is investigated in Chapters 3 and 4.

Overall, investigations in this thesis focus on two of the most important molecular hallmarks of neurodegenerative disease which carry promising translational potential for therapeutic intervention. Firstly, Chapter 3 and Chapter 4 explore the role of RBPs, with specific focus on the novel role of Scaffold Attachment Factor B1 (SAFB1) in polyQ disorders. Secondly, investigations in Chapter 5 focus on mitochondrial dysfunction, a well-established neurodegenerative disease hallmark, to identify novel pharmacological modulators of mitochondrial health and function.

1.2 Polyglutamine disorders

The polyglutamine (polyQ) disorders are a group of late-onset inherited neurodegenerative diseases caused by exonic CAG trinucleotide expansion and subsequent translation of pathological polyQ-containing protein (Table 1.3). Although rare diseases, the impact of the nine known polyQ disorders is substantial and there are currently no curative or disease-modifying therapies available for any of the conditions (Lieberman et al. 2019). Although they are caused by CAG expansions in many different genes which confer relatively diverse clinical presentations, common pathological features of all the disorders include correlation between CAG repeat number and disease phenotype, instability of CAG repeat number, and aggregation of polyQ proteins (Ghosh and Tabrizi, 2018).

Each polyQ disorder has a threshold number of CAG repeats above which disease symptoms occur (Table 1.3). It has been long established that an increasing number of CAG repeats correlates to earlier disease onset and increasing severity of clinical symptoms (Gusella and MacDonald 2000, Figure 1.2). As CAG expansions are located in exonic regions, the first stage of pathology is the transcription into expanded tandem repeat RNA (xtrRNA) (Rohilla and Gagnon 2017, Figure 1.3). The molecular pathology

of polyQ disorders is hypothesised to manifest at both the RNA and protein level, which is further discussed below in the context of HD and polyQ SCAs.

Disease	I.P.	Gene (protein)	Locus	Gene function	Normal CAG	Path. CAG
SCA1	A.D.	*ATXN1* (Ataxin1)	6p22.3	Gene expression	6-38	39-85
SCA2	A.D.	*ATXN2* (Ataxin2)	12q24.12	RNA metabolism	14-32	32-200
SCA3	A.D.	*ATXN3* (Ataxin3)	14q32.12	Deubiquitina-se	13-36	61-84
SCA6	A.D.	*CACNA1A* (Subunit-alpha of Cav2.1 calcium channel)	19p.13.13	Calcium channel	4-19	10-33
SCA7	A.D.	*ATXN7* (Ataxin7)	3p14.1	SAGA complex	4-35	37-306
SCA17	A.D.	*TBP* (TATA-box-binding protein)	6q27	Transcription factor	25-42	47-63
HD	A.D.	*HTT* (Huntingtin)	4p16.3	Scaffold protein	6-35	36-121
SBMA	X-linked	*AR* (Androgen receptor)	Xq12	Transcription factor	9-36	38-62
DRPLA	A.D.	*ATN1* (Atrophin 1)	12p13.31	Transcriptional co-repressor	7-34	49-88

Table 1.3 Neurodegenerative diseases caused by polyQ expansion repeats. Normal CAG refers to the physiological number of CAG repeats, Path. CAG refers to the number of CAG repeats associated with disease. A.D. autosomal dominant, DRPLA Dentatorubral-pallidoluysian atrophy, I.P. inheritance pattern, SBMA Spinal and bulbar muscular atrophy.

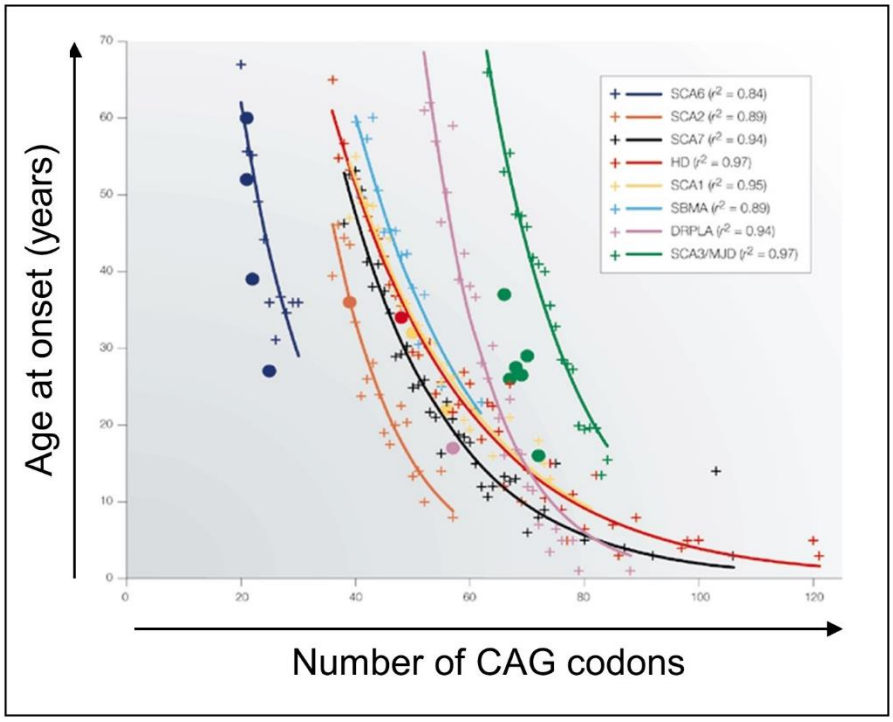

Figure 1.2 Relationship between age of onset of polyQ disorders and CAG repeat length. Data was obtained by Gusella and MacDonald (2000) by compiling literature searches and calculating mean patient age at disease onset before plotting best-fit curves. Filled circles represent age of onset for homozygotes, plotted according to the longest CAG expansion. Figure from Gusella and MacDonald (2000), reproduced with permission from Springer Nature under licence number 4845231063665.

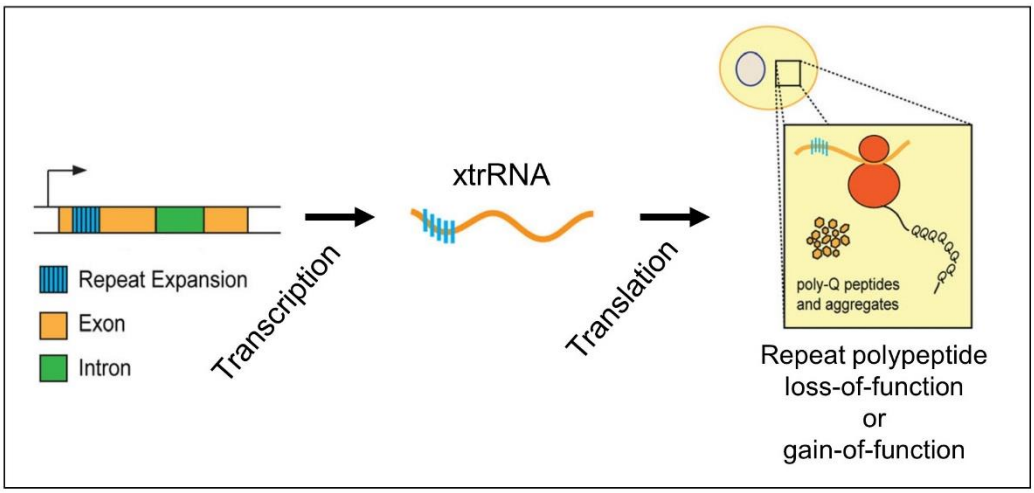

Figure 1.3 CAG expansion pathology is exerted at both the RNA and protein level. Exonic CAG repeat expansions are transcribed into xtrRNA (expanded tandem repeat RNA) which is translated into pathological peptides containing polyQ. Figure reproduced with adaptations from Rohilla and Gagnon (2017), under CC BY 4.0.

1.2.1 Neuropathology of HD

HD is caused by the autosomal dominant inheritance of an expanded CAG trinucleotide repeat in exon 1 of the *HTT* gene, which encodes the huntingtin protein (MacDonald et al. 1993). Huntingtin is highly expressed in the brain and is essential for normal development (Nasir et al. 1995). Despite its discovery nearly three decades ago, ongoing work continues to fully elucidate the exact functions of the huntingtin protein. Mutant huntingtin containing expanded amino-terminus polyQ tracts is highly aggregation prone (Labbadia and Morimoto 2013). Intracellular inclusions of huntingtin protein are found in the nucleus and cytoplasm of degenerating neurons where they may confer toxic gain of function (Labbadia and Morimoto 2013).

Average age of onset of HD is 40 years with most patients diagnosed between the ages of 30 and 50, although mild motor disturbance and cognitive dysfunctions may precede diagnosis by many years (McColgan and Tabrizi 2017). HD is currently fatal, and death occurs on average 15-20 years after symptom onset. HD is primarily classified as a movement disorder, with symptoms categorised as motor, cognitive or psychiatric. The dominant motor symptom is chorea, a term used to describe dyskinesia defined by abnormal rapid, irregular and involuntary movements. Chorea often develops into hypokinesia, rigidity and dystonia in later stages (Waldvogel et al. 2015). Motor symptoms are accompanied by neuropsychiatric and behavioural changes which can be highly distressing and difficult to manage, and manifest as both a direct consequence of neuronal degeneration and as a psychological response to living with the disease (Gray et al. 2013). Symptoms include agitation, anxiety, apathy, psychosis and sleep disorders (Anderson et al. 2018). The clinical symptoms of HD are caused by the selective degeneration of striatal dopaminergic neurons.

The striatum is the largest nucleus of the forebrain basal ganglia. It is comprised of several individual structures, including the caudate nucleus and the putamen (together forming the dorsal striatum) alongside the nucleus accumbens and olfactory tubercle (together forming the ventral

striatum) (Rub et al. 2016). The striatum projects to the closely associated external and internal segments of the globus pallidus (GPe and GPi, respectively), basal ganglia nuclei which are responsible for regulation of voluntary movement. The caudate and putamen are separated by a white matter tract (the internal capsule) which is overlaid by numerous tracts of grey matter, giving the structure its striated, or striped, appearance. The striatum is responsible for motor action and planning, cognition and reward perception (Waldvogel et al. 2015).

Over 95% of the striatal neuronal population comprises medium spiny neurons (MSNs), GABAergic inhibitory projection neurons which express D1 or D2 G-protein coupled dopamine receptors (Gerfen 2004). The striatum receives dopaminergic inputs from the cortex which converge onto D1 and D2-type MSNs which in turn form two efferent pathways, the direct pathway (mediated by D1) and the indirect pathway (mediated by D2). MSNs project to the basal ganglia, to either the substantia nigra or globus pallidus (Gerfen 2004).

Initial hyperkinesia and chorea arise as a result of degeneration of indirect pathway MSNs (Plotkin and Surmeier 2015). This confers reduced inhibitory action on the GPe, consequently increasing inhibition on the subthalmic nucleus (STN). STN hypoactivity results in disinhibition of the thalamus through reduced inhibitory action of the GPi, ultimately resulting in motor cortex overactivation (Waldvogel et al. 2015). Direct pathway MSN neuronal loss induces the hypokinesia characteristic of later stage disease, caused by increased inhibition of the thalamus by the GPi, resulting in decreased motor cortex activation (Waldvogel et al. 2015).

HD neuropathology is graded according to both gross and microscopic observations of the striatum from 0 to 4 using a system originally developed by Vonsattel et al. (1985) (Table 1.4). Macroscopic pathology manifests as bilateral atrophy of the striatum and the cerebral cortex (Waldvogel et al. 2015, Figure 1.4A). On the microscopic level, striatal histopathology is characterised by decreased numbers of neurons alongside reactive

astrogliosis. Astrogliosis is the response of astrocytes to pathological changes in the brain and is visible as an infiltration of small glial cell nuclei within the striatal neuropil (Figure 1.4B). The hallmark pathological inclusions in HD contain mutant huntingtin protein which accumulates in both the nuclei and cytoplasm of affected MSNs, forming various histological inclusion types (Herndon et al. 2009) (Figure 1.4C). HD striatum often exhibits clusters of dystrophic, degenerating neurons. Surviving MSNs may be morphologically normal, can appear shrunken (Waldvogel et al. 2015) or conversely may demonstrate a ballooned appearance (Rub et al. 2016). They are often tightly packed with lipofuscin (Vonsattel 2008).

Vonsattel Grade	**Macroscopic features**	**Microscopic features**	**Proportion of HD brains**
Grade 0	Indistinguishable from control brain	30% loss of striatal neurons, no RA	<1%
Grade 1	Slight shrinkage of the striatum	At least 50% loss of striatal neurons with RA	4%
Grade 2	Mild to moderate striatal atrophy	Moderate-severe neuronal loss with RA	16%
Grade 3	Severe striatal atrophy	Severe neuronal loss (less than 95%) with RA	52%
Grade 4	Severe striatal atrophy	At least 95% loss of striatal neurons with RA	28%

Table 1.4 Vonsattel grading of post-mortem striatum of HD patients. RA reactive astrogliosis. Information summarised from Vonsattel et al. 1985 and Waldvogel et al. 2015.

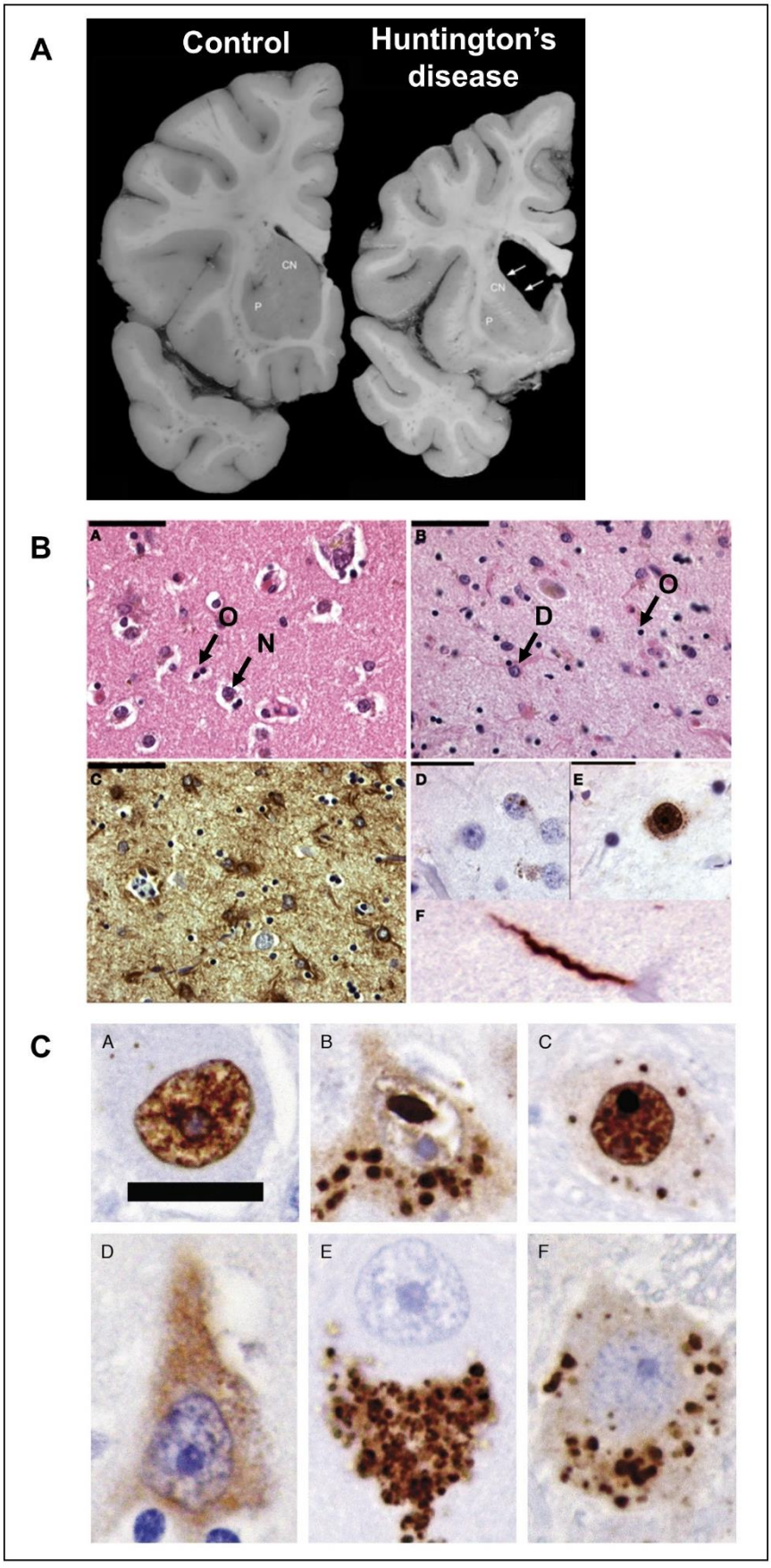

Figure 1.4 Figure legend on next page

Figure 1.4 (previous page) Gross and histological neuropathology of HD. **A**) Coronal brain sections at the level of the striatum and the nucleus accumbens from a control case and a patient with HD. Major shrinkage of the caudate nucleus (CN) and putamen (P) is apparent in the HD case (arrows). Figure reproduced with adaptations from Waldvogel et al. 2015, with permission from Springer Nature under licence number 4845250493940. **B**) Micrographs of HD striatum. a) Age-matched control striatum stained with haematoxylin and eosin b) HD striatum featuring reduced number of neurons and reactive astrogliosis. N=normal neuron, D=degenerating neuron, O=oligodendrocyte. c) HD striatum immunostained for GFAP highlights reactive astrogliosis (dark brown staining). d-f) immunostaining for polyQ using 1C2 antibody. PolyQ protein inclusions are present in the nuclei, cytoplasm and neurites of surviving striatal neurons. Figure reproduced from den Dunnen 2013 (CC BY 4.0). **C**) Staining patterns of polyQ inclusions in HD striatal neurons. Immunoreactivity with 1C2 antibody featuring (a) diffuse, (b) aggregated, (c) diffuse and aggregated nuclear staining and (d) diffuse, (e) aggregated and (f) diffuse and aggregated cytoplasmic staining. Scale bar is 20μm. Figure reproduced from Herndon et al. 2009, with permission from Oxford University Press under licence number 4845241143523.

There are currently no disease-modifying therapies available to patients with HD. Symptomatic medications are usually combined with physical, speech and occupational therapies to maintain patient quality of life for as long as possible (McColgan and Tabrizi 2017). Treatments which target the dopaminergic system have long been the mainstay of pharmacological treatment regimens. Anti-chorea medications counteract over activation of D2 indirect pathway circuitry either by blocking dopaminergic receptors or depleting presynaptic dopamine. Examples include haloperidol (a D2 receptor antagonist) and tetrabenazine (a vesicular monoamine transporter 2 (VMAT2) inhibitor which depletes synaptic monoamines) (Schwab et al. 2015). However, current pharmacological treatment regimens are unfortunately associated with potentially serious side effects including exacerbation of depression (tetrabenazine) (Poon et al. 2010). Furthermore, development of current treatment regimens has largely focussed on amelioration of motor symptoms, leaving neuropsychiatric and non-motor manifestations largely untreated (Schwab et al. 2015).

Taken together, this section demonstrates the devastating effect of HD and the substantial clinical need to further understand the neuropathology of HD in order to inform development of effective, disease-modifying therapies for current and future patients.

1.2.2 Neuropathology of polyQ SCAs

SCAs are a group of autosomal dominantly inherited neurodegenerative conditions characterised by degeneration of the cerebellum which causes coordination and balance problems (ataxia). Inherited SCAs are caused by mutations in specific genes which are most frequently conferred by point mutations or DNA rearrangements (found in SCA15, 16 and 20), or by trinucleotide repeat expansions (Sullivan et al. 2019). Expansion repeat mutations in non-coding regions cause SCA8, 10, 12, 31, 36 and Friedreich's ataxia (FA) (Sullivan et al. 2019). Which is caused by an intronic GAA expansion in the frataxin gene. This thesis focuses on autosomal dominant SCAs caused by exonic CAG trinucleotide repeat expansions (SCA1, 2, 3, 6, 7 and 17).

PolyQ SCAs are rare diseases which usually feature increased severity and shorter survival time in comparison to other inherited ataxias (Buijsen et al. 2019). Prevalence data indicates that polyQ SCAs overall affect around 3 in 100,000 people worldwide (Ruano et al. 2014). SCA3 is estimated as the most common type (Lieberman et al. 2019) whilst prevalence of some polyQ SCAs are extremely low, affecting <1 in 100,000 people (Buijsen et al. 2019, Table 1.5).

All polyQ SCAs are clinically characterised by progressive ataxias of the trunk and extremities, gaze nystagmus, dysarthria and cognitive decline (Lieberman et al. 2019). Additional clinical characteristics are summarised in Table 1.5. Gait ataxia is usually the first identified symptom, but age of onset is variable, falling between 30-50 years, and has been demonstrated to correspond with the number of CAG repeats (Tezenas du Montcel et al. 2014). In some rare and severe cases, juvenile onset can appear in patients below 13 years of age (Zoghbi et al. 1988). Prognosis is poor after symptom onset, with patients typically dying between 10-30 years after diagnosis (Table 1.5). SCA1 typically features the most rapid disease progression (Buijsen et al. 2019).

Neuropathology of SCAs is complex and varied but in all cases involves cerebellar and brainstem degeneration (Figure 1.5A). The cerebellum is responsible for motor control and coordination as well as regulating some cognitive functions. It receives inputs from the spinal cord and projects efferent fibres to motor neurons of the cerebral cortex via the thalamic nuclei. Degeneration of cerebellar motor systems alongside spinal cord proprioceptive pathways leads to characteristic progressive ataxias (Koeppen et al. 2013).

The external appearance of the cerebellum arises from the tightly folded cerebellar cortex, beneath which lies white matter containing the grey-matter deep cerebellar nuclei (dentate, emboliform, globase and fastigi). The cerebellar cortex forms distinctive histological layers which are readily identifiable: the granule cell layer, Purkinje cell layer and molecular cell layer (Figure 1.5B) (Koeppen 2018). The cerebellar cortex is densely packed with granule cells, small glutamatergic neurons with bifurcated axonal projections (parallel fibres) which run through the cortical layer making connections with Purkinje cells. Purkinje cells are very large specialised GABAergic neurons with a highly distinctive appearance (Figure 1.5D). Their cell soma form the Purkinje cell layer of the cerebellum (alongside Bergmann glia). They project extensive dendritic processes into the cerebellar molecular layer (the outermost layer of the cerebellar cortex which also contains parallel fibres alongside inhibitory stellate and basket neurons) (Binda et al. 2020).

The dentate nucleus (DN) is the largest of the cerebellar nuclei. It connects the cerebellum to the rest of the brain and is critical for the planning and control of voluntary movement (Koeppen 2018). It is highly convoluted and contains large principle neurons which mediate communication between the DN and the cerebellar cortex (Figure 1.5E). The cerebellar nuclei receive inhibitory inputs from Purkinje cells and from excitatory mossy fibre pathways.

The neurodegenerative pattern of the cerebellum in polyQ SCAs varies between type and is summarised in Table 1.6. The relative extent of degeneration of the molecular layer (including Purkinje cells) and DN in various polyQ SCAs was previously compared to control patients by Koeppen et al. (2013) (summarised in Table 1.7).

Loss and atrophy of Purkinje cells is characteristic, except in SCA3 where they are largely preserved (Koeppen et al. 2005). SCA2 usually features the most severe cerebellar cortical atrophy (Koeppen et al. 2018). Purkinje cell degeneration is characterised histologically by loss of cell number, reduction in cell soma size, and small nuclei with a “deflated” appearance. There is also simplification and thickening of the dendritic tree (Figure 1.5D). Proximal axonal swellings (known as torpedoes, Figure 1.5C) occasionally form in response to cerebellar injury and Purkinje cell stress in normal brain, and there is an increase in frequency of torpedoes associated with SCA (Louis et al. 2014). Torpedoes may not be apparent in cases with severe Purkinje cell loss.

Disease	Estimated prevalence (per 100,000)	Estimated duration (years)	Additional clinical symptoms
SCA1	1	10-30	Spasticity, weakness, hyperreflexia, dysphagia
SCA2	0.1-5.8	10-15	Postural tremor, hyporeflexia, chorea
SCA3	1-2	6-29	Weakness, spasticity, Parkinsonism
SCA6	0.02-0.03	Lifespan usually unaltered	Cerebellar signs (nystagmus, tremor, hypotonia)
SCA7	<1	10-30	Retinal degeneration, akinesia, oculomotor disturbance
SCA17	<1	10-20	Dementia, Parkinsonism, hyperreflexia, involuntary movement

Table 1.5 Prevalence, disease duration (from onset of clinical symptoms) and symptoms of polyQ SCAs. Additional clinical symptoms refer to those commonly manifesting alongside trunk and extremity ataxia, gaze nystagmus and dysarthria. Information summarised from Lieberman et al. 2018, Tezenas du Montcel et al. 2014 and Buijsen et al. 2019.

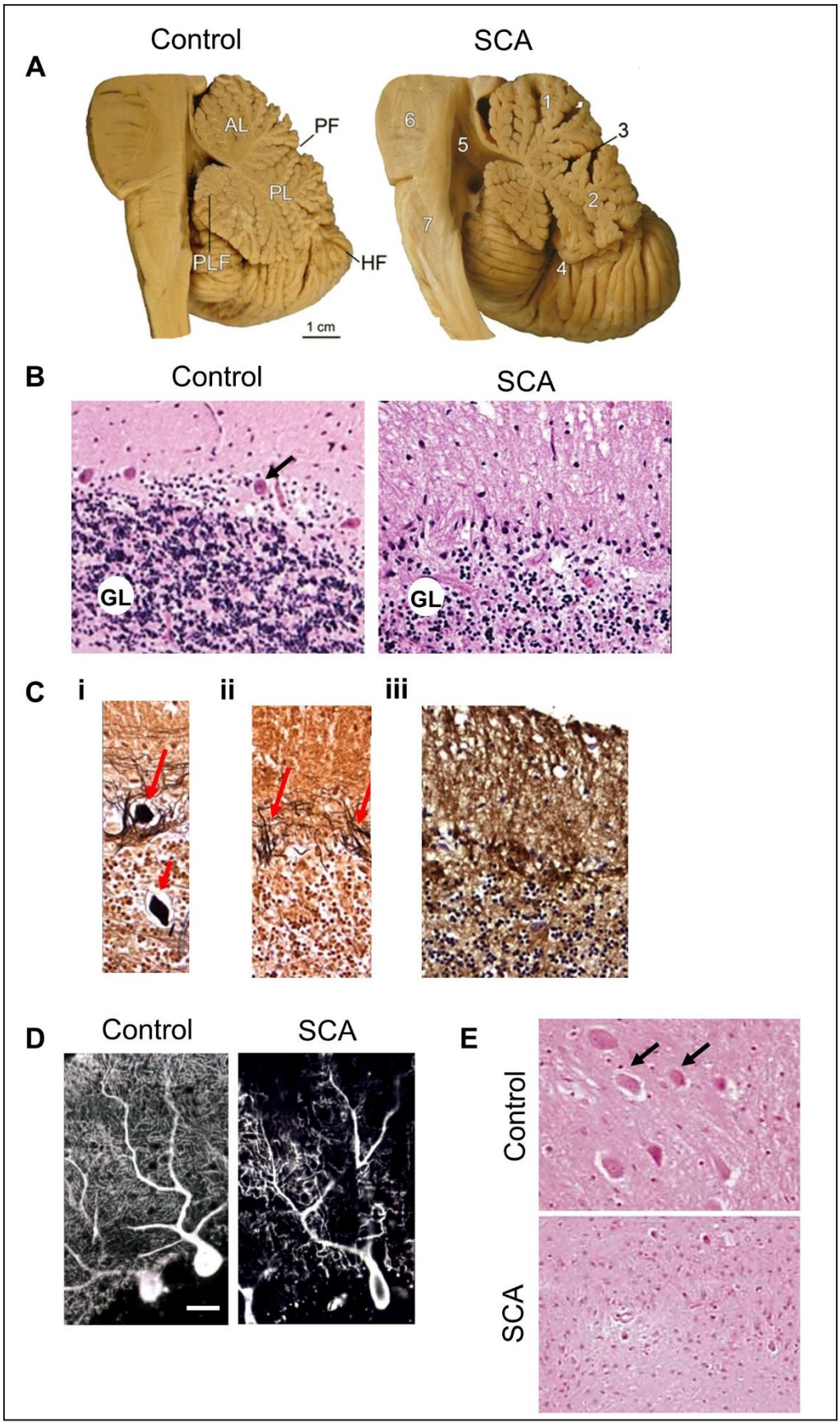

Figure 1.5 Figure legend on next page

Figure 1.5 (previous page) Gross and histological neuropathology of autosomal dominant SCA. **A**) Cerebellum and brainstem of a control case and a SCA1 patient. The SCA1 case features (1) atrophic anterior lobe (AL), (2) atrophic posterior lobe (PL), (3) widened posterior fissure (PF), (4), widened postereolateral fissure (PLF), (5) enlarged fourth ventricle, (6) flattened pons and (7) atrophic medulla oblongata. Figure reproduced from Seidel et al. 2012, with permission from Springer Nature under licence number 4845251122833. **B**) Micrographs showing control and SCA cerebellum stained with haematoxylin and eosin. In the SCA case, there is significant loss of granule layer cells (GL) and loss of Purkinje cells (arrow). Figure reproduced from den Dunnen 2013 (CC BY 4.0). **C**) Histological features of cerebellar degeneration in the Purkinje cell layer. i) Degenerating PC (longer arrow) associated with an axonal torpedo (shorter arrow). ii) Basket cell projections form “empty baskets” where Purkinje cells have been lost. iii) Bergman astrogliosis is apparent as dark brown staining. Figure reproduced with adaptations from den Dunnen 2013 (CC BY 4.0). **D**) Immunofluorescent staining of Purkinje cells with anti-calbindin antibody in a control case and patient with SCA6. The SCA6 Purkinje cell has reduced cell body size, a shrunken appearance and simplification of the dendritic tree. Scale bar is 50µm. Figure reproduced with adaptations from Koeppen 2005, with permission from Springer Nature under licence number 4845260114693. **E**) Haematoxylin and eosin staining of the cerebellar dentate nucleus from a control case and an autosomal dominant SCA patient. There is severe depletion of large principle neurons (arrows) in disease. Figure reproduced with adaptations from Houlden et al. 2007, with permission from Springer Nature under licence number 4845260447583.

DN neuronal loss and synaptic degeneration is a major histopathological characteristic of most types of polyQ SCA. It is hypothesised that DN neuronal atrophy may be a result of transsynaptic degeneration caused by reduced Purkinje cell GABAergic input (Koeppen 2018). There is extensive neuronal loss and synaptic degeneration in the DN in SCA1, 2 and 7, with general preservation of this region in SCA6 and 17 (Koeppen et al. 2005, Tables 1.6 and 1.7). SCA3 exhibits a unique histological “grumose reaction” in the DN, a hazy staining visible with cresyl violet and immunohistochemical staining, associated with neuronal pathology (Koeppen et al. 2005). Mutated disease-causing proteins containing expanded polyQ tracts form both nuclear and cytoplasmic protein inclusions in neurons affected by SCA (Table 1.6). The precise role of these inclusions in pathogenesis is not fully understood but is discussed further in section 1.3.1.

Disease	Purkinje cells	Dentate nucleus	Cellular inclusions
SCA1	Cell loss, atrophy	Neuronal loss	PolyQ positive nuclear inclusions in neurons
SCA2	Cell loss, atrophy	Neuronal loss, synaptic degeneration	Relatively small polyQ nuclear inclusions in neurons
SCA3	Generally preserved	Neuronal loss, synaptic degeneration, grumose reaction	Small ubiquitin and polyQ positive nuclear inclusions in neurons
SCA6	Cell loss, atrophy	Neurons mostly preserved	Cytoplasmic PolyQ inclusions in Purkinje cells. Nuclear inclusions are very rare.
SCA7	Cell loss, atrophy	Neuronal loss	Nuclear polyQ inclusions in neurons
SCA17	Cell loss, atrophy	Neurons mostly preserved	High abundance of nuclear inclusions in molecular cell layer and Purkinje cells. Inclusions present throughout the brain in grey matter.

Table 1.6 Neuropathological features of cerebellar degeneration in polyQ SCA. Cellular inclusions refers to intranuclear or intracytoplasmic bodies, positive for polyQ (1C2 staining) and/or ubiquitin. Summarised from Koeppen et al. 2005, Koeppen et al. 2013 and Rolfs et al. 2003.

Diagnosis	Molecular layer score	DN score
Normal	0	0
SCA1	9	14
SCA2	15	9
SCA3	0	13
SCA 6	11	11

Table 1.7 Summary of representative neuropathological grading in normal and polyQ SCA cerebellum by Koeppen 2018. Pathology of the molecular layer (Purkinje cells) and DN (dentate nucleus) was graded for abnormalities on a scale of 0-3 (0=normal, 1=mild, 2=moderate, 3=severe). Numbers in the table are the combined total scores for the following immunohistochemical stains from one representative patient per diagnosis: Calbindin-D28k, NSE (neuron-specific enolase), GAD (glutamic acid decarboxylase), VGluT1 (vesicular glutamine transporter 1) and VGluT2.

No drugs are approved for the specific treatment of polyQ SCA (Buijsen et al. 2019), and current treatment regimens are limited to supportive therapies, use of walking aids and home modifications (Opal 2017). Pharmacological treatment may be offered to alleviate some secondary symptomatic complications such as depression and pain (Opal 2017). Current research is aimed at developing disease-modifying therapies to prevent, halt or slow neuropathology.

Current opinion indicates that effective future treatments will aim to reduce mutated RNA and protein containing pathological expansions (Paulson et al. 2017). Candidate disease-modifying drugs include AAV (adeno-associated virus) mediated delivery of miRNA to prevent transcription of mutated genes, and in the case of SCA1, evidence for animal models indicates that an MSK1 inhibitor could reduce ataxin1 levels and alleviate pathology (Ashizawa and Paulson 2018). Overall, the polyQ SCAs are rare but devastating diseases with no approved treatments, indicating a large unmet clinical need to further investigate their molecular pathology and inform the development of disease-modifying therapies.

1.3 Molecular pathology of polyQ disorders

This section describes the current state of knowledge on the molecular biology underlying polyQ disease. Although characterised by their presence of neuronal polyQ protein inclusions, current research indicates an increasingly well understood role for CAG repeat xtrRNA. This section focuses on HD, the most common polyQ disorder, and polyQ SCAs, in particular SCA1, which features in the studies carried out in Chapters 3 and 4.

1.3.1 Protein-level pathology in polyQ disorders

It has been long established that the histopathology of HD is characterised by inclusions of polyQ huntingtin protein which are found primarily in the nucleus but also the cytoplasm of degenerating MSNs (section 1.2.1). Protein inclusions may also be present in peripheral tissues (Moffitt et al.

2009). More recently, the occurrence of mixed proteinopathies in HD has been discovered; 88% of HD patients with Vonsattel grade 4 neuropathology were found to exhibit at least one non-huntingtin proteinopathy (St-Armour et al. 2018).

Several hypotheses have been postulated to explain how polyQ huntingtin protein induces neurodegeneration, involving both loss and gain of function. There is evidence that altered protein folding, impaired protein degradation, mitochondrial dysfunction and disrupted neuronal circuitry may all be induced by the presence of mutant huntingtin (reviewed by Labbadia and Morimoto 2013). It is also hypothesised that the formation of neuronal inclusions of mutant huntingtin could be a cellular coping mechanism, rather than directly exerting neurotoxicity, as there is a disparity between the formation of aggregated protein and neurotoxicity in both animal models and patient tissues (Arrasate and Finkbeiner 2012). Disturbances to nucleocytoplasmic compartmentalisation have also been described in HD. Gasset-Rosa et al. (2017) demonstrated that polyQ huntingtin disturbs mRNA and protein transport between the nuclear and cytoplasmic compartments. Furthermore, this study discovered a role for compromised nuclear envelope integrity in polyQ pathology. More recently it has been hypothesised that huntingtin protein may spread inter-cellularly via a prion-like mechanism within the brain (Tang 2018, Srinageshwar et al. 2020).

In polyQ SCAs, it is hypothesised that misfolding and accumulation or aggregation of expanded polyQ proteins disrupts protein and RNA homeostasis. Some of the genes affected in polyQ SCAs are involved in the regulation of gene expression at the transcriptional and post-transcriptional level, so these processes would be disturbed by polyQ-induced loss of normal function. SCA1 is caused by mutation of the *ATXN1* gene (Orr et al. 1993, Banfi et al. 1994), which encodes a chromatin binding factor involved in RNA regulation (Tsai et al. 2004). Ataxin1 is also able to bind RNA in a manor dependent on the length of its polyQ tract (Yue et al. 2001). Like many other proteins involved in RNA processing, ataxin1 contains a nuclear

localisation sequence (NLS) motif and can shuttle between the nuclear and cytoplasmic compartments.

Neurons of SCA1 patients were initially discovered to contain nuclear inclusions of aggregated expanded ataxin1 protein associated with the nuclear matrix (Skinner et al. 1997). A single amino acid substitution in the NLS was later found to prevent expanded ataxin1 entering the nucleus and eliminated toxicity (Klement et al. 1998), indicating a pathogenic role of expanded ataxin1 protein in the nucleus. Indeed, Irwin et al. (2005) discovered that ataxin1-mediated neurodegeneration was dependent on its nuclear localisation, and that pathologically expanded ataxin1 is unable to export from the nucleus where it forms inclusions dependent on the presence of RNA. Ataxin1 polyQ expansion does not necessarily lead to aggregate formation (Krol et al. 2008), supporting the lack of correlation between neuronal polyQ inclusions and disease progression in SCA1 patients.

Both wildtype and expanded ataxin1 protein interact with components of nuclear DNA. Importantly, ataxin1 interacts via its HBP1 domain with capicua (CIC), a DNA binding protein and transcriptional repressor (Lam et al. 2006). Mice expressing both pathologically expanded ataxin1 and a loss-of-function CIC mutant had reduced cerebellar degeneration and fewer motor and cognitive deficits in comparison to mice with wildtype CIC (Fryer et al. 2011). Ataxin1 also binds the RNA splicing factor RBM17 (Lim et al. 2008). It is hypothesised that ataxin1 enters the nucleus and readily binds CIC. The ataxin1-CIC complex then binds DNA, targeting chromatin and transcription sites. Ataxin1 may shuttle between complexing with CIC and RBM17, with polyQ expansion conferring a dynamic shift in favour of RBM17 over CIC complexing (Lim et al. 2008, Paulson et al. 2017). This hypothesis was recently further explored by Rousseaux et al. (2018), who demonstrated that the interaction of ataxin1 with CIC is critical for cerebellar toxicity *in-vivo* in SCA1.

1.3.2 RNA-level pathology in polyQ disorders

Despite the research summarised above which explores the protein-level pathology of polyglutamine peptides in HD and polyQ SCAs, there is currently no causative evidence to demonstrate that any polyQ protein inclusions directly lead to neuronal degeneration. As genes containing polyCAG expansions are transcribed into xtrRNA, research is now leading us to further investigate the role of pathological RNA transcripts in the aetiology of polyQ disorders.

RNA-level pathology mediated by repeat expansions is a well-established feature of several neurodegenerative diseases; in SCA8, non-coding trinucleotide expansions confer neuronal toxicity in the absence of expanded peptides (excluding the possibility of those generated by RAN translation). In addition, the most common genetic cause of ALS and FTD is intronic hexanucleotide expansions in the *C9ORF72* gene, which causes formation of pathological sense and antisense repeat expansion RNA foci (Prudencio et al. 2015, Zu et al. 2013).

There is a so-called paradoxical absence of polyQ protein inclusions in the Purkinje cells of many hereditary ataxia patients (Koyano et al. 2002). This could be explained by assuming that damaged cells with nuclear inclusions are more likely to degenerate and be lost before those without inclusions, although the authors conclude that their finding is more likely to point towards a lack of correlation between polyQ protein inclusions and Purkinje cell degeneration (Koyano et al. 2002). A study in *Drosophila* found that interspersing CAG repeat tracts with glutamine-encoding CAA codons lessens ataxin3 degeneration, indicating that CAG triplicate expansion confers specific neuronal toxicity at the RNA level (Li et al. 2008). More recently, it was discovered that targeting CAG expansion *HTT* RNA *in-vivo* with an antisense oligonucleotide reduced neurodegeneration, and this was independent of huntingtin protein levels (Rue et al. 2016). Furthermore, a recent GWAS by Lee et al. (2019) demonstrated strong evidence that HD age of onset is determined by CAG repeat length, not polyglutamine length. Several mechanisms may underpin expanded CAG RNA toxicity, including

altered cellular localisation, dysregulated splicing and protein binding (Marti 2016). Some of these are further discussed below, with a focus on the aberrant interaction of CAG xtrRNA with RBPs.

1.3.3 Structure of CAG xtrRNA

Tandem repeats are naturally occurring simple sequence repeats within the genome comprising base pair motifs, usually up to six nucleotides long (Pan et al. 2018). Trinucleotide repeats are a form of this microsatellite DNA, located throughout the genome and most frequently formed of AAT, AAC and AAG codons. The presence of trinucleotide repeats affects the secondary structure of nucleic acids as defined by Watson-Crick base pairing. Whilst double stranded DNA forms double helices as a result of complementary base pairing, single stranded RNA transcripts may form multiple secondary structures. RNA often forms stem loops, also known as hairpin loops, comprising two stretches of base-paired nucleotides within the same strand, ending in an unpaired loop (Figure 1.6).

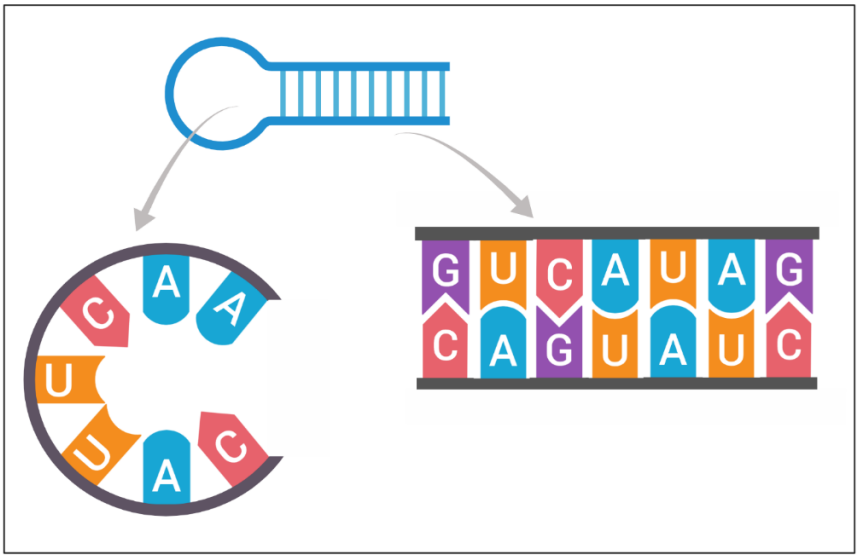

Figure 1.6 Illustration representing the 2D secondary structure of a single strand of RNA forming a stem loop, comprising paired nucleotides in the stem structure, ending in a loop of unpaired nucleotides.

Trinucleotide repeats are categorised into four structural RNA classes (Sobczak et al. 2010, Figure 1.7). Whilst RNA G-quadruplexes are associated with a number of human diseases (Kharel et al. 2020), here we will focus on the role of CAG-repeat containing hairpin loops. Biophysical and thermodynamic characterisation confirmed that CAG trinucleotides with 17 or more repeats form stable self-complimentary RNA hairpin structures, which are noted sites of interaction with RBPs (Sobczak et al. 2010). de Mezer et al. (2011) investigated the secondary structure of huntingtin mRNA *in-vitro*, determining that CAG expansion repeats alter secondary RNA structure, increasing the length of the hairpin loop. The same study also identified that CAG repeat expansion mRNA forms hairpin loops which accumulate in ribonuclear foci co-localised with RBPs.

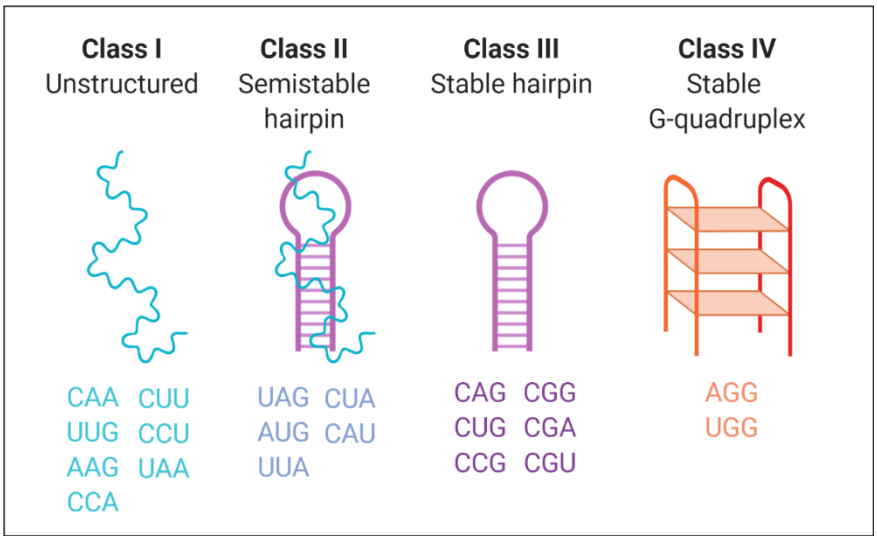

Figure 1.7 Illustration representing secondary RNA structures of trinucleotide repeats. CAG repeats which cause polyQ disorders form Class III stable hairpin structures. Adapted from Sobczak et al. 2010.

1.3.4 CAG expansion instability

PolyQ diseases are often associated with genetic anticipation, whereby as a genetic disorder is passed down generations, an earlier age of onset and increase in severity is observed (Nestor and Monckton, 2011). This is caused by the instability of CAG repeats and their propensity to expand in length through the insertion of extra CAG codons. This often occurs through replication slippage, or during DNA repair or recombination (Kraus-Perrotta and Lagalwar 2016).

1.3.5 CAT interruptions

Unexpanded CAG repeat tracts in *ATXN1*, *ATXN2* and genes associated with fragile x-associated disorders are interrupted by other codons (Kraus-Perrotta and Lagalwar 2016). For example, in wildtype *ATXN1*, tracts of up to 38 CAG repeats are interrupted by 1-3 CAT (histidine) codons, whilst mutated *ATXN1* does not contain interruptions (Paulson et al. 2017). CAT interruptions regulate DNA and RNA secondary structure. In *ATXN1* their inclusion inhibits replication slippage and destabilises hairpin structures, reducing the propensity of expanded CAG tracts to form long hairpins associated with pathogenesis (Sobczak and Krzyzosiak 2004). Interruptions can also change the secondary structure of RNA; in ATXN2, CAA interruptions induce formation of branched hairpins (Sobczak and Krzyzosiak 2005). As RNA secondary structure is important in mediating protein interactions (Sanchez de Groot et al. 2019), it is therefore possible that hairpin loop destabilisation by CAT interruption could alter transcript interaction with RBPs. It has been established that the number of CAT interruptions is critical in determining age of onset in SCA1 (Matsuyama et al. 1999), with age of onset inversely correlating to increased length of uninterrupted CAG stretch (Menon et al. 2013).

1.3.6 RAN translation

Repeat-associated non-ATG (RAN) translation occurs in the absence of a start codon and can be initiated in long hairpin structures of CAG repeats. This results in translation of additional proteins containing polyQ, polyserine or polyalanine repeats (Nalavade et al. 2013). RAN translation can also occur in the anti-sense direction, meaning that expanded CAG tracts can produce multiple potentially toxic transcripts (Pearson 2011). This mechanism may contribute to polyQ disease pathology as both sense and anti-sense RAN proteins accumulate in HD brains (Banez-Coronel et al. 2015). RAN translation has also been described in SCA8 (Zu et al. 2011), fragile x tremor ataxia syndrome (Todd et al. 2013) and C9ORF72-associated ALS (Ash et al. 2013). To date there is no evidence demonstrating that RAN translated peptides underly pathogenesis of polyQ

SCAs, but current opinion indicates that this is a potential disease mechanism (Paulson et al. 2017).

1.3.7 Protein interactions of CAG xtrRNA

Mutant xtrRNA transcripts have been previously shown to interact with RBPs which mediate critical cellular processes such as RNA processing (Osborne and Thornton 2006, Tsoi et al. 2012) and nucleocytoplasmic transport (Tsoi et al. 2011). The best well-characterised expansion repeat RNA-protein interaction is that between musclebind-like 1 (MBNL1) protein and CAU repeat RNA in DMPK transcripts, the mutation underlying type 1 myotonic dystrophy (Ciesiolka et al. 2017). CAG expansion repeat RNA is known to sequester and interact with proteins (McLaughlin et al. 1996, de Mezer et al. 2011, Nalavade et al. 2013). Current well-supported opinion describes abnormal structure-dependent interactions of xtrRNA with RBPs as a key contributing factor to the pathogenesis of expansion repeat disorders (Ciesiolka et al. 2017). Many polyQ disorders are characterised by binding of specific proteins to xtrRNA or colocalization of proteins with xtrRNA focal aggregates, including HD and polyQ SCAs (Rohilla and Gagnon 2017).

1.4 RNA binding proteins

1.4.1 Structure and function of RBPs

The human genome encodes at least 1500 RNA binding proteins (RBPs) (Dominguez et al. 2018) which are key mediators of transcriptional regulation. All RBPs contain at least one RNA binding domain (RBD) which facilitates direct interaction with RNA via van der Waals interactions, electrostatic bonds and hydrogen-bonding (Morozova et al. 2006). The “canonical” RBDs include RNA recognition motifs (RRM), zinc-fingers, K-homology (KH), double-stranded RNA binding domains (dsRBD), Asp-Glu-Ala-Asp (DEAD/DEAH) boxes and Pumillo homology (PUF) domains (Lunde et al. 2007). These are structurally well-defined and have been the most well-studied RBDs to date. RBPs are usually modular in structure (Lunde et al. 2007) and often contain multiple RBDs to confer substrate

binding specificity (Maris et al. 2005). Interdomain linker peptides allow flexibility of secondary structure to accommodate substrate interaction (Lunde et al. 2007). Short linker regions separating RRM domains are also directly involved in RNA binding (Daubner et al. 2013, Varadi et al. 2015).

Previous work has described RBP “interactomes”, characterisations of RNA-protein interactions across whole genomes. For example, Castello et al. (2012) generated an atlas of HeLa cell mRNA-protein interactions using cross-linking and mass spectrometry. This work discovered that repetitive, unstructured protein sequences comprise motifs which frequently interact with mRNA substrates. The discovery of novel RNA-protein interactions is a dynamic and rapidly advancing field of research and more recently, there have been several RBPs discovered which do not contain a well-characterised RBD (Beckmann et al. 2015 and reviewed by Hentze et al. 2018). This indicates that RNA-protein interactions cannot always be predicted by protein sequence or structural analysis.

Eukaryotic RNA processing in the nucleus involves 5’ capping, 3’ cleavage and polyadenylation, and splicing. The resultant functional mRNA is transported to the cytoplasm for further processing and translation. RBPs are important modulators of RNA processing, and regulate gene expression through transcription, mRNA stability, modulation of splicing and RNA transport and translation. They are usually multifunctional and often interact with other proteins as part of large macromolecular complexes, with multiple RBPs often interacting with individual RNA transcripts (Hegele et al. 2012). They bind transiently to their substrates to allow rapid assembly and disassembly of these complexes (Blanco and Montoya 2011), conferring highly dynamic control over RNA processing events. The interaction between RBPs and their RNA substrates also modulates the function, stability and localisation of the RBP itself (Hentze et al. 2018, Figure 1.8).

There are estimated to be over 400 RBPs which also bind DNA, termed DNA-RNA binding proteins (DRBPs) (Hudson and Ortlund 2014). DRBPs can interact with their nucleic acid targets in various ways: by competitive

binding of their DNA and RNA targets, by regulating gene expression at multiple levels (binding the promoters and RNA transcripts of a gene), and by simultaneously binding both DNA and RNA (Hudson and Ortlund 2014). The biology of DRBPs is especially interesting in the context of neurodegenerative disease because mutations in two DRBPs, transactive response DNA binding protein-43 (TDP-43) and fused in sarcoma (FUS), directly cause forms of ALS and fronto-termporal dementia (FTD). This sets a precedent for the involvement of RBPs in the pathology of neurodegenerative diseases, which is discussed in further detail below.

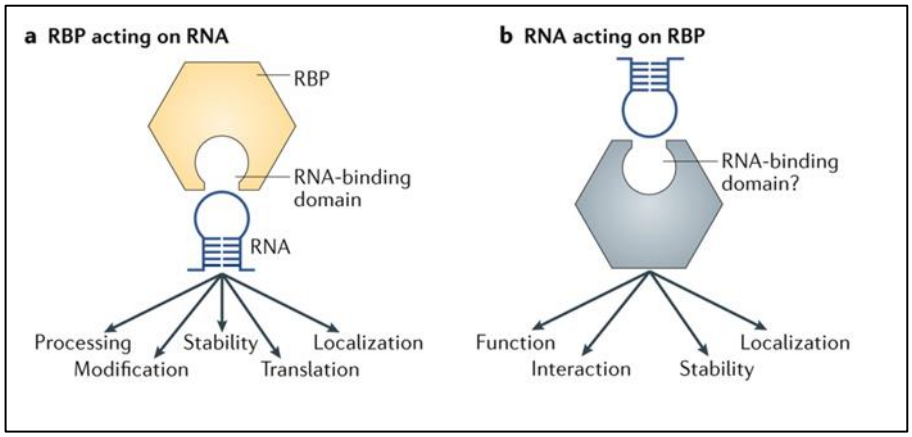

Figure 1.8 Diagram summarising the functional crosstalk between RBPs and RNA. The interaction of an RBP with its RNA substrate is highly complex and can modulate the processing, modification, stability and localisation of both the RNA transcript and the RBP itself. Figure reproduced from Hentze et al. 2018, with permission from Springer Nature under licence number 4845260765820.

1.4.2 RBPs in neurodegenerative disease

RBPs modulate complex processes required for the function and survival of neurons, including RNA transcription, RNA transport, pre-mRNA splicing and translation (De Conti et al. 2017, Figure 1.9). Dysregulated RBP function is implicated in both sporadic and inherited neurodegenerative disease (Cookson 2017, Table 1.8), and current opinion indicates that RBPs are important in mediating protein aggregation as well as RNA dysregulation in a range of neurodegenerative pathologies (Maziuk et al. 2017).

In this section the role of TDP-43 and FUS, two prototypical RBPs associated with neurodegenerative disease, are summarised. The

increasing knowledge contributing to the role of RBPs in neurodegeneration is discussed, particularly relating to alterations in their neuronal expression.

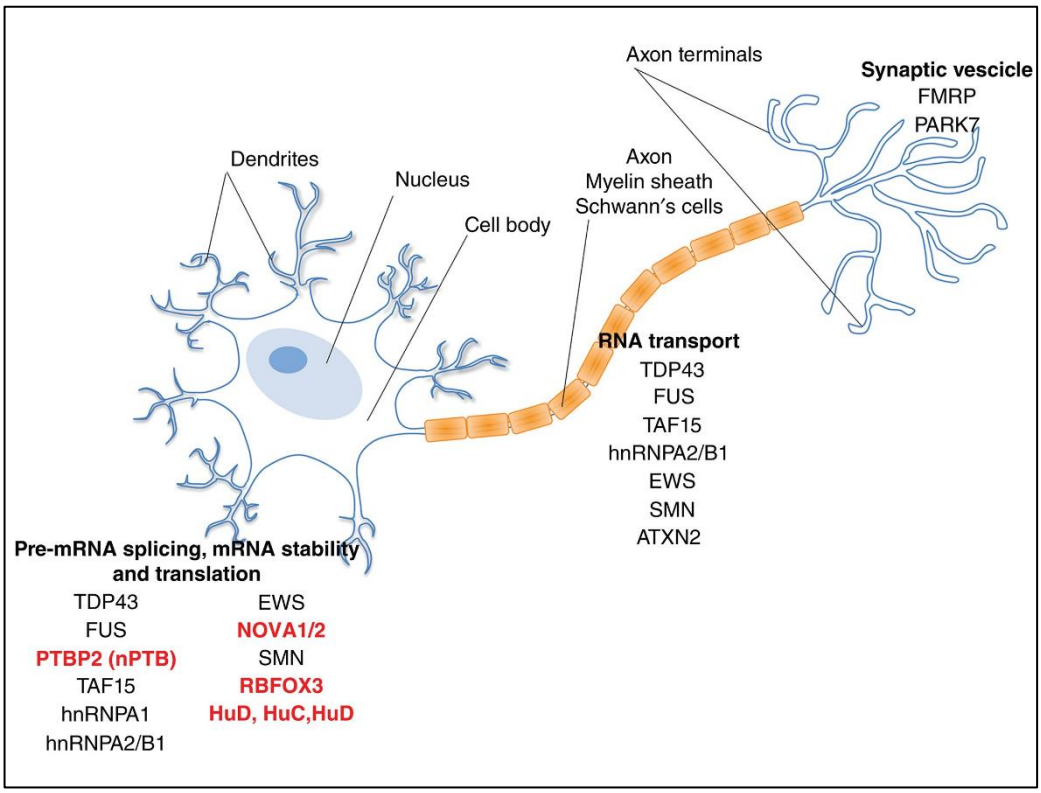

Figure 1.9 RBPs and their functions in neuronal metabolism. RBPs listed in red are predominantly or exclusively expressed in neurons. Many of these RBPs have been associated with neurodegenerative disease through altered expression levels, mutations or aberrant aggregation. Figure reproduced from De Conti et al. 2017, with permission from John Wiley and Sons under licence number 4845261151599.

1.4.2.1 TDP-43

TAR DNA binding protein 43 (TDP-43, encoded by the *TARDBP* gene) is a ubiquitously expressed and evolutionarily conserved DRBP. TDP-43 acts as a splicing factor and is involved in transcriptional repression and translational regulation (Conlon and Manley 2017). The critical role of TDP-43 is exemplified by the embryonic mortality induced in knockout mice (Kraemer et al. 2010). In neurons, TDP-43 binds thousands of individual RNA transcripts and is critical for normal neuronal function (Sephton et al. 2011, Sephton and Yu 2015).

RBP	Function	Associated diseases	Ref.
Ataxin1	RNA processing, RNA export	Repeat expansions cause SCA1	Orr et al. 1993, Irwin et al. 2005
Ataxin2	RNA binding	Expansions cause SCA2 and associated with ALS	Imbert et al. 1996, Elden et al. 2010
C9ORF72	RNA processing, transcription, translation and transport	Most commonly mutated protein associated with FTD and ALS (GGGGCC hexanucleotide repeats)	DeJesus-Hernandez et al. 2011
DJ-1	RNA processing, associates with mRNA transcripts	Associates with cytoplasmic RNA granules in PD. Mutations cause familial PD.	Repici and Giorgini 2019
EWSR1	RNA processing, transcription and transport	Mutations associated with ALS. Deletion induces motor dysfunction in mice.	Yoon et al. 2018
FUS	RNA processing, mRNA splicing, transcription and transport, translation	Mutations cause ALS and rare familial FTD. Implicated in the pathology of HD.	Kino et al. 2016
hnRNP A1	Packaging of pre-mRNA into hnRNP particles, mRNA transport	Mislocalised to the cytoplasm in MS. TDP-43 induces its upregulated expression and cytoplasmic accumulation.	Salapa et al. 2018, Deshaies et al. 2018
hnRNP A3	Cytoplasmic trafficking of RNA	Present in inclusions in FTLD and ALS neurons. Sequestered to RNA foci in ALS.	Cooper-Knock et al. 2015, Davidson et al. 2017
Matrin 3	mRNA stabilisation, splicing, RNA degradation	Mutations associated with ALS. Mislocalisation of non-mutated protein causes neurotoxicity.	Malik et al. 2018
TAF15	Involved in RNA polymerase II gene transcription	Mutations associated with ALS	Neumann et al. 2011, Couthouis et al. 2012
TDP-43	Transcriptional repression, translational regulation, splicing	Mutations associated with ALS and FTD. Also implicated in AD, HD, Lewy body dementia, PD and SCA.	Kabashi et al. 2008, Kwiatkowski et al. 2009
TIA1	Involved in induction of apoptosis	Mediates tau toxicity in AD. Mutations associated with ALS-FTD.	Mackenzie et al. 2017, Apicco et al. 2018

Table 1.8 Selected RBPs and their association with neurodegenerative disease

TDP-43 was identified as a component of neuronal cytoplasmic inclusions and dystrophic neurites in FTD and ALS (Arai et al. 2006, Neumann et al. 2006).Intracellular inclusions of phosphorylated TDP-43 were also later identified in brain tissue of patients with AD and dementia with Lewy bodies (Arai et al. 2009). In addition to its hyperphosphorylated and ubiquitin positive state, pathological TDP-43 was further characterised as featuring nuclear depletion and aberrant post-translational cleavage (Arai et al. 2006, Neumann et al. 2006).

It was later discovered that genetic mutations in TDP-43 are associated with rare familial cases of ALS and FTD (Kabashi et al. 2008, Kwiatkowski et al. 2009). There are now at least 55 known TDP-43 mutations associated with familial ALS (Conlon and Manley 2017), alongside several rare mutations associated with sporadic ALS and FTD (Buratti 2015). Almost all known mutations occur in the C-terminal domain of TDP-43 and would not be expected to directly affect RNA binding (Buratti 2015). However, recent research identified a mutation in close proximity to the RRM domain which promotes cytoplasmic mislocalisation and aggregation of TDP-43 (Chen et al. 2019). Furthermore, the ability of TDP-43 to bind mRNA in the cytoplasm was found to be critical for its pathological function as a translational enhancer of specific mRNAs linked to neurodegeneration (Neelagandan et al. 2018). A systematic study of disease-associated TDP-43 isoforms was performed in *Drosophila* and chicks, revealing that the RNA binding function of TDP-43 is required for *in-vivo* neurotoxicity (Voigt et al. 2010). This finding is supported by further evidence for the mechanistic importance of the RNA binding function of TDP-43 *in-vivo* presented by Ihara et al. (2013) who expressed human TDP-43 containing disease-associated mutations in *Drosophila* to induce neurodegenerative phenotypes. Neuronal degeneration was abolished when the RRM domain of TDP-43 was mutated to ablate its RNA-binding function. Although the majority (at least 90%) of ALS cases are sporadic and only rare cases are associated with TDP-43 mutations, TDP-43 proteinopathy is a feature of most ALS cases (Arai et al. 2006), and also features in a diverse set of neurodegenerative diseases including AD, HD, Lewy body dementia, PD and SCA. This indicates that

acquired functional abnormalities of wildtype TDP-43 in neurons underly its involvement in neurodegenerative pathology.

1.4.2.2 FUS

Fused in sarcoma (FUS) is one of the FET family of DRBPs which also includes EWSR1 and TAF15, originally discovered as oncogenes and now known to be associated with ALS (Kwiatkowski et al. 2009). In addition to ALS, mutations in FUS (for example in the NLS or DNA binding domain) can also more rarely cause familial FTD (Ederle and Dormann 2017). FUS has functional homology to TDP-43, being associated with many critical RNA processing functions such as pre-mRNA splicing, mRNA stabilisation, trafficking and translation, as well as DNA repair (Ederle and Dormann 2017). In ALS, FUS becomes mislocalised to the cytoplasm where it forms pathological inclusions (Vance et al. 2009).

In addition to their close association with ALS and FTD, the role of TDP-43 and FUS in other neurodegenerative diseases has also been investigated. TDP-43 aggregates were found to co-localise with huntingtin inclusions in HD patient brain (Schwab et al. 2008). In human cell lines, expanded huntingtin protein was found to induce the accumulation of phosphorylated TDP-43 (Coudert et al. 2019). Furthermore, FUS was previously shown to be a component of huntingtin aggregates in both a cell model (Doi et al. 2008) and mouse model of HD (Kino et al. 2016). The latter study also identified that FUS acts as a modifier of polyQ disease pathology, whereby degenerative phenotype was worsened with heterozygous FUS knockout. Tauffenberger et al. (2013) also discovered that both FUS and TDP-43 modified polyQ pathology *in-vivo* (in *C. elegans*), although their results conversely suggest that upregulating expression of the RBPs promotes polyQ toxicity.

1.4.2.3 Implications of RBP mislocalisation in neurodegenerative disease

Dysregulated nucleocytoplasmic transport of proteins is both a feature of normal ageing and an emerging mechanistic hallmark of neurodegenerative disease pathology (Fahrenkrog and Harel 2018, Benvegnu 2019). It is

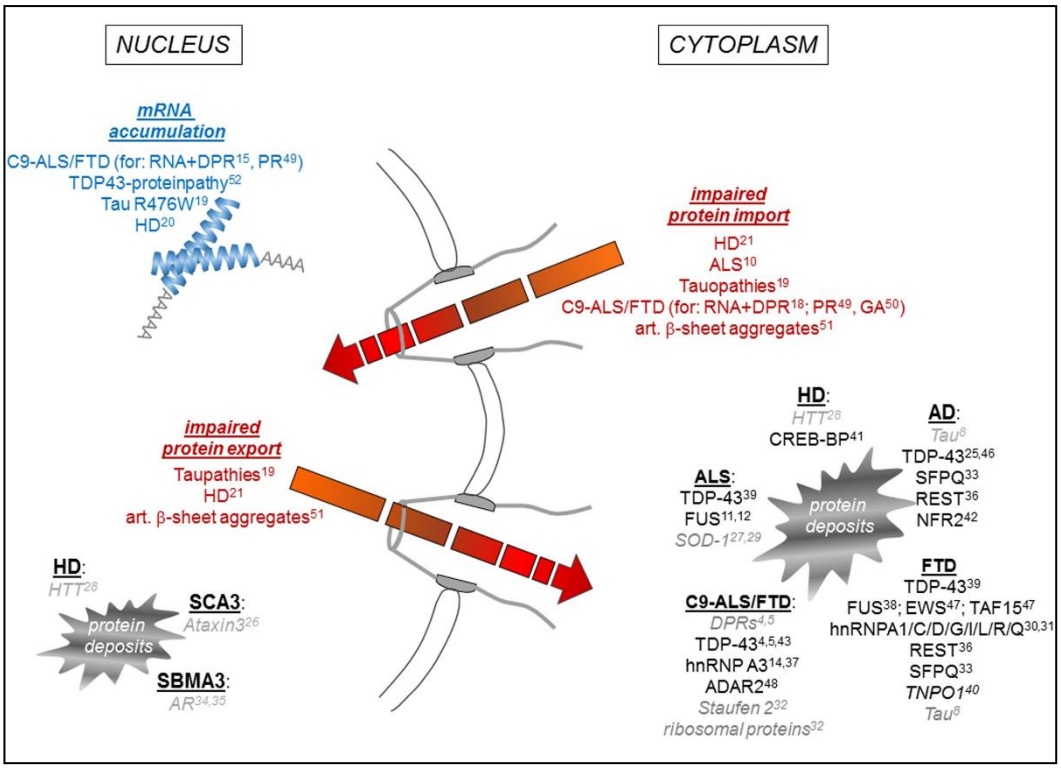

Figure 1.10 Nucleocytoplasmic transport deficits in neurodegeneration. Protein deposits that aggregate in the nucleus or cytoplasm are listed in black/grey. Proteins depleted form the nucleus and localised to the cytoplasm are listed in black. Disorders listed in red have confirmed protein import/export deficits. Figure from. Figure reproduced from Hutten and Dormann 2019, with permission from Elsevier under licence number 4845270056962.

possible that protein mislocalisation in neurons could occur through increased or decreased export from the nucleus, pathological nuclear retention, dysregulated nuclear import, disturbance to nuclear envelope integrity or altered expression of nuclear receptors or transporters. Dysregulation in the binding partners of mislocalised proteins which facilitate their nucleocytoplasmic shuttling may also play an important role. Proteins associated with neurodegeneration which are also involved in nucleocytoplasmic mislocalisation were recently summarised by Hutten and Dormann (2019) (Figure 1.10).

Control of protein subcellular localisation is especially important in the case of RBPs (Hutten and Dormann 2019), a number of which are featured in the summary in Figure 1.10. The RBPs FUS and TDP-43 are both predominantly expressed within the nucleus, and under normal conditions a proportion is expressed within the cytoplasm so that they can carry out

cytosolic functions including regulation of mRNA stability, mRNA transport and translation (Birsa et al. 2019). In ALS and FTD, TDP-43 (and more rarely, FUS) become depleted from the nucleus and accumulate in the cytoplasm, conferring a loss of nuclear function and potential toxic gain of function in the cytoplasm (Gao et al. 2018). Mutations in the NLS of FUS which affect its shuttling are associated with ALS, and impaired nuclear import has been identified as a key mechanism in ALS pathology (Dormann and Haass 2011, Hutten and Dormann 2019).

Mislocalisation of RBPs to both the nucleus and cytoplasm is now emerging as a more general mechanism of neurodegenerative disease. RBPs in the cytoplasm are often sequestered to stress granules, non-membranous aggregates comprising protein and mRNA molecules which assemble as part of the cellular stress response to supress the translation of non-essential proteins (Baradaran-Heravi et al. 2019). The regulated formation of stress granules and their sequestration of RBPs may act as a protective mechanism in neurons by initiating controlled translational arrest, but aberrant redistribution of RBPs to the cytoplasm and accumulation of excess stress granules is likely to be an important pathological mechanism (Hutten and Dormann 2019). Stress granule formation is associated with the pathogenesis of several neurodegenerative diseases including ALS (Li et al. 2013, Chen and Liu 2017, Wolozin 2012).

In addition to the prototypical examples of TDP-43 and FUS, many other RBPs have been described as mislocalised in neurodegenerative disease. As previously referred to, the pathological function of polyQ expanded ataxin1 is associated with its pathological retention in the nucleus. In addition, cytoplasmic redistribution of the RBP Matrin 3 was found to mitigate degeneration in primary neurons, indicating that nuclear Matrin 3 mediates toxicity (Malik et al. 2018). EWSR1, a FET family RBP similar to FUS and TDP-43, was discovered to be as mislocalised to the cytoplasm in sporadic ALS cases (Couthouis et al. 2012). Further evidence of RBP mislocalisation is described by Salapa et al. (2018), who observed that hnRNP1 aberrantly accumulates in the cytoplasm of MS patient neurons,

although this study looked at only a single patient case. It is not always clear from descriptive or observational studies whether this abnormal expression is related to impaired nucleocytoplasmic transport, or if alternative mechanisms are implicated.

Our research group is interested in the scaffold attachment factor B (SAFB) family of RBPs, which are emerging as important mediators of many cellular functions including the cellular response to stress (Norman et al. 2016). Like TDP-43 and FUS, SAFB proteins are DRBPs which contain RRM domains, are expressed in both the nucleus and the cytoplasm, they are important for RNA processing, critical for development and implicated in many aspects of neuronal function.

1.5 Scaffold Attachment Factor B 1 (SAFB1)

1.5.1 Discovery, structure and expression of SAFB1

The SAFB family of DRBPs includes SAFB1, SAFB2 and SLTM (SAF-like transcriptional modulator). SAFB1 was initially discovered through its ability to bind nuclear scaffold/matrix attachment regions (S/MARs), DNA sequences which confer attachment of chromosomes to the nuclear matrix (Renz and Fackelmayer 1996). The same protein was independently discovered by two separate research groups: Weighardt et al. (1999) identified SAFB1 as a protein interactor of the RBP hnRNPA1, whilst Oesterreich et al. (1997) reported its interaction with the heat-shock protein (HSP) 27 promoter. SAFB2 was later discovered as a gene paralogue of SAFB1, with which it shares a bidirectional dual promoter and high sequence homology (Townson et al. 2003, Figure 1.11). SLTM, the third and more distantly related member of the SAFB family, was identified as an epithelial mesenchymal transition factor by Colley et al. (2002) and later characterised as a mediator of apoptosis (Chan et al. 2007). The investigations in this thesis focus primarily on SAFB1.

SAFB1 is a large multifunctional protein which contains a characteristic AT-rich DNA binding domain (SAFBA/B Acinus and Pias (SAP)), an RNA

binding (RRM) domain and a nuclear localisation sequence (NLS). A C-terminal arginine-glycine rich motif (RGG or R/G domain) is the site of post-translational modifications e.g. by methylation and sumoylation, conferring increased functional complexity (Golebiowski et al. 2009). SAFB1 is larger than, but similar in structure to RBPs associated with neurodegenerative disease such as TDP-43 and FUS, which also contain RRM and glycine-rich domains, and N-terminal NLS (Figure 1.11).

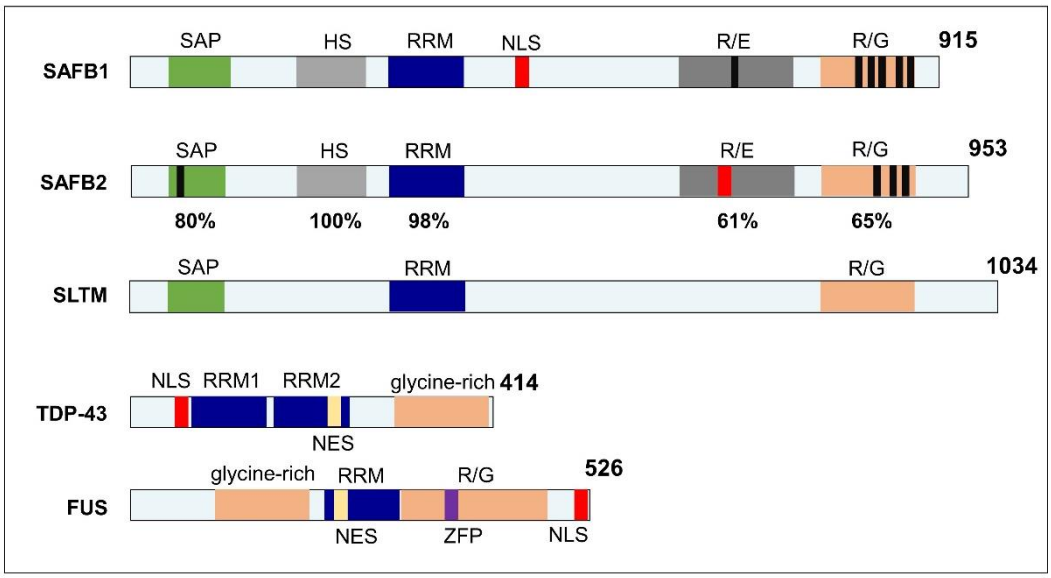

Figure 1.11 Functional domains of SAFB1, SAFB2, SLTM, TDP-43 and FUS. Black rectangles denote methylation sites. Red rectangles denote nuclear localisation sequence (NLS). Percentages indicate homology between SAFB1 and SAFB2. Numbers indicate amino acid length of each protein. HS High similarity region, NES Nuclear export signal, R/E Arginine/glutamic acid-rich motif, R/G Arginine-glycine rich motif, RRM RNA recognition motif, SAP SAF-A/B, Acinus and PIAS domain, ZFP zinc finger protein.

SAFB1 is expressed in tissues throughout the body but is enriched within the brain (Townson et al. 2003, The Human Protein Atlas (SAFB)), especially within the cerebellum and hippocampus (Rivers et al. 2015, Norman et al. 2016). In-house immunohistochemical characterisation demonstrates high SAFB1 and SAFB2 expression throughout the mouse brain including within the hippocampus, cortex, cerebellum and striatum (Figure 1.12). Characterisation of SAFB1 and SAFB2 expression in the rat brain confirms this distribution pattern, with high levels of both within the cerebral cortex, hippocampus, striatum and cerebellum (Hashimoto et al. 2020).

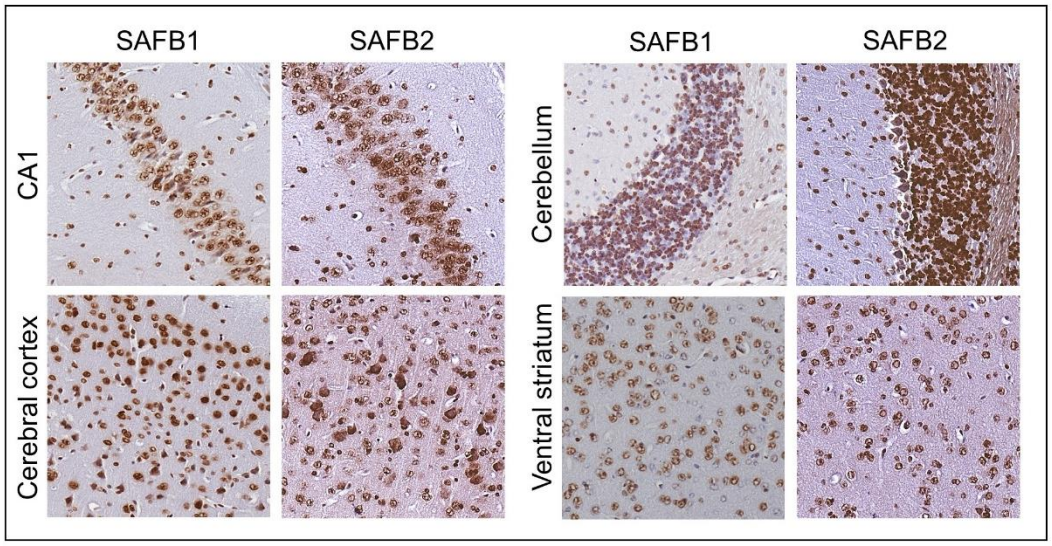

Figure 1.12 Expression of SAFB1 and SAFB2 visualised by immunohistochemical staining in various brain regions of wildtype mouse brain. High expression levels are observed in each area.

Despite their close structural homology, evolutionary retention of both SAFB1 and SAFB2 indicates functional distinction between the two proteins (Nadeau and Sankoff 1997). This differential function is also indicated by their subcellular distribution. Under baseline conditions in rodent cortical neurons, SAFB1 is expressed primarily in the nucleus whilst the distribution of SAFB2 is both nuclear and cytoplasmic (Norman et al. 2016, Hashimoto et al. 2020, Figure 1.13). This subcellular expression pattern is observed within primary cortical neurons *in-vitro*, as well as in mouse brain tissue (Figure 1.13). In HeLa cells, SAFB1 expression was observed as punctate within the nucleus with lack of expression within the nucleoli (Norman et al. 2016). This distribution pattern is also observed in human fibroblasts (Figure 1.13).

1.5.2 Functions of SAFB1 mediated by protein interaction

The extensive distribution of SAFB1 expression in the brain is indicative of its diverse and important functionality. The functions of SAFB1 are complex and involve RNA processing, regulation of transcription, alternative splicing, chromatin structure, DNA repair and nuclear stress body formation (Norman et al. 2016). Regulation of RNA processing is critical for the health and function of neurons, which are highly complex post-mitotic cells and extremely transcriptionally active (Andreassi et al. 2018).

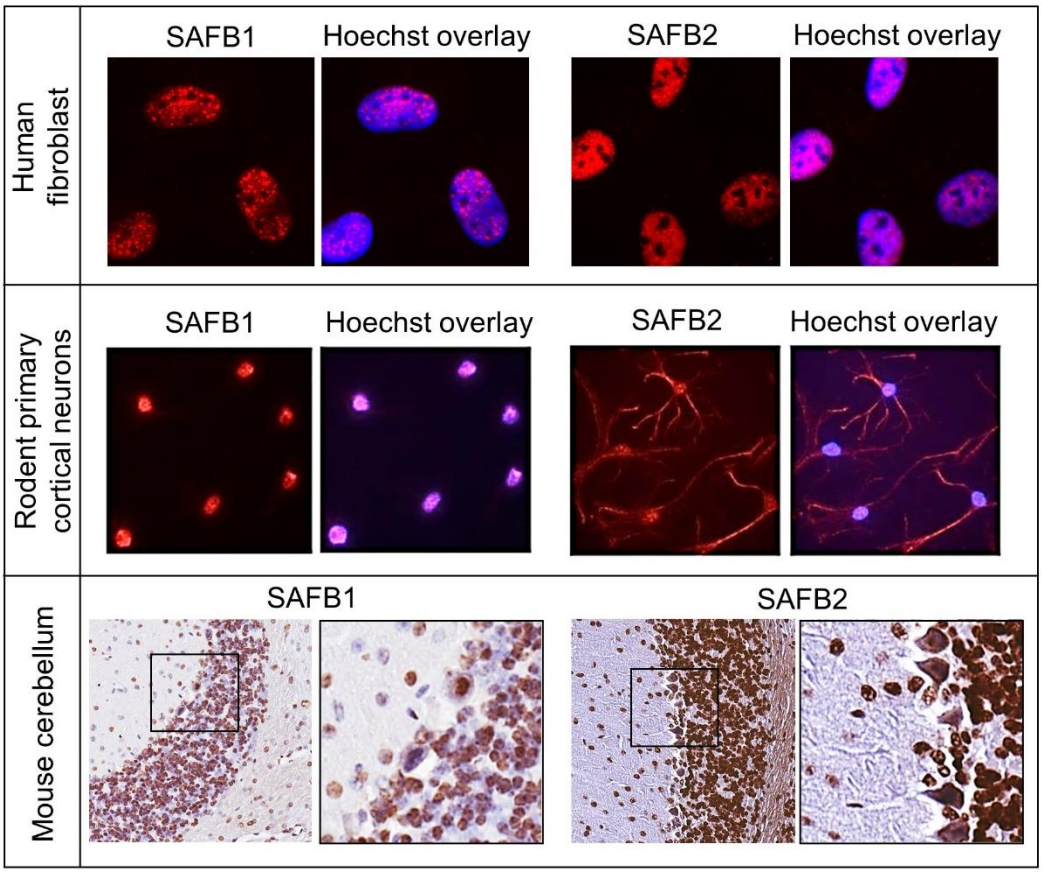

Figure 1.13 The subcellular distribution of SAFB1 and SAFB2. Human primary fibroblasts, rodent primary cortical neurons and mouse cerebellar tissue was immunostained using antibodies specific to SAFB1 or SAFB2. SAFB1 is distinctly nuclear whilst SAFB2 is expressed in the nuclei and cytoplasm of cortical neurons and cerebellar Purkinje cells. Images of rodent cortical neurons are reproduced with adaptations from Norman et al. 2016 (CC BY 4.0). Fibroblast and cerebellar staining was carried out in-house.

SAFB1 has been shown to interact with many proteins including splicing factors, transcriptional-related proteins (including RNA polymerase II) and steroid receptors (Norman et al. 2016). A summary of the known protein interactors of SAFB1 was comprised by Norman et al. (2016) and is reproduced in Table 1.9 with the addition of more recently discovered interacting partners. Since the discovery that SAFB1 binds RNA polymerase II with high affinity (Nayler et al. 1998), it has also been shown to associate with splicing factors such as SRSF1 (Denegri et al. 2002). SAFB1 also interacts with SLM-1 (Stoss et al. 2004) and Sam-68 (Sergeant et al. 2007), members of the STAR family of proteins which regulate pre-mRNA splicing, RNA export and translation.

Heterogenous ribonucleoprotein particles (hnRNPs) are nuclear RNA-protein complexes which regulate RNA transcription and post-transcriptional modification (Han et al. 2010). SAFB1 was demonstrated to interact with many of these proteins (Weighardt et al. 1999, Arao et al. 2000) but loss of co-immunoprecipitation of hnRNPs with SAFB1 in the presence of RNAse indicates that these interactions depend on binding to associated RNAs (Norman et al. 2016).

SAFB1 colocalises with the transcription factor and oestrogen receptor ER-alpha, mediating its association with the nuclear matrix and negatively regulating ER-alpha dependent transcription by influencing nuclear mobility of the receptor (Matsuda et al. 2018). The interaction of SAFB1 with ER-alpha was recently confirmed by immunoprecipitation in the rat brain (Hashimoto et al. 2020). Additional recently published evidence demonstrated that SAFB1 interacts with LC3, which is required for its secretion within extracellular vesicles (Leidal et al. 2020).

Interestingly, SAFB1 was shown to interact with FUS via its N-terminal SAP domain (Yamaguchi and Takanashi 2016). This interaction was demonstrated to tether FUS to chromatin, a function critical for the actions of FUS on RNA splicing and ligand-dependent transcription (Yamaguchi and Takanashi 2016). This demonstrates the importance of SAFB1 as an interacting partner with other RBPs and specifically with those directly associated with the pathology of neurodegenerative disease.

1.5.3 Functions of SAFB1 mediated by nucleic acid interaction

SAFB1 was first identified as a DNA binding protein, interacting with the nuclear matrix via its SAP domain (Renz and Fackelmayer 1996, Kipp et al. 2000). More recently it was discovered that SAFB1 mediates DNA damage-response signalling and is recruited to DNA double-strand breaks to facilitate repair (Altmeyer et al. 2013). Despite its discovery as a DNA binding protein, the study of nucleic acid binding functions of SAFB1 have so far primarily concerned its role as an interactor of RNA. The RRM domain of SAFB1 is likely to mediate its interaction with RNA, but the RGG domain may also be involved (Kiledjian and Dreyfuss 1992).

Process	Class	Interacting proteins
RNA processing	SAFB proteins	SAFB1/SAFB2 (homo- and hererodimerisation)
	hnRNP proteins	hnRNPA1, hnRNPC, hnRNPD, hnRNPG, hnRNPI, hnRNPK, hnRNPU
	SR proteins	SRSF1, SRSF7, SRSF9, SREK1, SRRM1
	SR protein kinase	SRPK1
	STAR proteins	Sam68, SLM-1
	TET proteins	FUS (Yamaguchi and Takanashi 2016)
	E(R) proteins	ERH (Drakouli et al. 2017)
Chromatin		CHD1, NCOR1, HDAC3, BRG1, Matrin 3
Transcription		RNA pol II, $TAF_{II}68$, steroid receptors, p53
Autophagy		LC3 (Leidal et al. 2020)
Miscellaneous		PIAS1, ZO-2, Zbed4

Table 1.9 Protein interacting partners of SAFB1. Table is reproduced with adaptations from Norman et al. 2016 (CC BY 4.0).

Mass spectrometry identified that SAFB1 directly binds mRNA (Baltz et al. 2012). In addition to its interaction with protein-coding transcripts, SAFB1 has been demonstrated to interact with various non-coding RNA (ncRNA) (Rivers et al. 2015, Hong et al. 2015). A key ncRNA mediated role for SAFB1 is in the cellular stress response, an orchestrated and evolutionarily conserved mechanism which has been characterised experimentally using heat-shock. Upon cellular stress, SAFB1 recruits to a locus encoding long-non coding microsatellite DNA at the pericentromeric region of chromosome 9 called satellite 3 (SatIII) where it recruits heat shock factor 1 (HSF1) (Denegri et al. 2002, Jolly et al. 2004). HSFs activate transcription of heat-shock proteins (HSPs), molecular chaperones which facilitate protein folding and assembly. During the cellular stress response, the cell undergoes many adaptations with the most marked change occurring within the nucleus; release of proteins from the nucleoli induce its disintegration, and formation of characteristic nuclear stress bodies (nSBs) (Velichko et al. 2013). nSBs are small electron-dense granules which form at the SatIII sequence. They are ribonucleoprotein complexes containing HSF1 and other associated RNA processing factors such as SRSF1 and RNA polymerase II (Velichko et al. 2013). Formation of nSBs alters cellular transcription to protect proteins and nucleic acids from the injurious effects of stress (Jolly et al. 2004). nSBs act as “molecular traps” sequestering constitutive splicing and transcription factors to temporarily prevent transcription and translation during stress (Weighardt et al. 1999, Norman et al. 2016). Recent research carried out in our lab has further characterised in detail the role of SAFB1 in the heat stress response (Raele 2020).

Recently published work by Huo et al. (2019) showed that SAFB1 binds major satellite RNAs to regulate chromatin condensation and the 3D organisation of heterochromatin. The interaction of SAFB1 with repeat element RNAs was disrupted upon treatment with RNase, indicating that the interaction of SAFB1 with repeat element RNAs to regulate chromatin structure is directly dependent on its RNA binding ability.

Individual nucleotide resolution cross-linking and immunoprecipitation (iCLIP) has been utilised to study the detailed interactions of SAFB1 with RNA in both human neuroblastoma cells (Rivers et al. 2015) and human breast cancer cells (Hong et al. 2015). In MCF-7 cells, SAFB1 cross-links were enriched at ncRNAs, intergenic regions and open reading frames as well as at intronic regions and 3' and 5' untranslated regions (UTRs) (Hong et al. 2015). This study also identified that SAFB1 interacts with and transcriptionally represses SHF (Src homology 2 domain containing F). SHF was previously described as a regulator of apoptosis (Lindholm et al. 2000), implicating a role for SAFB1 in regulation of programmed cell death. Indeed, redistribution of SAFB1 to the nucleolus, the site of extensive RNA processing, was discovered to be a critical step in the modulation of programmed cell death (Lee et al. 2007). Furthermore, overexpression of SAFB1 was previously shown to induce apoptosis (Norman et al. 2016).

The RNA interaction profile of SAFB1 in SH-SY5Y cells was investigated using iCLIP by Rivers et al. (2015). Gene ontology analysis of RNAs interacting with SAFB1 indicated involvement in chromosome organisation, RNA processing, the cellular stress response and neuronal morphogenesis. The study discovered that the highest density of SAFB1 cross-link sites was found at exons in proximity to intron-exon boundaries, indicating an important role of SAFB1 in gene splicing. This role was confirmed by knockdown of SAFB1 which altered the splicing pattern of various genes including NCAM1, an important regulator of neuronal development and synaptic function (Rivers et al. 2015). Results from this study also demonstrated that SAFB1 regulates dendritic spine density of hippocampal neurons, further defining an important neuronal role for SAFB1. An RNA-mediated neuronal function of SAFB1 is also indicated by a huge enrichment of SAFB1 tags at the *ATXN1* gene, corresponding to both within and adjacent to the CAG repeat tract (Rivers et al. 2015). Pathological CAG expansions in *ATXN1* cause the polyQ disorder SCA1, therefore this finding provides an insight into the potential role for SAFB1 in neurodegenerative disease.

1.5.4 SAFB1 in disease and neurodegeneration

The role of SAFB1 *in-vivo* was investigated by the creation of SAFB1 knockout in mice, which induced embryonic lethality with surviving animals exhibiting significant growth and developmental deficits (Ivanova et al. 2005). Interestingly, homozygous SAFB2 knockout mice are viable and do not exhibit the severe deficits induced in their SAFB1 knockout counterparts (Jiang et al. 2015). Deletion of the *C. elegans* homologue to SAFB1 affected eating behaviour and altered the lifespan of animals (Kumar et al. 2019) further indicating that the importance of SAFB1 *in-vivo* is evolutionarily conserved.

The association of SAFB proteins with nuclear hormone receptors underlies past investigations which established an association of SAFB1 with breast cancer progression and its role as a tumour suppressor gene (Hong et al. 2012). Although there are currently no known disease-causing mutations in SAFB1, mutations in the gene were previously discovered in primary breast tumour tissue (Oesterreich et al. 2001), and low SAFB1 expression levels have been associated with poor prognosis in breast cancer patients (Hammerich-Hille et al. 2010).

As detailed in section 1.4.2, RBPs have been implicated in several neurodegenerative diseases. Dysregulation of RBPs is exemplified by mutations in TDP-43 and FUS which directly cause ALS and FTLD. SAFB1 features several structural and functional similarities with both TDP-43 and FUS. Additionally, as mentioned above, SAFB1 was shown to directly interact with FUS (Yamaguchi and Takanashi 2016).

Although the SAFB-associated cellular stress response is not yet understood in neurons (San Gil et al. 2017), it is known that HSPs are implicated in mediating neurodegenerative disease pathology. For example, protein misfolding of expanded polyQ huntingtin is ameliorated by HSF1, and HSF1 expression levels have shown to be decreased in *in-vivo* models of HD and in striatum from HD patients (Gomez-Pastor et al. 2017). As SAFB1 is implicated in mediation of the cellular stress response, it is

possible that SAFB1 may play a role in neuronal stress associated with neurodegeneration, although to date no studies have been carried out to provide direct evidence of this speculation.

The discovery that SAFB1 directly interacts with *ATXN1* RNA (Rivers et al. 2015) provides evidence indicating a potential involvement of SAFB1 in SCA1, the condition caused by pathogenic *ATXN1* CAG expansion. Taken together with the increasing evidence that RBPs are involved in neurodegenerative processes in diseases including polyQ disorders, there emerges a precedent for dysregulated binding of xtrRNA transcripts to nucleic acid binding proteins in the aetiology of polyQ degeneration.

1.5.5 Hypotheses for Chapter 3 and Chapter 4

In summary, the RBP SAFB1 is highly expressed in the brain and has functions important for neuronal and synaptic maintenance. SAFB1 is also critical for neuronal development and mediates the cellular stress response. The dysregulation of similar RBPs including TDP-43 and FUS in neuronal pathology set a precedent for the potential involvement of other RBPs such as SAFB1 in neurodegeneration. SAFB1 also directly interacts with FUS, further implicating a role in mediation of neurodegenerative pathology. The highly enriched interaction of SAFB1 with *ATXN1* RNA at the site of disease-causing polyCAG expansion further supports the hypothesis that SAFB1 may be implicated in neurodegenerative disease.

Taken together, these findings represent a growing body of evidence indicating that SAFB1 is associated with neurodegenerative disease, and specifically that it may play a role in the neuropathology of polyQ disorders. The expression of SAFB1 in human neurodegenerative disease has not yet been studied, therefore Chapter 3 investigates the expression of SAFB1 in human post-mortem brain tissue from patients with neurodegenerative disorders including polyQ SCA and HD. Chapter 4 builds upon this to further explore methods to investigate the role of SAFB1 in polyQ expansion pathology, and to examine the interactions of SAFB1 protein with CAG expansion repeat RNA transcripts.

The second part of this thesis (Chapter 5) focuses on mitochondrial dysfunction as a key hallmark of neurodegenerative disease, which is exemplified in the pathogenesis of Parkinson's disease (PD) (Abou-Sleiman et al. 2006).

1.6.1 Neuropathology and treatment of PD

PD is the second most common form of neurodegenerative disease in the UK (Table 1.1). The average age of symptom onset is 55 years, but incidence increases markedly with age (Dauer and Przedborski 2003). PD is a debilitating disease characterised by disturbance to motor function. Clinical symptoms are caused by loss of dopaminergic neurons of the substantia nigra pars compacta (SNpc), resulting in massively reduced dopamine levels in the striatum. By the time symptoms become clinically apparent, up to 80% of dopaminergic neurons are already lost (Dauer and Przedborski 2003).

The substantia nigra is a subcortical nucleus of the basal ganglia comprised of the pars compacta (SNpc) and pars reticulata (SNpr) which are important for regulating reward processes and motor control. The SNpc contains dopaminergic neurons which form the main output pathways of the substantia nigra, projecting into the striatum via the nigrostriatal pathway. The dark neuromelanin pigment within dopaminergic neurons of the SNpc give the structure its characteristic dark appearance (Kandel et al. 2013).

The SNpc regulates movement by projecting excitatory input to the striatum via the D1 pathway, which in turn disinhibits the effect of the globus pallidus on the thalamic nucleus. Subsequent excitation of thalamocortical pathways stimulates cortical motor neurons to allow initiation of movement (Kandel et al. 2013). In PD, there is a loss of dopaminergic excitatory input to the striatum which results in decreased disinhibition of the globus pallidus and subsequently a reduced excitatory output from the thalamus to the motor cortex. This is the underlying cause of motor symptoms which include

tremor at rest, rigidity, slowness (bradykinesia) or reduction (hypokinesia) of voluntary movement, and postural instability (Postuma et al. 2015). Patients also suffer from impaired cognitive function which can develop into dementia, alongside mood disorders such as depression (Dickson et al. 2009).

Macroscopically, PD pathology presents as a loss of pigment in the substantia nigra caused by degeneration of neuromelanin-containing dopaminergic neurons. Histologically, surviving nigrostriatal neurons contain proteinaceous Lewy bodies within the cytoplasm. Smaller inclusions in neuronal processes (Lewy neurites) are also present, and both inclusions are ubiquitin-positive and composed primarily of alpha-synuclein (Dickson 2012).

Approximately 95% of PD cases are classified as sporadic with no clear genetic linkage (Dauer and Przedborski 2003). GWAS have identified single nucleotide polymorphisms (SNPs) associated with increased risk of developing PD including many in genes which affect mitochondrial and lysosomal function such as glucocerebrosidase (GBA) (Sidransky et al. 2009), which has exclusively enriched expression in neuronal cell types (Nalls et al. 2019). Rare monogenic inherited cases of PD are associated with mutations in specific genes (Bras et al. 2015), discussed in further detail below (section 1.9.1.1).

The selective vulnerability of dopaminergic neurons of the SNpc is not well understood. The formation of aminochrome during the oxidation of dopamine to neuromelanin could play a role in pathogenesis (Herrera et al. 2017). Axonal arborisation has also been implicated to render dopaminergic SNpc neurons vulnerable to neurodegenerative damage in PD (Pacelli et al. 2015).

There is currently no cure or readily available disease-modifying therapy for PD patients. The motor symptoms of PD are treated with dopamine replacement therapy, often delivered as levodopa or dopamine agonists (Emamzadeh and Surguchov 2018). Dopamine replacement drugs can

cause side effects for example levodopa is associated with dyskinesias (Charvin et al. 2018). Overall there is an unmet clinical need to further understand the molecular pathology of PD to inform development of disease-modifying therapies. In Chapter 5, dysregulated mitochondrial function in neurons is further investigated as a key hallmark of PD and as a potential target for disease modification.

1.7 Mitochondria

1.7.1 Structure and function of the mitochondrial network

Mitochondria are double membrane-bound organelles comprising of a central mitochondrial matrix, an inner mitochondrial membrane (IMM) which infolds to form cristae, and an outer mitochondrial membrane (OMM). Mitochondria contain maternally inherited mitochondrial DNA (mtDNA) in the form of nucleoids (circular double-stranded DNA complexed with protein) which encode 37 genes including 13 mitochondrial-specific proteins (Mishra and Chan 2014). The IMM and OMM are structurally and functionally distinct structures which surround the intermembrane space. The OMM is similar in composition to the cell membrane and contains various membrane-bound enzymes and many integral membrane proteins (porins) allowing the transport of molecules into and out of the organelle. The IMM contains specialist proteins comprising the electron transport chain (ETC) alongside specific transport proteins to regulate the selective movement of metabolites, and proteins which regulate mitochondrial fission and fusion (Labbe et al. 2014).

Mitochondria exist within a dynamic network of organelles which undergo continual remodelling. Motility and trafficking of mitochondria within the cytoplasm is facilitated by OMM proteins such as Miro (Mitochondrial Rho GTPase, encoded by the RHOT1 gene) which associate with microtubules via adaptor protein complexes (Mishra and Chan 2014). Mitochondria are closely associated with other organelles especially the endoplasmic reticulum (E.R.) and lysosomes. The physical and functional association of mitochondria with lysosomes is especially important for removal of

damaged mitochondria via mitophagy, and dysregulation of this process is closely associated with neurodegenerative conditions such as PD (Audano et al. 2018).

Mitochondria are required for cell survival. Key mitochondrial functions include oxidative phosphorylation, regulating levels of reactive oxygen species (ROS), mediation of apoptosis, and buffering of cytosolic calcium. The protein complexes of the ETC are responsible for the oxidation of nutrients to produce cellular energy in the form of ATP. Complexes I, III and IV pump protons across the inner mitochondrial membrane to establish an electrical potential between the cytoplasm and the mitochondrial matrix, described as the mitochondrial membrane potential, or mitochondrial polarisation. Protons flow back across this electrochemical gradient via ATP synthase (complex V), which uses the energy to generate ATP from ADP by phosphorylation. Loss of this proton gradient acts as a cellular signal for mitochondrial dysfunction.

In addition to normal physiological function and cell survival, mitochondria are important in regulating pathological processes and programmed cell death. Mitochondria regulate apoptosis via the intrinsic pathway by releasing molecules which activate the apoptotic initiator caspase-9, and are also critical for the function of proapoptotic proteins such as Bax and Bak (Wang and Youle 2009).

The mitochondrial permeability transition pore (mPTP) of the IMM is a non-selective channel of undefined structure (Baines and Guiterrez-Aguilar 2018). Channel opening induces massive release of calcium and other molecules below 1.5KDa (Narita et al. 1998), leading to mitochondrial matrix swelling, uncoupling of oxidative phosphorylation and eventual apoptotic or necrotic cell death. Pore opening has been associated with the pathogenesis of neurodegenerative diseases including AD, PD, HD and ALS (Kalani et al. 2018). For example, in PD pathological oligomeric alpha-synuclein protein was shown to induce mPTP opening and cell death in neurons derived from patient iPSCs (Ludtmann et al. 2018).

1.7.2 Mitochondrial dysfunction and quality control

Mitochondrial dysfunction is defined as abnormalities in the physiological processes of the mitochondrial network. This includes loss of mitochondrial membrane potential, uncoupling of oxidative respiration and altered ATP production, increased generation and dysregulated detoxification of ROS, dysregulated calcium homeostasis and altered mitochondrial trafficking and dynamics (biogenesis, fission, fusion and mitophagy) (Brand and Nicholls 2011).

The mitochondrial network exists in a state of balance to maintain overall cellular health and energy homeostasis (Figure 1.14A). In healthy cells, the balance is directed towards a network of properly functioning mitochondria which adapt appropriately to metabolic demands and regulate mitochondrial-associated cellular processes. Even under normal conditions, mitochondria are continually subjected to low levels of naturally occurring damage, for example as a result of exposure to ROS and as a part of normal ageing processes. This damage is offset by mitochondrial quality control systems which repair or remove damaged mitochondria (Sugiura et al 2014, Figure 1.15). In disease states including PD, an imbalance occurs as a result of increased exposure to mitochondrial damage and/or deficits in mitochondrial quality control mechanisms (Schapira 2012) (Figure 1.14B). This leads to pathological accumulation of dysfunctional organelles, resulting in loss of energy homeostasis and eventual cell death.

Figure 1.14 (next page) Mitochondrial homeostasis in health and disease. **A**) In normal cells, the mitochondrial network is balanced towards a healthy and functional phenotype. Damaged and dysfunctional mitochondria are kept at low levels and either removed or restored. In disease states including neurodegeneration, pathological factors disrupt mitochondrial balance in favour of a damaged and dysfunctional phenotype. This leads to disruption of cellular energy homeostasis associated with neurodegeneration. **B**) Factors which control the balance of mitochondrial health and damage. Healthy mitochondria maintain an active membrane potential ($\Delta\Psi m$) and carry out physiological functions critical for cellular survival such as oxidative respiration, calcium regulation and modulation of apoptosis. External stressors, mtDNA mutations and imbalances in quality control mechanisms can accumulate in non-dividing cells such as neurons, leading to build up of dysfunctional mitochondria. This results in dysregulation of cellular energy balance, increased ROS, release of pro-apoptotic factors and calcium imbalances associated with neurodegeneration. Physiological mitochondrial phenotype can be therapeutically restored through promotion of balanced mitochondrial quality

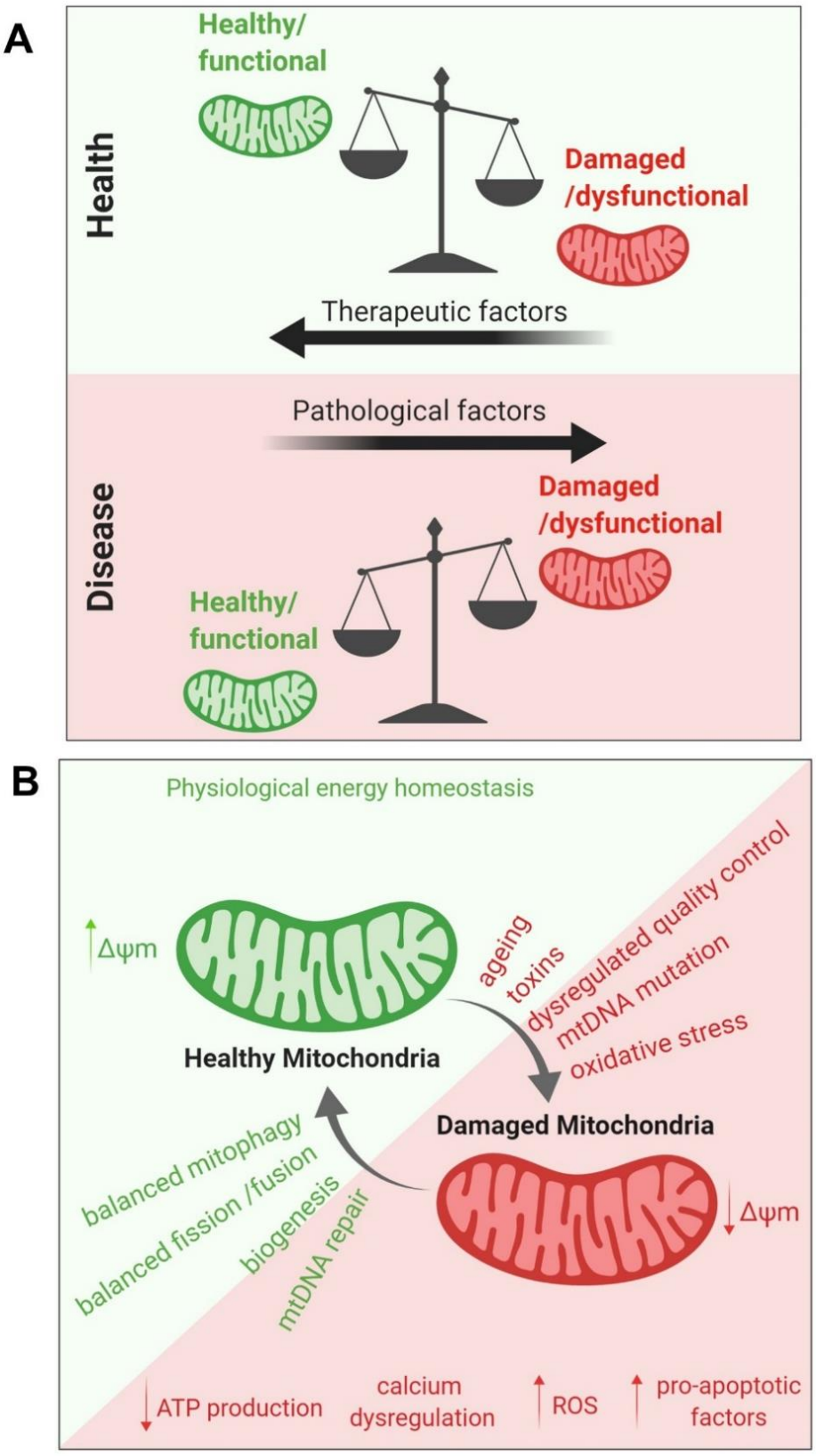

Figure 1.14 Figure legend on previous page

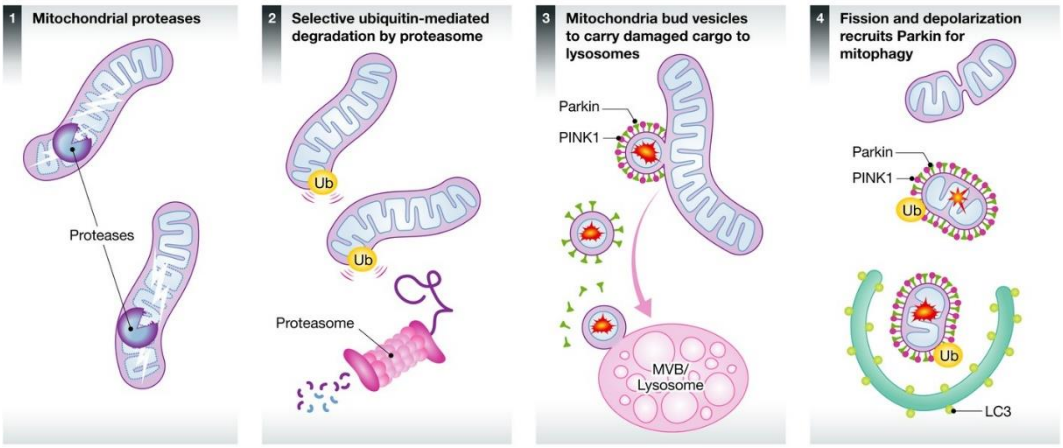

Figure 1.15 Diagram outlining the four main pathways of mitochondrial quality control. 1) Activation of mitochondrial proteases are a first-line defence against unfolded or oxidised proteins within the organelles. 2) Removal of damaged OMM proteins is mediated by ubiquitination and proteasomal degradation. 3) Components of more severely damaged mitochondria are removed by degradation in mitochondrial-derived vesicles (MDVs). 4) Irreparably damaged mitochondria undergo fission and are ubiquitinated before removal via LC3 expressing autophagosomes in PINK1/parkin dependent mitophagy. Figure reproduced from Sugiura et al. 2014, with permission from John Wiley and Sons under licence number 4845270703273.

1.7.3 Mitochondrial dynamics

The dynamic nature of mitochondria results in a highly complex, interconnected network of organelles which structurally and functionally interact not only with each other but with other organelles such as the E.R. and lysosomes (Bernard-Marissal et al. 2018). The mitochondrial network undergoes rapid and continual remodelling in response to cellular energy demands and cellular stress. Old or dysfunctional mitochondria are removed, and new organelles created by biogenesis. Mitochondria are also continually remodelled through fission (division of a single organelle into two or more separate mitochondria) and fusion (the combination of two or more organelles into a single mitochondrion) (Seo et al. 2010, Figure 1.16).

Mitochondrial biogenesis in neurons usually occurs in the cell soma due to the requirements of co-ordinating complex interactions between nuclear and mtDNA gene products (Uittenbogaard and Chiaramello 2014). Newly synthesised mitochondria are then trafficked within the neuron to maintain energetic homeostasis. The processes of biogenesis and removal of damaged mitochondria through mitophagy are coupled through AMPK

signalling (Palikaras et al. 2015), although the specific relation between the two processes in neurons is currently not understood. Disturbances in mitochondrial biogenesis may directly contribute towards development of mitochondrial dysfunction in neurons (Rugarli and Langer 2012), and recent research indicates that PD-associated mitochondrial damage reduces biogenesis (Lee et al. 2019a) whilst upregulation of biogenesis may counteract neuronal damage, indicating a potential mechanism for disease-modification (Chuang et al. 2019, Weng et al. 2019).

Mitochondrial fission and fusion are active processes which require several specialised proteins. Fission is mediated by a complex molecular machinery which includes Fis1, an OMM receptor for the cytosolic GTPase dynamin-related protein 1 (Drp1). Fusion is also dependent on dynamin-related GTPases, in particular the mitofusins (Mfns) 1 and 2 of the OMM and optic atrophy 1 (OPA1), a GTPase associated with the IMM and intramembrane space (Scott and Youle 2010).

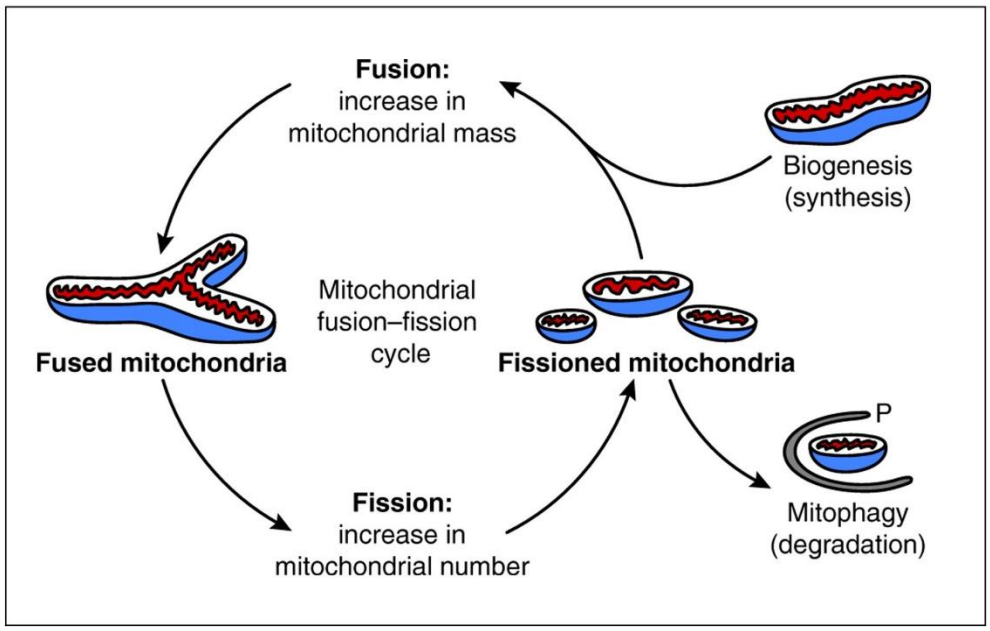

Figure 1.16 Under normal conditions, quality control of the mitochondrial network is maintained by continual re-modelling by fission, fusion, biogenesis and mitophagy. Figure reproduced from Seo et al. 2010, with permission from Company of Biologists under licence number 1040717-1.

The balance between the two processes regulates the morphology of the mitochondrial network, whereby increased fission promotes a high number of smaller, more rounded individual organelles and increased fusion results

in highly interconnected networks of extended mitochondrial tubules (Scott and Youle 2010). In neurons, the mitochondrial network is elongated in dendrites and within the cell body but becomes more fragmented in axons (Popov et al. 2005). Neurons also require extensive mitochondrial trafficking machinery and mitochondrial quality control mechanisms to regulate axonal energy demands (MacAskill et al. 2010).

Cycles of mitochondrial fission and fusion impart quality control. The importance of these processes in neuron survival are highlighted by inherited neurodegenerative disease; mutations in OPA1 (required for mitochondrial fission) cause dominant optic atrophy (Alexander et al. 2000), whilst GDAP1 mutations (encoding a protein important for mitochondrial fission) cause Charcot-Marie-Tooth disease 4A (Baxter et al. 2002). Fusion events are associated with baseline or low-stress conditions, whereas increased fission is an indication of stress within the mitochondrial network (Fischer et al. 2012). Moving the balance of mitochondrial dynamics towards increased fusion can be considered a rescue event against mitochondrial damage (Seo et al. 2010). Fusion promotes the mixing of mitochondrial protein and mtDNA within the cell, enabling mtDNA repair and redistribution of metabolites to maintain healthy mitochondria (Chen et al. 2007). Meanwhile, protective mechanisms prevent dysfunctional mitochondria from fusing with healthy ones. For example, loss of IMM potential causes proteolytic inactivation of OPA1 which halts membrane fusion (Head et al. 2009). Fragmentation of mitochondria by fission may be a pre-requisite for the autophagic removal of mitochondria through mitophagy (Twig et al. 2008), whilst stress-induced hyperfusion protects mitochondria against degradation and increases mitochondrial ATP production to promote cell survival (Gomes et al. 2011). Mitochondrial damage can induce imbalances in fission and fusion events. ROS induced stress results in fragmentation of the mitochondrial network and cell dysfunction (Wu et al. 2011). Furthermore, the mitochondrial toxins rotenone, MPP+ and MPTP (used to pharmacologically model Parkinson's disease) all promote increased mitochondrial fission (Barsoum et al. 2006, Thomas et al. 2011, Lee et al. 2019a).

1.8 Mitophagy

Repair of mitochondria can be achieved via regulation of mitochondrial dynamics or by selective degradation of damaged molecules in intact organelles (Roberts et al. 2016). Irreparably damaged mitochondria are removed by mitophagy to maintain cellular energy homeostasis and ameliorate mitochondrial dysfunction (Youle and Narendra 2011). Mitophagy is a mitochondrial-selective form of macroautophagy, characterised by the sequestration of damaged mitochondria into double-membrane bound autophagosomes (Rodriguez-Enriquez et al. 2006). Autophagosomes are identifiable by their expression of LC3-II which is recruited to their membranes from the cytosol (Kabeya et al. 2000). Autophagosomes deliver damaged mitochondria to lysosomes, acidic membrane-bound vesicles characterised by expression of lysosomal membrane associated proteins (LAMP) 1 and 2 (Schwake et al. 2013). Lysosomal-autophagosomal fusion results in the degradation of mitochondria by lysosomal hydrolases.

It is important to differentiate between basal mitophagy which is responsible for the continual turnover of organelles, and induced mitophagy which is activated as a protective stress-response mechanism under conditions of starvation, oxidative stress or mitochondrial damage (Martinez-Vicente 2017). Three types of mitophagy have been previously characterised (Lemasters 2014). Type 1 occurs in response to nutrient deprivation and is dependent on PI3K signalling. Type 2 occurs following stress-induced mitochondrial damage and sustained depolarisation. Type 3 (micromitophagy) involves formation of mitochondria-derived vesicles (MDVs) which transit into multivesicular bodies prior to lysosomal fusion. MDV formation occurs under baseline conditions and as an early response to oxidative stress, selectively removing damage macromolecules from otherwise intact mitochondria (Roberts et al. 2016).

1.8.1 PINK1/parkin mediated mitophagy

Damage-induced (Type 2) mitophagy can be mediated by various OMM receptors facilitating direct interaction with LC3, or by indirect association with autophagosomes via IMM proteins such as cardiolipin (Martinez-Vicente 2017). However, the best characterised signalling pathway in mammalian cells involves the ubiquitin ligase parkin, and the serine-threonine kinase protein phosphatase and tensin homologue (PTEN)-induced kinase 1 (PINK1) (Figure 1.17). Mutations in parkin (*PARK2*) and PINK1 (*PARK6*) cause autosomal recessive PD (Bras et al. 2015, Table 1.10), highlighting the importance of this signalling pathway in maintaining dopaminergic neuronal health and function.

Parkin-mediated mitophagy was first described by Narendra et al. (2008), and since this discovery extensive research has elucidated detailed insights into PINK1/parkin mediated signalling (as reviewed by Eiyama and Okamoto 2015). Figure 1.18 and Figure 1.19 summarise the stages of PINK1/parkin mediated mitophagy signalling. Parkin is a RBR (RING-between-RING) type E3 ubiquitin ligase with several known splice variants. Parkin mediates the transfer of active ubiquitin from ubiquitin-conjugating UbE2 enzymes to target proteins on the OMM. Under baseline conditions, parkin exists in an auto-inhibited cytoplasmic form, with its N-terminal UBL (ubiquitin-like) domain blocking the E2 binding site. Activation of parkin results in its translocation to the OMM. This is triggered by phosphorylation

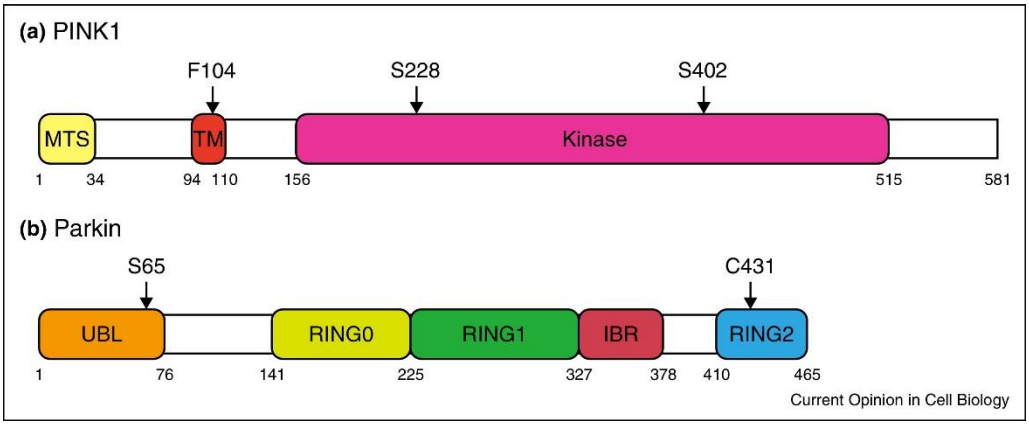

Figure 1.17 Functional domains of PINK1 and parkin. MTS mitochondrial targeting sequence, TM transmembrane domain, IBR in between RING. Figure reproduced from Eiyama and Okamoto 2015, with permission from Elsevier under licence number 4845280254276.

at ser65 which induces a conformational change, releasing the RING2 domain and permitting binding of E2 ligases to the RING domain (Gladkova et al. 2018). This facilitates discharge of ubiquitin onto a catalytic cysteine in the RING2 domain, yielding a thioester intermediate which is then conjugated as ubiquitin onto the substrate protein. Recent work showed that parkin ubiquitinates mitochondrially-tagged artificial proteins, indicating it has low substrate specificity which is not determined by a consensus sequence (Koyano et al. 2019).

PINK1 is responsible for the phosphorylation and activation of parkin, through both direct phosphorylation of parkin's UBL domain at ser65, and by phosphorylation of cytosolic ubiquitin which subsequently activates parkin (Kane et al. 2014). PINK1 is ubiquitously expressed, and constitutively imported from the cytoplasm into the mitochondrial intermembrane space via translocase of the outer membrane (TOM) and into the mitochondrial matrix by translocase of the inner membrane (TIM). Under baseline conditions it is cleaved by presenilins-associated rhomboid-like protein (PARL), an IMM protease, which inactivates and degrades PINK1 (Spinazzi and De Strooper 2016, Pickrell and Youle 2015). This results in rapid turnover of PINK1 at healthy mitochondria.

PINK1 acts as a mitochondrial damage detector. Import of PINK1 via TIM is disrupted when mitochondrial membrane potential is lost (i.e. the IMM becomes depolarised), resulting in accumulation of uncleaved PINK1 at the OMM (Jin et al. 2010). Uncleaved PINK1 is free to activate parkin via phosphorylation. Once PINK1-activated parkin is localised to the OMM, a feed-forward loop of ubiquitination occurs with activated parkin linking numerous cytosolic and OMM proteins with K48- and K63-linked ubiquitin chains (Newton et al. 2008). Polyubiquitinated proteins coating the mitochondria are recognised by adaptor proteins (such as p62/SQSTM1) which facilitate connection of the damaged mitochondria to an autophagosome via an LC3-interacting region (Pankiv et al. 2007).

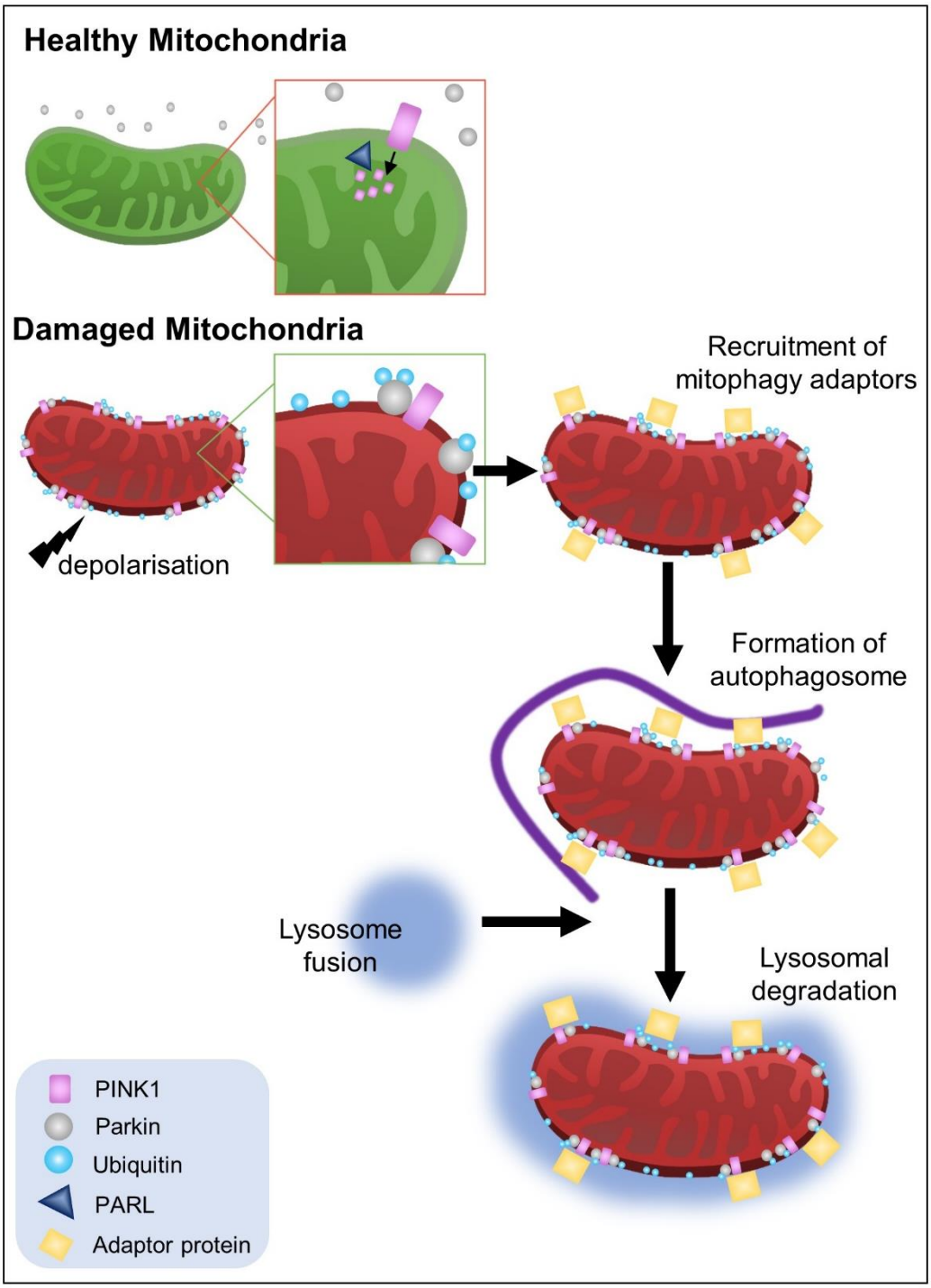

Figure 1.18 PINK1/Parkin signalling mediates mitochondrial quality control by mitophagy. Schematic diagram illustrating PINK1-dependent parkin recruitment to the outer mitochondrial membrane of damaged/depolarised mitochondria, resulting in autophagosome recruitment and eventual degradation of damaged mitochondria by lysosomal fusion.

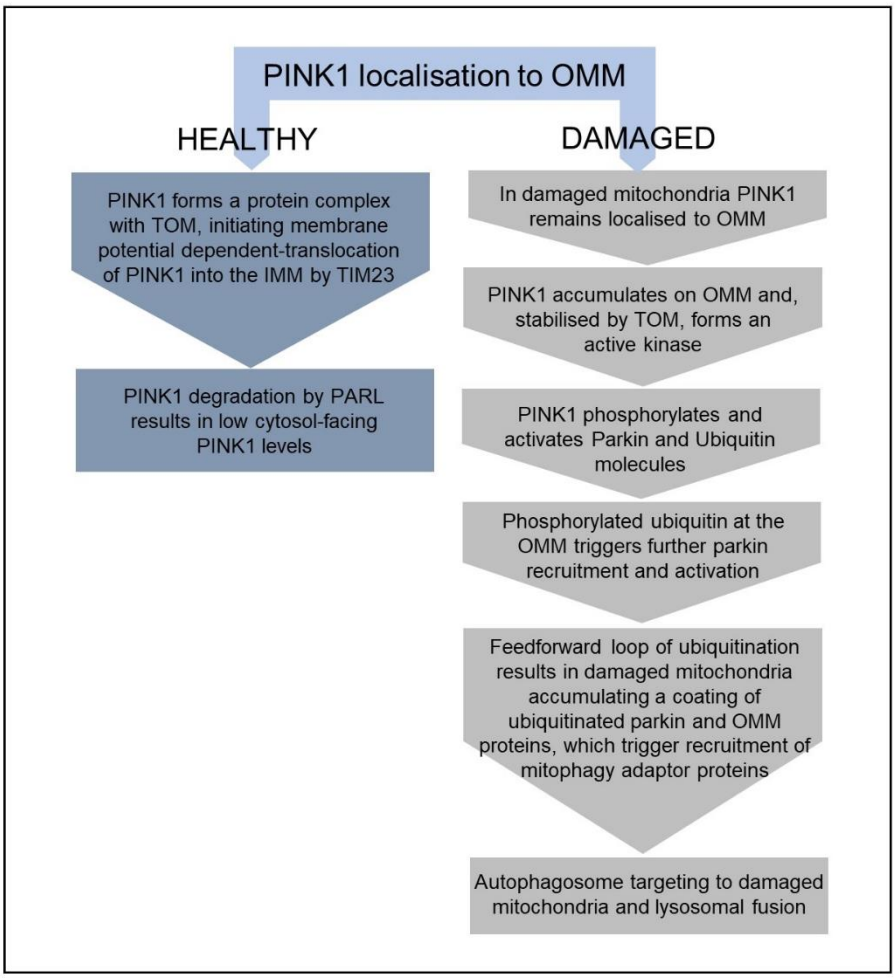

Figure 1.19 Flow diagram summarising the key stages of PINK1/Parkin mediated mitophagy.

1.8.2 Induction and measurement of mitophagy

Basal mitophagy is not readily apparent in cell lines under standard culture conditions and it is therefore necessary to experimentally induce mitophagy. This is often achieved pharmacologically using ionophores such as carbonyl cyanide m-chlorophenyl hydrazine (CCCP) or valinomycin. These drugs disrupt the ion gradient across the IMM, resulting in depolarisation of mitochondria and uncoupling of oxidative phosphorylation. Inhibitors of cellular respiration are also used to experimentally induce mitochondrial damage and subsequent mitophagy. Examples include antimycin A which binds to and inhibits cytochrome C reductase in the ETC, inhibiting ATP production. Rotenone inhibits the transfer of electrons from ETC complex I, inducing reduction of cellular oxygen to damaging ROS. 1-methyl-4-phenyl-

1,2,3,6-tetrahydropyridine (MPTP) and its metabolite 1-methyl-4-phenylpyridinium (MPP+) also inhibit complex I, likewise generating damaging free radicals and inducing mitochondrial damage by oxidative stress. Both rotenone and MPTP are used to induce Parkinsonian symptoms in animal models of PD.

These pharmacological insults represent acute severe mitochondrial stress by inducing global damage to mitochondria. To more closely mimic mitochondrial damage as it might occur in disease, use of optogenetic tools to inactivate subsets of mitochondria has been reported. KillerRed is a fluorescent protein which produces high levels of ROS upon illumination. Expression of mitochondrial KillerRed in subsets of *C. elegans* neurons followed by *in-vivo* illumination results in specific disruption to neuronal function (Williams et al. 2013). It is also possible to induce a more mild pharmacologically-induced damage to subsets of organelles within the same cell by plating neurons across microfluidic chambers and restricting perfusion of drugs such as antimycin A to either cell soma or axonal compartments (Ashrafi et al. 2014).

Experimental cell lines such as HeLa express almost no endogenous parkin (Denison et al. 2003). Parkin recruitment to mitochondria can readily be visualised and measured by expressing fluorescently-tagged parkin in cultured cells. As a straightforward system which is easily quantifiable, this technique is especially suitable for use in screening assays (Villace et al. 2016, Scott et al. 2020). Although it represents a critical stage of mitophagy signalling, parkin recruitment alone does not offer direct measurement of mitophagy. Direct detection relies on measurement of mitochondrial targeting to autophagocytic vesicles or lysosomes. This is made possible by expression of specific fluorescently-tagged proteins; lysosomes can be visualised by expressing GFP-tagged LC3, whilst autophagosomes are identifiable by fluorescently tagging LAMP1. For example, quantification of GFP-LC3 vesicles and LAMP1/GFP-LC3 (late endosome/lysosome) overlap was utlilsed by Chandrachud et al. (2015) in a high-content compound screening assay.

Direct measurement of mitophagy *in-vivo* is possible through the expression of fluorescent reporter proteins with readouts dependent on the delivery of mitochondria to acidic lysosomal compartments (McWilliams et al. 2016, Rodger et al. 2018). The mito-QC mouse expresses a tandem mCherry-GFP tag at the OMM, and mitochondrial targeting to lysosomes quenches the GFP signal (McWilliams and Ganley 2016). Keima is a fluorescent protein which has an excitation spectrum dependent on pH. Mitochondrial targeting of mt-Keima therefore allows detection of mitochondrial engulfment in lysosomes (Sun et al. 2015). These tools have been utilised to further understand the role of mitophagy signalling and mitochondrial dysfunction in complex neuronal systems.

1.8.3 The role of mitophagy in neurons and in-vivo

Neurons are highly dependent on balanced mitochondrial function and quality control systems. Maintenance of normal neuronal function is incredibly energetically "expensive", with the brain requiring at least 20% of the body's energy budget, most of which is utilised in synaptic transmission (Rolfe and Brown 1997, Harris et al. 2012). Furthermore, neurons contain extensive mitochondrial networks and generate energy almost entirely through oxidative phosphorylation (Rangaraju et al. 2014, Yamano et al. 2016). Neurons have the most complex architecture of all cells in the body and form a highly polarised structure. Their extensively arborised axonal and dendritic projections require widespread transportation and maintenance of the mitochondrial network (Mandal and Drerup 2019). Furthermore, neurons are differentiated, post-mitotic cells which do not divide and therefore must remain functional throughout the entire lifespan of the organism. This necessitates precise control over mitochondrial quality through biogenesis, fission/fusion cycles and mitophagy (Corti 2019).

The majority of studies which established our understanding of mammalian mitophagy use *in-vitro* immortalised cell lines, raising questions about the relevance of these findings in post-mitotic neurons or *in-vivo*. Much work has been carried out in recent years to answer these questions. It was shown that endogenous parkin is activated in mature murine primary

neurons in response to mitochondrial depolarisation (McWilliams et al. 2018). Cai et al. (2012) report direct evidence of mitophagy in primary mouse neurons challenged with CCCP by demonstrating that parkin-positive mitochondria are engulfed by lysosomal vesicles. When endogenous parkin expression was knocked down using RNAi in the same study, depolarised mitochondria accumulated within cells, indicating a role for mitophagy in clearing damaged mitochondria in neurons. Conversely, similar studies have reported absence of parkin recruitment to mitochondria and mitochondrial recruitment to autophagocytic vesicles (Van Laar et al. 2011). Other recent evidence indicates that damaged mitochondria in neurons may be removed by parkin-independent retrograde transport as opposed to by mitophagy (Lin et al. 2017). Cultured dopaminergic neurons derived from human iPSCs and treated with mitochondrial toxins have been shown to recruit endogenously expressed parkin to mitochondria in a PINK1-dependent manner (Wang et al. 2011, Cai et al. 2012, Seibler et al. 2011). Parkin also translocates to mitochondria in human iPSC-derived dopaminergic neurons challenged with CCCP or rotenone (Oh et al. 2017).

It should be noted that these *in-vitro* studies utilise mitochondrial toxins such as CCCP, valinomycin or rotenone to induce global mitochondrial depolarisation and subsequent mitophagy, a severe stress scenario which is unlikely to occur *in-vivo*. Baseline mitophagy was observed in cultured hippocampal neurons via lysosomal mt-Keima accumulation, which was reduced when parkin or PINK1 expression was knocked down (Bingol et al. 2014). Induction of a milder stress could more accurately represent the chronic mitochondrial dysfunction which occurs in neurodegenerative disease. To more closely mimic the removal of deploarised fragments of mitochondria, mt-KillerRed was used to induce selective ROS-mediated damage to mitochondria within rat hippocampal neurons which resulted in parkin recruitment and autophagosome formation (Ashrafi et al. 2014).

In addition to the experimental study of neuronal mitophagy *in-vitro*, research efforts have focussed on further defining the role of mitophagy *in-vivo*. Evidence of PINK1/parkin-dependent mitophagy was first discovered

in *Drosophila* by measurement of protein turnover (Vincow et al. 2013). PINK1-dependent mitophagy was later directly demonstrated by Cornelissen et al. (2018) using flies expressing mtKeima. This finding is supported by that of Kim et al. (2019) who also detected mitophagy *in-vivo* using the mtKeima model, and abolished mitophagy induction in response to hypoxic stress with knockdown of PINK1 or parkin using RNAi.

Mice with either PINK1 or parkin knockout do not have dopaminergic neuron degeneration but do exhibit neurochemical abnormalities and evidence of mitochondrial dysfunction (Goldberg et al. 2003, Perez and Palmiter 2005, Gispert et al. 2009). Basal levels of mitophagy in the dopaminergic midbrain neurons of mito-QC mice has been demonstrated, but this was not altered with PINK1 knockout or parkin mutation (McWilliams et al. 2018, McWilliams et al. 2018a). In rats, knockout of PINK1 or DJ-1 induced 50% nigral dopaminergic neuron loss by 8 months of age, whereas rats with parkin knockout did not have any neuropathological changes (Dave et al. 2014).

Models combining knockout of PINK1 or parkin with mitochondrial stress have also shown variable results, indicating a complex dynamic between mitophagy signalling and mitochondrial dysfunction. Parkin knockout mice which also accumulate dysfunctional mitochondria through accelerated generation of mtDNA mutations exhibit dopaminergic neuron death (Pickrell et al. 2015). In contrast, combining parkin deletion with knockout of a mitochondrial biogenesis transcription factor did not induce dopaminergic neuron loss, and parkin was found to be dispensable for the clearance of damaged mitochondria in these mice (Sterky et al. 2011). Further recent evidence for mammalian mitophagy *in-vivo* comes from the findings of Sliter et al. (2018). This research demonstrates that mitochondrial stress *in-vivo* induced by ether exhaustive exercise or mtDNA mutation triggers mitophagy which was directly measured in heart tissue and which was dependent on PINK1. This provides direct evidence for PINK1-dependent clearance of damaged mitochondria *in-vivo*, although this was demonstrated in cardiac cells not neurons.

In terms of clinical translation, PINK1/parkin dependent mitophagy has been of great interest to researchers in part due to the causative association between mutations in these genes and familial PD (discussed further in section 1.9.1.1). Ubiquitin phosphorylated at ser65 partially overlaps with mitochondrial and lysosomal markers and was upregulated in post-mortem brains of patients with neurodegenerative diseases (Fiesel et al. 2015), providing indirect evidence for PINK1/parkin mediated mitophagy in the human brain. This staining pattern in human brain was also observed by Shiba-Fukushima et al. (2017) in midbrain dopaminergic cells.

Overall, *in-vitro* studies in immortalised cell lines which have been the mainstay in mitophagy research have been followed-up by several studies which collectively provide evidence that PINK1/parkin mediated mitophagy occurs in neurons *in-vitro*. However, this has not always been consistently replicated across studies. There is also a scarcity of evidence to convincingly directly demonstrate PINK1/parkin mediated mitophagy in mammalian neurons *in-vivo*. *Drosophila* and mouse studies indicate that PINK1/parkin-mediated mitophagy occurs at both basal levels and in response to stress in neurons *in-vivo*, but the exact role of this mitochondrial quality control mechanism and how it is regulated is still uncertain.

The wider context should be considered, as mitophagy represents just one aspect of overall organelle-level mitochondrial quality control. Non-mitophagic pathways alongside mitochondrial fission, fusion and biogenesis are likely to act in synergy with mitophagy to maintain overall mitochondrial health (Gustafsson and Dorn 2019). It is therefore important to recognise the contribution of various aspects of mitochondrial quality control and dysfunction in PD pathogenesis, and as potential targets for therapeutic intervention.

1.9.1 Evidence for mitochondrial dysfunction and dysregulated quality control as a key pathological hallmark of PD

Impaired biogenesis, altered mitochondrial dynamics and trafficking, defective mitophagy, ETC dysfunction, oxidative stress and calcium imbalance have all been implicated as contributing to mitochondrial dysfunction in PD (Park et al. 2018). This relationship has been confirmed by extensive genetic, molecular and clinical evidence.

The earliest example of such evidence was the discovery that the mitochondrial toxin MPTP replicated the motor and non-motor symptoms of PD in seven drug users who had inadvertently administered the toxin (Ballard et al. 1985). This finding lead to the development of MPTP-induced neurotoxicity in animals as a model of PD. Later, post-mortem studies demonstrated reduced complex I activity in the substantia nigra of idiopathic PD patients (Schapira et al. 1989). Mitochondrial dysfunction was further demonstrated clinically by magnetic resonance spectroscopy revealing reduced ATP levels in the putamen and midbrain of both early and advanced stage PD patients (Hattingen et al. 2009). Genetics and molecular biology also contribute to the knowledge that mitochondrial dysfunction is a critical driver of PD pathogenesis.

1.9.1.1 Evidence from clinical genetics

Loss of normal function in genes important for mitochondrial function directly causes familial PD (Bras et al. 2015) (Table 1.10). The first gene to be associated with genetically inherited PD was PARK1 (*SNCA*) which encodes alpha-synuclein, a cytoplasmic protein involved in vesicular trafficking which is the main component of Lewy bodies. Increasing evidence now links alpha-synuclein pathology to mitochondrial dysfunction, for instance accumulation of alpha-synuclein is associated with increased ROS production in post-mortem PD brain (Devi et al. 2008). Furthermore, aggregated alpha-synuclein was shown to inhibit mitochondrial complex I (Reeve et al. 2015).

Mutations in parkin were first linked to inherited PD in 1998 by Kitada et al. Shortly after, PINK1 mutations were discovered to cause hereditary early-onset PD (Valente et al. 2004), providing evidence linking mitophagy dysfunction to disease pathogenesis in PD patients. Ongoing research is continually identifying various mutations in parkin, for example a recent study describes a ser65 deletion mutation discovered in two patients, which also induces parkinsonian phenotype in mice (McWilliams et al. 2018).

The most common form of monogenetic PD is caused by mutations in LRRK2, and SNPs in this gene are a risk factor for development of sporadic PD (Bras et al. 2015). Extensive evidence links LRRK2 with mitochondrial function (reviewed by Singh et al. 2019). Mitochondrial impairment is a neuropathological feature of patients carrying the G2019S mutation in LRRK2 (Mortiboys et al. 2010). Mechanistic studies demonstrate that the same mutation promotes mitochondrial uncoupling (Papkovskaia et al. 2012), excess mitochondrial fission (Ho et al. 2019), increased ROS release and impaired respiratory capacity (Walter et al. 2019).

Other genes with PD-causing mutations include DJ-1, which binds mitochondrial complex I subunits (Hayashi et al. 2009) and is a negative modulator of mitophagy signalling (Joselin et al. 2012). DJ-1 deficiency also reduced mitochondrial membrane potential, decreased ATP levels and induced aberrant complex I assembly in neurons (Heo et al. 2012) as well as inducing defective mitochondrial morphology in patient cells (Irrcher et al. 2010). Mutations in ATP13A2 cause juvenile-onset PD characterised by lysosomal and mitochondrial dysfunction (Park et al. 2015). Meanwhile, recent work has revealed that PD-causing mutations in the phospholipase PLA2G6 induces dopaminergic neurodegeneration via mitochondrial dysfunction (Chiu et al. 2019).

In addition to genes which cause monogenic mendelian inheritance of PD, evidence for the critical role of mitochondrial function in PD pathogenesis emerges from the study of SNPs associated with increased disease risk. Mutations in the lysosomal hydrolase GBA are the biggest genetic risk factor

for development of PD (Sidransky et al. 2009, Gegg and Schapira 2016). Reduced GBA activity leads to deficits in autophagic-lysosomal functions, and GBA mutation was shown to induce early mitochondrial dysfunction in 3D neurospheres, impairing clearance of damaged mitochondria (Moren et al. 2019). This indicates a further link between development of PD and mitochondrial quality control. A recent GWAS meta-analysis by Billingsley et al. (2019) identified that genes associated with mitochondrial function underly the heritability of sporadic PD, demonstrating robust evidence for the involvement of mitochondrial processes in PD pathogenesis.

Finally, somatic mutations in mtDNA and mtDNA copy-number loss are known to contribute to mitochondrial dysfunction (Dolle et al. 2016). mtDNA does not contain histones and is around ten times more susceptible to mutations than nuclear DNA, with over 200 different mtDNA mutations reported in human patients (Schapira 2012). No mtDNA mutations have been discovered to directly cause PD, but deletions were shown to occur at higher levels in dopaminergic neurons of the substantia nigra in human tissue in comparison to other brain areas (Bender et al. 2006).

1.9.1.2 Evidence from dopaminergic neuron vulnerability

It is currently not understood why specific subsets of neurons in the brain degenerate in different neurodegenerative disease. As previously discussed, dopaminergic neurons of the SNpc have several traits which may render them vulnerable to pathologic changes in PD. Specifically, it is hypothesised that their extensive arborisation and metabolic profile may leave SNpc neurons especially vulnerable to imbalances in energy homeostasis caused by stress-induced mitochondrial dysfunction (Pacelli et al. 2015, Surmeier et al. 2017).

	Gene (locus)	Protein	Mitochondrial function	Inheritance pattern
Mendelian	*SNCA* (*PARK1*)	Alpha-synuclein	Aggregated protein inhibits complex I and promotes ROS formation and mitochondrial dysfunction	A.D.
	PRKN (*PARK2*)	Parkin	Mitophagy signaling	A.R.
	PINK1 (PARK6)	PTEN-induced kinase 1	Mitophagy signaling	A.R.
	LRRK2 (*PARK8*)	Leucine-rich repeat kinase 2	Localises to mitochondria, regulation of mitochondrial function. Mutations promote mitochondrial fission.	A.D.
	DJ-1 (*PARK7*)	Parkinsonism associated deglycase	Binds to and maintains activity of mitochondrial complex I. Also implicated in mitophagy signaling.	A.R.
	ATP13A2 (*PARK 9*)	ATPase type 13A2	Lysosomal transmembrane protein, supports mitochondrial function	A.R.
	PLA2G6 (*PARK14*)	Phospholipase A2 group 6	Supports mitochondrial function, mutations induce mitochondrial dysfunction	A.R.
	VPS35 (*PARK17*)	Vacuolar protein sorting-associated protein 35	Endosomal/lysosomal trafficking, supports mitochondrial function	A.D.
Risk	*GBA*	glucocerebrosidase	Autophagy and lysosomal degradation	NA
Somatic	mtDNA mutations	Multiple proteins	Multiple functions	NA

Table 1.10 Selected genes associated with PD pathogenesis and their mitochondrial functions. A.D. autosomal dominant, A.R. autosomal recessive, NA not applicable.

The differential role of mitochondria throughout the brain was recently investigated by Fecher et al. (2019), who profiled mitochondria from specific cerebellar cell types, revealing distinctive mitochondrial composition within individual neuronal populations. This premise that mitochondrial-specific

phenotypes exist throughout the brain complements a previous study which demonstrated that reduced rates of mitophagy and increased numbers of defective mitochondria were present in mouse substantia nigra when compared to cortex (Diedrich et al. 2011). This further implicates dopaminergic mitochondrial phenotype as a risk factor for neurodegeneration.

Interestingly, the most extensively arborised nigral dopaminergic cells *in*-vitro were shown to contain elevated rates of mitochondrial oxidative phosphorylation and associated levels of pathological oxidative stress (Wong et al. 2019). Furthermore, parkin deletion in mouse dopaminergic SNpc cultures was shown to preferentially pathologically affect highly arborised DA neurons (Giguere et al. 2018).

1.9.1.3 Evidence from patient cells and tissue

In addition to the mitochondrial dysfunction associated with monogenically inherited PD, there is also evidence to demonstrate its importance in non-familial (also called sporadic or idiopathic) PD, which accounts for the vast majority of cases. The genetic evidence presented by Billingsley et al. (2019) (section 1.9.1.1) clearly demonstrates the association between mitochondrial dysfunction and the aetiology of sporadic PD. Evidence from molecular biology using cells and tissues derived from PD patients further evidences the role of mitochondria in PD pathogenesis.

Reduced mitochondrial biogenesis leading to decreased mitochondrial mass and altered respiratory function was observed in stem cells of patents with non-genetic Parkinsonism (Angelova et al. 2018). Furthermore, cells derived from the platelets of sporadic PD patients featured fragmented mitochondrial networks alongside increased Drp1 and decreased OPA1 expression, evidencing a role for disease-associated imbalance of fission and fusion (Santos et al. 2015). There is also evidence to suggest altered mitochondrial respiratory function in non-familial PD. The activity of mitochondrial ETC complex I is downregulated and subjected to significantly increased oxidative damage in the cortex of PD patients (Keeney et al.

2006). In a further study, neurons from patients with idiopathic PD had significantly reduced expression of mitochondrial ETC complexes I and II (Grunewald et al. 2016). Alongside the overall decrease in mitochondrial proteins in PD, a more recent study discovered that individual surviving dopaminergic axons and synapses in PD patient brain in fact expressed increased levels of complex I and IV and higher numbers of mitochondria compared to control brains. This indicates a pathological compensatory mechanism potentially associated with oxidative damage (Reeve et al. 2018).

Alongside evidence of altered mitochondrial dynamics and ETC function in PD patients, dysregulated mitophagy signalling has been demonstrated in PD brain tissue (Hou et al. 2018, Shaltouki et al. 2018). Dopaminergic neurons differentiated from iPSCs of PD patients with parkin mutations have impaired mitophagy (Suzuki et al. 2017). In a separate study also using iPSC-derived dopaminergic neurons from familial PD patients, parkin mutations were found to induce mitochondrial dysfunction and imbalance in mitochondria-associated apoptosis (Konovalova et al. 2015). Using iPSC-derived dopaminergic neurons, Hsieh et al. (2016) identified both disrupted mitophagy and impaired mitochondrial motility in both familial LRRK2 associated and sporadic PD patient cells.

Taking together the evidence from clinical genetics, animal models, patient tissue and patient-derived neurons, the importance of dysregulated mitochondrial dynamics and impaired quality control systems leading to mitochondrial dysfunction is clear. Modulation of the signalling pathways which control these processes could therefore be neuroprotective and represent a potential therapeutic approach in PD to ameliorate neuronal cellular stress caused by mitochondrial dysfunction (Schapira et al. 2014, Lee 2016, Gao et al. 2017).

1.9.2 Modulation of mitochondrial health and function as a therapeutic approach to neurodegenerative disease

Considerable efforts in recent years have been made investigating mitochondrial rescue agents as potentially disease-modifying treatments

Drug	Mechanism	Clinical trial results
Coenzyme Q10 (Ubiquinone)	Antioxidant electron carrier for ETC complex I and II	Phase III demonstrated safety and tolerability but no clinical benefit
Creatine	Improves mitochondrial bioenergetics	Phase III trial terminated due to lack of efficacy over placebo
MitoQuinone (MitoQ)	Antioxidant, enhances mitochondrial bioenergetics	Phase III trial had no benefit over placebo (small sample size)
N-acetylcysteine	Antioxidant	Well tolerated in Phase I trials
Pioglitazone	Anti-inflammatory, enhances mitochondrial bioenergetics,	No clinical efficacy in Phase II trial
Exenatide	GLP-1 receptor agonist, anti-inflammatory, enhances mitochondrial biogenesis *in-vitro*	Clinical efficacy in PD patient motor symptoms in a randomised double-blind trial
AZD3241	Myeloperoxidase inhibitor, neuroprotective in MPTP rodent models	Tolerated in PD and MSA patients in Phase IIa trials

Table 1.11 Summary of clinical trial outcomes for pharmacological disease-modifying therapies targeting mitochondrial dysfunction in neurodegenerative disease. MSA multiple systems atrophy

(Mortiboys et al. 2018). Indeed, selective modulation of mitophagy is currently regarded as one of the most promising approaches to developing neuroprotective therapies for disorders such as PD (Scrivo et al. 2018).

Several potentially disease-modifying drugs for PD and other neurodegenerative conditions which target the mitochondrial system have been taken to clinical trials in recent years (Table 1.11). Although ongoing trials indicate promise for some drugs such as AZD3241, many compounds have unfortunately failed to translate into clinical efficacy for PD patients (Athauda and Foltynie 2015). A contributing

factor may be that patients are not stratified enough to reflect the differential extent of mitochondrial dysfunction underlying their symptoms. An ongoing trial aims to develop a biochemical protocol for grouping PD patients based on mitochondrial biomarkers (SysMedPD, accessed January 2020). The results could have important implications for the way disease-modifying mitochondrially targeted drugs are tested in clinical trials in future and for the targeting of future disease-modifying therapeutics.

1.9.3 Hypothesis for Chapter 5

Taken together, sections 1.7-1.9 demonstrate the unmet clinical need for development of disease-modifying therapies and detail the importance of mitochondrial dysfunction in PD. The evidence demonstrating that the mitochondrial network offers a promising option for potential therapeutic intervention is also outlined. Identification and development of pharmacological modulators of the mitochondrial network, especially using repurposed drugs, offers timely therapeutic promise in the treatment of PD. In Chapter 5, an *in-vitro* phenotypic screen is developed and utilised for this purpose.

1.10 Overall thesis hypotheses and aims

Overall, this thesis aimed to investigate two important molecular hallmarks of neurodegenerative disease: RBP dysfunction and mitochondrial dysfunction. Chapters 3 and 4 hypothesise that the RBP SAFB1 is associated with the pathology of polyQ disease. Chapter 3 aimed to characterise the expression of SAFB1 in human tissue from patients with the polyQ disorders SCA and HD. Chapter 4 aimed to further investigate the potential mechanisms underlying the association of SAFB1 with the pathology of polyQ disorders. The second part of this thesis investigates mitochondrial dysfunction in neurodegenerative conditions such as PD. Chapter 5 hypothesises that novel modulators of mitochondrial function could be therapeutically useful and aims to use an *in-vitro* screening approach to identify novel pharmacological modulators of mitochondrial function which may have potentially neuroprotective actions.

2. Chapter 2

General Methods

2.1 Overview

This chapter provides descriptions of experimental procedures used in this thesis. Additional information relating to the experiments in Chapter 3, Chapter 4 and Chapter 5 can be found within the Methods section of each chapter.

2.2 Materials and resources

This section summarises the materials and resources used in this thesis. Recipes for reagents and solutions are listed in Table 2.1. Details of materials and resources can be found in Table 2.2. A list of the primary and secondary antibodies used in this study can be found in Table 2.3 and Table 2.4, respectively. Guide RNA and primer sequences are detailed in Table 2.5.

Reagent or solution	Recipe (all chemicals from Sigma unless stated)
Cell culture	
Media for H4 cells and HeLa cells	High glucose Dulbecco's Modified Eagle's Medium (DMEM), 10% (v/v) foetal bovine serum (Thermo Fisher Scientific), 10mM l-glutamine, 100U/ml penicillin, 0.1mg/ml streptomycin
Media for SH-SY5Y cells	Dulbecco's Modified Eagle's Medium: Nutrient Mixture F-12 (DMEM/F12), 10% (v/v) foetal bovine serum (Thermo Fisher Scientific), 10mM l-glutamine, 100U/ml penicillin, 0.1mg/ml streptomycin
Media for primary human fibroblasts	High glucose Dulbecco's Modified Eagle's Medium (DMEM), 1% (v/v) MEM non-essential amino acids solution, 10% (v/v) foetal bovine serum (Thermo Fisher Scientific), 10mM l-glutamine, 100U/ml penicillin, 0.1mg/ml streptomycin
Media for Kolf2 iPSCs	Essential 8 medium + supplement (Thermo Fisher Scientific)
Media for plasmid DNA and siRNA transfections	Opti-MEM Reduced Serum Media (Gibco)
Media for Seahorse Mito Stress Test	Seahorse XF DMEM medium, pH 7.4 (Agilent 103575-100) freshly supplemented with 10mM glucose, 1mM sodium pyruvate and 2mM L-glutamine
Media for live cell imaging	20mM HEPES pH7.4, 137mM NaCl, 5mM KCl, 2mM $MgCl_2$, 1.5mM $CaCl_2$, 5.6mM glucose, 1mg/ml BSA, 0.5mM NaH_2PO_4
Media for hfNPC maintenance	High glucose Dulbecco's modified Eagle's medium (DMEM) (Invitrogen), F12 (Invitrogen) (DMEM/F12 ratio: 3:1), 2% (v/v) Glutamax (Invitrogen), 2% (v/v) B27 supplement, 20 ng/ml fibroblast growth factor (FGF-2) (Peprotech), 20 ng/ml epidermal growth factor (EGF), 5µg/ml heparin, 100U/ml penicillin, 0.1mg/ml streptomycin.
Media for hfNPC differentiation	High glucose Dulbecco's modified Eagle's medium (DMEM) (Invitrogen), F12 (Invitrogen) (DMEM/F12 ratio: 3:1), 2% (v/v) Glutamax (Invitrogen), 1% (v/v) N2 supplement, 100U/ml penicillin, 0.1mg/ml streptomycin.
Western Blotting	
2x SDS Laemmli sample buffer	125mM Tris base, 20% (v/v) glycerol, 4% (w/v) SDS, 0.04% (w/v) bromophenol blue, pH 6.8, 100mM DTT (added fresh)
RIPA buffer	150mM sodium chloride, 50mM Tris-HCl pH 8, 1% (v/v) Triton-X 100, 1% (w/v) sodium deoxycholate, 0.1% (w/v) SDS, protease inhibitors (11836170001 Roche, 1 tablet per 10 ml added fresh)
Running buffer	25mM Tris base, 250mM glycine, 0.1% (w/v) SDS
Transfer buffer	48mM Tris base, 39mM glycine, 0.037% (w/v) SDS, 20% (v/v) methanol

Table 2.1 General reagents and solutions (continued next page)

Reagent or solution	Recipe (all chemicals from Sigma unless stated)
Immunostaining	
IHC wash buffer for FFPE tissue staining	PBS (phosphate-buffered saline), 0.1% (v/v) Triton-X 100
IHC wash buffer for frozen tissue staining	TBS (Tris-buffered saline), 50mM Tris-Hcl, 150mM NaCl, pH 7.4, 0.1% (v/v) Triton-X 100
IHC wash buffer for cell staining	PBS (phosphate-buffered saline), 0.1% (v/v) Triton-X 100
Mowiol mounting medium	40% (v/v) Mowiol 4-88 (Millipore), 200mM Tris-HCl, pH 8.5 in glycerol
Phosphate-buffered saline (PBS)	137mM sodium chloride, 2.7mM potassium chloride, 10mM phosphate buffer solution (pH 7.4)
Sodium citrate buffer	10mM tri-sodium citrate in distilled water, pH to 6 using hydrochloric acid, 0.05% (v/v) Tween-20
RNA immunoprecipitation	
Cross-linking wash buffer	PBS pH 7.4 + 0.02% (v/v) Tween-20
Cross-linking coupling buffer	0.2M Triethanolamine in PBS + 0.01% (v/v) Tween, (pH 9)
Cross-linking quenching buffer	50mM ethanolamine in PBS + 0.01% (v/v) Tween
Cross-linking elution reagent	0.2M glycine + 0.01% Tween (v/v) (pH 2.5)
Lysis buffer	50mM Tris (pH 7.5), 150mM NaCl, 1mM EDTA, 1% (v/v) IGEPAL CA-630, 1 tablet/10ml protease inhibitor, 10 U/ml RNase inhibitor, 10 U/ml RNase-free DNAse (inhibitors and enzymes added fresh)
CRISPR	
Cas9 storage buffer	10mM Tris-HCl pH 7.4, 300mM NaCl, 0.1mM EDTA, 1mM DTT (added fresh from frozen 1M stock)

Table 2.1 General reagents and solutions (continued from previous page)

Reagent or resource	Source	Identifier/cat. #
Antibodies		
Donkey anti-mouse Cy3 conjugated	Jackson immunoresearch	715-165-151
Donkey anti-rabbit IgG Cy2 conjugated	Jackson Immunoresearch	711-225-152
Donkey anti-rabbit IgG Cy3 conjugated	Jackson Immunoresearch	711-165-152
Donkey anti-mouse peroxidase-linked IgG	GE Healthcare	NA931
Donkey anti-rabbit peroxidase-linked IgG	GE Healthcare	NA934
Goat anti-mouse Alexa Fluor 488	Invitrogen	A-11001
Goat anti-rabbit Alexa Fluor 555	Invitrogen	A27039
Horse anti-mouse/rabbit biotin conjugated	Vector Laboratories	PK-6200
Mouse anti-polyglutamine	Merck	5TF1-1C2
Mouse anti-hyperphosph. neurofilament	BioLegend	Smi-34
Mouse anti-calbindin	Abcam	CB-955
Mouse anti-alpha-tubulin	Sigma	T5168
Mouse anti-FLAG	Millipore	F3165
Mouse anti-TUBB3	BioLegend	MMS-435P
Rabbit anti-SAFB1	Bethyl	IHC 00142
Rabbit anti-SAFB1	Bethyl	A300-811 A
Rabbit anti-SAFB1	Invitrogen custom	AB1895
Rabbit anti-SAFB2	Bethyl	A301-112A
Rabbit anti-SAFB2	Invitrogen custom	AB1897
Rabbit normal IgG	Cell signalling technology	2729S
Biological samples		
FFPE human tissue sections and frozen human tissue samples	MRC Neurodegeneration Brain Bank	See Chapter 3 for ethics details
FFPE human tissue sections (Cerebellar tissue from MS patients)	Kind gift from Dr. Kevin Kemp, Univeristy of Bristol	See Chapter 3 for ethics details
Commercial kits and assays		
DAB substrate kit	Vector Labs	SK-4100
ECL Prime Western Blotting detection reagent	Amersham	RPN2236
GoScript Reverse Transcription System	Promega	A5000
*mir*VANA PARIS kit	Invitrogen	AM155
P3 primary cell nucleofector kit	Lonza	V4XP-3012
Pierce BCA Protein Assay kit	Thermo Fisher	23225
QuickStart HiFi PCR kit	Roche	3553400001
ReliaPrep RNA Cell Miniprep System	Promega	Z6010
Seahorse XFp Cell Mito Stress Test Kit	Agilent	103010-100
SuperSignal West Pico PLUS substrate	Thermo Fisher	34580
Vectastain Elite ABC HRP kit	Vector Labs	PK-6200
Wizard genomic DNA purification kit	Promega	A1120

Table 2.2 Key resources table (continued next page)

Reagent or resource	Source	Identifier/cat. #
Experimental cell lines		
C1 control human fibroblasts	Kind gift from Dr. Lucy Crompton, University of Bristol	N/A
H4	N/A	N/A
H4 eGFP-parkin	Cell line created by Dr. Helen Scott	N/A
HeLa	N/A	N/A
Kolf2	Kind gift from Professor Nick Allen, Cardiff University and HipSci	HPSI0114i-kolf_2
SH-SY5Y	N/A	N/A
SH-SY5Y eGFP-parkin	Cell line created by Dr. Fella Hammachi	N/A
hfNPCs	Kind gift from Dr. Oscar Cordero-Llana, University of Bristol	See Chapter 5 for ethics details
Oligonucleotides and plasmid DNA		
pEGFP-ATXN1-2Q	Addgene	33239
PEGFP-ATXN1-30Q	Addgene	33238
PEGFP-ATXN1-52Q	Addgene	32492
pcDNA1 Flag ATXN1[2Q]	Addgene	33235
pcDNA1 Flag ATXN1[30Q]	Addgene	33236
pcDNA1 Flag ATXN1[85Q]	Addgene	33237
crRNA	Integrated DNA Technologies	N/A
PCR primers	ThermoFisher Scientific	N/A
Software		
INCell Analyzer Workstation	GE Healthcare	Version 3.7.1
Fiji	Image J	Version 1.51r
Forna	ViennaRNA Web Services	Accessed via http://rna.tbi.univie.ac.at/forna/ (Sep 2019)
GraphPad Prism	GraphPad	Version 7.04
ImageScope	Aperio	Version 12.3.3
Image Studio Lite	Licor	Version 5.2
Seahorse Wave	Agilent	Version 2.6.1
SerialCloner	SerialCloner	Version 2.6.1
SnapGene Viewer	SnapGene	Version 4.3.4

Table 2.2 Key resources table (continued from previous page)

Antigen	Cat. #	Supplier	Clonal Type	Species raised in	Application	Dilution
Alpha-tubulin	T5168	Sigma	Mono	Mouse	Western blot	1:2000
Calbindin	CB-955	Abcam	Mono	Mouse	IF (FFPE human)	1:250
FLAG	F3165	Millipore	Mono	Mouse	IF (cells)	1:500
					Western blot	1:500
Hyperphosphorylated neuro-filament	Smi-34	BioLegend	Mono	Mouse	IF (FFPE human)	1:500
SAFB1	A300-811A	Bethyl	Poly	Rabbit	IHC (FFPE human)	1:50
					IF (FFPE human)	1:200
					Western blot	1:1000
SAFB1	IHC-00142	Bethyl	Poly	Rabbit	IHC (FFPE human)	1:50
SAFB1	AB1895	Invitrogen custom antibody services	Poly	Rabbit	RNA IP	0.75mg per 100mg protein
SAFB2	AB1897	Invitrogen custom antibody services	Poly	Rabbit	IHC (FFPE mouse)	1:100
TBP (Poly-glutamine)	1C2	Millipore	Mono	Mouse	IHC (FFPE human)	1:1000
TOMM20	Sc-11415	Santa Cruz Biotech.	Poly	Rabbit	IF (cells)	1:300
TUBB3	MMS-435P	BioLegend	Mono	Mouse	IF (cells)	1:500

Table 2.3 Primary antibodies and their applications

Species raised in	Species raised against	Conjugation	Cat. #	Supplier	Application	Dilution
Donkey	Mouse	Cy3	715-165-151(JIR)	Stratech	IF	1:300
Donkey	Rabbit	Cy2	711-225-152(JIR)	Stratech	IF	1:300
Donkey	Rabbit	Cy3	711-165-152-JIR	Stratech	IF	1:300
Donkey	Mouse	Peroxidase	NA931	GE Healthcare	Western blotting	1:10000
Donkey	Rabbit	Peroxidase	NA934	GE Healthcare	Western blotting	1:10000
Goat	Mouse	Alexa Fluor 488	A-11001	Invitrogen	IF	1:500
Goat	Rabbit	Alexa Fluor 555	A27039	Invitrogen	IF	1:500
Horse	Mouse/ Rabbit	Biotin	PK-6200	Vector Laboratories	IHC	1:50

Table 2.4 Secondary antibodies and their applications

Application	Target	F sequence	R sequence
CRISPR (gRNA)	SAFB dual promoter	gRNA 1: GGGCAGAGTCTCCGCCATCG	gRNA 2: CCTCGTCAGAGACCGGGACG
CRISPR PCR screening	SAFB dual promoter	GTGTCCAGGTTCCGCTTCTTC	CGCTCGAGTCCACATTCCGTTT
qPCR	Ataxin1	TCCAGCACCGTAGAGAGGAT	GCCCTGTCCAAACACAAAAA
qPCR	Beta-actin	CCCCTGAACCCAAGGC	CAGAGGCCTACAGGGATAG
qPCR	SAFB1	GAGGGACCGAACGGACTGTAG	TGGCTGATTTGCGATCCTG

Table 2.5 PCR primer and guide RNA (gRNA) sequences

2.3.1 Human cell lines

Human neuroglioma (H4), human neuroblastoma (SH-SY5Y) and human cervical carcinoma (HeLa) cell lines were used in this study. H4 and SH-SY5Y cell lines which stably express eGFP-parkin were used in Chapter 5. All cells were maintained in a humidified incubator at 37^{o}C, with 5% CO_2. Cells were regularly tested for mycoplasma by PCR analysis of conditioned media, which determined that the lines were free of contamination. H4 cells and HeLa cells were maintained in high-glucose Dulbecco's Modified Eagle's Medium (DMEM) (Sigma) and SH-SY5Y cells were maintained in DMEM/F-12 (Sigma), both supplemented with foetal bovine serum, l-glutamine and penicillin-streptomycin (Table 2.1). For siRNA and plasmid transfections, cells were cultured in media without antibiotics. Cells were passaged when they reached confluency of approximately 80%, by harvesting with 0.5% (w/v) trypsin with EDTA. After inactivating the enzyme with complete media, cell suspensions were centrifuged at 1200rpm for 2 minutes and the cell pellet quickly and gently resuspended in fresh culture media. Stock flasks were maintained by splitting cells in a ratio of between 1 in 8 and 1 in 20 every 3-4 days. For experiments, H4 cell lines and SH-SY5Y cell lines were used up to passage 20 and HeLa cells were used up to passage 25. Prior to seeding cells into plates for experimental assays, a sample of the cell suspension was stained with 50% trypan blue (v/v) and the viable cells counted using a standard haemocytometer.

2.3.2 Transient transfection of human cell lines

Cell lines were transiently transfected with either siRNAs to knockdown gene expression, or with DNA plasmids to induce gene expression. Cell lines were plated without antibiotics and transfected 24 hours later. In siRNA knockdown experiments, a non-targeting control (NTC) siRNA was transfected as a control on each plate. Plasmid DNA or siRNAs were diluted in Opti-MEM reduced serum media (ThermoFisher Scientific) and combined with Lipofectamine 2000 (ThermoFisher Scientific) or Fugene 6 (Promega)

transfection reagent. The combined reagents were mixed gently and left to equilibrate for up to 15 minutes at room temperature. The resultant transfection mixture was added dropwise to cells, on top of a reduced volume of their usual growth media and the culture vessel rocked gently to mix. After transfection, cells were left for 6 hours in transfection media before carrying out a full media change. Cells were left for 48 hours post-transfection before further use in experimental assays.

2.3.3 Primary human cells

Skin fibroblasts from a 49 year-old patient with no history of neurological disease were a kind gift from Dr. Lucy Crompton (School of Biochemistry, University of Bristol). Human fibroblasts were maintained in high-glucose DMEM with non-essential amino acids, foetal bovine serum, l-glutamine and penicillin-streptomycin (Table 2.1). Fibroblasts were grown in culture vessels or on glass coverslips coated in sterile 0.1% gelatin.

2.3.4 Human induced pluripotent stem cells (iPSCs)

Human iPSCs were a kind gift from the research group of Professor Nicholas Allen (School of Biosciences, Cardiff University). Undifferentiated iPSCs were maintained in E8 media (Gibco) in culture vessels pre-coated with vitronectin. Culture media was changed a minimum of every 48 hours. iPSC colonies were observed to ensure maintenance of stem-cell like morphology. When iPSC colonies were approximately 80% confluent, they were passaged by incubating in ReLeSR (stem cell technologies) at 37^{o}C for approximately 3 minutes, until the edges of colonies began to detach from the culture vessel. The ReLeSR was aspirated leaving iPSC colonies adhered to the vessel. Dulbecco's phosphate-buffered saline with no calcium or magnesium (DPBS) was gently washed over the culture vessel to lift the colonies, and the cell suspension centrifuged at 1000rpm for 3 minutes. Supernatant was removed from the cell pellet, and colonies gently resuspended in E8 media. Cultures were typically split at a ratio of 1 in 6 by adding the resuspended colonies drop-wise into a new vitronectin-coated culture vessel containing fresh pre-warmed E8 media. If colonies became

overly dissociated during passaging, 1µl/ml ROCK inhibitor (StemCell Technologies) was added to the media and removed after 24 hours.

2.3.5 Human foetal neuroprogenitor cells (hfNPCs)

hfNPCs were a kind gift from the research group of Dr. Oscar Cordero-Llana, and were utilised with the technical assistance of Ms. Andriana Gialeli (University of Bristol). Human foetal tissue was collected from medical terminations of pregnancy with full donor consent, through the SWIFT human foetal tissue bank at Cardiff University and with ethical approval of the project from the local research ethics committee (SWIFT-RTB 46). hfNPCs were grown as neurospheres in non-adherent culture in high-glucose Dulbecco's modified Eagle's medium (DMEM)/F12 (Invitrogen) with Glutamax, fibroblast growth factor (FGF-2) (Peprotech), epidermal growth factor (EGF) (Sigma) and heparin (Sigma) (Table 2.1). hfNPCs were cultured in flasks coated with or without poly-2-hydroxyethyl methacrylate (poly-HEMA). Growth medium was replenished twice a week, and the cells were mechanically passaged with a McIlwain tissue chopper.

2.4 High-content florescent cell imaging and analysis

2.4.1 High-content image acquisition

Automated image capture of fluorescence in fixed and live cells was carried out using an INCell Analyzer 2200 (GE Healthcare). Cells were plated in black-walled 96-well plates (either Corning 3904 or Greiner 655090). The INCell Analyzer laser autofocus trace tool was used to calculate and set plate bottom height and thickness. Images were acquired using laser autofocus with power set between 10-50%. Two acquisition modes were utilised in this study: 2D imaging (image from a single focal plane with no post-processing) and 2D deconvolution imaging (image from a single focal plane with post-processing to reverse blurring caused by the objective). Images were capturing using either a 10x objective (Nikon 10x/0.45 NA Plan Apo, CFI/60), 20x objective (Nikon 20x/0.45, Plan Fluor, correction collar 0-2.0 CFI/60) or 40x objective (Nikon 40x/0.6 NA Plan Fluor, correction collar

0-2.0, CFI/60). Details of the fluorescent excitation channels used for cell imaging in this study can be found in Table 2.6.

Cell component	Fluorophore	Channel name	Excitation filter	Emission filter
Nuclei	Hoechst	DAPI	390/18	432.5/48
Cell	eGFP	FITC1	475/28	511.5/23
Cell	MitoTracker Red	Cy3	542/27	597/45
Parkin	eGFP	FITC1	475/28	511.5/23
Mitochondria	MitoTracker Red	Cy3	542/27	597/45

Table 2.6 Excitation and emission wavelengths (nm) for fluorescence imaging of cellular components using the INCell Analyzer 2200

2.4.2 Quality control of high-content imaging

The INCell Analyzer 2200 uses a laser autofocus to assess the location of interface between the bottom of the well and the liquid in the well, to identify the location of the biological sample and obtain an automatically focussed image. However, due to various factors (e.g. small imperfections in the wells from the manufacturing process) a small percentage of acquired images may be out of focus. The small size of the organelles of interest in this study (parkin puncta and mitochondria, which can be less than 1µm long), necessitate accurate segmentation by the analysis software. Images therefore were required to be of the highest possible standard of quality and focus. To avoid error caused by out of focus objects being inaccurately identified by the analysis software, images from each field were manually checked after acquisition and any wells which contained an image which was not in focus were removed from the final data set. An excess number of wells replicating each experimental condition ensured that the minimum number of well replicates was met per plate (see 2.8.2 Experimental replicates).

2.4.3 High-content image analysis

All images acquired using the INCell Analyzer 2200 were quantified using INCell Analyzer Workstation software (version 3.7.1, GE Healthcare). Cell analysis protocols were created within the Multi Target Analysis (MTA) mode. Pre-programmed algorithms within the software, designed to identify objects within cells (granularity assays) were modified to create assays to segment cellular organelles. Assays were used to quantify parkin recruitment, mitochondrial network morphology, MitoTracker Red CMX Ros fluorescence intensity and cell counts. A description of the individual MTA output measures utilised in this study can be found in Table 2.7. Details of the settings used for each Workstation analysis protocol can be found in Table 2.8, Table 2.9, Table 2.10 and Table 2.11. Data was outputted from the Workstation software as Microsoft Excel .xlsx files. Raw data files remained unedited, and summarisation of data was carried out within separate Excel files.

Segmentation	MTA measure	Description
Nuclei	Count	Number of nuclei
Cell	Intensity	Mean intensity of pixels within the cytoplasm region, in the cells channel
Organelles	Count	Number of inclusions attributed to the cell
Organelles	Total Area	Total area of inclusions attributed to the cell
Organelles	Distance to Nucleus	Mean distance from the inclusion centre to the nucleus centre (averaged by all inclusions within the cell)
Organelles	Elongation	Mean ratio of the short axis of the inclusion to the long axis of the inclusion (averaged by all inclusions within the cell). If the value is 1 then the object is center-symmetric (not elongated)
Organelles	Inclusion/Cell Intensity	Ratio of the average pixel intensity within inclusions to the average pixel intensity in the cell region immediately adjacent to the inclusions (both intensities measured in the Inclusion channel)

Table 2.7 Multi-target analysis (MTA) parameter descriptions as specified by INCell Workstation software

Experiment		**Parkin recruitment (Primary Screening)**	**Parkin recruitment (Secondary screening)**
Cell Line		**H4 eGFP-parkin**	**H4 eGFP-parkin, SH-SY5Y eGFP-parkin**
Objective		10x	20x
Fields per well		2	3-4
Nuclei	Channel	DAPI	DAPI
	Acquisition	2D	2D
	Segmentation	Top-Hat	Top-Hat
Cells	Channel	FITC1	FITC1
	Acquisition	2D	2D
	Segmentation	Multiscale Top-Hat	Multiscale Top-Hat
Organelles	Channel	FITC1	FITC1
	Acquisition	2D	2D
	Segmentation	Multiscale Top-Hat	Multiscale Top-Hat
Organelles 1	Channel	N/A	Cy3
	Acquisition	N/A	2D
	Segmentation	N/A	Multiscale Top-Hat
Reference 1	Channel	N/A	FITC1
	Segmentation	N/A	Pseudo
Reference 2	Channel	N/A	Cy3
	Segmentation	N/A	Pseudo
Key output measures	Nuclei	Cell count	Cell count
	Cell	N/A	N/A
	Organelles	% cells with >3 organelles	% cells with >3 organelles, Total area*, Count*, Inclusion/cell intensity*
	Organelles 1	N/A	N/A

Table 2.8 INCell Workstation MTA protocol settings for quantification of parkin puncta in compound testing experiments. *used for SH-SY5Y eGFP-parkin cells only, N/A not applicable.

Experiment		Mitochondrial analysis	MPP+ assay
Cell Line		**H4 eGFP-parkin**	**H4 eGFP-parkin**
Objective		40x	20x
Fields per well		4	4
Nuclei	Channel	DAPI	DAPI
	Acquisition	2D	2D
	Segmentation	Top-Hat	Top-Hat
Cells	Channel	Cy3	Cy3
	Acquisition	2D	2D
	Segmentation	Multiscale Top-Hat	Multiscale Top-Hat
Organelles	Channel	Cy3	N/A
	Acquisition	2D deconvolution	N/A
	Segmentation	Multiscale Top-Hat	N/A
Organelles 1	Channel	N/A	N/A
	Acquisition	N/A	N/A
	Segmentation	N/A	N/A
Reference 1	Channel	N/A	N/A
	Segmentation	N/A	N/A
Reference 2	Channel	N/A	N/A
	Segmentation	N/A	N/A
Key output measures	Nuclei	Cell count	Cell count
	Cell	N/A	Intensity
	Organelles	Total area, Count, Elongation, Distance to nucleus	N/A
	Organelles 1	N/A	N/A

Table 2.9 INCell Workstation MTA protocol settings for quantification of mitochondria in compound testing experiments. N/A not applicable.

Experiment	**Parkin recruitment (primary screening)**	**Parkin recruitment (secondary screening)**	**Parkin recruitment (secondary screening)**
Cell line	**H4 eGFP-parkin**	**H4 eGFP-parkin**	**SH-SY5Y eGFP-parkin**
Nuclei (Top-Hat)			
Minimum area (μm^2)	100	100	60
Sensitivity	80	70	50
Cells (Multiscale Top-Hat)			
Area (μm^2)	450	200	350
Sensitivity	30	5	5
Organelles (Multiscale Top-Hat)			
Minimum area	1	1	1
Maximum area	5	3	3
Number of scales	1	2	1
Sensitivity/Advanced sensitivity	5/1.95	1/2.3	8/2
Detect	In the cells	In the cells	In the cells
Organelles 1 (Multiscale Top-Hat)			
Minimum area	N/A	2	N/A
Maximum area	N/A	11	N/A
Number of scales	N/A	1	N/A
Sensitivity/Advanced sensitivity	N/A	1/1.5	N/A
Detect	N/A	In the cells	N/A
Filters			
Type	Threshold	Threshold	Threshold
Measure	Organelle count	Organelle count	Nuclei 1/form factor
Value	False if ≤3	False if ≤3	False if >1.8

Table 2.10 INCell Workstation MTA protocol settings for parkin recruitment assays. N/A not applicable.

Experiment	**MPP+ assay**	**Mito H4**
Cell Line	**H4 eGFP-parkin**	**40x**
Nuclei (Top-Hat)		
Minimum area (µm^2)	100	100
Sensitivity	70	50
Cells (multiscale Top-Hat)		
Area (µm^2)	200	70
Sensitivity	5	2
Organelles		
Minimum area	1	1
Maximum area	3	100
Number of scales	2	1
Sensitivity/Advanced sensitivity	1/2.3	1/1.4
Detect	In the cells	In the cells
Organelles 1		
Minimum area	2	N/A
Maximum area	11	N/A
Number of scales	1	N/A
Sensitivity/Advanced sensitivity	1/1.5	N/A
Detect	In the cells	N/A
Filters		
Type	N/A	Threshold
Measure	N/A	Cell area
Value	N/A	False if >4966.89

Table 2.11 INCell Workstation MTA protocol settings for mitochondrial assays. Mito H4 refers to mitochondrial morphology analysis in H4 cells. N/A not applicable.

2.5 Mitochondrial analysis

2.5.1 Parkin recruitment assay

Parkin recruitment to mitochondria was used to screen drug compounds for their effect on the mitochondrial network *in-vitro*. Briefly, H4 and SH-SY5Y cells stably expressing eGFP-tagged parkin plated in 96-well plates were fixed in 4% PFA and the cell nuclei stained with 1µg/ml Hoechst dye (Sigma). Under baseline conditions, eGFP-parkin appears diffuse throughout the cell cytoplasm. Upon induction of mitophagy by depolarisation of the mitochondrial membrane with CCCP, parkin is recruited to the mitochondrial membrane where it appears as small bright dots (puncta). The INCell Analyzer 2200 was used to image fluorescent signal from Hoechst (nuclear) channel and the eGFP (parkin) channel. The formation of parkin puncta was quantified using INCell Analyzer Workstation software. Details of the analysis protocol settings can be found in Table 2.10.

2.5.2 High-content imaging of mitochondria

Mitochondria in live cells were stained with 100nM MitoTracker Red CMX Ros (ThermoFisher Scientific) for 1 hour at 37^{o}C. MitoTracker Red enters mitochondria when the organelles maintain a healthy membrane potential. The dye is retained after fixation using 4% PFA. Cell nuclei were counterstained with 1µg/ml Hoechst. Mitochondria in cells were imaged using the INCell Analyzer 2200 using a 40x objective and 2D-deconvolution imaging. An analysis protocol was developed using INCell Analyzer Workstation software to segment mitochondria. Output measures of the shape and size of the mitochondrial network include the total mitochondrial cross-sectional area per cell, and a ratio measure of the elongation of each mitochondrial object. Details of the analysis protocol settings can be found in Table 2.11.

2.5.3 MPP+ toxicity assay

H4 eGFP-parkin cells grown in 96-well plates were treated with MPP+ iodide (Sigma) for 24 hours in the presence of kenpaullone (5µM) or vehicle control (DMSO). MPP+ iodide was dissolved in sterile distilled water and frozen in stock aliquots at -80ºC until use. MPP+ was protected from light during use. Cells were stained with 100nM MitoTracker Red for 1 hour at 37ºC, then fixed in 4% PFA and cell nuclei stained using 1µg/ml Hoechst. Plates were imaged using the INCell Analyzer 2200 and analysed using the INCell Workstation software to measure cell number and MitoTracker Red intensity within the cytoplasm (Table 2.11).

2.5.4 Analysis of mitochondrial function in live cells

Oxygen consumption rate (OCR) and extracellular acidification rate (ECAR) in live cells was measured using a Seahorse XFp analyser (Agilent). H4 eGFP-parkin cells or SH-SY5Y eGFP-parkin cells were plated into Seahorse XFp microplates at a density of 15000 or 20000 cells per well, respectively. 24 hours later, cells were treated with kenpaullone (5µM) or vehicle control (DMSO) for 24 hours. In the presence of kenpaullone or DMSO, cells were challenged with CCCP (15µM) or DMSO for 2 hours before OCR analysis. A mitochondrial stress test assay was carried out using a Seahorse XFp Cell Mito Stress Test kit (Agilent). Cells were washed with assay medium (Seahorse XF DMEM medium supplemented with 10mM glucose, 1mM pyruvate and 2mM L-glutamine) and kept at 37ºC with no CO_2 for 45 minutes before the assay. The mitochondrial stress test involves injecting selective inhibitors of the electron transport chain into the cell assay media. Cells were exposed to a final concentration of 1µM oligomycin, 2µM FCCP and 0.5µM rotenone/antimycin A. OCR was calculated using the standard Mito Stress Test protocol on the XFp analyser. Metabolic parameters were calculated from OCR data using the formulae in Table 2.12. After the assay, cell media was carefully removed, the cells gently washed once in PBS and 20µl RIPA buffer was added to each well. The plates were agitated for 15 minutes and 2µl of lysate was

used for quantification using a BCA assay (Pierce BCA assay kit). OCR was normalised to protein concentration in each well.

Parameter Value	Equation
Basal Respiration	(Last rate measurement before first injection) – (Non-mitochondrial respiration rate)
Spare Respiratory Capacity	(Maximal respiration) – (Basal respiration)
Maximal Respiration	(Maximum rate measurement after FCCP injection)- (Non-mitochondrial respiration)
ATP Production	(Last rate measurement before oligomycin injection) – (Minimum rate measurement after oligomycin injection)
Non-mitochondrial Oxygen Consumption	Minimum rate measurement after rotenone/antimycin A injection
H+ (Proton) Leak	(Minimum rate measurement after oligomycin injection) – (Non-mitochondrial respiration

Table 2.12 Seahorse XF Cell Mito Stress Test parameter formulae. Table adapted from Seahorse XF Report Generator User Guide (accessed November 2019).

2.6 Molecular biology

2.6.1 Gene knockout using CRISPR-Cas9

Knockout of the SAFB1/2 dual promoter in human iPSCs was carried out using the CRISPR-Cas9 system. In brief, guide RNAs (gRNAs) complementary to sequences flanking the promoter sequence were combined with a fluorescent tracer RNA (tracrRNA). Cas9 protein was combined with the gRNA/tracrRNA complex to make the ribonucleoprotein (RNP) complex. iPSC colonies were treated with ROCK inhibitor and dissociated to a single cell suspension. One million cells were nucleofected with the RNP complex by electroporation and allowed to recover overnight. Individual cells were sorted by FACS (fluorescence activated cell sorting) and cells in the top 10% of fluorescence intensity were plated to form clonal

iPSC colonies. Individual colonies were screened for promoter knockout by PCR and the deletion confirmed by Sanger sequencing.

2.6.2 Genomic DNA extraction

Genomic DNA was extracted from cells using a Wizard Genomic DNA Purification Kit (Promega) according to the protocol for Tissue Culture Cells. Cells were harvested and pelleted before washing in PBS, and the manufacturer's protocol followed. For PCR screening of iPSC colonies, genomic DNA was extracted using DNA QuickExtract solution (Lucigen) according to manufacturer's instructions. Samples were stored at -20^{o}C until use.

2.6.3 RNA extraction and purification

RNA from frozen human tissue was extracted using a mirVana PARIS kit (Life Technologies) according to manufacturer's instructions. RNA from precipitated immunocomplexes and protein lysates from the RNA immunoprecipitation protocol were purified using a ReliaPrep RNA cell miniprep kit (Promega). Immunocomplexes bound to Proten G magnetic beads (Dynabeads, ThermoFisher) were mixed with 250µl of fresh BL+TG buffer, vortexed and left to stand for 10 minutes at room temperature. The bead supernatant was then used in the kit manufacturer's protocol. Protein lysates were pre-mixed with BL+TG buffer before freezing, or freshly mixed with BL+TG buffer, before standing at room temperature for 10 minutes and proceeding with the manufacturer's protocol. RNA samples were handled with RNase-free plasticware and reagents, were kept on ice at all times and were stored at -80^{o}C.

2.6.4 Reverse transcription

Reverse transcription of RNA into cDNA was carried out using a GoScript Reverse Transcription System kit (Promega) according to manufacturer's instructions. A maximum of 4µl RNA was added to 1µl of random primers or Oligo(dT) primers and incubated at 70^{o}C for 5 minutes before immediately cooling to 4^{o}C. Reverse transcription mix was prepared with 4.5mM $MgCl_2$

according to the kit protocol and 15µl added to each RNA/primer sample. Reactions were annealed at 25ºC for 5 minutes, extended at 42ºC for 1 hour and transcriptase was inactivated at 70ºC for 15 minutes. cDNA was stored at -20ºC.

2.6.5 Quantification of DNA and RNA

RNA, gDNA, cDNA and plasmid DNA was quantified using either a NanoDrop 2000 spectrophotometer (ThermoFisher Scientific) or an Implen Nanophotometer (GeneFlow) using a minimum of 1µl of sample. DNA with an A260/A280 ratio of at least 1.8 and an A260/A230 ratio of 2-2.2 was used in experiments. RNA with an A260/A280 ratio of at least 2 and an A260/A230 ratio of 2-2.2 was used in experiments.

2.6.6 Quantitative PCR (qPCR)

cDNA was used in qPCR reactions neat or diluted 1:10. A qPCR mastermix was made using Power SYBR Green (ThermoFisher Scientific) including a final concentration of 300nM of forward and reverse primers. qPCR was carried out using a StepOnePlusTM Real Time PCR system (Thermo Fisher Scientific) using a default 2-hour PCR protocol. Sequences for qPCR primers can be found in Table 2.5.

2.6.7 Protein extraction from cells

Cell culture media was removed and cells washed in ice-cold PBS. PBS was removed and cell lysis buffer (typically RIPA buffer) added, and the cells scraped on ice to lyse the cells. Lysate was mixed on a rocker for 20 minutes at 4ºC before centrifuging at 14,000rpm at 4ºC for 15 minutes. The cell debris pellet was discarded and the protein supernatant stored in a fresh microtube at -80ºC until use.

2.6.8 Protein extraction from tissue

Protein extraction from frozen human brain tissue was carried out using a mirVana PARIS kit (Life Technologies) according to manufacturer's instructions (see section 3.3.7 for further details).

2.6.9 Protein quantification

Total protein content of lysed cell samples or tissue extracts was quantified using a bicinchoninic acid assay (Pierce BCA protein assay kit, Thermo Scientific). A standard curve of albumin protein standards was used on each plate. Samples were diluted in lysis buffer to ensure that the optical density readings from the BCA assay fell within the linear portion of the standard curve within each plate. 2µl of sample or standard was incubated in 100µl of BCA assay reagent (made up according to manufacturer's instructions) in a 96-well plate and incubated at 37^{o}C for 30 minutes. The optical density of each well was measured using a Glomax plate reader (Promega).

2.6.10 RNA immunoprecipitation

A detailed description of RNA immunoprecipitation (IP) techniques can be found in Chapter 4. In brief, HeLa cells were transfected with DNA plasmids expressing the *ATXN1* gene containing either 2, 30 or 85 CAG repeats, with an N-terminal FLAG tag (Table 2.2). Protein extracted from transfected HeLa cells was pre-cleared by incubating with Protein G magnetic beads (Dynabeads, ThermoFisher). Protein concentration of lysates was established using a BCA assay (Pierce BCA assay kit, Thermo Fisher Scientific), and a known quantity of protein incubated overnight at 4^{o}C with Protein G beads cross-linked to either SAFB1 antibody or concentration-matched rabbit IgG (Cell Signalling Technology). Beads were isolated using a magnetic rack and washed before dissociating immunocomplexes from the beads. RNA was purified using a Reliaprep RNA cell miniprep system (Promega). RNA was reverse transcribed to cDNA and quantified by qPCR using primers against *ATXN1*. Relative quantities of *ATXN1* were calculated by comparison to a standard curve of serial diluted *ATXN1*- expressing DNA plasmid included on each plate.

2.6.11 Western blotting

Typically, 20-30µg of protein per sample was added 1:1 to 2x SDS sample buffer and heat denatured at 95^{o}C for 5 minutes. Samples were loaded onto a polyacrylamide gel (8-10%) and electrophoresis at 100-150V carried out

in a TRIS-glycine running buffer. Protein was transferred onto PVDF membrane by either wet or semi-dry transfer. Semi-dry transfer was carried out using a Trans-Blot Turbo transfer system (BioRad) for 10 minutes using a high molecular weight transfer protocol with a mini PVDF transfer pack (BioRad). For wet transfer, gels were sandwiched against PVDF membrane in a transfer cassette and immersed with an ice pack in TRIS-glycine transfer buffer with 20% methanol. The transfer cassette was run at 200mA for 2 hours. Following transfer, protein on PVDF membranes was blocked in 5% milk powder in PBS (w/v) for 1 hour at room temperature on a rocker. Membranes were then probed with primary antibody diluted in 1% milk powder in PBS on a rocker overnight at 4^{o}C. Membranes were washed 3 times in PBS with 0.05% Tween (PBS-T) for 5 minutes on a rocker at room temperature before probing with secondary antibody diluted 1:10000 in 1% skimmed milk powder. For primary antibodies raised in rabbit, membranes were incubated in peroxidase-linked anti-rabbit IgG (NA934, GE Healthcare). For primary antibodies raised in mouse, membranes were incubated in peroxidase-linked anti-mouse IgG (NA931, GE Healthcare). Membranes were washed 3 times for 5 minutes with PBS-T. Antibody-bound protein was visualised using enhanced chemiluminescence (ECL) (either ECL Prime reagent (Amersham) or Supersignal West Pico PLUS reagent (Thermo Fisher Scientific)). The light signal was imaged using either a gel doc CCD (charge-coupled device) imaging system (G:Box F3, Syngene), or by exposing the membrane to x-ray film inside a cassette before developing the film using a developing machine.

2.7 Immunostaining

2.7.1 Immunohistochemical staining of FFPE tissue sections

Sections were deparaffinised and rehydrated. Antigen retrieval was carried out by immersing slides in heated 0.1mM sodium citrate buffer (pH 6) with 0.05% (v/v) Tween 20. Endogenous peroxidases were neutralised by incubating sections in 1% (v/v) hydrogen peroxide diluted in distilled water. Immunohistochemical staining was carried out using an avidin-biotin complex staining kit (Vectastain Elite ABC HRP Kit (Peroxidase, Universal),

PK-6200, Vector Laboratories). Protein blocking to reduce non-specific binding was carried out by incubating sections in normal horse serum (Vectastain blocking solution) diluted 1:100 in PBS-T. Sections were incubated with primary antibody diluted in protein blocking solution overnight at 4ºC. Sections incubated in antibody diluent only served as no primary antibody controls. Sections were incubated in secondary antibody (Vectastain biotinylated horse anti-rabbit/mouse, 1:50) diluted in Vectastain blocking solution. Following PBS washes, sections were incubated in ABC reagent (Vectastain Elite ABC Reagent, 1:50), and antibody binding was visualised using 3,3'-diaminobenzidine (DAB) (Vectorlabs DAB substrate kit, no nickel). After washing in distilled water, nuclei were visualised by counterstaining in Ehrlich's haematoxylin. Sections were dehydrated, cleared and mounted under glass coverslips using DPX mountant.

2.7.2 Immunofluorescent staining of FFPE and frozen tissue sections

FFPE sections were placed in an oven at 56ºC for at least 1 hour to aid de-waxing and reduce auto-fluorescence. Slides were dewaxed in Clearene, immersed in 100% alcohol then washed in running tap water for 10 minutes. Antigen retrieval was carried out as described for immunohistochemical staining. Slides were washed in running tap water, then washed in PBS (pH 7.4). Protein block was carried by incubating with protein blocking solution (10% (v/v) normal goat serum diluted in PBS with 0.01% (v/v) Triton X-100) for 1 hour at room temperature. Sections were incubated in primary antibodies diluted in blocking solution overnight at 4ºC. Sections were washed in PBS before incubation with fluorescently conjugated secondary antibodies diluted in blocking solution for 1 hour, protected from light. Sections were washed in PBS, then incubated with DAPI (1µg/ml in PBS) (ThermoFisher Scientific, UK) for 5 minutes. Following a final PBS wash, sections were mounted in 50% PBS/50% glycerol under glass coverslips sealed with clear nail varnish. Slides were stored at 4ºC in the dark prior to imaging.

2.7.3 Immunofluorescent staining of cells

Cells grown on coverslips were fixed in 4% PFA for 15-20 minutes at room temperature, then washed in PBS. Cells were incubated in 5% (v/v) donkey serum in PBS with 0.03% (v/v) Triton X-100 for 1 hour at room temperature to block proteins and permeabilise the cells. Cells were then incubated in primary antibody diluted in 1% (v/v) donkey serum in PBS overnight rocking gently at 4^{o}C. Cells were washed in PBS before incubating for 1 hour at room temperature with fluorescent-conjugated secondary antibody raised in the same species as the serum used for blocking, which was always a different species in which the primary antibody was raised. Cells were washed in PBS, then the nuclei counterstained using 1µg/ml Hoechst or DAPI (ThermoFisher Scientific). Coverslips were mounted using mowiol mounting medium, sealed with clear nail varnish and stored at 4^{o}C prior to imaging.

2.7.4 Microscopy

Image capture of immunohistochemically stained sections was carried out using a Nikon eclipse i80 microscope with a Nikon Ci-SMS camera, and Image-Pro plus software, or using an Aperio Scanscope CS2 digital slide scanner (Leica) and Leica ImageScope software. Immunofluorescent cells and tissue sections were imaged using either a Leitz DMRB fluorescence microscope (Leica) with a Leica DC500 camera and Leica imaging software, or with a Nikon C1 confocal microscope with EZ viewer software.

2.8 Statistics and data presentation

2.8.1 Statistical tests and reporting

Prior to statistical analysis, data distribution of experimental results was carried out using a Shapiro-Wilk normality test. For normally distributed datasets, parametric statistical tests were carried out. Comparisons between two groups were made using a student's t-test (unpaired, two tailed). T-test results are reported in the following format: "t(degrees of freedom)=t value, p-value". Comparisons between multiple (at least two)

groups with a single factor (variable) were made using one-way analysis of variance (ANOVA) tests. Comparisons between multiple groups with two factors (variables) were made using two-way ANOVA tests. If ANOVA tests detected a significant difference, an appropriate multiple comparison post-hoc test was employed to confirm where significant differences occurred between groups. Post-hoc test details are included alongside the reporting of statistical results. Results of ANOVA tests are reported as p-values. Relationships between two sets of parametric data were analysed using Pearson's correlation tests. Non-parametric comparisons between two groups were performed using Mann-Whitney tests, the results of which are reported as follows: "(group 1 median, group 2 median) U-value, p-value". Non-parametric correlation analysis was carried out using Spearmann's correlation. Parametric data is displayed in bar graphs as group means with error bars representing ± standard error of the mean (SEM). Non-parametric data is displayed in bar graphs representing the median of each group. Individual datapoints (biological replicates) are plotted as circular or square symbols on bar graphs. Lines of best fit displayed on scatter plots were drawn using a linear regression function. All statistical tests were carried out using GraphPad Prism (version 7.04). In all cases, p-values of <0.05 were considered statistically significant. P-value significance levels when displayed in figures are denoted as follows: ns not significant, * $p<0.05$, ** $p<0.01$, *** $p<0.001$.

2.8.2 Experimental replicates

Biological replicates (n) in cell-based assays were defined as individual plates of cells, prepared on different days and used at different times according to the same experimental protocol. Technical replicates were included in plate-based assays as replicate wells of the same experimental condition within each plate. A minimum of three technical replicates was included in each plate-based experiment. In experiments involving human tissue, a biological replicate was defined as a single tissue section or sample from an individual patient. Statistical analysis was carried out on experiments with a minimum of 3 biological replicates (n=3).

2.8.3 Figures

Figures 1.1, 1.6, 1.7, 1.10, 3.1, 3.19, 4.1, 4.2, 4.9, 4.11, 5.1 and 5.14 contain components created with Biorender.com. Figures reproduced either with or without amendment from previously published works are reproduced under appropriate licencing, as specified in the figure legend. The licence for content reproduced under Creative Commons Attribution 4.0 International (CC BY 4.0) can be found at creativecommons.org/licenses/by/4.0/.

3. Chapter 3

Immunohistochemical characterisation of SAFB1 in human neurodegenerative disease

3.1 Overview

3.1.1 Chapter overview

This chapter aimed to carry out a novel characterisation of the RNA binding protein (RBP) SAFB1 in human neurodegenerative disease. Immunohistochemical staining of tissue from patient and control donors was performed and the staining patterns quantified. In neurons of control cases and patients with the non-polyQ diseases MS and PD, SAFB1 was expressed almost exclusively in the nucleus. In contrast, SAFB1 was abnormally expressed in the cytoplasm of damaged Purkinje cells of SCA patients and striatal neurons of HD patients. Overall this chapter presents the finding that SAFB1 expression in the cytoplasm of degenerating neurons is a novel pathological hallmark of human polyQ disorders.

3.1.2 Graphical abstract

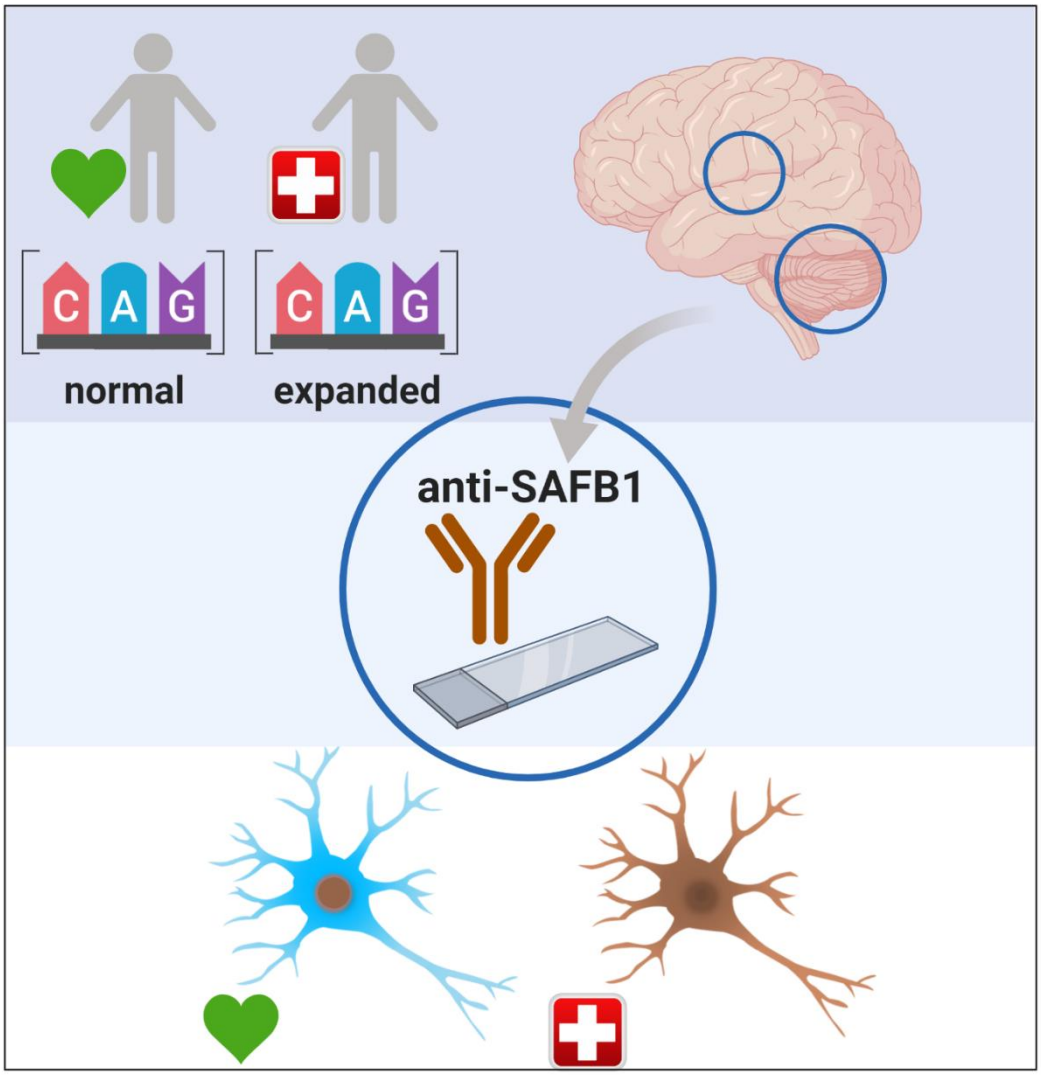

Figure 3.1 Graphical abstract for Chapter 3

3.2 Introduction

RBPs are critical for the regulation of gene expression and are highly expressed in neurons, cells which have very complex and active transcriptomes (Licatalosi and Darnell 2010, Andreassi et al. 2018). RBP dysfunction is now established as an important feature of many neurodegenerative diseases (Cookson 2017), and the preservation of RBP function is emerging as a potential approach for disease-modifying therapy (Nussbacher et al. 2019). The critical role of RBPs in neurodegenerative pathology is exemplified by mutations in TDP-43 and FUS which cause some inherited forms of ALS and FTD (Kwiatkowski et al. 2009). Pathological accumulation of TDP-43 and FUS in the cytoplasm occurs frequently in both ALS and FTD (Arai et al. 2006), which may induce a nuclear loss of function and/or cytoplasmic gain of function (Birsa et al. 2019). Recent work showed that the dual nucleic acid binding protein SAFB1 binds FUS, regulating its localisation within chromatin and being required for its splicing functions (Yamaguchi and Takanashi 2016). SAFB1 also interacts with Matrin 3, another RBP in which mutations cause familial ALS (Johnson et al. 2014).

Like TDP-43 and FUS, SAFB1 is a DRBP which is characterised structurally by the presence of an RRM motif and is highly expressed in the brain (Norman et al. 2016). SAFB1 has been shown to exert important RNA regulatory functions in neurons, including the splicing of neuronal genes, and modulation of dendritic spine formation (Rivers et al. 2015). The same study explored the RNA-binding function of SAFB1 in detail using individual-nucleotide resolution crosslinking and immunoprecipitation (iCLIP) (Figure 3.2). RNA-protein interactions of purified SAFB1 extracted from cultured cells were identified with high resolution to reveal the precise site of interaction with gene sequences. This work revealed a significant enrichment of SAFB1 iCLIP tags within the *ATXN1* gene. SAFB1 tags were localised exclusively to exon 8, both within and immediately 5’ to the *ATXN1* CAG repeat site (Rivers et al. 2015). CAG expansions in *ATXN1* cause spinocerebellar ataxia type 1 (SCA1), a polyQ disorder characterised by

severe degeneration of neurons within the cerebellum, a brain region which highly expresses SAFB1 (Norman et al. 2016).

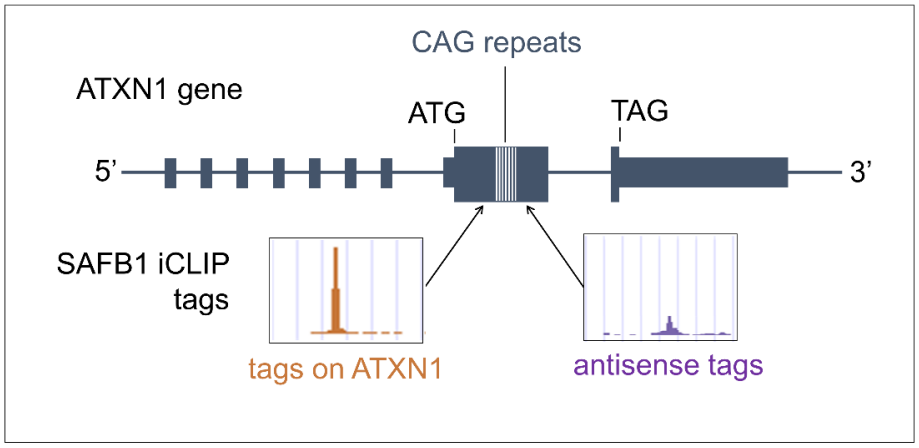

Figure 3.2 SAFB1 iCLIP tags are enriched in exon 8 of the *ATXN1* gene, both within and immediately 5' of the CAG repeat site (representation of data from Rivers et al. 2015).

Overall, SAFB1 binds RBPs directly implicated in neurodegenerative disease, is highly expressed in the human brain and cerebellum, regulates neuronal function and associates with the polyQ disease-causing gene *ATXN1*. This chapter therefore hypothesised that SAFB1 could contribute to the pathogenesis of SCA1 and potentially to other polyQ disorders such as HD. The expression of SAFB1 has not previously been characterised in the human brain or in any neurodegenerative disease. This chapter therefore aimed to carry out a detailed investigation into the expression of SAFB1 in human brain from control cases and patients with polyQ and non-polyQ neurodegenerative conditions.

3.3 Methods

3.3.1 Donor tissue

Human post-mortem tissue was collected via prospective donor schemes through the UK Brain Banks Network and utilised under local ethics approval. Formalin-fixed paraffin embedded (FFPE) sections from patients diagnosed with SCA, HD, PD and control cases with no history of neurological disease were obtained from the MRC London Neurodegenerative Diseases Brain Bank, UK. This tissue was utilised in this study under ethics approval number LNDBB1778. Cerebellar tissue sections from patients diagnosed with secondary progressive MS were obtained from the Multiple Sclerosis Tissue Bank, Imperial College, London, UK and utilised in this study under research ethics committee approval 08/MRE09/31. Post-mortem donor brain tissue was fixed in neutral buffered formalin and embedded in paraffin. Tissue sections were cut to 7-10μm and mounted onto glass slides. Clinicopathological details of donors of FFPE tissue are given in Table 3.1. Frozen striatal tissue (200mg pieces) from patients diagnosed with HD or control cases were obtained from the MRC London Neurodegenerative Diseases Brain Bank and utilised under ethics approval number LNDBB1788. Clinicopathological details for donors of frozen tissue are given in Table 3.2.

3.3.2 Immunohistochemical staining of human brain tissue

FFPE sections were immunostained with antibodies raised against SAFB1 (either A300-811A (1:50) or IHC-00142 (1:50), both Bethyl Laboratories, UK). Details of primary antibodies used for human tissue immunostaining can be found in Table 2.3. Sections were deparaffinised in Histo-clear and rehydrated in graded alcohol solutions. Antigen retrieval was carried out by microwaving slides immersed in 0.1mM sodium citrate buffer (pH 6) with 0.05% (v/v) Tween 20 until boiling. Slides were left to stand for 5 minutes, re-heated again and boiled for 1 minute, left to cool in buffer for 20 minutes and then transferred to running tap water.

Case	Brain region	Path. Diagnosis	Age (yrs)	PMD (hrs)	Sex (M/F)	Cause of death
1	Cerebellum	Control	74	66	F	Pneumonia
2	Cerebellum	Control	90	45	M	Myocardial infarction
3	Cerebellum	Control	66	78	F	Metastatic colorectal cancer
4	Cerebellum	Control	65	26	M	Metastatic prostate cancer
		Mean	**73.8**	**53.8**	**50% F**	
		SEM	**5.8**	**11.5**		
5	Cerebellum	SCA1	76	24	M	Cancer (unknown primary)
6	Cerebellum	SCA	54	31.5	F	Not available
7	Cerebellum	SCA	68	48	M	Not available
8	Cerebellum	SCA	74	33	F	Not available
9	Cerebellum	SCA	86	Not available	M	Bronchopneumonia
		Mean	**71.6**	**34.1**	**60% F**	
		SEM	**5.3**	**5**		
10	Striatum	Control	51	33	F	Lung cancer
11	Striatum	Control	63	23	M	Colon cancer
12	Striatum	Control	89	43	F	Cancer
13	Striatum	Control	85	45	M	Urethrial cancer
14	Striatum	Control	65	26	M	Metastatic prostate cancer
15	Striatum	Control	82	47	M	Congestive cardiac failure
16	Striatum	Control	84	34	F	Sepsis; metastatic breast cancer
		Mean	**74.1**	**35.9**	**43% F**	
		SEM	**5.4**	**3.6**		
17	Striatum	HD (grade 2)	83	55	F	Myocardial infarction
18	Striatum	HD (grade 2)	79	26	M	Huntington’s disease
19	Striatum	HD (grade 3)	54	19	M	Huntington’s disease
20	Striatum	HD (grade 3)	57	66	F	Bronchopneumonia
21	Striatum	HD (grade 3)	83	24	F	Not available
22	Striatum	HD (grade 4)	64	47	M	Not available
23	Striatum	HD (grade 4)	55	60	F	Not available
24	Striatum	HD (grade 4)	79	45	F	Acute myocardial infarction
		Mean	**69.3**	**42.8**	**63% F**	
		SEM	**4.6**	**6.3**		

Table 3.1 Clinicopathological details for donors of FFPE tissue (continued next page)

Case	Brain region	Path. Diagnosis	Age (yrs)	PMD (hrs)	Sex (M/F)	Cause of death
25	Cerebellum	MS	78	5	F	Metastatic bronchial carcinoma
26	Cerebellum	MS	64	7	F	GI bleed, aspirational pneumonia
27	Cerebellum	MS	49	31	F	Chronic renal failure, heart disease
28	Cerebellum	MS	49	7	F	Bronchopneumonia
		Mean	**60**	**12.5**	**100% F**	
		SEM	**7**	**6.2**		
29	Substantia nigra	Control	85	45	M	Not available
30	Substantia nigra	Control	82	47	M	Not available
		Mean	**83.5**	**46**	**100% M**	
		SEM	**1.5**	**1**		
31	Substantia nigra	PD	80	20	M	Not available
32	Substantia nigra	PD	65	26	M	Not available
		Mean	**72.5**	**23**	**100% M**	
		SEM	**7.5**	**3**		

Table 3.1 Clinicopathological details for donors of FFPE tissue (continued from previous page)

Case	Brain region	Path. Diagnosis	Age (yrs)	PMD (hrs)	Sex (M/F)	Cause of death
33	Striatum	Control	67	26	M	Prostate cancer
34	Striatum	Control	63	51	M	Colon cancer
35	Striatum	Control	82	25	M	Not available
36	Striatum	Control	91	103	F	Cardiac failure
37	Striatum	Control	92	9	F	Not available
38	Striatum	Control	84	53	F	Myocardial infarction
39	Striatum	Control	82	47	M	Cardiac failure
40	Striatum	Control	66	50	F	Not available
41	Striatum	Control	76	20	F	Kidney cancer
42	Striatum	Control	90	70	M	Myocardial infarction
		Mean	**79.3**	**45.4**	**50% F**	
		SEM	**3.4**	**8.7**		
43	Striatum	HD	48	65	F	Not available
44	Striatum	HD (grade 3)	70	33	M	Sepsis
45	Striatum	HD (grade 3)	31	54	F	Not available
46	Striatum	HD (grade 3)	68	72	M	Chest infection
47	Striatum	HD (grade 4)	29	102	F	Huntington's disease
48	Striatum	HD	83	24	F	Not available
		Mean	**54.8**	**58.3**	**67% F**	
		SEM	**9.1**	**11.5**		

Table 3.2 Clinicopathological details for donors of frozen striatal tissue

Endogenous peroxidases were neutralised by incubating sections for 15 minutes in 1% hydrogen peroxide diluted in distilled water. Immunohistochemical staining was carried out using an avidin-biotin complex staining kit (Vectastain Elite ABC HRP Kit (Peroxidase, Universal), PK-6200, Vector Laboratories). After washing in phosphate-buffered saline (PBS pH 7.4) with 0.05% Triton X-100 (v/v), non-specific binding was blocked using normal horse serum (Vectastain blocking solution) diluted 1:100 in PBS-T for 45 minutes. Sections were incubated with primary antibody diluted in blocking solution overnight at 4^{o}C. Sections incubated in antibody diluent only served as no primary antibody controls. Sections were washed in PBS, then incubated in secondary antibody (Vectastain biotinylated horse anti-rabbit/mouse, 1:50) diluted in Vectastain blocking solution. Following PBS washes, sections were incubated in ABC reagent (Vectastain Elite ABC Reagent, 1:50), and antibody binding was visualised using 3,3'-diaminobenzidine (DAB) (Vectorlabs DAB substrate kit, no nickel). After washing in distilled water, nuclei were counterstained in Ehrlich's haematoxylin, before rinsing slides in running tap water. Sections were dehydrated in graded alcohol solutions, cleared in xylene and mounted under glass coverslips using DPX mountant.

3.3.3 Immunofluorescent labelling of human brain tissue

FFPE sections were dewaxed in Clearene, immersed in 100% alcohol then washed in running tap water for 10 minutes. Antigen retrieval was carried out as described for immunohistochemical staining. Slides were washed in running tap water, then in PBS. Protein block was carried by incubating with protein blocking solution (10% normal goat serum diluted in PBS with 0.01% Triton X-100 (v/v)) for 1 hour at room temperature. Cerebellar sections were double immunolabelled with rabbit anti-SAFB1 (1:200) (A300-811A, Bethyl Laboratories), and either mouse anti-calbindin-D-28K (1:500) (Sigma-Aldrich, UK) or mouse anti-SMI-34 (hyperphosphorylated neurofilament, 1:500) (Covance, US). Striatal sections were double labelled with anti-SAFB1 and anti-polyQ (1:1000) (1C2, Millipore). Sections were incubated in primary antibodies diluted in blocking solution overnight at 4^{o}C. Sections

were washed in PBS before incubation with fluorescently conjugated secondary antibodies diluted in blocking solution for 1 hour at room temperature, protected from light (Alexa Fluor 488 goat anti-mouse (1:500) or Alexa Fluor 555 goat anti-rabbit (1:500) (Invitrogen)). Sections were washed in PBS, then incubated with DAPI for 5 minutes (1µg/ml in PBS) (ThermoFisher Scientific). Following a final PBS wash, sections were mounted in 50% PBS/50% glycerol under glass coverslips sealed with clear nail varnish. Slides were stored at 4^{o}C in the dark and imaged within 1 week.

3.3.4 Analysis of SAFB1 immunohistochemistry in cerebellar Purkinje cells

Prior to all immunohistochemical analysis, sections were coded, and the investigator blinded to their identity by covering the slide label with opaque coloured tape. To analyse DAB immunolabelling of SAFB1 in Purkinje cells, cerebellar sections were scanned using an Aperio Scanscope digital slide scanner. The Purkinje cell layer was traced, and the distance measured using annotation tools within Aperio ImageScope software (Figure 3.3A and B). Purkinje cells were identified by their characteristic morphology and localisation within the cerebellar sections. The number of Purkinje cells was counted and normalised to the total length of the Purkinje cell layer to obtain a count of Purkinje cells per unit length (mm) (Figure 3.3E). The perikaryon of each Purkinje cell that had a clearly visible nucleus was traced and the area in µm^2 of each perikaryon measured. Each Purkinje cell was individually graded as either positive or negative for SAFB1 immunoreactivity within the nucleus and cytoplasm (Figure 3.3F). This methodology was based on that previously described by Kemp et al. (2016).

3.3.5 Analysis of SAFB1 immunohistochemistry in cerebellar white matter neurons

To analyse DAB immunolabelling of SAFB1 in large neurons within cerebellar white matter, the dentate nucleus was identified at low microscopic magnification as a characteristic grey matter ribbon running through the cerebellar white matter (Figure 3.3C). Images were taken at regular intervals along the whole of the dentate nucleus tissue tract within

each section. A minimum of 15 images were acquired per section. Large principle neurons were identified within each image by their characteristic size and morphology and graded as either positive or negative for SAFB1 immunoreactivity within the nucleus and cytoplasm.

3.3.6 Analysis of SAFB1 immunohistochemistry in striatal neurons

To analyse DAB immunolabelling of SAFB1 in the striatum, images were captured across the whole stained striatal section using a Nikon eclipse i80 microscope with a Nikon Ci-SMS camera, and Image-Pro plus software. Between 15 and 20 regions of interest were imaged and analysed per section (Figure 3.4A). Images containing histological artefacts such as air bubbles, tears, high background staining or features such as large blood vessels were excluded from quantification. In single labelled sections immunohistochemically stained for SAFB1, cells in the striatal tissue were categorised by size as neuronal (large) or non-neuronal (small) (Figure 3.4B). To ensure the same categorisation judgement was utilised between micrographs, an initial test count across three randomly selected micrographs was carried out, and the nuclear diameter of cells categorised as either large or small was recorded. During staining quantification, a scale bar equal to the smallest nuclear diameter categorised as large/neuronal was used to categorise any cells which were of indeterminate size. Large/neuronal cells containing SAFB1 staining in either the nucleus or the cytoplasm were counted manually using ImageJ software.

In tissue dual labelled for SAFB1 and polyQ by immunofluorescence, sections were imaged using a Nikon C1 confocal microscope with EZ viewer software. Ten micrographs were captured and analysed per section (Figure 3.4C). The number of neurons positive for polyQ inclusions was counted, and within this cell population the number of cells positive for SAFB1 in the cytoplasm was counted.

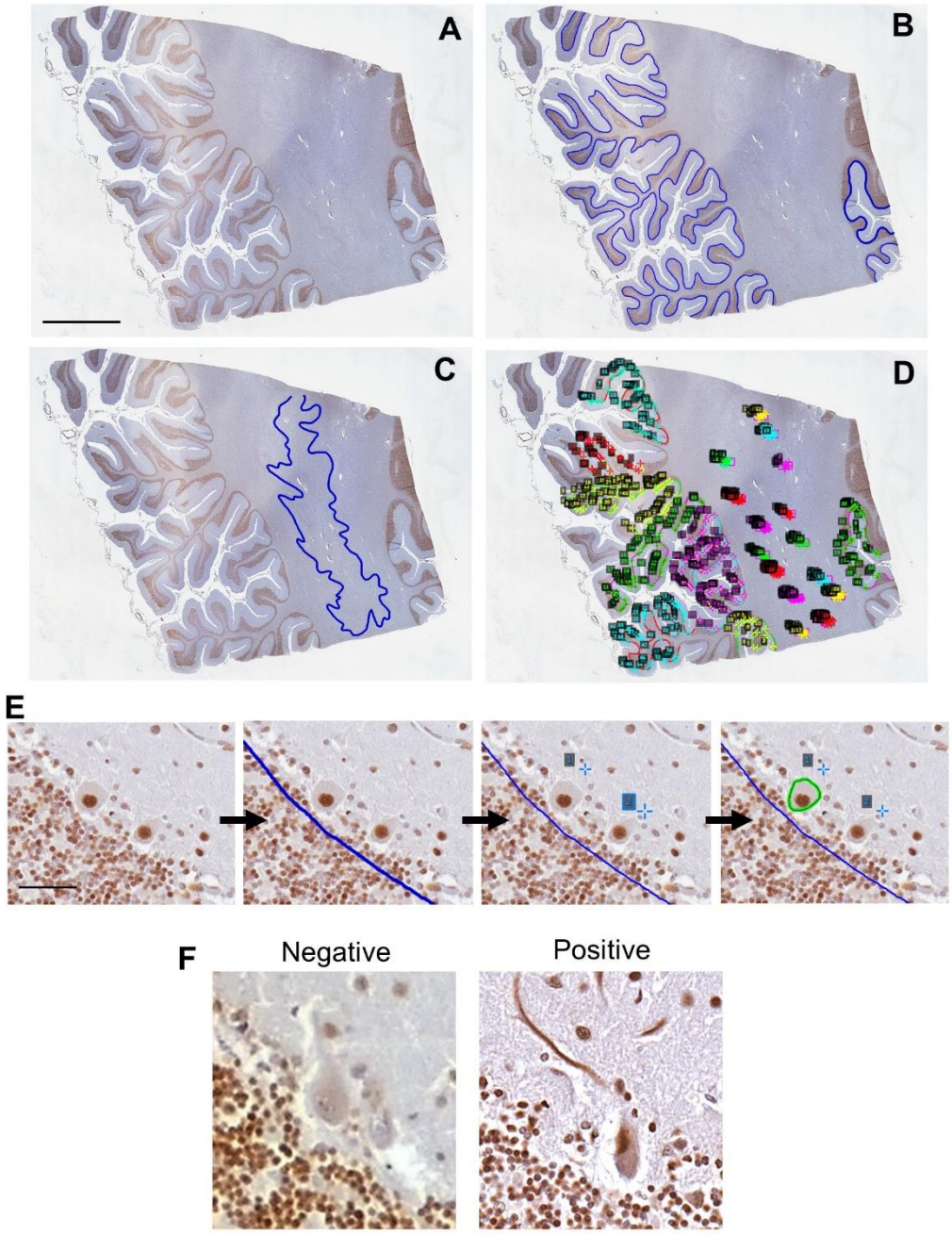

Figure 3.3 Method for analysis of cerebellar sections immunostained for SAFB1. **A**) Whole human cerebellar section stained for SAFB1 and counterstained with haematoxylin (scale bar is 5mm). The Purkinje cell layer (**B**) and dentate nucleus (**C**) are highlighted in blue. **D**) Purkinje and dentate cell measurement annotations. **E**) Magnified section of cerebellar tissue featuring annotations to measure the length of the Purkinje cell layer, count individual cells, and measure the cross sectional area of the cell soma (scale bar is 50µm). **F**) Purkinje cells negative and positive for SAFB1 staining in the nucleus and cytoplasm. Note the dystrophic morphology observed within the SAFB1 positive cell.

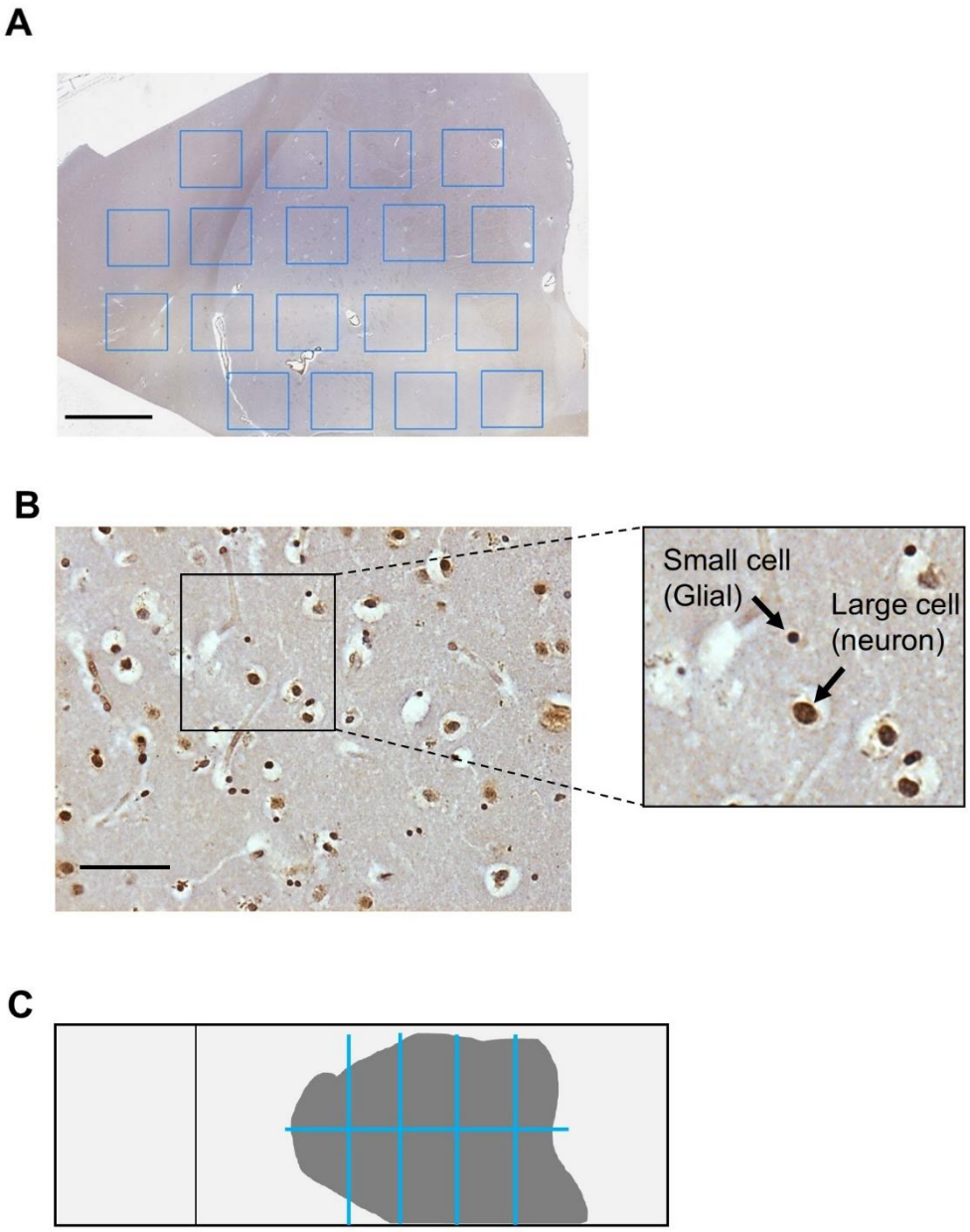

Figure 3.4 Method for analysis of striatal sections immunostained for SAFB1. **A**) Whole human striatal section immunostained with SAFB1 counterstained with haematoxylin. Blue boxes represent example of regions of interest across the section, within which an image was captured for quantification (scale bar is 5mm). **B**) Sample image of striatum immunostained for SAFB1 (scale bar is 75µm). Magnified region with annotation showing the appearance of both small and large cell nuclei within the tissue. **C**) Illustration of a whole striatal section mounted on a slide. Blue lines show the delineation of the sections and the regions of interest that were labelled using immunofluorescent techniques. An image was taken within each region using a confocal microscope for quantification.

3.3.7 RNA and protein extraction from human striatum

Frozen samples of human striatum were processed under RNase-free conditions using a mirVana PARIS kit (Life Technologies). All surfaces and materials in contact with tissue were treated with RNaseZap (ThermoFisher Scientific) and all plasticware was RNase-free. Samples of striatum weighing 200mg were removed from -80ºC storage on dry ice and ground to a course powder using a pre-chilled granite pestle and mortar. Tissue was bathed in liquid nitrogen to ensure that the sample remained completely frozen. Powdered tissue was rapidly transferred into 700µl of pre-chilled cell disruption buffer, mixed, and homogenised using a chilled 2ml glass tissue homogeniser. Half the volume was used for RNA extraction and half for protein extraction. Extraction of total RNA was carried out in accordance with the mirVana PARIS kit manufacturer's protocol. In brief, the sample was mixed with a denaturing solution to prevent RNA degradation, followed by organic extraction using acid-phenol chloroform. The aqueous phase was precipitated with ethanol, and RNA isolated by centrifuging the sample through a proprietary filter cartridge. After washing the filter, RNA was eluted in 100µl of pre-warmed nuclease-free water and stored at -80ºC. Tissue homogenate reserved for protein extraction was incubated on ice for 5 minutes before repeatedly passing the sample through a sterile needle to reduce viscosity. Samples were centrifuged at 14000 rpm at 4ºC for 15 minutes and the cell debris pellet discarded. Protein lysates were quantified by BCA assay and stored at -80ºC.

3.3.8 Analysis of striatal SAFB1 protein by Western blotting

Protein denaturation was carried out by combining 50µg of extracted striatal protein with 2xSDS sample buffer and heating at 95ºC for 5 minutes. Samples were resolved on an 8% polyacrylamide gel by electrophoresis, before transferring onto a polyvinylidene difluoride (PVDF) membrane using a Trans-blot Turbo Transfer System (Bio Rad). Protein bound to the membrane was blocked in 5% (w/v) skimmed milk in PBS for 1 hour at room temperature, before incubating with anti-SAFB1 antibody (A300-811A, Bethyl Laboratories) diluted 1:1000 in 1% (w/v) milk overnight at 4ºC. After

washing, the membrane was incubated in peroxidase-linked secondary antibody (Table 2.4) diluted in 1% skimmed milk for 1 hour at room temperature. After washing, protein bands were visualised using enhanced chemiluminescence (Amersham ECL Prime Western Blotting Detection Reagent, GE Healthcare). Digital images were quantified using densitometric analysis in Image Studio Lite (Licor). The density of each SAFB1 protein band was normalised against total SAFB1 (according to BCA assay results) to obtain a relative quantification of SAFB1 protein for each striatal tissue sample.

3.3.9 Analysis of striatal SAFB1 mRNA by qPCR

RNA extracted from striatal tissue samples was reverse transcribed into cDNA with oligoDT primers using a GoScript Reverse Transcription kit (Promega). 1µl of undiluted cDNA was added to 19µl of Power SYBR Green qPCR mastermix (Thermo Fisher Scientific) containing 300nM of forward and reverse primers against SAFB1 or beta-actin (Table 2.5). qPCR reactions were carried out using a StepOnePlus Real-time PCR system (Applied Biosciences). Comparative threshold (CT) analysis was carried out by normalising SAFB1 expression to housekeeping gene expression within each sample.

3.3.10 Statistical analysis

Results from immunostaining quantification did not pass Shapiro-Wilk normality testing. This, alongside the categorical nature of staining quantification, indicated that statistical analysis should be carried out non-parametrically. Non-parametric comparisons between two groups were performed using Mann-Whitney tests. Non-parametric correlative analysis was carried out using Spearman's tests. Parametric testing was applied to normally distributed data sets, using unpaired two-tailed t-tests to compare two groups, and using Pearson's test for correlative analysis.

3.4.1 the anti-SAFB1 antibody A300-811A is specific and suitable for immunostaining human brain

Investigations by our research group have established that some historic studies investigating the function of SAFB1 relied upon antibodies which were unable to differentiate between SAFB1 and SAFB2. The immunogen peptide sequence for the anti-SAFB1 antibody A300-811A (Bethyl Laboratories) shares 77% sequence homology with the equivalent epitope region of SAFB2, indicating a possibility of cross-reactivity (Table 3.3). With this in mind, we previously validated that A300-811A specifically detects SAFB1 (Rivers et al. 2015). The first aim of this chapter was to confirm that this antibody was appropriate for analysing SAFB1 expression in human tissue.

Prior to carrying out staining in human tissue, antibody specificity was tested using an siRNA knockdown approach based on the Rimm Algorithm for antibody specificity (Bordeaux et al. 2010). HeLa cells transfected with siRNA against SAFB1 or SAFB2 were lysed and the protein run on a Western blot probed using A300-811A (Figure 3.5A). The blot showed reduced signal with SAFB1 siRNA knockdown but no change with SAFB2 siRNA in comparison to non-targeting control (NTC) transfected and control (untransfected) samples (Figure 3.5A). This result confirmed that A300-811A does not cross-react with the closely related protein SAFB2.

To ensure that immunostaining in human tissue visualised by both DAB and fluorophores was specific to antibody binding and not background tissue reactivity, sections incubated without antibody were included in each immunostaining experiment as a negative control. Representative images of control staining are shown in Figure 3.5B and C. Sections without primary antibody were negative for DAB staining (Figure 3.5B). Representative images from a cerebellar section with primary antibody omitted shows minimal non-specific auto-fluorescent signal in this tissue (Figure 3.5C). The auto-fluorescent properties of striatal tissue sections are further discussed

in section 3.4.7. Overall these results show that antibody A300-811A is specific for SAFB1 in human tissue.

Antibody	Immunogen	Immunogen peptide sequence	homology of immunogen with human SAFB2	homology of immunogen with mouse SAFB1
Bethyl IHC 00142	Amino acids 875 – C-terminal end of human SAFB1	GSFAPGGASRGH PIPHGGMQGGFG GQSRGSRPSDAR FTRRY	46%	93%
Bethyl A300-811 A	Amino acids 775-825 of human SAFB1	REGQHYPERHGG PERHGRDSRDGW GGYGSDKRMSEG RGLPPPPRRDWG DHG	77%	92%

Table 3.3 Immunogen properties of commercially available polyclonal antibodies raised against human SAFB1

3.4.2 SAFB1 is expressed in the cytoplasm of damaged Purkinje cells in SCA1

Previous data obtained by our research group demonstrated the interaction between SAFB1 protein and *ATXN1* RNA using iCLIP. A CAG expansion mutation in the *ATXN1* gene causes the polyQ disorder SCA1, therefore the initial investigation in this chapter characterised the expression of SAFB1 in the cerebellum of a SCA1 patient in comparison to a control case with no history of neurological disease (Figure 3.6). In both control and SCA1 cerebellum, frequent SAFB1 immunoreactivity was observed within the nuclei of cells within the granular and molecular layers of the folia (Figure 3.6). In control tissue, SAFB1 staining in Purkinje cells was almost always limited to within the nuclei, where it presented in a diffuse pattern spread throughout the nucleus (Figure 3.6).

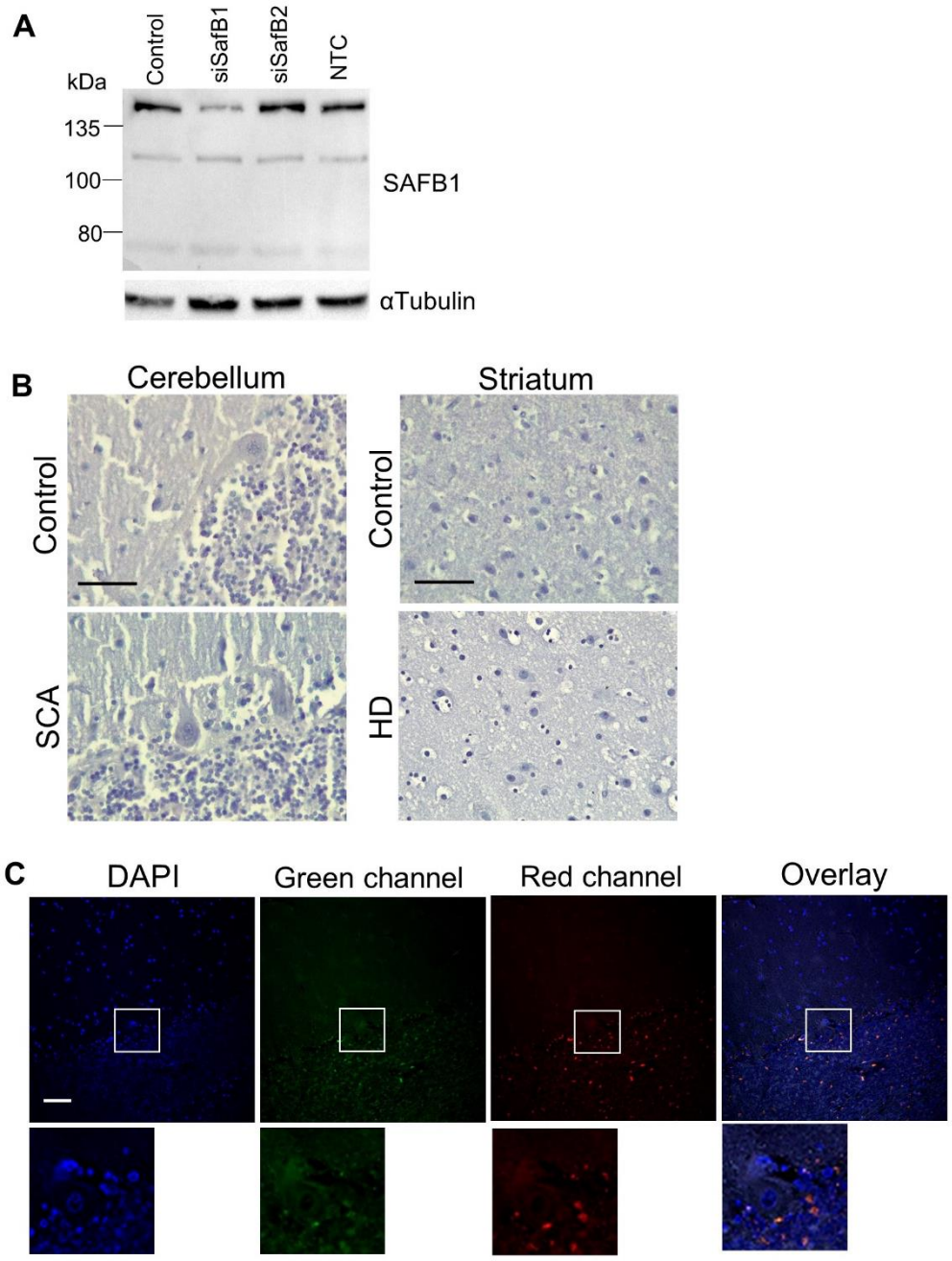

Figure 3.5 Control studies for SAFB1 antibody staining. **A**) Western blot of lysates from HeLa cells (either non-transfected (control), siRNA knockdown of SAFB1, knockdown of SAFB2 or non-targeting control (NTC)), probed with anti-SAFB1 antibody (A300 811-A, Bethyl). The antibody detected a reduction in expression of SAFB1 but did not detect a change in SAFB2 indicating specificity for SAFB1 (uppermost bands). **B**) Cerebellum and striatum from control and disease patients immunohistochemically stained with no primary antibody were negative for DAB reactivity. Scale bars are 100µm. **C**) Cerebellar tissue immunofluorescently stained with no primary antibody. There was some minimal autofluorescence in the granule cell layer, but no non-specific fluorescence in Purkinje cells. White boxes indicate magnified region highlighting a Purkinje cell. Scale bar is 100µm.

In SCA1 Purkinje cells SAFB1 immunoreactivity was frequently present in both the nucleus and within the cytoplasm of the perikaryon and dendrites (Figure 3.6). Cytoplasmic SAFB1 staining was evident in SCA1 Purkinje cells with mild, moderate and substantial morphological alterations indicating increasing severity of neurodegenerative injury (Figure 3.6). It has been previously established that under normal conditions, SAFB1 protein is localised to within the nucleus (Norman et al. 2016, Hashimoto et al. 2020), therefore the presence of cytoplasmic staining in damaged Purkinje cells was considered a novel and unusual finding and prompted further investigation.

3.4.3 Cytoplasmic accumulation of SAFB1 in SCA is a novel histopathological hallmark

Post-mortem cerebellar tissue from patients with a neuropathological diagnosis of SCA was compared against a control group of patients with no history of neurological disease (Table 3.1). There was no significant difference in patient age ($t(7)=0.27$, $p=0.79$) or post-mortem delay (PMD) ($t(6)=1.57$, $p=0.17$) between groups (unpaired, two-tailed t-tests). The neuropathological findings of the patient autopsies are summarised in Table 3.4.

SAFB1 expression in Purkinje cells was quantified by counting the percentage of cells positive for SAFB1 (Figure 3.7). The percentage of control Purkinje cells with nuclear SAFB1 immunopositivity ranged between 57% and 83%, which was not significantly different compared to SCA patient cerebellum which ranged between 50% and 99% (Figure 3.7B). There was, however, a significantly higher percentage of Purkinje cells with cytoplasmic SAFB1 staining in SCA patients (between 14% and 80%) compared to controls (between 0.6% and 3.1%) (Figure 3.7C). There was substantial loss of Purkinje cell numbers and reduction in the cross-sectional area of Purkinje cell soma in SCA patients compared to control cases (Table 3.5).

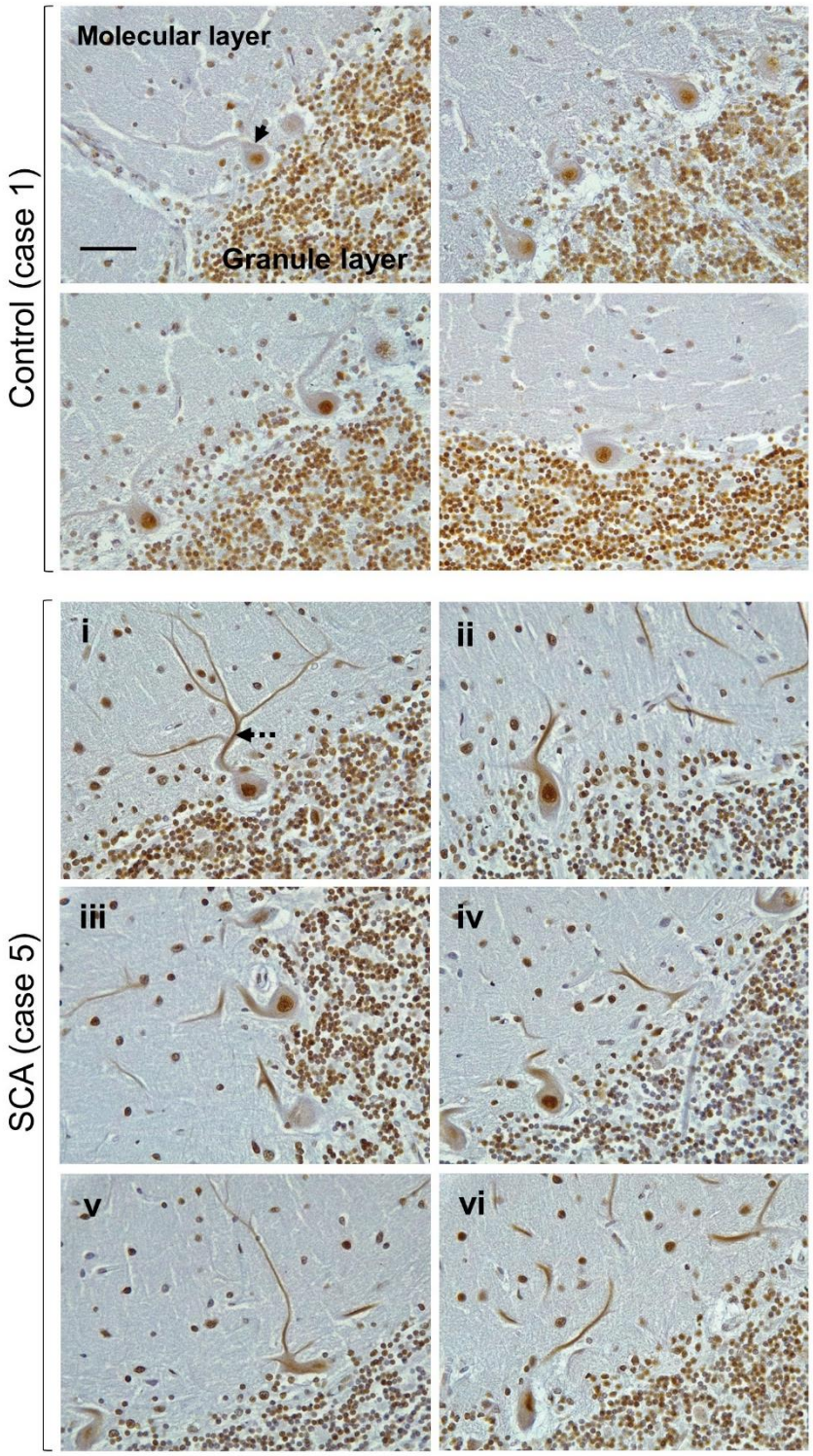

Figure 3.6 SAFB1 is abnormally expressed in the cytoplasm of Purkinje cells in SCA1**.** Representative images of cerebellar tissue from a control case and SCA1 patient immunostained for SAFB1. In control cerebellum, Purkinje cells often featured SAFB1 immunostaining within the nucleus, but cytoplasmic SAFB1 staining was not present (arrow). In SCA1 cerebellum, Purkinje cells had cytoplasmic SAFB1 staining in the soma and dendrites (dotted arrow) in addition to strong nuclear staining. Cytoplasmic SAFB1 staining appeared in SCA1 Purkinje cells with mild (**i-ii**), moderate (**iii-iv**) and substantial (**v-vi**) morphological alteration in comparison to control Purkinje cells. Scale bar is 50µm.

			Cerebellar neuropathological findings			
Case	Path. diagnosis	Genetic diagnosis	Purkinje cells	Dentate nucleus	Granule cells	PolyQ positivity?
5	SCA1	SCA1	Depleted, with shrinkage of remaining cells	Atrophy/ shrinkage of neurons	Reduction in density	Staining not carried out
6	SCA (A.D.)	Not available	Severe loss, with severe shrinkage of remaining cells. No torpedoes.	Some loss and shrinkage of neurons	Reduction in density	Staining not carried out
7	SCA	Not available	Depleted with empty baskets. No torpedoes	Atrophy/ shrinkage of neurons	Reduction in density	Staining not carried out
8	SCA	Not available	Depleted, with heterotypic PCs in granule cell layer. No P62 positivity. PolyQ positivity in surviving PCs.	Atrophy/ shrinkage of neurons	P62 positive inclusions	Strong polyQ staining in surviving PCs
9	SCA	Not available	Severe loss, with severe shrinkage of remaining cells.	Some loss and shrinkage of neurons	Reduction in density	Staining not carried out

Table 3.4 Diagnoses and cerebellar neuropathological findings summarised from the autopsies of SCA patients included in this study**.** A.D. autosomal dominant, PC Purkinje cells.

Axonal torpedoes (swellings) in Purkinje cells are a cerebellar response to injury (Takahashi et al. 1992) which have been previously observed in SCA patients (Louis et al. 2014). In the present study, torpedoes were not observed in any SCA Purkinje cells. Visualisation of torpedoes may be occluded by the dense SAFB1 staining of the granule cell layer. Furthermore, severe Purkinje cell pathology can be associated with lower frequency of torpedoes in ataxias (Louis et al. 2014).

In addition to atrophy and loss of Purkinje cells within the cerebellar cortex, the pathology of polyQ SCA also affects the large principle neurons within the dentate nucleus (DN) of the cerebellar white matter. Notably, SAFB1 staining was not detected in the majority of dentate neurons in control cases (Table 3.6, Figure 3.8). However, there was significantly increased

expression of SAFB1 in both the nucleus (Figure 3.8A and B) and cytoplasm (Figure 3.8A & C) of DN neurons in SCA patients.

Case	Diagnosis	PCs counted	Mean PCs/mm	Nuclear SAFB1	Cytoplasmic SAFB1	Mean PC size (μm^2)
1	Control	326	2.36	226	3	775.5
2	Control	315	3.17	262	2	611.9
3	Control	321	3.05	182	10	639.2
4	Control	310	3.35	247	3	598.1
	Total or *Mean*	**1272**	***2.98***	**917**	**18**	***656.2***
5	SCA	242	1.91	241	137	556.5
6	SCA	20	0.05	18	16	202.6
7	SCA	39	0.26	30	12	386.6
8	SCA	29	0.07	20	4	451.0
9	SCA	22	0.04	11	11	308.8
	Total or *Mean*	**352**	***0.46***	**320**	**180**	***381.1***
25	MS	316	1.91	298	17	454.5
26	MS	417	2.9	404	7	494.3
27	MS	371	2.41	192	38	595.7
28	MS	208	3.26	192	6	419.8
	Total or *Mean*	**1312**	***2.62***	**1086**	**68**	***491.1***

Table 3.5 Number of cerebellar Purkinje cells (PC) with SAFB1 staining, and their morphology (PC perikaryon size) in control, SCA and MS patient tissue.

Nuclear SAFB1 staining was present in 6 - 18% of control DN neurons and 27 - 80% of SCA DN neurons, and cytoplasmic SAFB1 staining was present in 0.6 - 3.9% of control and 32 - 87% of SCA DN neurons. The DN neurons of SCA patients appeared smaller and more shrunken, and SAFB1 staining was diffuse and distributed throughout the cell bodies (Figure 3.8A), as was observed in Purkinje cells. There was, however, less DN neuron cell loss compared to that seen in the Purkinje cell population (Table 3.6). Taken together, this data shows that abnormal cytoplasmic SAFB1 expression is a feature of two neuronal populations specifically affected by polyQ-induced neurodegenerative damage in SCA.

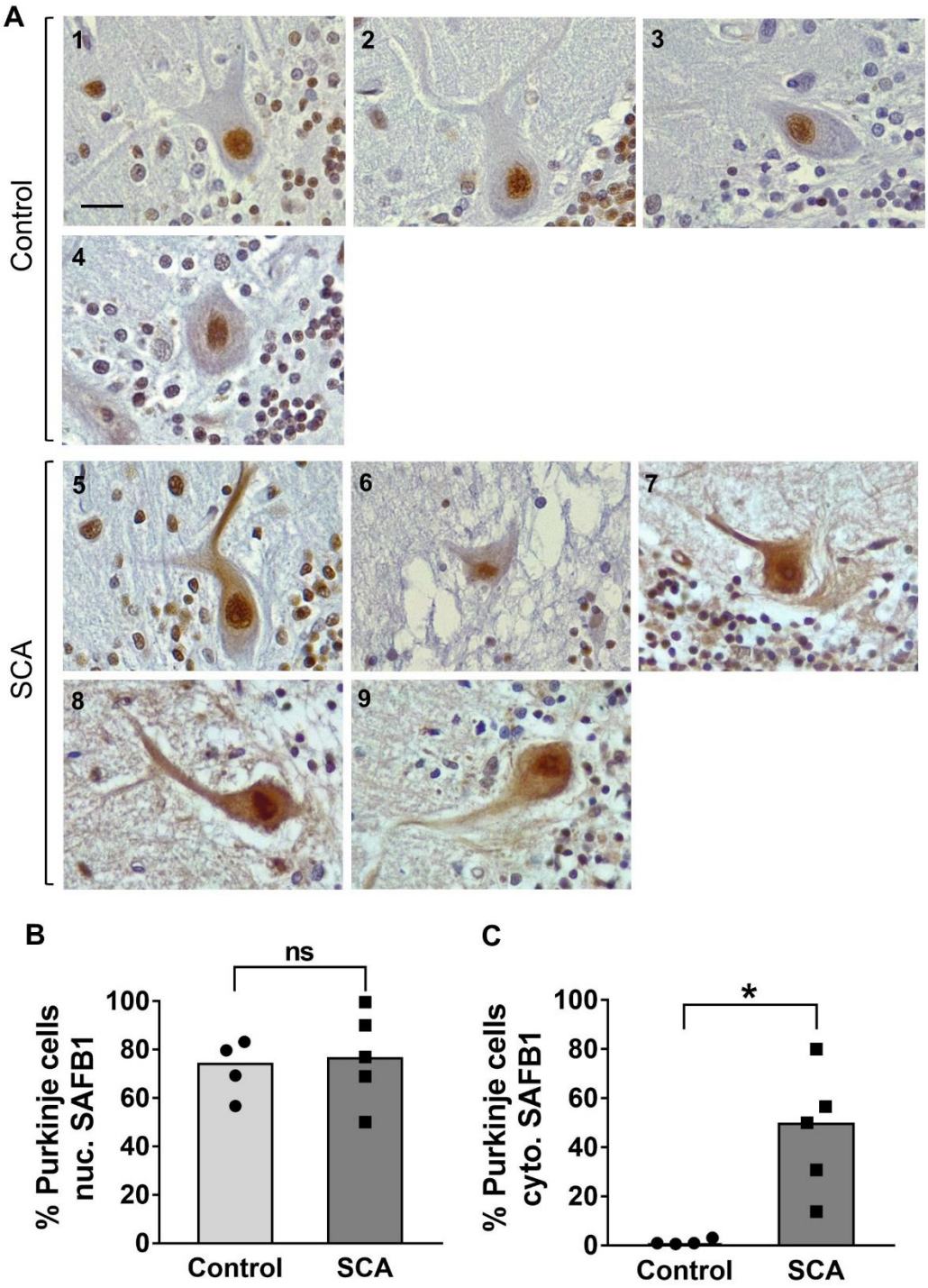

Figure 3.7 SAFB1 expressed in the cytoplasm of cerebellar Purkinje cells is a feature of SCAs. **A**) Representative images of Purkinje cells immunostained for SAFB1. In control cases (n=4), SAFB1 was expressed in the nucleus but not in the cytoplasm. In SCA patients (n=5), Purkinje cells were positive for SAFB1 in the nucleus and frequently featured abnormal SAFB1 expression in the soma and dendrites. Inset numbering represents patient case number, scale bar is 25µm. SAFB1 staining was quantified by counting the percentage of Purkinje cells with nuclear or cytoplasmic immunopositivity. **B**) There was no difference between the percentage of cells positive for nuclear SAFB1 in SCA patients compared to control. **C**) There was a significant increase in frequency of SAFB1 cytoplasmic staining in the SCA patient group compared to control ((ctl=0.94, SCA=50) U=0, p=0.02, Mann-Whitney test). ns=not significant, * $p<0.05$. Data is presented as median values.

Case	Diagnosis	DN neurons counted	Nuclear SAFB1	Cytoplasmic SAFB1
1	Control	143	21	1
2	Control	133	27	1
3	Control	126	17	4
4	Control	148	10	7
	Total	**550**	**75**	**13**
5	SCA	112	81	76
6	SCA	135	90	46
7	SCA	148	39	48
8	SCA	181	135	155
9	SCA	267	216	233
	Total	**843**	**561**	**558**

Table 3.6 Number of cerebellar dentate nuclei (DN) neurons with SAFB1 staining in control and SCA patient tissue.

To confirm that cytoplasmic SAFB1 staining in SCA was specific to Purkinje cells, dual immunofluorescent labelling was performed using antibodies against SAFB1 and calbindin-D28k (a calcium binding protein widely used as a Purkinje cell marker). Representative images show that cytoplasmic SAFB1 was present in cerebellar Purkinje cells, as determined by co-localisation with calbindin immunoreactivity (Figure 3.9A). To assess whether cytoplasmic SAFB1 expression was localised to injured or damaged Purkinje cells in SCA, cerebellar sections were dual labelled for SAFB1 and SMI-34, an antibody which recognises hyperphosphorylated neurofilament as a marker of Purkinje cell damage (Redondo et al. 2015). SCA Purkinje cells featuring hallmark morphological features of neurodegenerative injury (such as reduced perikaryon size and deflated appearance of nuclei) and positive for SMI-34 staining also contained abnormal cytoplasmic SAFB1 expression (Figure 3.9B). Dense SMI-34 staining of basket cell projections surrounding damaged Purkinje cells was noted, and has been previously described as a feature of cerebellar degeneration (Erickson-Davis et al. 2010).

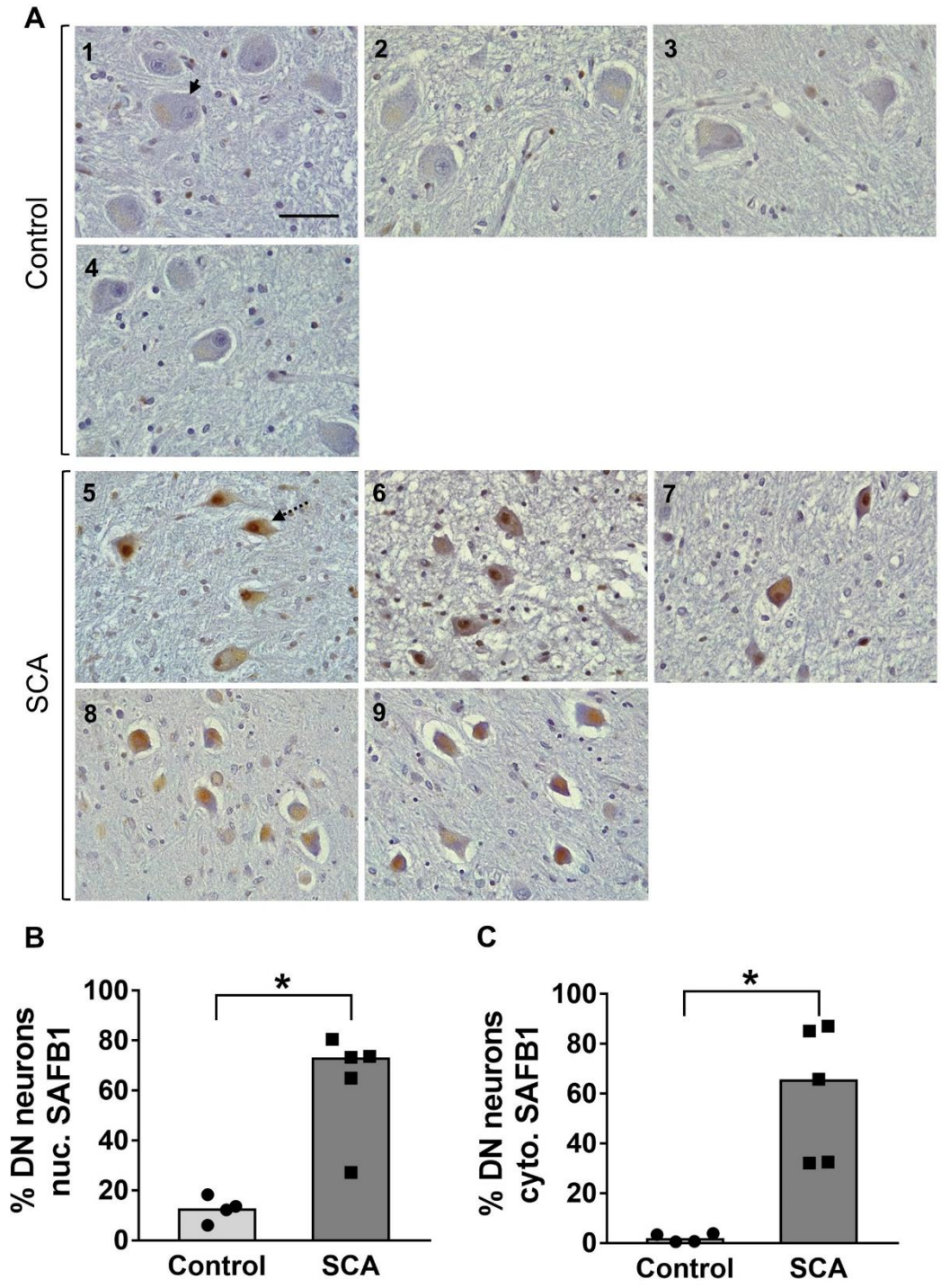

Figure 3.8 SAFB1 expression is increased in the nucleus and cytoplasm of cerebellar dentate nucleus (DN) neurons in SCA patients. **A**) Representative images of cerebellar DN immunostained for SAFB1 show large principle neurons (identifiable by their morphology) within the neuropil of the DN in control (n=4) and SCA (n=5) cases (arrow). Cells within SCA patient DN appeared smaller and shrunken (dotted arrow) and showed increased nuclear and cytoplasmic SAFB1 expression. Numbering represents patient case number, scale bar is 50µm. (continued next page).

Figure 3.8 (continued from previous page) SAFB1 Immunoreactivity expressed as the percentage of large principle neurons positive for SAFB1 in either the nucleus or the cytoplasm. **B**) In SCA patients, a significantly higher percentage of neurons were positive for SAFB1 within the nuclei compared to control cases ((ctl=12.94, SCA=59.31) U=0, p=0.02, Mann-Whitney test). **C**) Cytoplasmic SAFB1 was expressed in a significantly higher percentage of neurons of SCA patients compared to control cases ((ctl=2, SCA=65.8) U=0, p=0.02, Mann-Whitney test). * p<0.05. Data is presented as median values.

3.4.4 Cytoplasmic SAFB1 expression correlates to a measure of Purkinje cell injury in SCA

The neuropathology of polyQ SCAs has been well characterised and frequent pathological hallmarks include a reduction in Purkinje cell number and size (Koeppen 2005, Babij et al. 2013). Across the SCA patient cases analysed in this study, there was a reduction in the number of Purkinje cells per mm length of the cell layer, and in Purkinje cell size, compared to control (Table 3.5).

To determine whether there was a relationship between Purkinje cell histopathological characteristics and the frequency of SAFB1 staining, correlative analysis was carried out (Figure 3.10). There was no significant correlation between Purkinje cell perikaryon area and nuclear SAFB1 staining (Figure 3.10A). However, there was a significant correlation between cytoplasmic SAFB1 staining and Purkinje cell perikaryon area (Figure 3.10B). Increasing frequency of abnormal SAFB1 in the cytoplasm was associated with Purkinje cell injury, as measured by shrinkage of the cell soma and loss of cell number. In a single SCA case (case 5), who died as a result of cancer, there was a larger number of surviving Purkinje cells (compared to four other SCA patients, Table 3.5) and over 56% of these cells stained positive for cytoplasmic SAFB1.

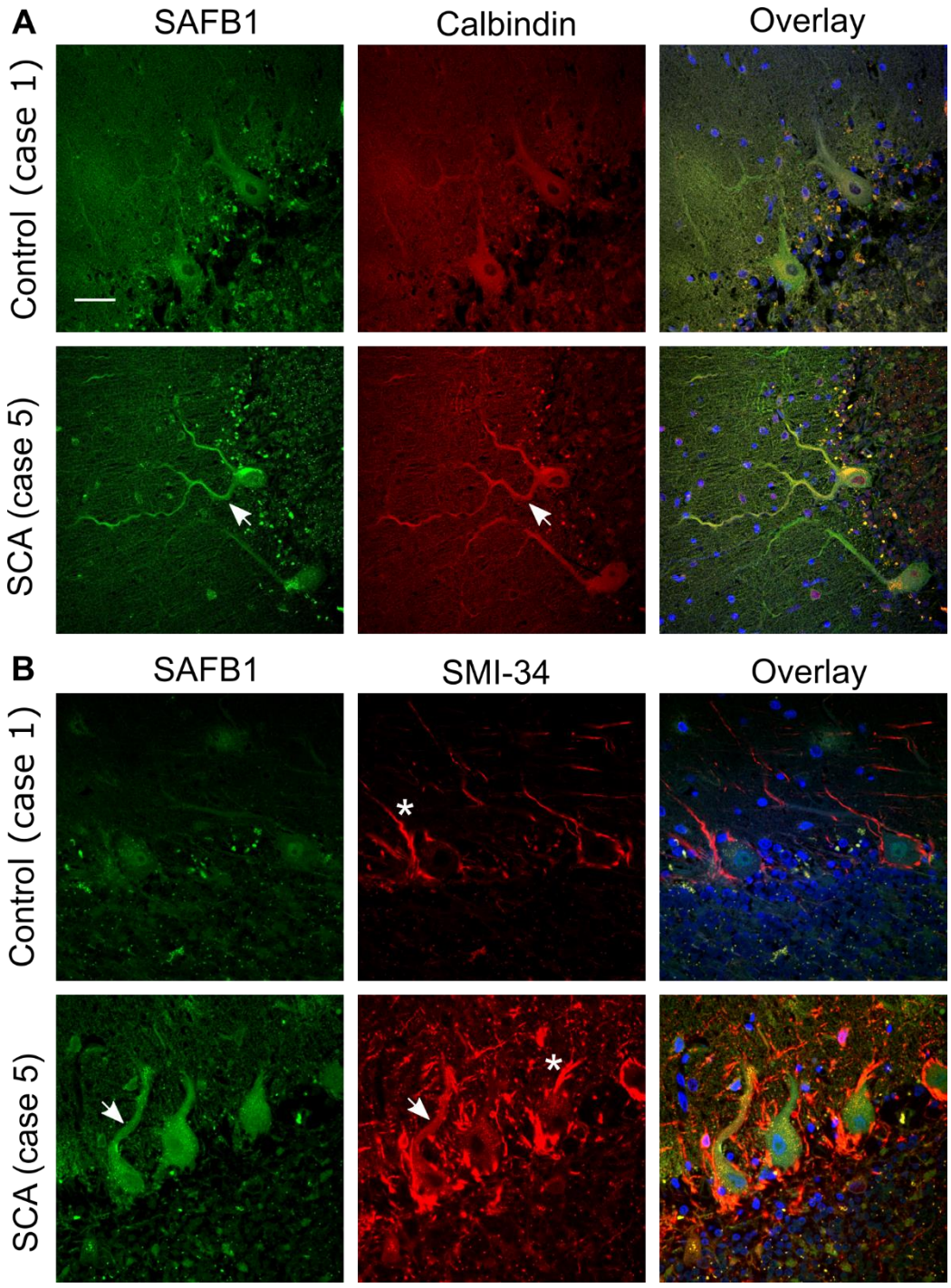

Figure 3.9 Cytoplasmic SAFB1 in SCA Purkinje cells colocalises with calbindin and SMI-34. **A**) Calbindin immunopositivity specifies Purkinje cell soma and dendrites. SAFB1 staining was absent from the cytoplasm of control Purkinje cells but colocalised with calbindin in SCA (arrows). (**B**) SMI-34 staining, a marker of Purkinje cell damage, colocalised with SAFB1 in the soma and dendrites of SCA cerebellum (arrows) but not in control tissue. SMI-34 also stained basket cell projections (asterisks), which appear hypertrophied in SCA. Cell nuclei were stained using DAPI (blue). Scale bar is 50µm.

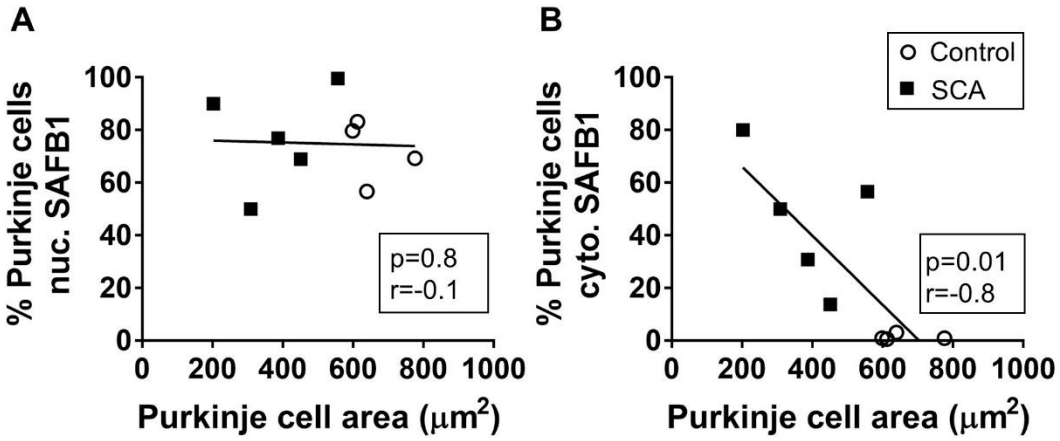

Figure 3.10 Abnormal cytoplasmic SAFB1 expression is associated with reduced Purkinje cell size. **A**) There was no significant correlation between SAFB1 staining in the nucleus and Purkinje cell area. **B**) Increased frequency of cytoplasmic SAFB1 expression is correlated with a decrease in Purkinje cell perikaryon area. P and r values were calculated by performing Spearman correlation tests.

3.4.5 Cytoplasmic SAFB1 expression is not a feature of non-polyQ diseases

To assess whether abnormal cytoplasmic SAFB1 expression is specifically associated with Purkinje cell injury induced by polyQ disease, cerebellar tissue sections from four patients diagnosed with multiple sclerosis (MS) were immunolabelled for SAFB1 (Figure 3.11). MS causes Purkinje cell damage and degeneration (Redondo et al. 2015, Wilkins 2017), but this is not caused by polyQ pathology. Analysis of Purkinje cells across whole cerebellar sections including those with both normal and dystrophic phenotypes showed that SAFB1 immunostaining was confined to the nucleus, following the same pattern to that of control patients (Figure 3.11, Table 3.5).

To further investigate SAFB1 expression in non-polyQ neurodegenerative disease, substantia nigra from two patients with PD was compared to two control patients (Figure 3.12). Overall, SAFB1 immunoreactivity was much lower in this area compared to the striatum and cerebellum, but where staining was present SAFB1 was confined to the nuclei. There was no

difference in the SAFB1 staining pattern in the substantia nigra of PD patients compared to control (Figure 3.12). This finding further demonstrates that abnormal SAFB1 expression in the cytoplasm is associated specifically with polyQ-associated injury in neurons.

3.4.6 SAFB1 accumulates in the cytoplasm of striatal neurons in HD

As SAFB1 has not previously been characterised in human polyQ disorders, its expression was next investigated in HD, the most common neurodegenerative disease caused by CAG expansion (Figure 3.13). Post-mortem striatal tissue was obtained from a cohort of patients diagnosed with HD (ranging between Vonsattel grade 2-4) and from control cases with no history of neurological disease (Table 3.1). There was no significant difference in age ($t(13)=0.69$, $p=0.5$) or P MD ($t(13)=0.92$, $p=0.38$) between groups (unpaired, two-tailed t-tests).

SAFB1 immunostaining was present within the nuclei of cells throughout striatal sections (Figure 3.13A). There was a significant increase in nuclear SAFB1 staining in HD patients compared to control striatum (Figure 3.13B). In control patients, between 18 - 60% of cells were positive for SAFB1 in the nucleus whereas in HD patients nuclear SAFB1 positivity ranged from 61 - 87%.

Cytoplasmic SAFB1 staining in HD cases was of greater intensity and present in significantly more cells in the striatum of HD patients compared to controls (Figure 3.13A and C). In control striatum, the frequency of cells positive for cytoplasmic SAFB1 ranged from 5 - 19%, whereas between 23 - 68% of cells in HD patient tissue contained cytoplasmic SAFB1 staining (Figure 3.13C). The numbers of striatal neurons counted are recorded in Table 3.7

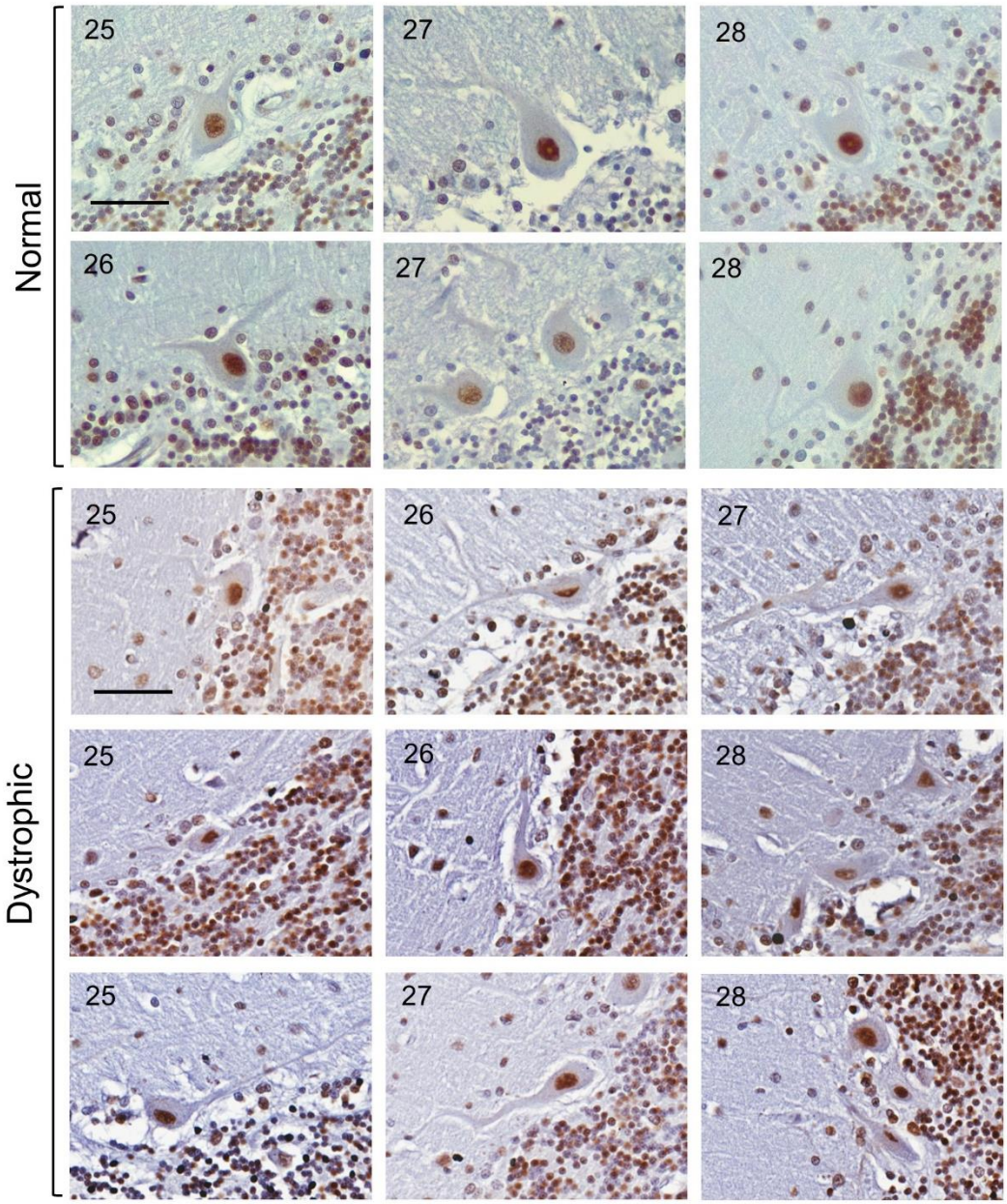

Figure 3.11 SAFB1 expression is unaltered in MS patient Purkinje cells. Cerebellar Purkinje cells in patients with MS immunostained for SAFB1 (representative images from n=4 patients, inset number represents patient case, scale bar is 25µm). SAFB1 staining within Purkinje cells with both morphologically normal and dystrophic phenotypes was nuclear without immunoreactivity in the cytoplasm of the cell soma or dendrites. The percentage of Purkinje cells positive for SAFB1 staining in the nucleus in each patient group are as follows (mean ± SEM); Control (72.09 ± 4.8), MS (83.3 ± 10.7), SCA (77.1 ± 8.6). The percentage of Purkinje cells positive for SAFB1 in the cytoplasm per group are as follows; Control (1.7 ± 0.5), MS (5.1 ± 1.9) SCA (46.2 ± 11.3).

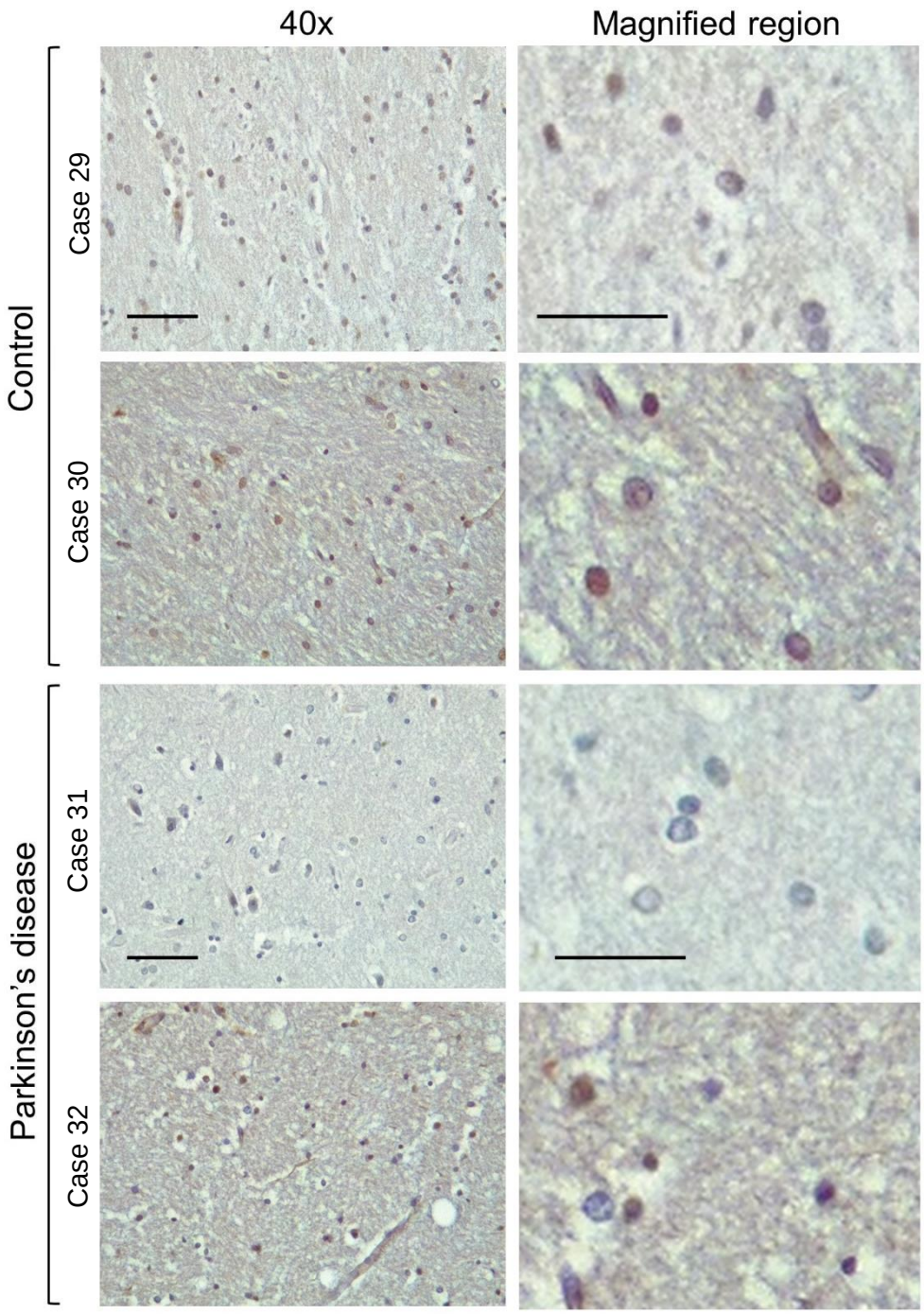

Figure 3.12 SAFB1 is not abnormally expressed in PD patient substantia nigra. Control (n=2) and PD patient (n=2) substantia nigra, immunostained for SAFB1. Overall levels of SAFB1 staining in the substantia nigra were low compared to the cerebellum and striatum. SAFB1 staining was localised to the nuclei. There was no clear difference in the SAFB1 staining pattern in control patients compared to PD patients. There was no evidence of cytoplasmic SAFB1 staining in control or PD patient substantia nigra. 40x scale bar is 50µM, magnified region scale bar is 25µm.

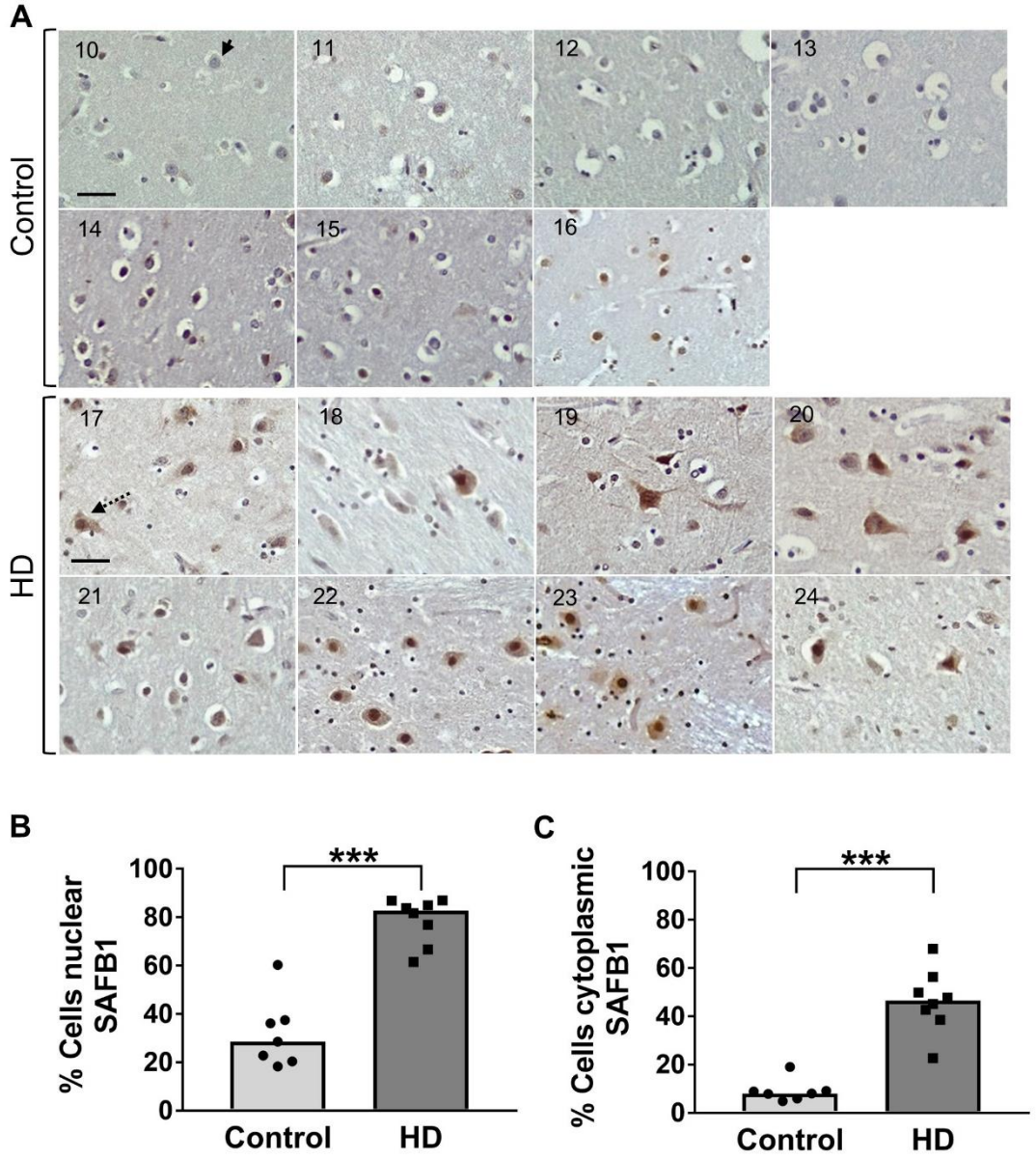

Figure 3.13 SAFB1 is expressed within HD patient striatal cell cytoplasm. **A**) Representative images of striatum immunostained for SAFB1. Within the striatal neuropil, large (neuronal) cells can be distinguished (arrow). Dystrophic neurons were present within HD striatum (dotted arrow). Numbers inset represent patient case, scale bar is 50µm. **B**) There was a significantly higher percentage of large (neuronal) cells with nuclear SAFB1 positivity in HD cases (n=8) compared to control cases (n=7) ((ctl=28.52, HD=82.75) U=0, p=0.0003, Mann-Whitney test). **C**) There was a significantly higher percentage of neurons in HD striatum with cytoplasmic SAFB1 staining compared to control cases ((ctl= 8.03, HD=46.48) U=0, p=0.0003, Mann-Whitney test)). *** p<0.001. Data is presented as median values.

Comparison of SAFB1 staining in HD striatum with a published histopathological image (Waldvogel et al. 2015) shows that SAFB1 positive cells match the morphology of degenerating MSNs in HD (Figure 3.14). The staining pattern of striatal SAFB1 staining with antibody A300-811A was replicated when sections were labelled with an alternative commercially available antibody raised against SAFB1 (IHC 00142, Bethyl) (Figure 3.15, Table 3.3). This control adds further validation to the discovery of abnormal cytoplasmic SAFB1 expression as a novel histopathological hallmark of polyQ neurodegeneration.

Case	Diagnosis	Striatal neurons counted	Nuclear SAFB1	Cytoplasmic SAFB1
10	Control	380	229	30
11	Control	610	174	49
12	Control	382	143	34
13	Control	412	84	20
14	Control	329	75	30
15	Control	486	89	29
16	Control	299	108	57
	Total	**2898**	**902**	**249**
17	HD (grade 2)	307	236	153
18	HD (grade 2)	213	131	91
19	HD (grade 3)	249	166	119
20	HD (grade 3)	186	152	84
21	HD (grade 3)	213	181	120
22	HD (grade 4)	192	167	74
23	HD (grade 4)	365	317	83
24	HD (grade 4)	228	191	155
	Total	**1953**	**1541**	**879**

Table 3.7 Number of striatal neurons with SAFB1 staining in control and HD patient tissue.

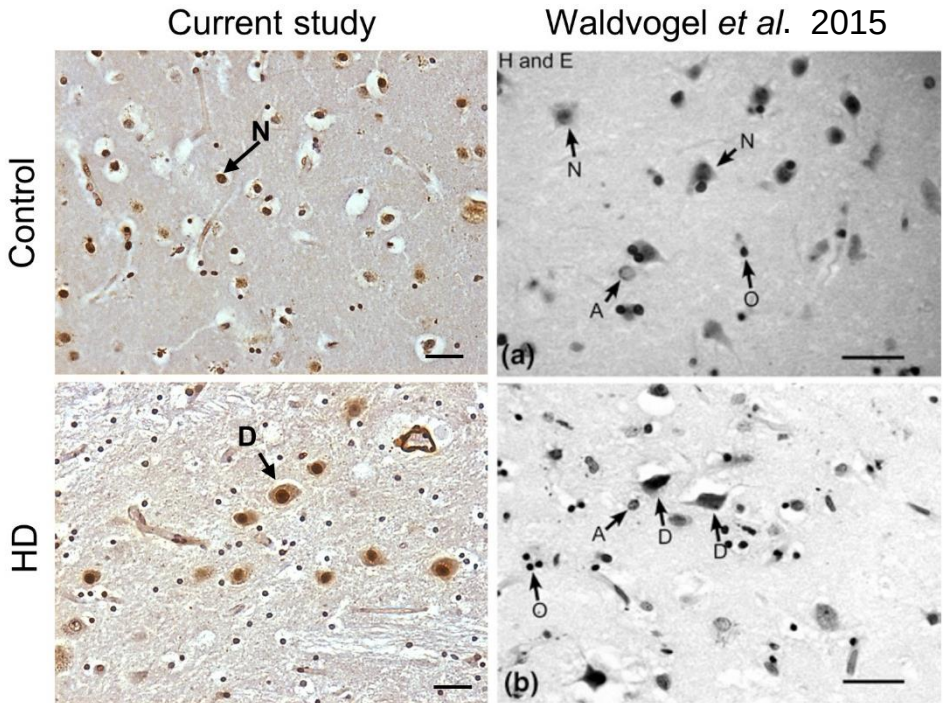

Figure 3.14 Morphology of cells within HD striatum immunostained for SAFB1 in comparison to an H&E stained histological image labelled by a neuropathologist (Waldvogel et al. 2015, p45). Image comparison demonstrates that the large cells immunopositive for SAFB1 have the same morphology as degenerating medium spiny neurons. N=normal medium spiny neuron, D=degenerating neuron, A=astrocyte, O=oligodendrocyte. Scale bars are 25 µm. Image from Waldvogel et al. 2015 reproduced with permission from Springer Nature under licence number 4844250973302. Original work: link.springer.com/chapter/10.1007%2F7854_2014_354

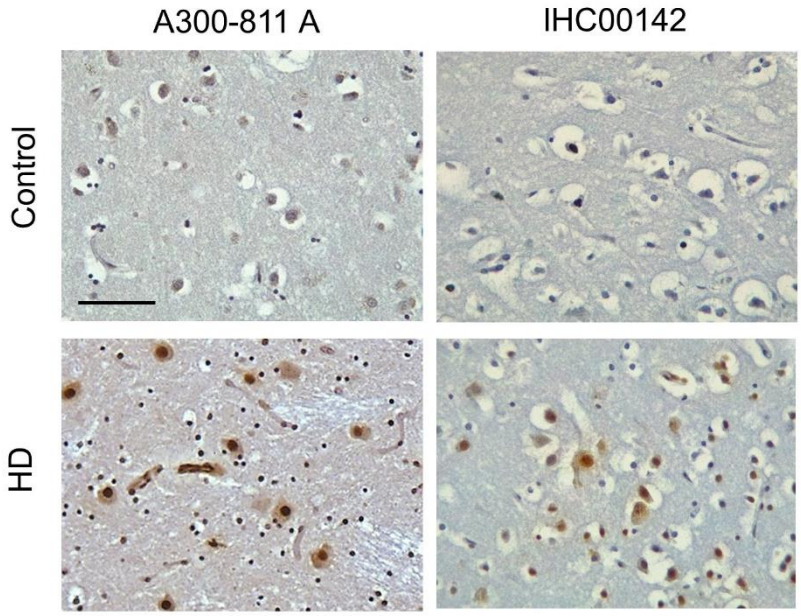

Figure 3.15 Control and HD striatum immunostained with two commercially available antibodies raised against SAFB1 both showed the same cellular staining pattern. Scale bar is 50µm.

3.4.7 Cytoplasmic SAFB1 is present in polyQ-positive HD neurons, but does not co-localise with polyQ inclusions

To further explore the expression of SAFB1 in relation to polyQ pathology, striatal sections from patients with HD and control cases were dual immunolabelled with antibodies against polyQ-containing protein (1C2) and SAFB1 (Figure 3.16). Representative images of immunofluorescent staining in control and HD striatum are shown in Figure 3.16A. Substantial non-specific intracellular fluorescence was observed within the sections, especially in the cytoplasm of large neurons. This fluorescence was attributed to the presence of lipofuscin, lipid-containing residue often present within aged brain cells. Several protocols were employed in this study to quench lipofuscin auto-fluorescence, including incubation of the tissue in copper sulphate solution, glycine solution, or Sudan Black. None of these methods were effective in reducing auto-fluorescence, so quantification was carried out with the caveat of its presence within the cells, and every effort was made to distinguish specific staining from auto-fluorescence. SAFB1 staining in the cytoplasm of striatal cells was overall less easily distinguishable in fluorescent sections compared to detection using DAB.

There were significantly more striatal cells positive for polyQ inclusions in HD striatum compared to control tissue, indicating that the staining protocol was able to specifically detect pathological inclusions (Figure 3.16B). As polyQ inclusions in HD are found in degenerating neurons, immunopositivity may be considered as a surrogate neuronal marker in this tissue. Within this neuronal population, the majority of cells (median 83%) also contained cytoplasmic SAFB1 staining, compared to just 13% cytoplasmic positivity in cells which did not contain polyQ inclusions (Figure 3.16C). This result demonstrates that abnormal cytoplasmic SAFB1 expression is a feature associated with striatal neurons containing pathological polyQ inclusions.

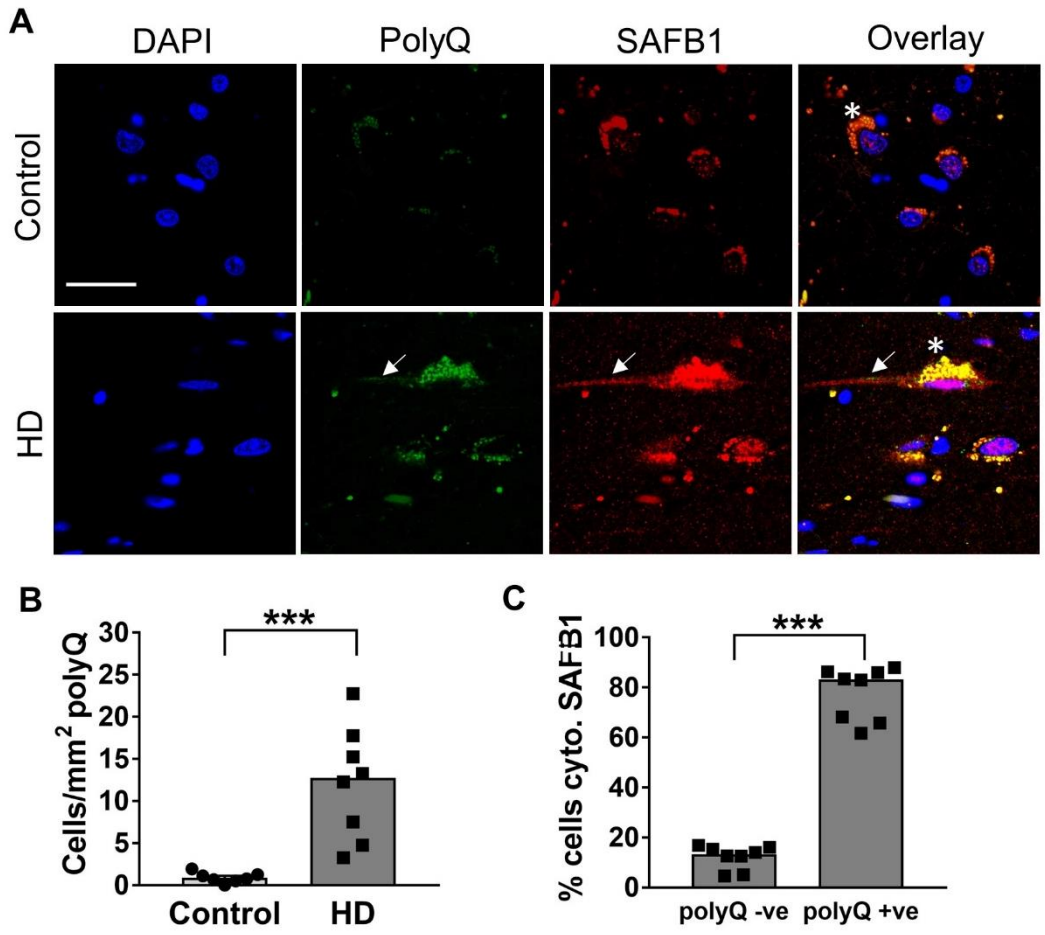

Figure 3.16 Cytoplasmic SAFB1 is present in polyQ-positive neurons in HD striatum. **A**) Dual immunofluorescent labelling of polyQ (green) and SAFB1 (red) in control (n=7) and HD (n=8) striatum. SAFB1 staining was mostly nuclear in control tissue and cytoplasmic SAFB1 was observed in large cells of HD striatum which were also positive for polyQ (arrows). Substantial auto-fluorescent lipofuscin deposits (asterisks) were observed in both control and HD tissue. Scale bar is 25µm. **B**) HD striatum contained significantly more cells per mm^2 positive for polyQ inclusions compared to control (ctl=0.75, HD=12.75) U=0, p=0.0003, Mann Whitney test. **C**) Cytoplasmic SAFB1 expression was associated with a significantly higher percentage of polyQ positive cells than polyQ negative cells (polyQ -ve=13.31, polyQ +ve=83.17) U=0, p=0.0002, Mann Whitney test. ***p<0.001.

Due to the auto-fluorescence in the dual labelled striatal sections, serial sections from a patient with HD were stained for SAFB1 and 1C2 using DAB to obtain a comparison of the distribution of each protein in the same area of tissue (Figure 3.17). Control staining demonstrated the specificity of the 1C2 antibody (Figure 3.17Ai). The frequency of SAFB1 cytoplasmic staining compared to polyQ staining in striatal neurons is represented in Figure 3.17Aii. Quantification showed that the frequency of abnormal SAFB1 staining and polyQ inclusions was similar (38.6 and 34.5%, respectively). High magnification images showed polyQ inclusions in both the nucleus and cytoplasm of degenerating neurons which often presented as concentrations of large puncta/aggregates (a pattern previously described by Herndon et al. 2009). SAFB1 staining was more homogenous and diffusely spread throughout the nucleus and cytoplasm, with some evenly distributed small puncta present throughout the cytoplasm (Figure 3.17B). These differing staining patterns suggest that SAFB1 protein is spatially not closely associated with polyQ aggregates in HD neurons.

3.4.8 There is no overall change in SAFB1 expression levels in the striatum of HD patients

To further investigate the expression of SAFB1 in human polyQ disease, frozen striatal tissue from HD patients and control cases was obtained for RNA and protein analysis (Table 3.2). HD tissue was donated from patients who were significantly younger than control cases, but there was no significant difference in PMD between groups (Figure 3.18A). Striatal tissue from HD patients yielded a significantly lower amount of protein compared to control cases (Figure 3.18A). This could be a result of cell loss within the striatum of these patients, although there was no significant difference in RNA yield between groups (Figure 3.18A). Correlative analyses determined that there was no significant relationship between either age or PMD, and total RNA or protein yield (Figure 3.18B and C). qPCR analysis did not identify a difference in SAFB1 mRNA expression levels (relative to a housekeeping gene, beta-actin) in HD patient striatum compared to control (Figure 3.18Di).

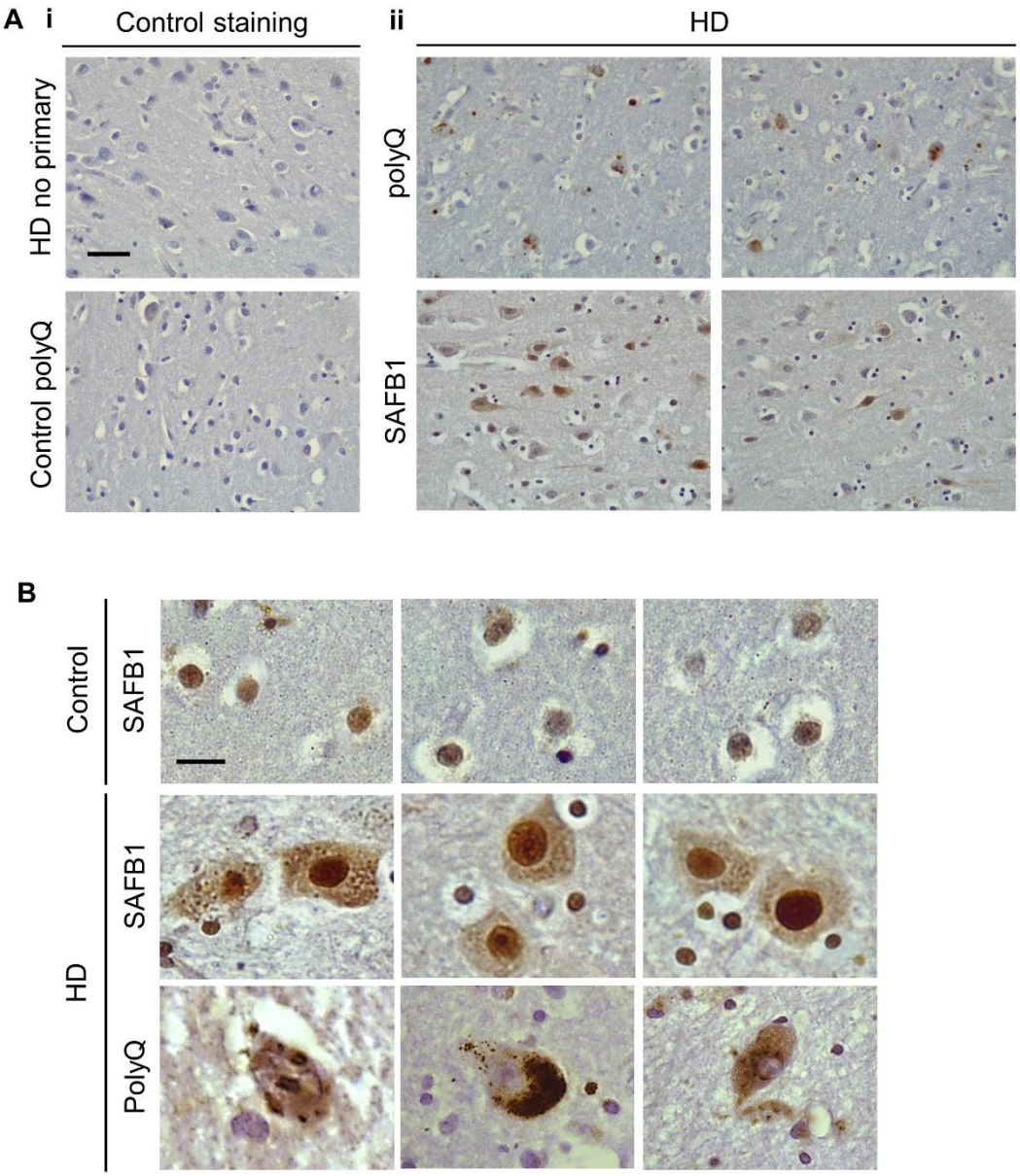

Figure 3.17 PolyQ immunohistochemistry compared with SAFB1 immunohistochemistry in a patient with HD. PolyQ inclusions were visualised using the monoclonal antibody 1C2. (**A**) **i**) Control staining with no primary antibody in HD striatum and using 1C2 to stain the striatum of a control patient shows no immunoreactivity. **ii**) Representative immunostaining for polyQ and for SAFB1 in separate, serial striatal sections of an HD patient (case 23). In this patient, 34.3% of neurons were polyQ positive and 38.6% of neurons were SAFB1 positive. **B**) SAFB1 and polyQ staining in striatal neurons. SAFB1 staining is quite consistent, with diffuse staining throughout the nucleus and cytoplasm, alongside some small dark foci throughout the cytoplasm of degenerating neurons. PolyQ staining patterns were more variable, presenting as either diffuse or aggregated, within both the nucleus and cytoplasm of degenerating neurons. Scale bar in (**A**) is 50µm, in (**B**) is 10µm.

Based on recommendations from the literature (Welinder and Ekblad 2011) SAFB1 quantified by Western blotting and densitometry was normalised to total protein, rather than to a housekeeping protein. There was no difference in SAFB1 protein levels in HD patient striatum compared to control, when normalised to total protein (Figure 3.18Dii). One HD patient (case 47) expressed substantially higher protein levels in the striatum compared to the other cases in this study, and also expressed the highest relative level of SAFB1 mRNA of all the HD patients analysed. This patient died in her 20s as a result of complications from HD symptoms, and was the only patient with Vonsattel Grade 4 neuropathology in this group.

Figure 3.18 (next page) Analysis of protein and mRNA in control (n=10) and HD (n=6) patient frozen striatal tissue. **A**) Descriptive statistics for age, PMD, protein yield and mRNA yield. The age of HD patients is significantly lower than that of control patients (t(14), t=2.983, p=0.01). There is no significant difference in PMD time between control cases and HD patients (t(14), t=0.903, p=0.382). **B**) Across all samples there is no significant correlation between patient age (**Bi**) or PMD (**Bii**) with total yield of mRNA. **C**) Across all samples there is no significant correlation between age (**Ci**) or post-mortem delay (**Cii**) with total protein yield. **D**) SAFB1 expression was analysed at the mRNA and protein level in patient striatal tissue. Analysis by qPCR showed no significant difference in SAFB1 mRNA expression in HD patients compared to control cases when normalised to beta-actin expression (**Di**) (t(14), t=0.778, p=0.45). Analysis by Western blotting showed no significant difference in SAFB1 protein expression in HD patients compared to control, when normalised to total protein (**Dii**) (t(14), t=1.11, p=0.29). Correlative analyses were carried out using Pearson's tests. Comparisons between two groups were carried out using student's unpaired, two-tailed t-tests. Data is shown as mean ± SEM.

A	Control n=10 mean (± SEM)	HD n=6 mean (± SEM)	*P* value	Sig. level
Age (yrs)	79.3 (3.4)	54.8 (9.8)	0.01	**
PMD (hrs)	45.4 (8.7)	58.3 (11.5)	0.38	ns
Protein yield (mg/ml)	13.9 (2.5)	5.8 (1.1)	0.04	*
RNA yield (ng/ul)	242.7 (50.7)	363.7 (64.2)	0.16	ns

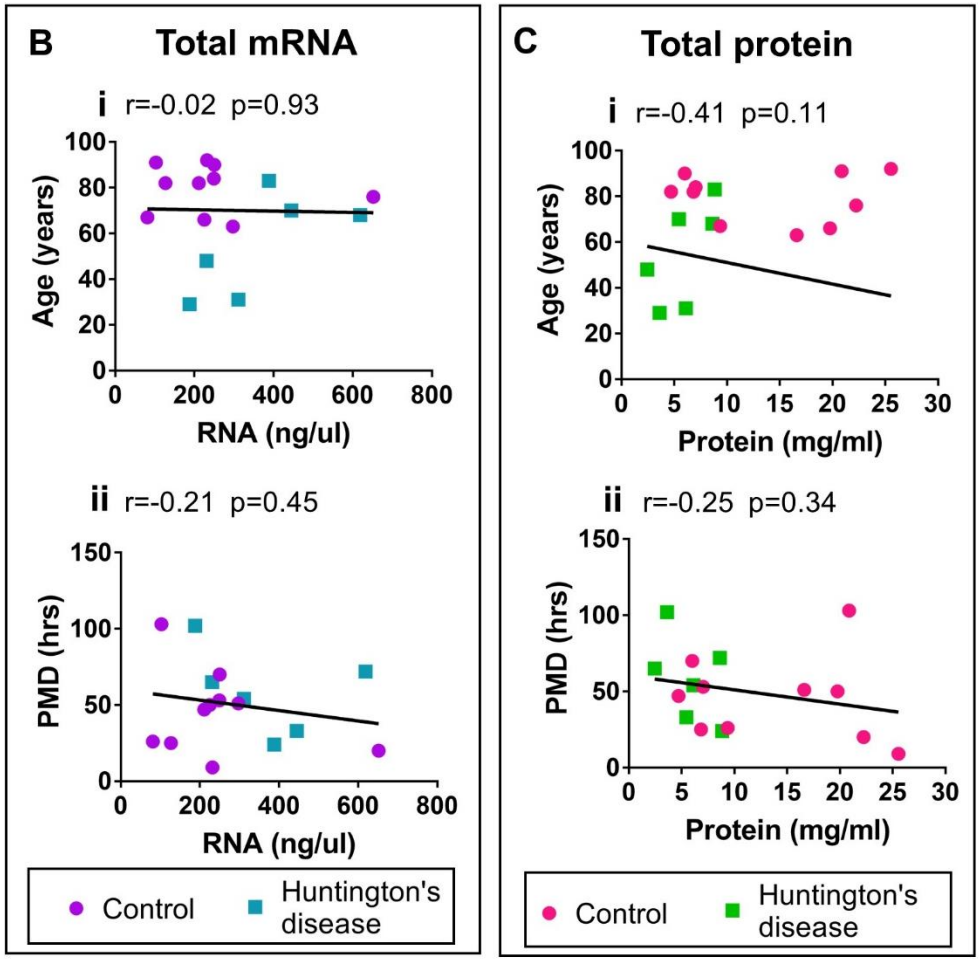

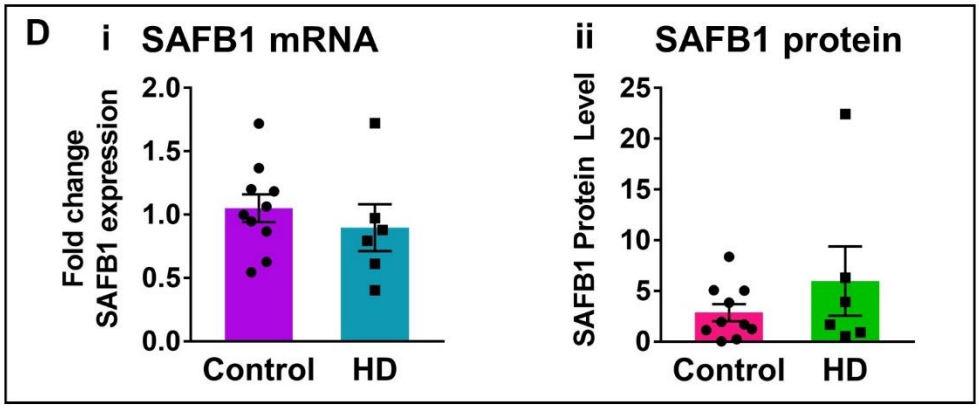

Figure 3.18 See previous page for figure legend

3.5 Discussion

3.5.1 Key findings

This chapter utilised brain tissue from 48 patient cases to carry out a novel investigation of SAFB1 expression in human neurodegenerative disease. SAFB1 is an RBP with important neuronal regulatory functions, which is primarily expressed in the nucleus. The current findings show that abnormal cytoplasmic expression of SAFB1 in degenerating neurons is a newly discovered histopathological feature of human polyQ disorders including SCA and HD. Cytoplasmic SAFB1 was present in 56% of Purkinje cell neurons and 73% of DN neurons in a SCA1 patient with less severe Purkinje cell loss compared to the other SCA cases. This could indicate that abnormal SAFB1 expression is associated with relatively early stages of pathology in polyQ disease. There was no evidence of abnormal SAFB1 expression in the brains of control cases, or in patients diagnosed with MS or PD.

There was no overall change in SAFB1 RNA or protein levels in HD patient striatum. This may reflect the fact that SAFB1 becomes mislocalised to the cytoplasm in the absence of changed expression levels in HD. Alternatively, this finding could be a consequence of the experimental techniques not being sensitive enough to detect potential changes in the level of SAFB1 in degenerating MSNs. This is because any changes in MSN SAFB1 expression levels will be diluted within the striatal tissue samples, which contain MSNs at differing stages of degeneration, amongst many other non-neuronal cell types. The finding that one patient, who died very early from complications of HD, had high SAFB1 protein levels in the striatum, further supports the hypothesis that SAFB1 may be associated with the earlier stages of polyQ pathology.

Donated patient tissue is a highly valuable resource which provides direct and unparalleled insight into the pathology of neurodegenerative disease. The work presented in this chapter is therefore highly translational, directly characterising the role of SAFB1 in human disease.

3.5.2 Evaluation of experimental design and methods

Specificity of the anti-SAFB1 antibody A300-811A was confirmed using siRNA knockdown, and non-specific staining was controlled for by the inclusion of control sections with no primary antibody. This follows the recommendations of Bordeaux et al. (2010), who established the Rimm Algorithm for antibody validation. Furthermore, the methods utilised in this chapter closely followed the principles outlined by Gibson-Corley et al. (2013) in their frequently cited manuscript outlining important principles for valid scoring in histopathological research. The analysis of Purkinje cells through counting and measuring cross-sectional area have also been previously validated as methods of quantifying cell degeneration (Babij et al. 2013, Redondo et al. 2015, Kemp et al. 2016).

There is potential for significant biological variation between patient cases (Stan et al. 2006). It is also important to consider variations in the post-mortem processing of samples including delays in PMD time, alongside variations or artefacts conferred from the fixation and embedding processes. Control patient tissue was carefully selected based on clinical, pathological and diagnostic criteria, as outlined by Ferrer (2015). Every effort was made to balance patient groups for age, PMD and sex, although this was not always possible given tissue availability. Variations in PMD are often of concern in experimental design, because the post-mortem period is associated with autolytic activity and subsequent changes in tissue pH which can differentially affect tissue quality, morphology and protein expression (Scudamore et al. 2011, Blair et al. 2016). A large comprehensive study of PMD times in tissue obtained from UK brain banks found no significant correlation between brain pH and either PMD or agonal state (Robinson et al. 2016). Therefore, extended post-mortem delays do not necessarily preclude the utility of individual patient samples in research.

Immunostaining with a second SAFB1 antibody, IHC 00142, demonstrated the same expression pattern in HD striatal tissue as seen using A300-811A. Both antibodies are raised against antigens corresponding to C-terminal sequences spanning the arginine-glycine (R/G) rich domain of SAFB1

(Figure 3.19, Table 3.3). SAFB1 can be post-translationally modified by methylation within its R/G domain (Thandapani et al. 2013) and has also been shown to be cleaved (Lee et al. 2007). In this study, it is presumed that the antibodies are not sensitive to post-translational modifications such as methylation. Recognition of SAFB1 in the cytoplasm of disease patient neurons by these antibodies indicates that cytoplasmic SAFB1 detected by IHC is without substantial C-terminal cleavage, as loss of this part of the peptide would prevent antibody binding. However, this does not exclude the possibility that a proportion of SAFB1 cleaved at the C-terminal could exist undetected by the current methods.

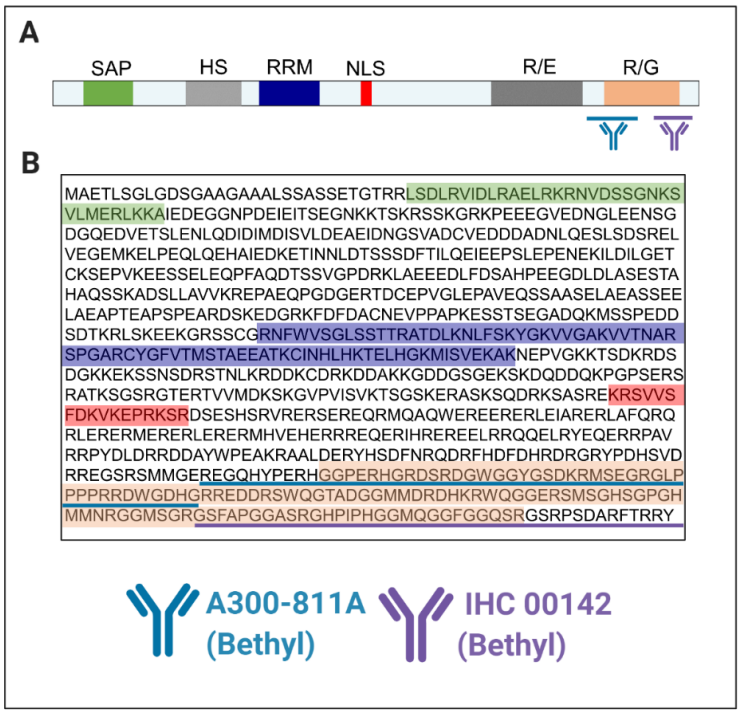

Figure 3.19 Diagram summarising SAFB1 antibody binding to SAFB1 protein domains. **A**) Diagram of SAFB1 protein domains with binding regions of antibodies indicated. **B**) Amino acid sequence of SAFB with binding regions of antibodies indicated in underline. Highlighted sequences correspond to the colours representing each functional domain in (**A**).

3.5.3 Study limitations

3.5.3.1 Patient diagnoses

SCA1 is a very rare disease, and there was only one genetically confirmed patient case available within the UK Brain Banks Network. There is also a scarcity of patient tissue available with any other genetically confirmed polyQ SCA types. The London Neurodegenerative Diseases brain bank has

confirmed that no other researchers who have accessed the non-genetically confirmed SCA cases used in this study (cases 6, 7, 8 and 9) have carried out any genetic analyses.

The cerebellar neuropathological findings summarised in Table 3.4 justify the inclusion of these cases in the present study. Pathological diagnosis of SCA is indicated in the post-mortem reports in all cases. Case 8 features strong polyQ-positive inclusions in Purkinje cells, strongly suggestive of polyQ SCA. Unfortunately, polyQ immunostaining was not carried out in the remaining cases (cases 6, 7, and 9) due to tissue availability. It should also be noted that lack of 1C2-positive inclusions in surviving Purkinje cells would not necessarily exclude the cases as polyQ SCA, as the abundance and distribution of inclusion bodies in Purkinje cells does not always correlate with disease (Koyano et al. 2002, Koeppen 2005). There is evidence to classify case 6 as autosomal dominantly inherited SCA based on patient clinical family history, again indicating a likely diagnosis of polyQ SCA.

By a process of exclusion and based upon the observations from the single cerebellar section studied from each patient, it can be speculated that the undefined cases (6-9) may have suffered from either SCA1, SCA2 or SCA7. These patients did not feature grumose reaction in the DN, but all featured atrophied DN neurons, alongside substantial Purkinje cell degeneration, indicating that SCA3 is unlikely (Koeppen 2018). A diagnosis of SCA6 or SCA17 may also be excluded, as DN neurons are mostly preserved in these cases (Koeppen 2005, Seidel et al. 2012). The confirmed SCA1 case featured a less severe loss of Purkinje cell number, although this does not necessarily rule out a diagnosis of SCA1 for the unspecified cases, as there are likely to be significant variations in disease progression between patients.

It cannot be ruled out that the undefined cases may have suffered from SCA12, caused by a CAG repeat in the non-coding 5’ UTR of the *PPP2R2B* gene (Holmes et al. 1999). Characterisation of SAFB1 in SCA12 patient

tissue would provide further valuable insight to the mechanisms underpinning the abnormal expression of SAFB1.

As the work in this chapter does feature one case of genetically confirmed SCA1, alongside multiple cases of confirmed polyCAG expansion in HD patients, the current study overall offers strong histopathological evidence for abnormal cytoplasmic expression of SAFB1 being associated with polyQ disease.

3.5.3.2 Dual immunolabelling

As concluded from Figure 3.16, technical limitations were encountered when performing dual fluorescent immunolabelling in human striatal tissue due to the accumulation of lipofuscin within cells. Lipofuscin is an auto-fluorescent pigment made of lipids, metals and misfolded proteins which aggregates within neurons, and which is a general feature of aged human tissue especially in neurodegenerative disease (Moreno-García et al. 2018). Despite considerable attempts to quench this auto-fluorescence, its presence unfortunately occluded the clarity of immunostaining in the striatal tissue. There were no major accumulations of lipofuscin found in the cerebellar tissue of control or disease patients.

3.5.4 Recommendations for future work

To further explore the relationship between SAFB1 and other RBPs associated with neurodegenerative disease, human tissue sections could be immunostained with antibodies raised against FUS, and TDP-43. Furthermore, our lab has recently developed an antibody raised against SAFB2 (AB1897, Invitrogen custom antibody services) which does not cross-react with SAFB1. This antibody could be used to further characterise the expression of SAFB proteins in human polyQ disease. In future immunostaining studies, increasing the number of confirmed polyQ SCA patient cases is recommended, which may require donor tissue to be accessed from international repositories. The number of control cases should also be increased. As a further control, it may also be useful to study

SAFB protein expression in brain regions or tissues unaffected by SCA pathology, in polyQ SCA patient cases.

The frozen striatal samples from control cases and HD patients are a valuable resource which should be used for further investigation. It is recommended that when performing Western blotting, normalisation of proteins of interest should not carried out in relation to specific housekeeping genes. This is because it is unknown whether there is differential vulnerability of proteins to degradation. Indeed, differential patterns of protein degradation in human post-mortem tissue were observed in Western blotting by Blair et al. (2016). In the current study, SAFB1 protein levels were normalised against total protein levels measured using a BCA assay. In future, it may be more accurate to normalise to whole protein content within each sample quantified by gel electrophoresis and Coomassie blue staining (Welinder and Ekblad 2011). It was not possible to take this approach in the current study due to unforeseen limitations in access to tissue samples.

It was previously demonstrated that SAFB1 protein can be successfully isolated from human striatal tissue lysate by immunoprecipitation (data not shown). SAFB1 protein isolated from these samples could be utilised in proteomic analysis by tandem-mass tagging to gain further novel quantitative insight into the protein-protein interactions of SAFB1 in HD. Furthermore, it would also potentially be possible to isolate SAFB1 protein from these samples to investigate SAFB1 RNA interactions by iCLIP. These detailed biochemical analyses would complement the results of the current study and ensure that the valuable human tissue is utilised to its full potential.

3.5.5 Conclusions

This chapter demonstrates that the RBP SAFB1 is abnormally expressed in the cytoplasm of degenerating neurons of polyQ patients. This finding contributes to a wider body of evidence which implicates RBPs in neurodegenerative disease aetiology, a rapidly developing field of research

which could provide insight into potential future therapeutic interventions. The use of human tissue confers high translational value to the current findings. However, as the experiments were observational, it is not possible to obtain any mechanistic insight from this data. Possible hypotheses to explain the altered expression of SAFB1 in polyQ disease include aberrant interaction of SAFB1 with polyQ protein or polyCAG RNA transcripts, or dysregulated nuclear export or import of SAFB1. The role of SAFB1 in polyQ disease and possible mechanistic explanations are further discussed in Chapter 4

4. Chapter 4

Investigating the mechanism of SAFB1 expression in polyglutamine pathology

4.1 Overview

4.1.1 Chapter overview

This chapter investigated the mechanism by which SAFB1 protein may contribute to polyglutamine (polyQ) pathology. An RNA immunoprecipitation (IP) protocol to quantify the interaction of SAFB1 protein with RNA containing expanded polyCAG tracts was successfully developed. Using this technique, it was confirmed that SAFB1 protein binds *ATXN1* RNA containing both physiological and expanded CAG trinucleotide repeats. Furthermore, compared to *ATXN1* containing a normal CAG tract, there was a relative increase in the amount of *ATXN1* RNA containing pathologically expanded CAG repeats associated with SAFB1 protein. This is a novel mechanistic insight into the RNA binding function of SAFB1 in polyQ disease. In addition, this chapter describes the establishment of human iPSCs with SAFB1 and SAFB2 deletion which can be used in the future to further understand the role of SAFB1 in polyQ disease.

4.1.2 Graphical abstract

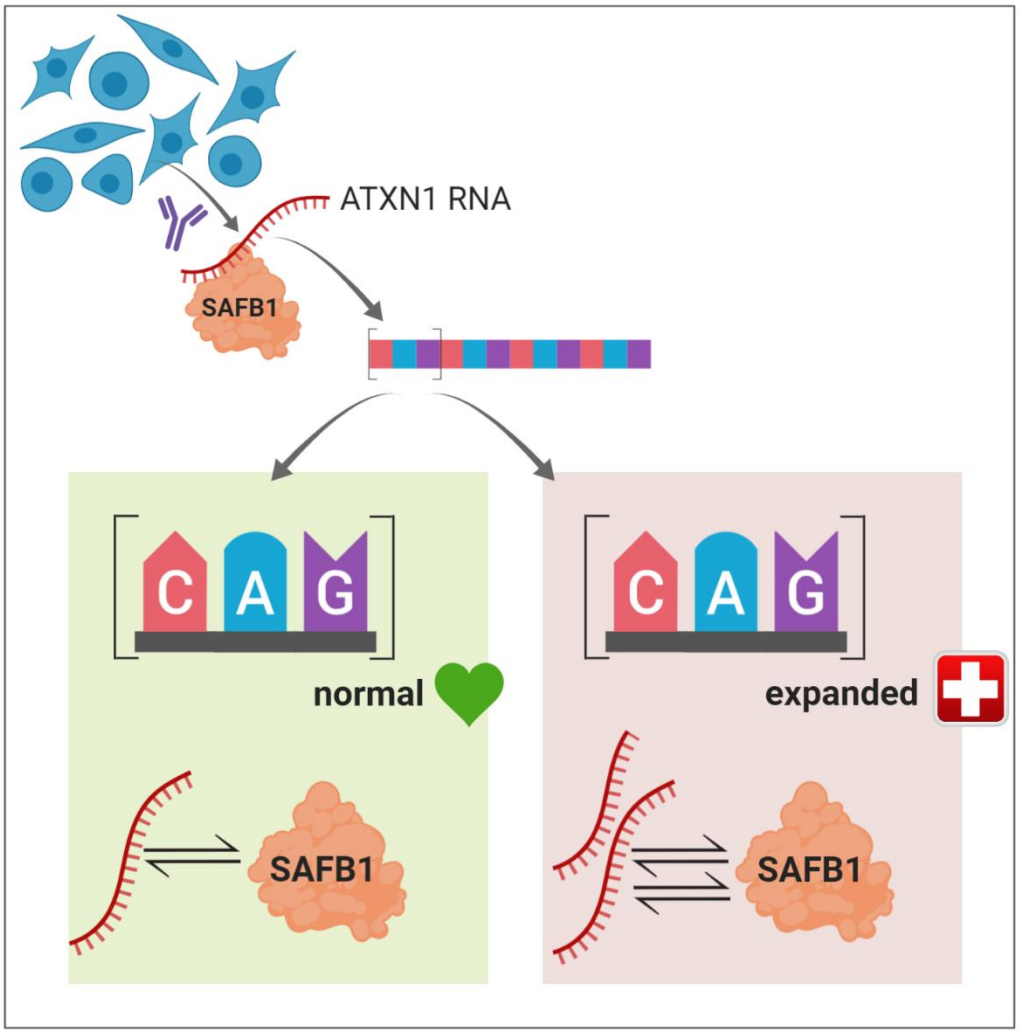

Figure 4.1 Graphical abstract for Chapter 4

4.2 Introduction

PolyQ disorders are caused by an expansion of the CAG trinucleotide repeat tract in the coding regions of specific genes. The threshold number of CAG codons causing disease varies with the affected gene (Table 1.3). Genes containing expanded CAG sequences are transcribed into expansion repeat-containing RNA (xtrRNA) and subsequently translated into peptide gene products containing polyQ tracts.

The molecular pathology underlying the process of neuronal loss in polyQ disorders is not yet fully understood. Much research has focussed on understanding the role of polyQ proteins, as their propensity to aggregate and form proteinaceous intracellular inclusions is considered a pathological hallmark of polyQ disorders. Modifying the misfolding and aggregation of polyQ protein has therefore been considered a key therapeutic target (Takeuchi and Nagai 2017). However, it is still not understood whether formation of polyQ aggregates or inclusions in neurons directly causes neuronal loss (Arrasate and Finkbeiner 2012).

It is now recognised that xtrRNA transcripts are likely to be important mediators of polyQ pathology. CAG repeat number correlates to age of disease onset across polyQ disorders (Gusella and MacDonald 2000) (Figure 1.2) and the number of CAG repeats is the most important predictor of pathology, independent of the glutamine tract length of the corresponding gene product (Lee et al. 2019).

RBPs are one of the most important elements of RNA regulation. RBP dysregulation in neurodegenerative disease is exemplified by mutations in TDP-43 and FUS which cause ALS and FTD. RBPs are implicated in the molecular pathology of polyQ disorders including HD (Doi et al. 2008, Kino et al. 2016) and SCA (Irwin et al. 2005, Ostrowski et al. 2017). Our research group is interested in the RBP SAFB1, which has structural and functional similarities to both TDP-43 and FUS (section 1.5, Figure 1.11).

Although there are currently no known disease-causing mutations in SAFB1, our research group has previously established that SAFB1 is highly expressed in the brain and mediates neuronal functions (Rivers et al. 2015, Norman et al. 2016). SAFB1 is also required for development (Ivanova et al. 2005) and is involved in the cellular stress response (Norman et al. 2016). SAFB1 interacts strongly with RNA transcripts of the *ATXN1* gene, which is mutated with an expanded polyCAG tract in the polyQ disorder SCA1 (section 3.2, Figure 3.2). Proteomic analysis in cell lines does not indicate a protein-protein interaction between SAFB1 and ataxin1 (Zhang et

al. 2018, Allahyani 2020). The novel findings presented in Chapter 3 demonstrate that SAFB1 is abnormally expressed in the cytoplasm of degenerating neurons, a pathology specific to patients with polyQ disorders including SCA1.

Based on these findings, this chapter aimed to further understand the pathology of SAFB1 in polyQ disease, specifically the interaction of SAFB1 with *ATXN1* RNA. This chapter also describes the creation of human iPSCs with knockout of SAFB1 and SAFB2 which can be used as a tool to further understand the role of SAFB proteins in polyQ pathology.

4.3 Methods

4.3.1 Immunofluorescent labelling of transfected cells

SH-SY5Y cells (section 2.3.1) were plated in antibiotic-free media at a density of $1x10^5$ cells per well in a 24-well plate on sterilised glass coverslips pre-coated in poly-d-lysine. After 24 hours, SH-SY5Y cells were transiently transfected with DNA plasmids containing N-terminal eGFP-tagged ataxin1 (*ATXN1*) with either a subphysiological length CAG tract (pEGFP-ATXN1-2Q), a normal length CAG repeat tract (pEGFP-ATXN1-30Q) or a pathologically expanded CAG repeat tract (pEGFP-ATXN1-52Q). All *ATXN1* plasmids were kind gifts from Huda Zhoghbi via Addgene (Figure 4.2). Transfection mixture containing 1.3µl FuGENE 6 transfection reagent (Promega) mixed with 48.7µl Opti-MEM reduced serum media (ThermoFisher Scientific) was combined with 500ng of DNA plasmid and left to stand for 15 minutes. The transfection mixture was added to SH-SY5Y cells in a well containing 200µl of growth media. Control cells were incubated with transfection mixture but no DNA plasmid. A full media change was carried out 6 hours after transfection. Transfected cells were left for 48 hours before fixing in 4% PFA and carrying out immunofluorescent staining (section 2.7.3). SAFB1 was visualised using antibody A300-811A or IHC 00142 (Bethyl) at 1:200 and anti-rabbit Cy3 conjugated secondary antibody (Stratech) at 1:300. HeLa cells grown on glass coverslips were transfected as above using FLAG-*ATXN1* plasmids (section 4.3.2.1) and

immunostained according to the protocol in section 2.7.3. FLAG-tagged protein was visualised using antibody F3165 (Millipore) at 1:500 and anti-mouse Cy3 conjugated secondary antibody (Stratech) at 1:300. Cells were imaged using a Leitz DMRB fluorescence microscope (Leica) with a Leica DC500 camera and Leica imaging software.

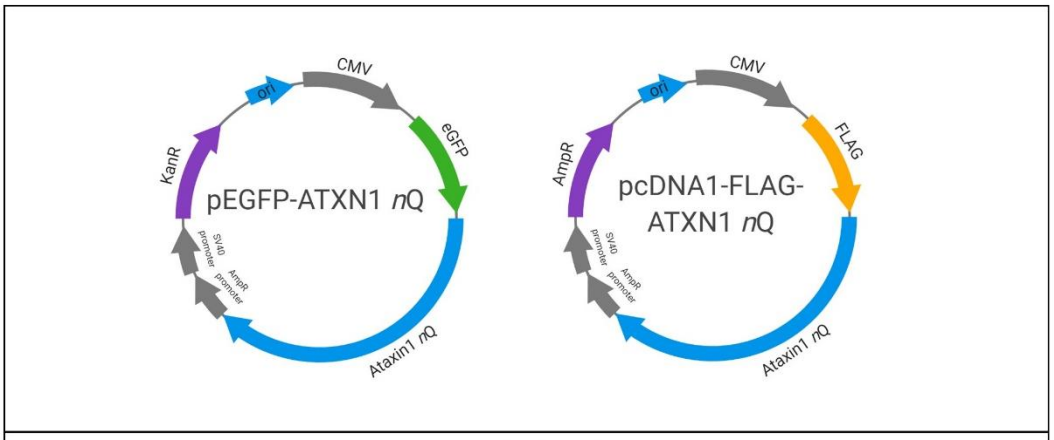

Plasmid name	Addgene Ref.	Number of CAG repeats	Tag	Backbone	Promoter
pEGFP-ATXN1-2Q	33239	2	eGFP	pEGFP-C1	CMV
pEGFP-ATXN1-30Q	33238	30 (with 2 CAT interruptions)	eGFP	pEGFP-C1	CMV
pEGFP-ATXN1-52Q	32492	52	eGFP	pEGFP-C1	CMV
pcDNA1 Flag ATXN1[2Q]	33235	2	FLAG	pcDNA1.1	CMV
pcDNA1 Flag ATXN1[30Q]	33236	30 (with 2 CAT interruptions)	FLAG	pcDNA1.1	CMV
pcDNA1 Flag ATXN1[85Q]	33237	85	FLAG	pcDNA1.1	CMV

Figure 4.2 Details of DNA plasmids expressing *ATXN1* used in this study

4.3.2 RNA immunoprecipitation (IP) of SAFB1 protein and ATXN1 *RNA*

4.3.2.1 Transfection of cell lines with ATXN1 *plasmids*

HeLa cells (section 2.3.1) were plated in antibiotic-free growth media at a density of $9x10^5$ cells per 10cm culture dish. After 24 hours, cells were transiently transfected with DNA plasmids containing N-terminal FLAG-tagged ataxin1 (*ATXN1*) with either a subphysiological length CAG tract (pcDNA1 Flag ATXN1[2Q]), a normal length CAG repeat tract (pcDNA1

Flag ATXN1[30Q]) or a pathologically expanded CAG repeat tract (pcDNA1 Flag ATXN1[85Q]). All *ATXN1* plasmids were kind gifts from Huda Zhoghbi via Addgene (Figure 4.2). Transfection media containing 45µl FuGENE 6 transfection reagent (Promega) mixed with 925µl Opti-MEM reduced serum media (ThermoFisher Scientific) was combined with 15µg of DNA plasmid and left to stand for 15 minutes. The transfection mixture was added dropwise to HeLa cells in a 10cm dish containing 8ml of growth media. Control cells were incubated with transfection mixture but no DNA plasmid. A full media change was carried out 6 hours after transfection, and cells were left for 48 hours before use in RNA immunoprecipitation (IP) experiments.

4.3.2.2 Cross-linking of antibodies to Protein G beads

Protein G beads (Dynabeads, ThermoFisher Scientific) were vortexed into suspension and the desired volume of bead slurry was pelleted using a magnetic rack before washing beads in an equal volume of PBST (wash buffer). Wash buffer was added to bring the total volume to 1ml. Anti-SAFB1 (AB1895, Invitrogen custom antibody services) or rabbit IgG (Cell signalling technology) at a concentration of 15µg per 100µl of bead slurry was added to the washed beads and rotated overnight at 4^{o}C. Antibody-bound Protein G beads were pelleted using a magnetic rack, and washed 3 times in 1ml of wash buffer, then 3 times in 1ml of coupling buffer. Beads were pelleted and resuspended in freshly prepared 20mM DMP (dimethyl pimelimidate) before rotating for 30 minutes at room temperature. This step was repeated with another solution of freshly made DMP. The cross-linking reaction was quenched by washing beads in 1ml quenching buffer and rotating for 30 minutes at room temperature. Un-crosslinked antibody was removed from the beads by washing 3 times in 1ml of elution reagent. Cross-linked beads were resuspended to their original volume in PBST with 0.02% sodium azide and stored at 4^{o}C for up to 4 weeks.

4.3.2.3 RNA IP

All stages of the RNA IP procedure were carried out in RNase-free conditions. Transfected HeLa cells were washed in ice-cold PBS and

scraped on ice in 1ml of lysis buffer containing protease inhibitors and RNAse inhibitors. Lysates were centrifuged and the supernatant pre-cleared by incubating with Protein G magnetic beads washed in lysis buffer. Pre-cleared protein lysates were quantified using a bicinchoninic acid assay (Pierce BCA protein assay kit, Thermo Scientific). Protein was diluted to 1µg/µl, and a 500µl aliquot incubated with 25µl Protein G beads cross linked to either 3.75µg SAFB1 antibody (AB1895, Invitrogen custom antibody services) or 3.75µg rabbit IgG (Cell Signalling Technology). Lysates were rotated overnight at 4^{o}C with antibody-linked beads. Protein G beads bound to immunocomplexes were isolated using a magnetic rack and washed 4 times with 500µl lysis buffer and once with 500µl RNAse-free PBS. A sample of beads in solution from each experimental condition was reserved for Western blot analysis. Beads were pelleted and resuspended in fresh BL/TG buffer from a Reliaprep RNA Cell Miniprep kit (Promega) and left at room temperature for 10 minutes to dissociate immunocomplexes from the beads. RNA was purified from immunocomplexes using a Reliaprep RNA Cell Miniprep Kit according to manufacturer's instructions and eluted in 12µl nuclease-free water. In each experiment, RNA was purified from a sample of input protein, Protein G beads conjugated with antibody and Protein G beads conjugated with rabbit IgG.

4.3.2.4 Western blotting of protein lysates from RNA IP experiments

To confirm SAFB1 protein was successfully isolated using antibody-linked Protein G beads, samples of pre-cleared input were analysed by Western blotting (section 2.6.11) alongside samples of antibody-linked and IgG-linked Protein G beads associated with immunocomplexes. Protein was dissociated by resuspending beads in 2xSDS sample buffer and heating at 95^{o}C for 5 minutes. To quantify relative FLAG-ataxin1 protein expression levels, input samples from each experiment were also analysed by Western blotting. Samples were run on an 8% polyacrylamide gel then transferred to a PVDF membrane using a TransBlot Turbo Transfer System (Bio-Rad). Membranes were blocked in 5% milk (in PBS) then probed with either anti-SAFB1 antibody (1:1000 in 1% (v/v) milk in PBS) (A300-811 A) or anti-FLAG (1:500 in 3% (v/v) milk in TBS) overnight at 4^{o}C. Membranes were incubated

with anti-rabbit or anti-mouse peroxidase conjugated secondary antibody (1:10000) (GE Healthcare) and antibody signal visualised using ECL. Membranes probed for FLAG expression were densitometrically analysed using Image Studio Lite (Licor) to quantify the intensity of protein bands.

4.3.2.5 Quantification of ATXN1 *cDNA by qPCR*

RNA was reverse transcribed using a GoScript Reverse Transcription System kit (Promega) using random primers according to manufacturer's instructions. cDNA was analysed by qPCR with Power SYBR Green (ThermoFisher Scientific) using primers to recognise *ATXN1* (Forward:TCCAGCACCGTAGAGAGGAT, Reverse: GCCCTGTCCAAACACAAAAA) with a StepOnePlusTM PCR system (ThermoFisher Scientific). cDNA from each condition was run in triplicate.

4.3.2.6 Analysis of RNA IP qPCR data

To quantify the relative amount of *ATXN1* RNA bound to SAFB1 protein, the mean CT value for each experimental condition was compared against the CT values of a standard curve of serially diluted *ATXN1* DNA which was run alongside the experimental wells on each qPCR plate. Each serial dilution of the standard curve was assigned a relative value. The relative level of *ATXN1* in the experimental samples was then determined by comparison to the standard curve. For each sample, the mean relative quantity was expressed per µg of SAFB1 protein. The mean relative quantity for each condition was normalised to the densitometric quantification of FLAG protein expression as analysed by Western blotting. Data from n=3 independent experiments was analysed using a one-way ANOVA with Tukey's post-hoc test to evaluate statistical significance between groups.

4.3.3 CRISPR-Cas9 knockout of SAFB1/2 dual promoter

4.3.3.1 Ribonucleoprotein complex preparation

Guide RNAs (gRNAs) flanking the SAFB1/2 dual promoter were designed and compared against the WT genome using BLAST in order to minimise off-target effects. Lyophilised gRNAs and fluorescent tagged tracrRNA (Integrated DNA Technologies, IDT) were resuspended in 1xTE solution

(IDT) to 200µM. Each gRNA was combined with tracrRNA in equimolar concentration in nuclease-free duplex buffer (IDT). Oligos were denatured at 95ºC then annealed by cooling to room temperature for at least 20 minutes. Cas9 (IDT) was diluted in Cas9 storage buffer to a 1M stock then combined with each crRNA/tracrRNA complex before incubating at room temperature for 20 minutes. The two ribonucleoprotein (RNP) complexes were combined into a single RNP solution prior to nucleofection.

4.3.3.2 Nucleofection

Kolf2 iPSCs were obtained from the research lab of Professor Nick Allen (Cardiff University) via HipSci. iPSCs were grown in 6-well plates pre-coated with vitronectin and maintained as undifferentiated colonies in E8 media (Gibco) until reaching 80% confluency. One well of cells was used for each nucleofection. Cells were treated with 1µl ROCK inhibitor (Stemcell Technologies) per ml culture medium for 30-60 minutes. Media was aspirated and cells washed in PBS (no magnesium). Cells were incubated with pre-warmed Accutase (Stemcell Technologies) at 37ºC for around 5 minutes until colonies began dissociating. PBS was swirled into each well and the suspension collected into a 15ml falcon tube before centrifuging at 1000rpm for 3 minutes. Cells were resuspended in 1ml PBS and $1x10^6$ cells aliquoted in suspension into a fresh 15ml falcon tube. After pelleting again, cells were resuspended in 100µl nucleofection solution (P3 primary cell nucleofector kit, Lonza) prepared according to manufacturer's instructions. The pre-prepared RNP solution was added, and the whole suspension transferred to a cuvette before nucleofecting in an Amaxa 4D nucleofector X unit (Lonza). Cells were left to recover for 10 minutes at 37ºC post-nucleofection before combining the suspension with 1ml pre-warmed E8 media with ROCK inhibitor. Cells were transferred drop-wise to a single well of a 6-well dish pre-coated in vitronectin and returned to the incubator overnight.

4.3.3.3 FACS sorting

Cells were FACS sorted 24 hours after nucleofection with fluorescent tracrRNA. Cells were dissociated in Accutase and resuspended in 500µl E8

media with ROCK inhibitor as a single-cell suspension in a 15 ml falcon tube and placed on ice. FACS sorting was carried by Mr. Mark Bishop (Cardiff University) using a BD FACS Aria Fusion. The top 10% of cells expressing the highest tracrRNA fluorescence were collected (typically around 3000 cells) and kept on ice until plating. Cells in suspension were plated drop-wise into a well pre-coated in vitronectin containing E8 media plus ROCK inhibitor. A full media change was carried out after 24 hours.

4.3.4 PCR screening of iPSC clones

iPSC colonies were individually picked and plated into vitronectin-coated wells of a 96-well plate. After the colonies became well-established, they were passaged to create a duplicate 96-well plate. One plate was kept as a growing stock for expansion following PCR screening. Genomic DNA was extracted from the duplicate plate using DNA QuickExtract solution (Lucigen) according to manufacturer's instructions. For optimisation of PCR screening conditions, genomic DNA from cell lines was extracted using a Wizard genomic DNA Purification kit (Promega). To screen iPSC genomic DNA for SAFB1/2 dual promoter deletion, PCR reactions were set up using a FastStart High Fidelity PCR System kit (Roche) in accordance with Table 4.1 and run on a thermocycler according to the programme specified in Table 4.2 with 35 annealing cycles.

Reaction component	µl
10x buffer	5
$MgCl_2$ (25mM)	4
dNTPs (20mM)	1
DMSO	2.5
F primer (4µM)	5
R primer (4µM)	5
gDNA (100ng/µl)	1
Taq polymerase	0.5
Water	26
TOTAL	**50**

Table 4.1 PCR reaction conditions for screening iPSC gDNA for SAFB1/2 promoter deletion

Cycle stage	Temperature (°C)	Time
Initial denaturation	95	2 minutes
Denaturation	95	20 seconds
Annealing	50	30 seconds
Extension	72	60 seconds
Final Extension	72	5 minutes

Table 4.2 Thermocycler parameters for PCR screening of iPSC SAFB1/2 promoter deletion

4.4.1 SAFB1 and expanded polyQ ataxin1 protein do not co-localise in SH-SY5Y cells

To model polyQ protein expression, high copy number DNA plasmids expressing *ATXN1* with various lengths of CAG repeat tract were transiently transfected into cell lines to artificially express *ATXN1* RNA and ataxin1 protein. Constructs were tagged at the N-terminal with either eGFP or FLAG to aid visualisation of ataxin1 protein. Figure 4.2 summarises the DNA plasmids used in this study.

To investigate whether overexpression of ataxin1 containing a polyQ expansion affected SAFB1 protein expression, SH-SY5Y cells were transiently transfected with eGFP-tagged *ATXN1* and immunostained using a SAFB1-specific antibody (Figure 4.3). Large protein inclusions of eGFP-ataxin1 were expressed in the nucleus (Figure 4.3A). Less frequently, some cells transfected with pathologically expanded eGFP-ataxin1 featured cytoplasmic eGFP-ataxin1 expression (Figure 4.3Bi). Nuclear ataxin1 protein inclusions varied in size between cells within each polyQ repeat length, but an overall trend was observed that the size of the inclusions appeared to increase with increasing glutamine tract length (Figure 4.3A). There was no clear co-localisation of ataxin1 inclusions with immunopositive SAFB1 puncta in the nucleus (Figure 4.3A). Furthermore, expression of eGFP-ataxin1 did not appear to affect the overall level or distribution of SAFB1 nuclear immunopositivity. In some cells transfected with 52Q expanded ataxin1, infrequent small cytoplasmic SAFB1 positive inclusions were observed in the cytoplasm (Figure 4.3Bii). This staining pattern was not present in untransfected cells, or in cells expressing ataxin1 with 2 or 30 CAG repeat tracts. This finding supports the evidence presented in Chapter 3, which indicated that SAFB1 protein and expanded polyglutamine peptides do not necessarily co-localise in degenerating neurons of patients with polyglutamine disorders. Investigations into the interactions of SAFB1 protein with *ATXN1* RNA transcripts were therefore carried out.

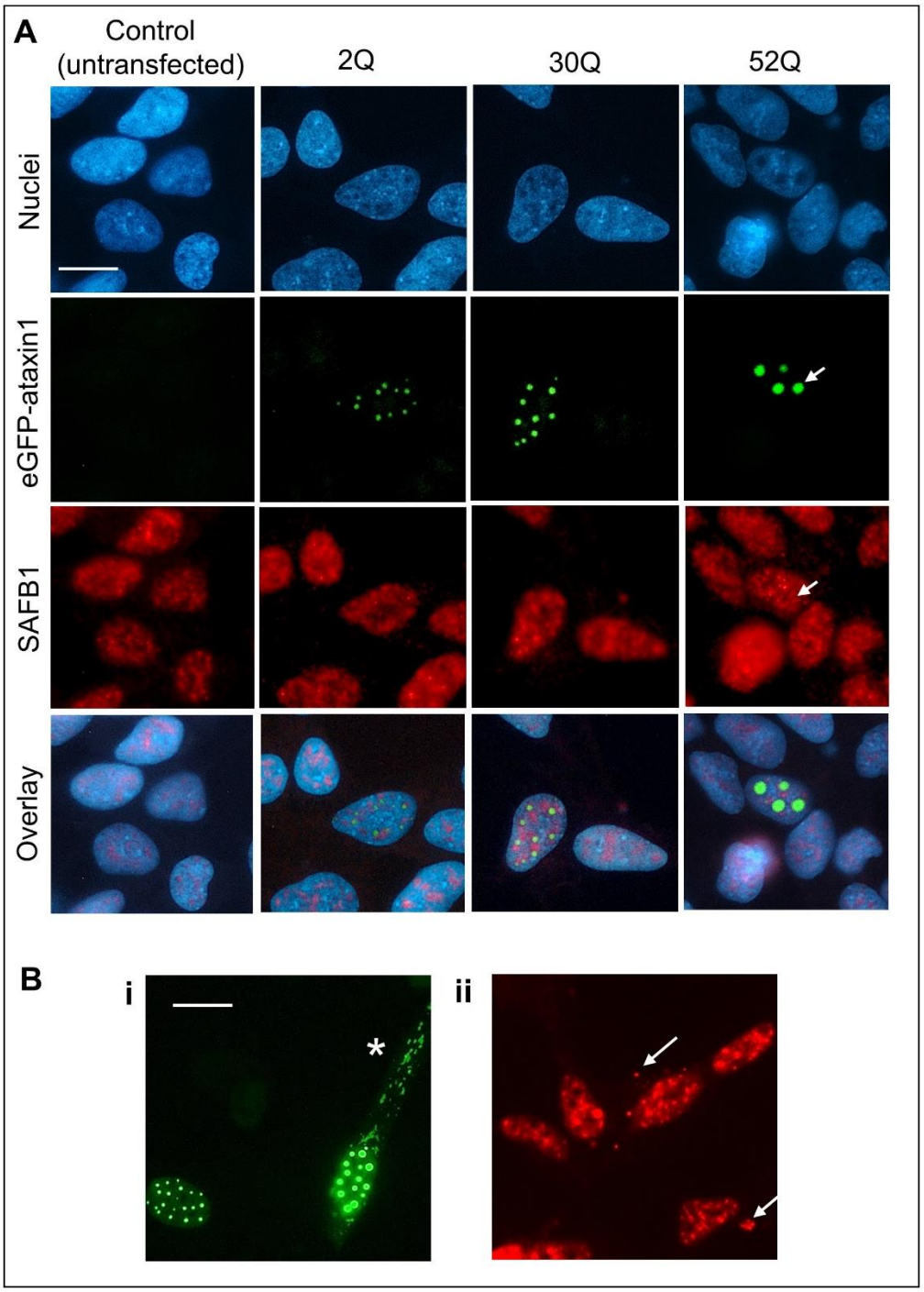

Figure 4.3 SAFB1 immunostaining in SH-SY5Y cells transfected with eGFP-ataxin1 constructs with varying CAG repeat lengths. **A**) eGFP-ataxin1 protein was expressed as large well-defined inclusions mostly within the nucleus. Inclusion size was variable within conditions, but in some cells there appeared to be an increasing size with increasing CAG length. eGFP-ataxin1 inclusions did not co-localise with areas of bright SAFB1 staining within the nucleus (arrows). Images captured with assistance from Mr. Ben Clennel. **B**) Two separate images representing less frequently occurring features observed amongst cells transfected with pathologically expanded ataxin1-52Q. **i**) eGFP-ataxin1 expressed both as nuclear inclusions and within the cytoplasm (asterisk). **ii**) SAFB1 immunostaining was present as small inclusions within the cytoplasm of some cells (arrows). Images are representative of cells across duplicate coverslips. Scale bars are 15µm.

4.4.2 *Development of an RNA IP technique to study the interaction of SAFB1 protein with* ATXN1 *RNA*

To investigate the interaction between SAFB1 protein and *ATXN1* RNA, an IP technique was developed. This allowed SAFB1 protein from HeLa cells transfected with *ATXN1* of varying CAG repeat lengths to be isolated, and the relative levels of associated *ATXN1* RNA to be quantified. eGFP is a 32.7KDa protein (239 amino acids) and contains multiple base-pair motifs predicted to interact with SAFB1 (Table 4.3). In contrast, FLAG (DYKDDDDK) is an eight amino acid tag of just 24 base pairs, containing only one possible motif predicted to interact with SAFB1 protein (Table 4.3). RNA IP experiments were therefore carried out using FLAG-tagged *ATXN1* constructs to minimise the likelihood of aberrant interaction of SAFB1 protein with tagged-*ATXN1* RNA transcripts.

RNA IP experiments were carried out in HeLa cells because they are readily transfected with DNA plasmids. Immunostaining of HeLa cells transfected with FLAG-*ATXN1* plasmids confirmed a good transfection efficiency (Figure 4.4A) and demonstrated that the expression pattern of FLAG-ataxin1 was similar to that observed for eGFP-ataxin1 (Figure 4.4B).

Based on protocols described in the literature (especially Konig et al. (2011), Izumikawa et al. (2017) and Volkening et al. (2018)), a workflow for RNA IP experiments was established (Figure 4.5).

Motif	Number occurring in eGFP	Number occurring in FLAG
Pentameric	**5**	**0**
GAAGA	1	0
AAGAA	1	0
AGAAG	2	0
Trimeric	**39**	**1**
GAA	11	0
AAG	21	1
AGA	7	0

Table 4.3 Pentameric and trimeric purine-rich motifs likely to be recognised by SAFB1 (Rivers et al. 2015) and their frequency of occurrence in eGFP and FLAG tags

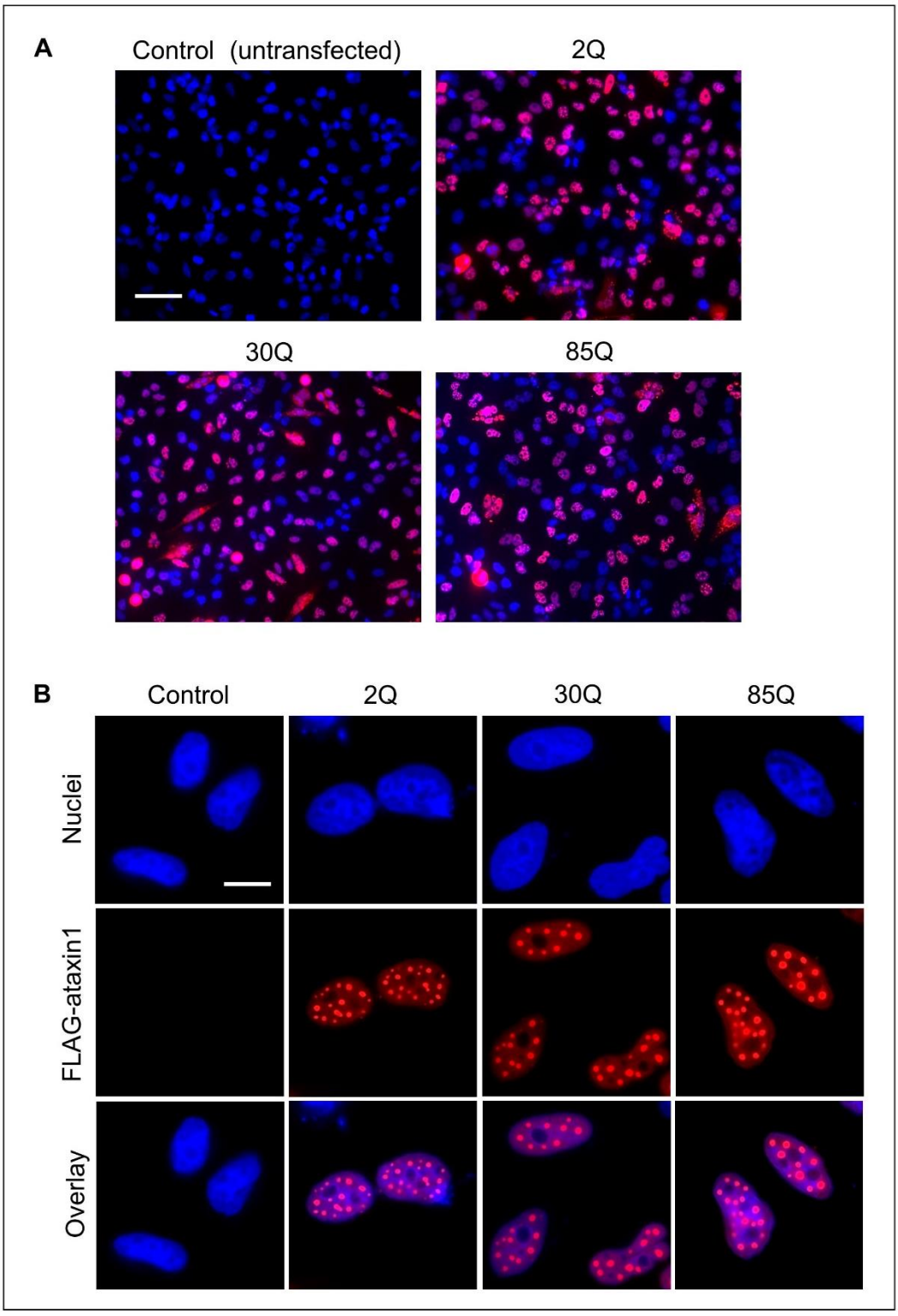

Figure 4.4 FLAG immunostaining in HeLa cells transfected with pcDNA1-FLAG-ataxin1 plasmids containing 2, 30 or 85 CAG repeats. **A**) Overlay of Hoechst fluorescence (blue) and FLAG immunostaining (red). Approximately 70% of cells expressed FLAG-ataxin1 48 hours after transfection. Scale bar is 50µm. **B**) Distribution of FLAG-ataxin1 in the nuclei of HeLa cells. Scale bar is 10µm.

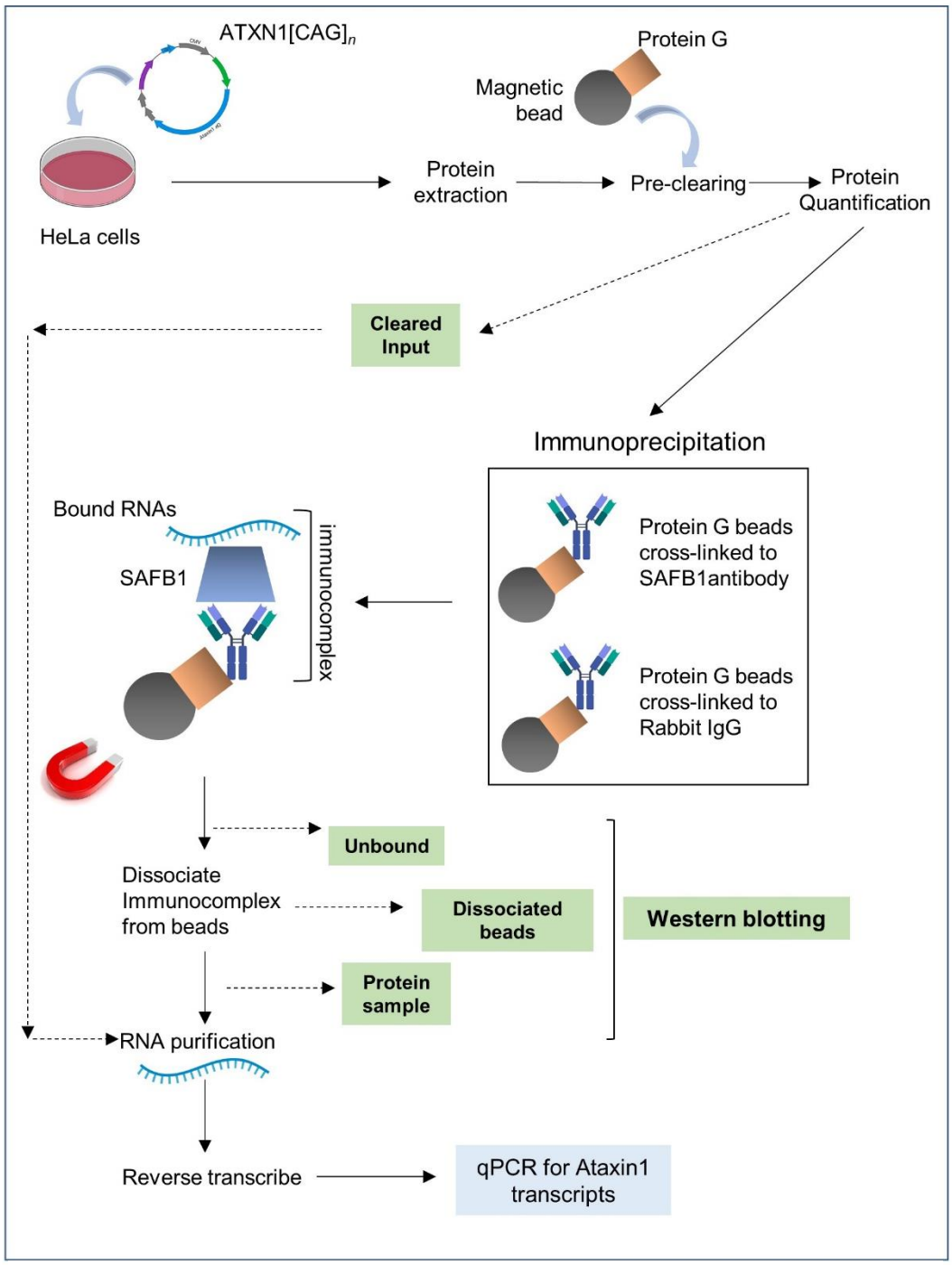

Figure 4.5 Diagram summarising stages of the RNA IP protocol used in this chapter

4.4.3 Confirmation of SAFB1 protein isolation using RNA IP protocol

Samples of input protein lysate, unbound lysate, protein bound to SAFB1 antibody-linked beads (IP) and protein bound to IgG-linked beads (IgG)

were reserved for Western blotting (Figure 4.6). A clear protein band corresponding to SAFB1 was present in the input of each experimental condition, and a weaker SAFB1 band was observed in the sample of immunoprecipitated protein in each experimental condition. This confirmed that SAFB1 protein was successfully isolated by the IP protocol. Furthermore, there was no SAFB1 protein present in the isotype control (IgG) samples.

A sample of unbound lysate (UB) was also analysed by Western blotting (Figure 4.6). There was no SAFB1 protein present in the unbound lysate following overnight immunoprecipitation with SAFB1, confirming that the antibody incubation protocol effectively bound and removed SAFB1 protein from the input lysates, therefore demonstrating that the antibody concentration to protein ratio was optimal.

To confirm that the protein-RNA immunocomplexes were effectively dissociated from the Protein G beads prior to RNA purification, a sample of dissociated beads (DB) was analysed by Western blot (Figure 4.6). There was a trace of SAFB1 protein remaining in the dissociated beads for the 2 CAG transfected sample, but overall the low/absent SAFB1 signal indicates that the immunocomplex was indeed successfully dissociated from the beads. Taken together, these results show that the protein isolation stage of the RNA IP was successfully optimised.

4.4.4 Pathological CAG expansion may increase the association of ATXN1 *RNA with SAFB1 protein*

Following qPCR analysis, the relative levels of *ATXN1* RNA were normalised per µg of SAFB1 protein (Table 4.4). The relative *ATXN1* expression in the IgG control samples was very low compared to in the IP samples. This isotype control, alongside the Western blot results (Figure 4.6), demonstrate that SAFB1 was specifically purified using the custom antibody AB1895.

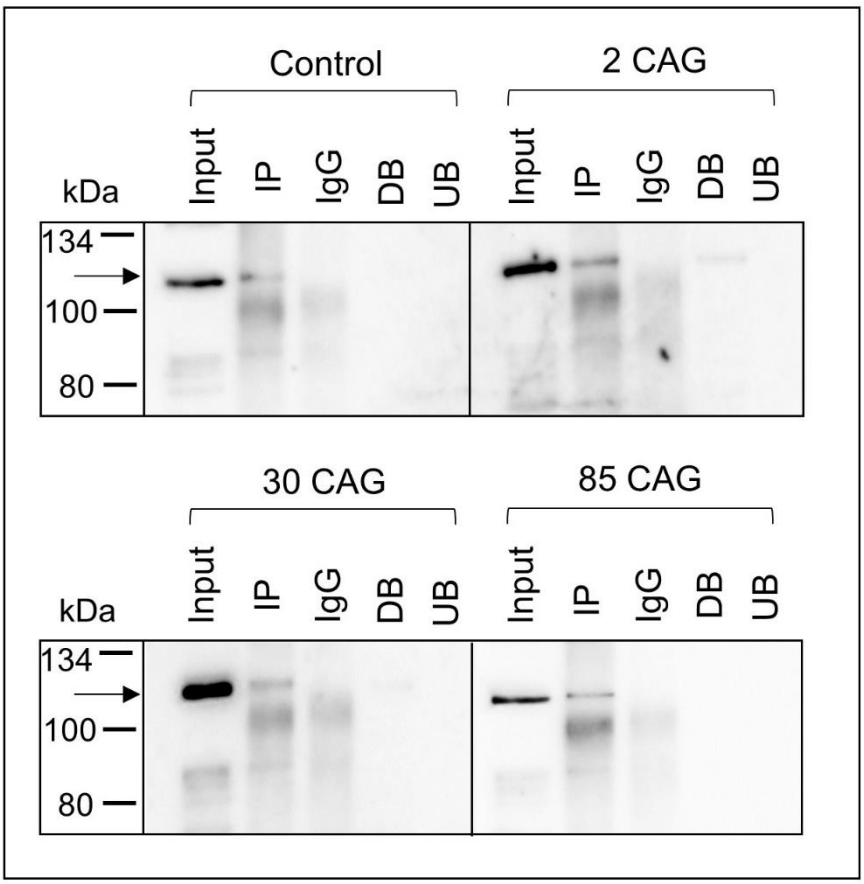

Figure 4.6 Western blots of protein samples from RNA IP experiments, probed for anti-SAFB1. Protein bands corresponding to the approximate molecular weight of SAFB1 (arrows) are visible in Input and IP samples but not in IgG samples, DB samples or UB samples. Input=protein lysate before IP. IP=protein associated with SAFB1 antibody-bound Protein G beads after IP. IgG=protein associated with rabbit IgG-bound Protein G beads after IP. DB=dissociated beads (Protein G beads after immunocomplex dissociation), UB=unbound lysate (protein unbound to SAFB1 antibody-bound Protein G beads after IP). n=1 IP experiment.

There was an increased relative amount of *ATXN1* RNA in the control IP samples (non-transfected) compared to the corresponding IgG control. This indicates the association of endogenous *ATXN1* with SAFB1. There were very low endogenous *ATXN1* levels relative to the 2, 30, and 85 CAG *ATXN1* transfected samples. This indicates that a) *ATXN1* expression is highly enriched in the transfected samples, confirming successful transfection and transcription of exogenous *ATXN1*, and b) the interaction

of SAFB1 protein with endogenous *ATXN1* transcripts accounts for a small proportion of the total quantified in transfected cells.

ATXN1 RNA was detected in all the transfected samples which were immunoprecipitated using the SAFB1 antibody, confirming that SAFB1 protein interacts with *ATXN1* RNA with varying length CAG tracts. Finally, results show an overall increase in the mean relative *ATXN1* expression in IP samples with an increasing CAG repeat length (Table 4.4)

The original experimental protocol was designed to quantify *ATXN1* levels in each input sample alongside its associated IP and IgG sample. Relative levels of *ATXN1* would then be expressed as a percentage of the ATXN1 levels in the input of each sample. This would correct for transfection and transcriptional variations between *ATXN1* plasmids. In each of the three experimental replicates, the CT values for the input samples were extremely low and therefore the relative levels of *ATXN1* could not be calculated. This meant that the relative *ATXN1* levels could not be normalised to account for variations in plasmid expression levels.

To correct for this, protein lysates from the input of each experimental condition were analysed for protein-level expression of FLAG-ataxin1 by Western blotting with a monoclonal antibody raised against the FLAG tag. The relative *ATXN1* expression levels were then normalised to their respective FLAG-ataxin1 levels as quantified by densitometric analysis (Figure 4.7). This analysis aimed to compare the interaction of SAFB1 protein with *ATXN1* with 2, 30 and 85 CAG transcripts and therefore does not include the control (non-transfected) samples.

Upon FLAG protein normalisation of the data, the apparent increase in relative 30 CAG *ATXN1* levels compared to 2 CAG *ATXN1* levels (Table 4.4) was eliminated, demonstrating the importance of normalisation when interpreting the results of RNA IPs.

Condition	n (experimental replicate)	Relative *ATXN1* IgG	Relative *ATXN1* IP
Control	1	0.03	1.68
	2	0.01	2.0
	3	0.04	2.71
	Mean	**0.03**	**2.13**
	SEM	**0.01**	**0.3**
2 CAG	1	0.14	11.80
	2	0.02	4.01
	3	0.20	58.76
	Mean	**0.12**	**24.86**
	SEM	**0.05**	**17.1**
30 CAG	1	0.23	27.22
	2	1.88	19.72
	3	0.44	140.21
	Mean	**0.85**	**62.38**
	SEM	**0.52**	**38.97**
85 CAG	1	0.41	50.83
	2	0.01	54.12
	3	1.0	177.58
	Mean	**0.47**	**94.18**
	SEM	**0.29**	**41.71**

Table 4.4 Relative levels of *ATXN1* RNA associated with SAFB1 protein immunoprecipitated from HeLa cells transfected with *ATXN1* with 2 (subphysiological), 30 (physiological) or 85 (pathological) length CAG repeat tracts. Control refers to untransfected cells. IgG refers to immunoprecipitations carried out with rabbit isotype control.

After normalisation to FLAG-tagged ataxin1 protein expression, RNA IP results showed that pathological expansion of *ATXN1* (85 CAG) resulted in an increased association of *ATXN1* RNA with SAFB1 protein when compared to 2 CAG and 30 CAG *ATXN1* (Figure 4.7). The effect size was large, but varied considerably between experimental replicates. In particular, experimental replicate 2 (n2) resulted in an approximately 20-fold higher percentage increase in 85 CAG vs. 30 CAG *ATXN1* levels compared to replicates 1 and 3 (Figure 4.7B). The data did not reach statistical significance. Given the large yet variable effect size, it is recommended that the number of experimental replicates is increased to afford better power in statistical testing.

The secondary structure of RNA transcripts alters binding to RBPs, therefore the secondary structure of *ATXN1* containing various CAG repeat tracts was modelled using Forna software (Figure 4.8). Modelling showed

that CAG expansion results in the formation of a typical hairpin loop, the length of which was extended with increasing numbers of CAG repeats.

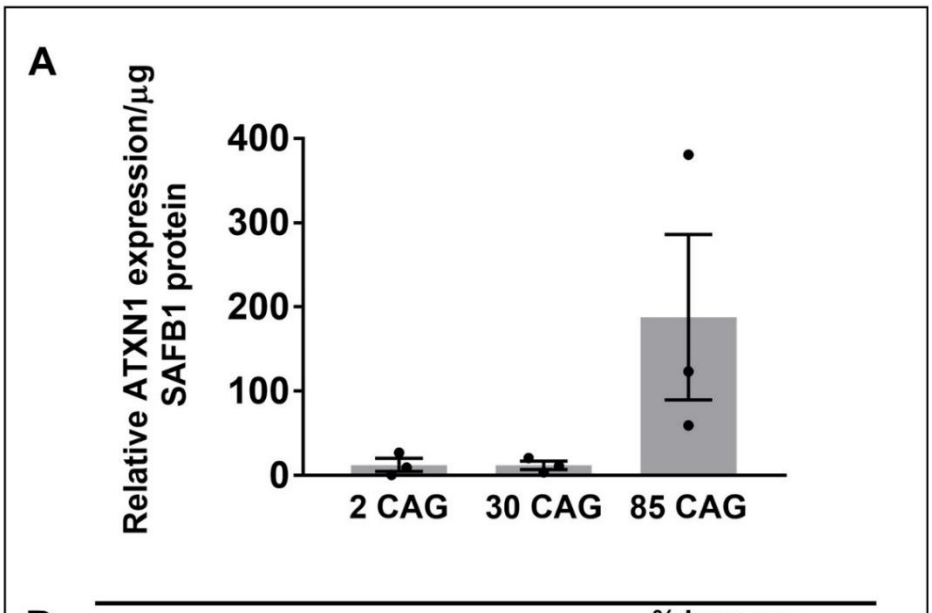

B

	2 CAG	30 CAG	85 CAG	% increase (30 vs. 85 CAG)
n1	27.30	20.91	123.44	590.40
n2	0.88	3.73	380.80	10199.23
n3	9.59	11.66	59.51	510.55
Mean	**12.59**	**12.10**	**187.92**	**3766.73**
SEM	**7.77**	**4.96**	**98.19**	**3216.33**

Figure 4.7 Pathological CAG expansion in *ATXN1* may increase its association with SAFB1 protein. **A**) Relative *ATXN1* RNA levels per µg of SAFB1 protein, normalised to FLAG-ataxin1 protein expression. There was no statistically significant difference between experimental groups (One-way ANOVA with Tukey's post-hoc test, n=3). **B**) Table detailing descriptive statistics of the RNA IP data summarised in (**A**).

4.4.5 Establishing human iPSCs with SAFB1/2 dual promoter deletion

CRISPR-Cas9 was used to genetically modify human iPSCs in collaboration with Professor Nick Allen's research group (School of Biosciences, Cardiff University). The aim was to create human iPSCs which can be differentiated into neurons which do not express SAFB1 or SAFB2, by deletion of the dual promoter. Kolf2 cells derived from the fibroblasts of a control patient were used in the CRISPR-Cas9 protocol (Figure 4.9).

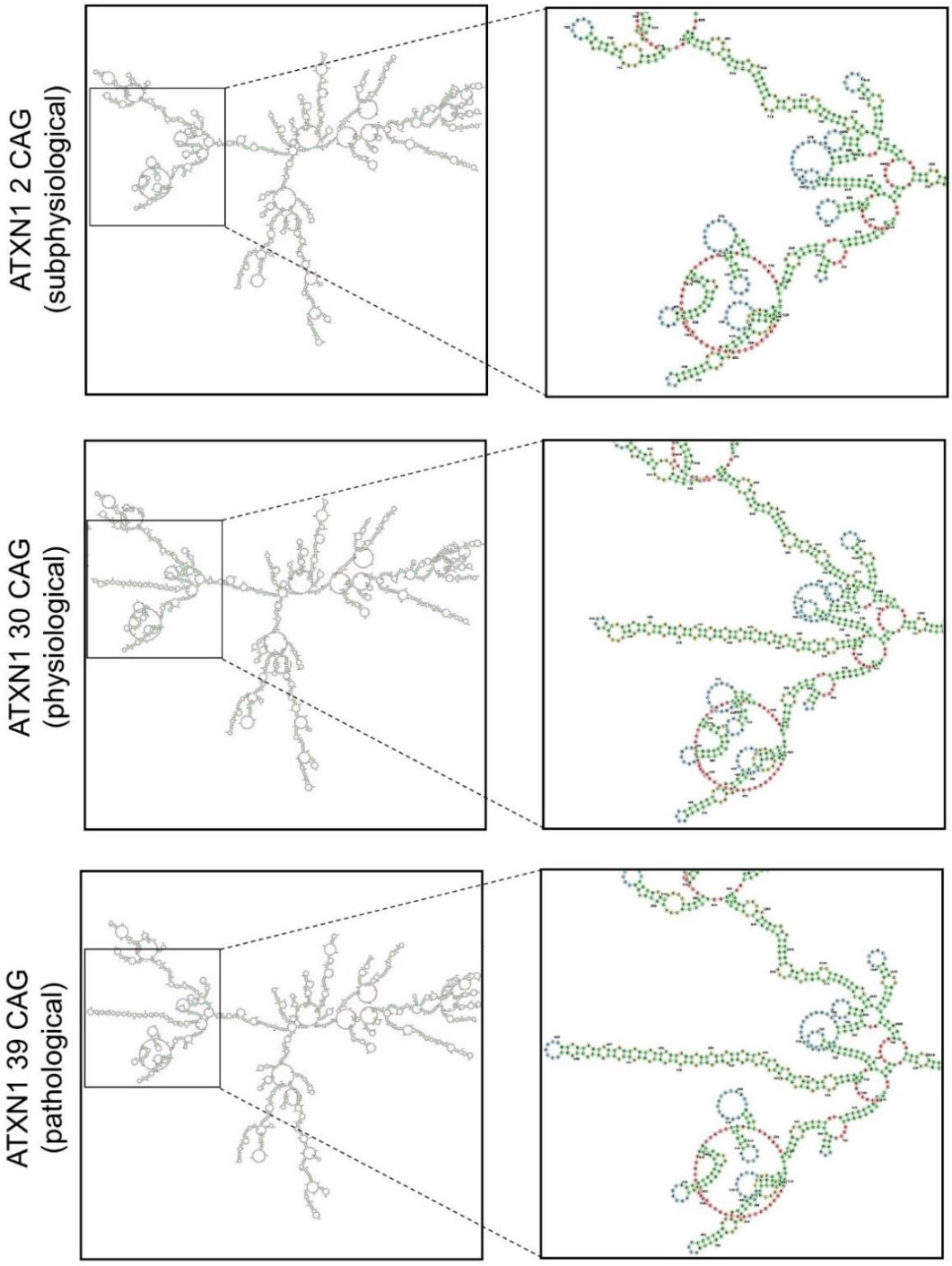

Figure 4.8 Secondary structure of *ATXN1* mRNA with 2 CAG repeats (below normal), 30 CAG repeats with one CAT interruption (normal range) and 39 uninterrupted CAG repeats (pathologically expanded). CAG repeats begin at nucleotide 589 in the *ATXN1* mRNA sequence, which is shown magnified in the inset box.

Graphics generated using Forna software (http://rna.tbi.univie.ac.at/forna/)

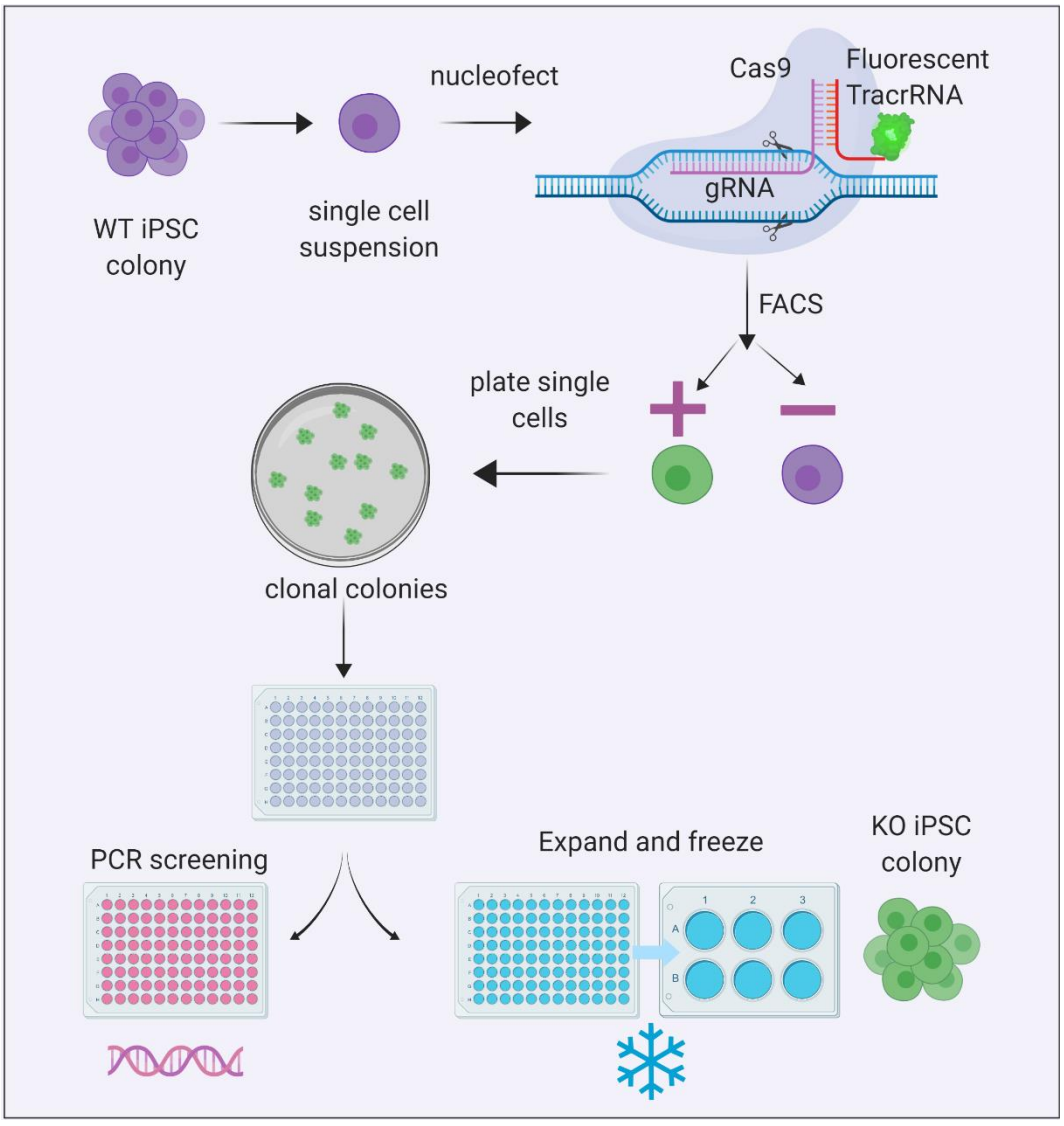

Figure 4.9 Diagram outlining the protocol for SAFB1/2 promoter knockout in human iPSC lines using CRISPR-Cas 9. KO knockout, WT wildtype.

Screening to determine which iPSC clones carried the deletion was carried out by PCR using primers flanking the dual promoter region. PCR conditions were optimised by adjusting reaction parameters until a single clear band of PCR product was visible (Figure 4.10Ai-iii). Following implementation of the CRISPR protocol, PCR was used to screen genomic DNA extracted from a 96-well plate of individual iPSC clones. Wildtype cells, heterozygous knockout cells and homozygous knockout cells were successfully detected (Figure 4.10Aiv). Confirmatory Sanger sequencing demonstrated deletion of the SAFB1/2 dual promoter (Figure 4.10B), and clones were frozen in liquid nitrogen for future use.

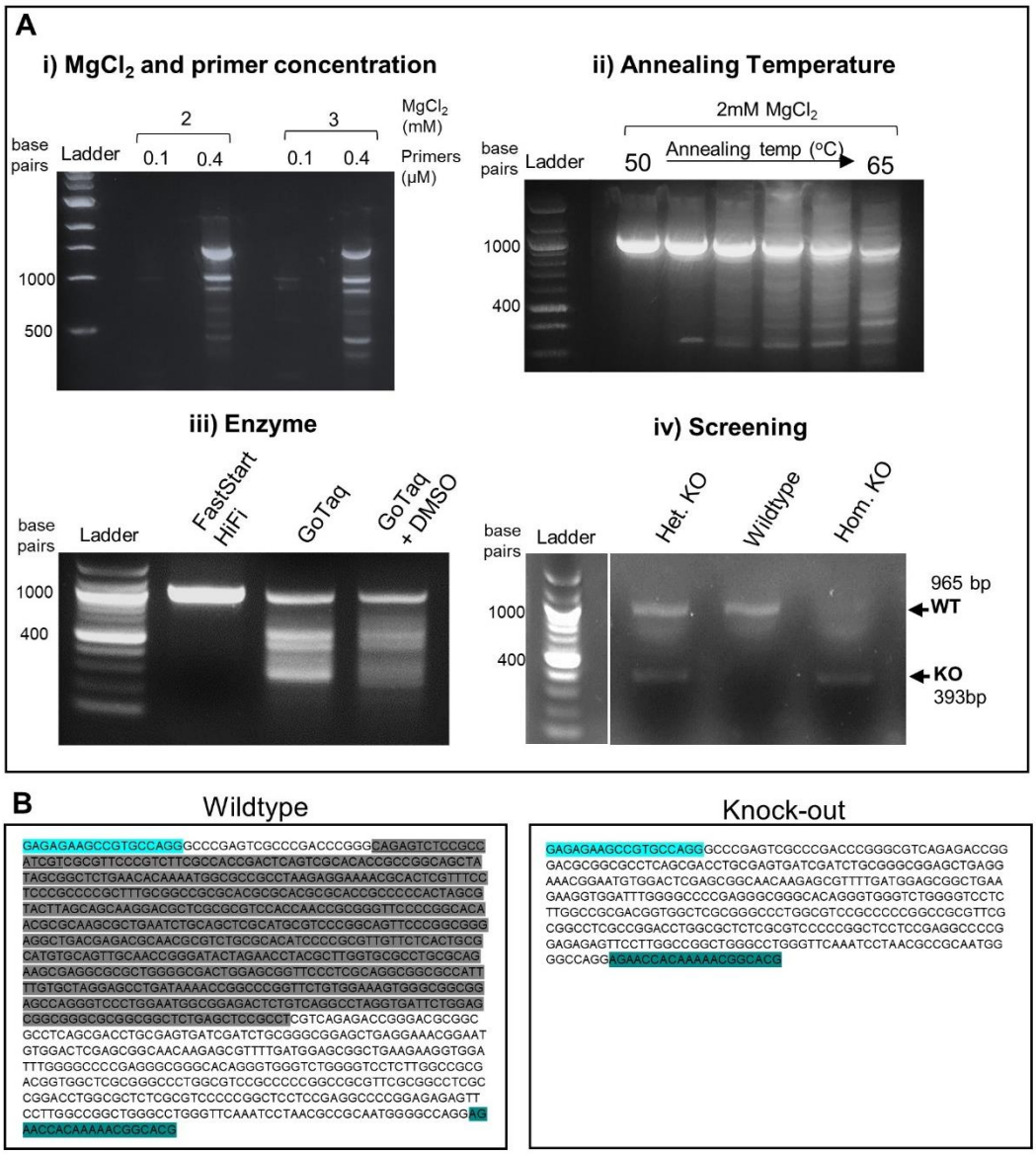

Figure 4.10 Screening Kolf2 iPSCs for deletion of SAFB1/SAFB2 dual promoter. **A**) Optimisation of conditions for PCR screening of SAFB1/2 dual promoter deletion. Genomic DNA extracted from iPSCs was amplified by PCR using primers complementary to sequences flanking the SAFB1/2 dual promoter sequence. In wildtype (WT) iPSCs the PCR product is 965bp, in knockout (KO) iPSCs the PCR product is 393bp. PCR conditions were optimised for primer concentration, $MgCl_2$ concentration (**i**) and annealing temperature (**ii**). Using optimised conditions (2mM $MgCl_2$, 0.4μM primers and 50ºC annealing), various PCR enzymes were tested. FastStart HiFi polymerase resulted in a clean band at 965bp in WT iPSC gDNA. Following CRISPR-Cas9 nucleofection, DNA was screened from clonal colonies of iPSCs. **A**) (**iv**) demonstrates the results from heterozygous (het. KO), WT and homozygous (hom. KO) colonies. **B**) Sanger sequencing was used to confirm deletion of the SAFB1/2 dual promoter in Kolf2 iPSCs. The WT promoter is highlighted in grey, whilst forward and reverse PCR primer sequences are highlighted in light and dark blue respectively.

4.5 Discussion

4.5.1 Key findings

This chapter used RNA IP to purify SAFB1 protein from HeLa cells, demonstrating that it associated with artificially expressed *ATXN1* RNA with 2, 30 or 85 CAG repeats. Pathological expansion of the CAG tract conferred an increase in the relative level of *ATXN1* RNA associated with SAFB1 protein. In addition to the RNA IP experiments, a human iPSC line with deletion of the SAFB1/2 dual promoter was established.

4.5.2 Evaluation of RNA IP methodology

To study RNAs which interact with a protein of interest, most established methods require protein purification which is usually carried out by IP (Ramanathan et al. 2019). This is often combined with chemical cross-linking of protein with its associated nucleic acids by irradiation with 245-nm UV light. Techniques which do not require protein purification are currently less well-established, and are based on chemical modification of RNA by artificially fusing the RBP of interest to either an ADAR enzyme (McMahon et al. 2016), or poly(U) polymerase (Lapointe et al. 2015), and sequencing either deaminated or poly(U) tailed RNAs, respectively. CLIP-seq methods combine protein purification and cross-linking with high-throughput sequencing to identify multiple RNA binding partners of a protein of interest. Many iterations of CLIP-seq exist, utilising different methods of cross-linking and RNA processing (reviewed by Ramanathan et al. (2019)). iCLIP was used previously by Rivers et al. (2015) to characterise the direct RNA binding partners of SAFB1, which include *ATXN1*.

In this chapter, protein IP was combined with RNA purification and qPCR to quantify the relative levels of *ATXN1* transcripts with varying CAG tract lengths associated with SAFB1. In preliminary optimisation experiments (not shown), HeLa cells were irradiated with UV to cross-link SAFB1 to *ATXN1* RNA transcripts. However, this requires an additional proteinase K processing step, and did not change the yield of SAFB1-associated RNA in comparison to un-crosslinked samples. As the IP was carried out under non-

denaturing conditions, *ATXN1* RNAs may either be directly bound to SAFB1, or associate to it via “bridging” molecules as part of a larger complex. Previous iCLIP results showed that SAFB1 binds to both the CAG tract and its flanking regions in *ATXN1*. The dynamics of RNA-protein interactions are highly complex, and it is also possible that even more distal regions of the RNA sequence may additionally contribute to the interaction of SAFB1 and *ATXN1*. This study utilised full-length *ATXN1*, permitting the transcript to form into its complete secondary structure, therefore more closely representing the *in-vivo* interaction between molecules.

RNA IP is a useful and appropriate tool for understanding the interactions between SAFB1 and *ATXN1* RNA transcripts. It is, however, important to consider any limitations of this experimental technique when interpreting the results of this chapter.

4.5.2.1 Variability between experimental replicates

Although each of the RNA IP experimental replicates showed that pathological CAG expansion increased the association of *ATXN1* RNA with SAFB1, there was variability in the relative increase between experiments. It is not clear where this variability arose. Despite this variability in effect size, in each experimental replicate the percentage increase in relative 85 CAG *ATXN1* levels associated with SAFB1 compared to 2 or 30 CAG *ATXN1* levels was substantial and consistent. As previously stated in section 4.4.4, further experimental replicates should be carried out to confirm statistical significance of the current result.

4.5.2.2 Copy number of transfected ATXN1 *plasmid*

The same molar amount of each *ATXN1* DNA plasmid was transfected into HeLa cells. The variation in size of the *ATXN1* inserts (arising from CAG expansion), resulted in a different copy number of plasmid under each experimental condition (Table 4.5). Compared to *ATXN1* 2Q, there were 1.7% fewer *ATXN1* 30Q plasmid copies, and 5% fewer *ATXN1* 85Q plasmid copies transfected. It was not considered necessary to correct for this relatively small variation, as it was deemed unlikely to have a significant

effect on the overall result. If the current results were subsequently corrected for copy number variation, the reduced number of 85 CAG *ATXN1* plasmids would further increase the difference between the amount of expanded *ATXN1* compared to non-expanded *ATXN1* associated with SAFB1. It is important to consider that correcting for plasmid copy number does not account for potential variation between transfection efficiency, or for variations in transcription or translation rates which could be caused by the pathological CAG expansion.

4.5.2.3 Correcting for transfected ATXN1 *RNA levels*

The RNA IP protocol was designed to express *ATXN1* RNA levels in the experimental IP samples relative to that expressed in their respective input sample (total levels prior to isolation of SAFB1). This corrects for variations in *ATXN1* RNA expression levels in the different experimental conditions.

It was not possible to carry out this correction in the current study, because the CT values of *ATXN1* expression in input samples were very low. Instead, a surrogate measure of transfection efficiency was used by quantifying FLAG-ataxin1 protein expression. This is an acceptable method of correcting for transfection efficiency, but not ideal as the experiment measures *ATXN1* RNA not ataxin1 protein. As previously established in the literature, CAG expansion is likely to affect translation efficiency (Raca et al. 2000, Krauss et al. 2013, Nalavade et al. 2013), therefore the levels of FLAG-ataxin1 protein may not correlate equally to levels of *ATXN1* RNA across experimental conditions.

Insert	Insert base pairs	Plasmid base pairs	Copies of plasmid transfected
FLAG-ATXN1 2Q	786	4819	2.88×10^{12}
FLAG-ATXN1 30Q	870	4903	2.83×10^{12} (-1.7% vs. 2Q)
FLAG-ATXN1 85Q	1035	5068	2.74×10^{12} (-5% vs. 2Q)

Table 4.5 Base pair lengths and approximate copy numbers of *ATXN1* plasmids transfected into HeLa cells for RNA IP experiments. Plasmid copy number was estimated by assuming an average base pair mass of 650 Daltons.

4.5.2.4 Other considerations for quantifying CAG expansion repeat sequences

ATXN1 RNA was converted to cDNA to facilitate qPCR analysis. The current experimental protocol assumes equal efficiency of reverse transcription between samples. However, it cannot be disproved that the CAG expansion may have conferred differences in the efficiency of reverse transcription. It has previously been established that variations in RT efficiency may be an important consideration for data interpretation (Schwaber et al. 2019).

4.5.3 Mechanisms of altered SAFB1 expression in polyQ disease

4.5.3.1 Causes of altered SAFB1 expression

As shown in Chapter 3, degenerating neurons in polyQ disease feature abnormal expression of SAFB1. In SCA Purkinje cells and HD MSNs, SAFB1 is expressed in the cytoplasm, and its expression in the nucleus is upregulated in cerebellar DN neurons. Mechanisms underpinning this change in SAFB1 expression are currently uncertain but could include binding of SAFB1 to expanded polyQ peptides, binding of SAFB1 to expanded polyCAG RNA, association of SAFB1 with other peptides altered in polyQ disease, or alterations in the nucleocytoplasmic transport of SAFB1 (Figure 4.11).

The work in this thesis, combined with published evidence, indicates that SAFB1 does not directly associate with expanded polyQ peptides, or with wildtype huntingtin or ataxin1: In this chapter it was shown that SAFB1 did not co-localise with artificially expressed ataxin1 in SH-SY5Y cells. Chapter 3 demonstrated that there was also no clear co-localisation of SAFB1 with polyQ huntingtin in HD patient striatal cells. Furthermore, proteomic analysis of the protein binding partners of SAFB1 in HeLa cells did not identify non-pathologically expanded ataxin1 or huntingtin as an interactor of SAFB1 (Allahyani 2020). In addition, SAFB1 was not identified as a protein interactor of pathologically expanded ataxin1 in mouse neuroblastoma cells, under either baseline or stress conditions (Zhang et al. 2018), nor was it

identified as an interacting partner of either physiological or pathological huntingtin (Ratovitski et al. 2012).

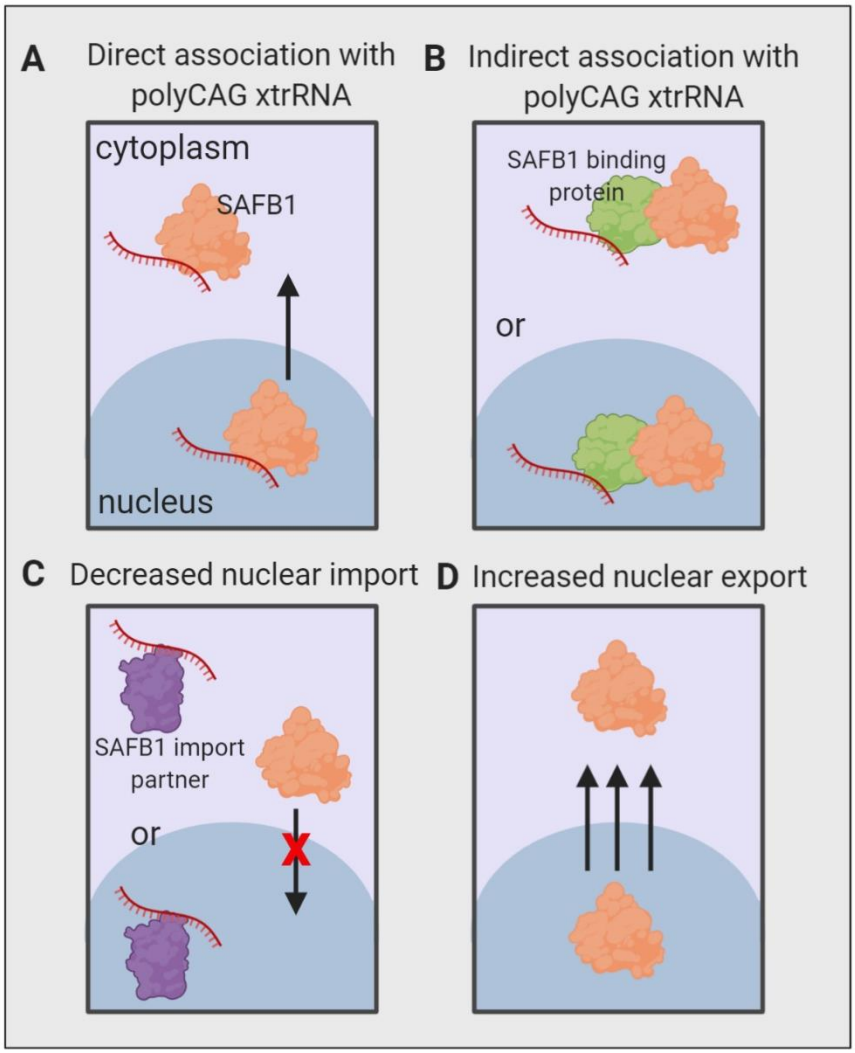

Figure 4.11 Illustration summarising the potential mechanisms by which SAFB1 protein is abnormally expressed in polyQ disease neurons.

The current results indicate that *ATXN1* RNA with 2 CAGs does not contain a hairpin loop, yet still interacts with SAFB1 at a similar level to *ATXN1* RNA containing a 30 CAG hairpin loop. Although this indicates that the hairpin loop itself may be dispensable for the interaction between SAFB1 protein and wildtype *ATXN1* RNA, previous iCLIP results demonstrated the enrichment of SAFB1 tags within both the CAG repeat tract itself and in the adjacent region. This indicates that both the CAG tract and its flanking sequence are important in mediating the interaction of *ATXN1* RNA with

SAFB1. Indeed, RNA hairpins comprising CAG repeats were previously shown to mediate protein interaction (de Mezer et al. 2011), and have been specifically shown to modulate binding to RRM motifs (Law et al. (2006), Clery and Allain (2011)). Flanking regions of RNA hairpin loops can mediate both RNA secondary structure (Sobczak and Krzyzosiak 2004), and RNA interaction with proteins (Sobczak et al. 2010). Taken together this indicates that both the CAG tract and flanking sequences of *ATXN1* may be important in the interaction with SAFB1.

In the case of pathologically expanded *ATXN1*, it is likely that the CAG repeat tract itself mediates the altered interaction with SAFB1. Highly structured regions in RNA transcripts (including stable hairpins) confer increased potential for protein interaction (Sanchez de Groot et al. 2019). As the inclusion of an uninterrupted 85 CAG stretch in *ATXN1* induces the formation of a highly structured stable hairpin loop, this is likely to directly influence the interaction of the RNA transcript with SAFB1, conferring an increased association between the two molecules.

The pathological expression of SAFB1 in the cytoplasm was identified as a feature of degenerating neurons in both SCA1 and HD. SAFB1 protein was not identified to interact with wildtype or expanded *HTT* RNA in a recent study by Schilling et al. (2019). If SAFB1 does indeed not interact with *HTT*, this would indicate that a) the presence of a CAG hairpin alone is not sufficient to mediate an interaction with SAFB1, and b) there may be mechanisms underpinning the abnormal expression of SAFB1 in polyQ disease additional to its direct association with polyCAG RNA.

However, the limitations of this single study by Schilling et al. should be considered; the work was carried out in *Drosophila* which only express one form of SAFB. Furthermore, the expression levels of SAFB1 itself and its potential RNA binding partners may not have been at high enough levels to observe an interaction. To date no studies have been carried out to quantify the protein binding partners of *HTT* RNA in patient tissue. These considerations are combined with the knowledge that some SAFB1 iCLIP

tags were present within *HTT* RNA transcripts (unpublished observation, Rivers et al. (2015)), indicating potential for a direct interaction between SAFB1 and polyCAG *HTT* RNA transcripts in HD.

The processing and transport of RNA containing polyCAG tracts could be altered by the increased binding of SAFB1. It is possible that polyCAG *ATXN1* RNA directly sequesters SAFB1 in the nucleus, then becomes exported into the cytoplasm (Figure 4.11A). A preprint (non-peer reviewed publication) by Zhang et al. (2018a) reports that expression of *ATXN1* with 85 CAG repeats disrupts multiple nuclear transporters, resulting in the increased localisation of CRM1 (a key mRNA nuclear transporter known to be involved in the export of xtrRNA) to the nucleus, indicating a possible mechanism for the increased export of polyCAG RNA into the cytoplasm.

SAFB1 binds proteins implicated in neurodegenerative disease pathology and repeat expansion disorders including SRSF1 (Denegri et al. 2002, Hautbergue et al. 2017), FUS (Yamaguchi and Takanashi 2016), Matrin 3 (Tada et al. 2018), Sam68 (Sergeant et al. 2007, Sellier et al. 2010) and hnRNP K (White et al. 2010). As CAG expansion repeats sequester diverse proteins (Nalavade et al. 2013), it is possible that pathological *ATXN1* transcripts in the cytoplasm or nucleus could aberrantly associate with proteins which are in turn binding partners of SAFB1, forming a protein-RNA complex in the cytoplasm or nucleus (Figure 4.11B).

Dysregulation of nucleocytoplasmic transport is emerging as an important mechanism in neurodegenerative disease (Dormann et al. 2010, Fahrenkrog and Harel 2018) and the transport of RBPs is known to be altered in polyQ disorders and ALS (Chan et al. 2011, Malik et al. 2018). It is possible that expanded *ATXN1* RNA in the cytoplasm or nucleus sequesters important protein binding partners of SAFB1 which facilitate its post-translational nuclear import, rendering SAFB1 trapped in the cytoplasmic compartment (Figure 4.11C). This could subsequently lead to a nuclear loss of function of SAFB1, inducing a compensatory increase in expression which allows SAFB1 to enter the nucleus via an alternative

mechanism, thus explaining the increased nuclear expression of SAFB1 observed in polyQ DN neurons. This hypothesis is supported by the findings that polyCAG RNA forms pathological complexes with RNA export proteins including the nuclear export receptor NXF1, resulting in abnormal nucleocytoplasmic transport of repeat expansion protein and RNA (Tsoi et al. 2011). SAFB1 binds SRSF1 (a splicing factor and nuclear export adaptor) to mediate the export of pathological repeat RNA into the cytoplasm, a process implicated in neurodegeneration (Hautbergue et al. 2017). It is also possible that an upregulation of SAFB1 export into the cytoplasm occurs in polyQ disease neurons, perhaps via increased expression of nuclear transporters or SAFB1 export partners (Figure 4.11D).

4.5.3.2 Consequences of altered SAFB1 expression

As SAFB1 is a multifunctional protein which is involved in regulating gene expression, DNA repair, apoptosis, dendritic function and the cell stress response, it is likely that dysregulated expression of SAFB1 has many functional consequences in affected neurons.

Pathological expression of SAFB1 in the cytoplasm of neurons may cause a toxic gain of function. SAFB1 binds to many proteins (Table 1.9) which could be sequestered in the cytoplasm by abnormally expressed SAFB1. This could affect the functions usually carried out by these proteins, including transcriptional regulation and RNA transport in affected neurons. Cytoplasmic SAFB1 could also aberrantly bind to both coding and non-coding RNA transcripts in the cytoplasm, inducing a range of functional consequences in affected neurons.

Altered SAFB1 expression in polyQ disorders could induce a loss or gain of function in the nucleus. Nuclear SAFB1 is important in regulating neuronal transcription and splicing of many genes, which may become dysregulated if SAFB1 levels in the nucleus are disrupted. Variation in DNA repair gene expression contributes to age of onset and progression of polyQ disorders (Lee et al. 2015, Holmans et al. 2017). Nuclear SAFB1 mediates the DNA

damage response (Altmeyer et al. 2013), therefore its altered expression in the nucleus could contribute to disrupted DNA damage repair processes in neurons affected by polyQ pathology. A recent study showed that loss of DNA damage response function in FUS was important in mediating its pathological effects, and leads to formation of cytoplasmic FUS inclusions (Naumann et al. 2018). As SAFB1 both binds to and shares structural and functional similarities to FUS, this study draws into consideration the possibility that alterations in the DNA damage response function of SAFB1 could be linked to its altered cytoplasmic expression. As SAFB1 was recently discovered to mediate heterochromatin structure (Huo et al. 2019), its altered expression in the nucleus could also result in dysregulation of chromatin stability.

During the cellular stress response *in-vitro*, SAFB1 localises to the SatIII locus and recruits HSFs at the site of nSB formation (Denegri et al. 2002, Jolly et al. 2004, Norman et al. 2016). nSBs sequester transcription factors as a protective response against cellular stress. Neuronal stress response pathways have been previously described (Farley and Watkins 2018), and may act as protective mechanisms against *in-vivo* insults which contribute to neurodegenerative cell loss in the brain. These insults include mitochondrial stress, oxidative stress, neuroinflammation, proteasomal dysfunction and toxin exposure (Tofaris and Buckley 2018). Although the role of SAFB1 in the cellular stress response *in-vivo* or in neurons is not yet understood, it is hypothesised that SAFB1 may play an important role (Norman et al. 2016). Altered expression of SAFB1 (resulting from either dysreguated expression levels or protein mislocalisation) could therefore potentially dysregulate the protective cell stress response in neurons, rendering them more vulnerable to neurodegenerative damage.

The expression of SAFB1 and SAFB2 is controlled by a bidirectional promoter (Townson et al. 2003). It has previously been shown that SAFB1 and 2 regulate each other's expression levels; depletion of SAFB1 expression increases the expression of SAFB2 (Hong et al. 2015). Therefore, disturbances in SAFB1 expression may consequently affect the

expression of SAFB2, potentially inducing further dysregulation of neuronal functions.

4.5.4 Recommendations for future work

4.5.4.1 Future work using RNA IP

The RNA IP protocol developed here could be used to further understand the role of SAFB proteins in polyQ disease. For example, the experiment could be repeated using an antibody raised against SAFB2. This could be carried out in parallel with protein-level characterisation of SAFB2 in patient tissue to characterise a second member of the SAFB family in neurodegenerative disease. Future RNA IP experiments should aim to normalise *ATXN1* RNA levels in IP samples to that of the corresponding input sample. It should be noted that in this study, reverse transcription was carried out using random primers. To specifically study the levels of *ATXN1* mRNA, reverse transcription could be carried out in future experiments using oligo(dT) primers.

To further understand the importance of SAFB1 interaction with polyCAG RNA transcripts, the RNA IP could be repeated with plasmids containing *ATXN1* with a mutated or absent start codon. This would prevent translation of exogenous *ATXN1* into polyQ peptides. If a differential interaction of SAFB1 protein with *ATXN1* RNA was still found, then this would prove that this interaction is independent of polyQ protein. Conversely, if the effect was lost, this would indicate that the expression of expanded polyQ peptides could be important in mediating the interaction of SAFB1 protein and *ATXN1* polyCAG RNA (for example, SAFB1 might interact with both polyQ peptides and polyCAG RNA transcripts in a protein-RNA complex).

The RNA IP technique may be sensitive enough to measure the interaction of SAFB1 with endogenous *ATXN1* RNA. For example, neurons differentiated from a SCA1 patient-derived iPSC line (Buijsen et al. 2018) could be compared to control neurons. This would give a more direct insight into the mechanisms of SAFB1 and its interaction with polyCAG RNA in

human disease cells, with a higher translational potential than using the HeLa line.

4.5.4.2 Future work using iPSCs

Following successful deletion of the SAFB1/2 dual promoter in Kolf2 iPSCs, the frozen stocks of iPSCs should be expanded to create a large stock of low-passage cells. Undifferentiated iPSCs should be characterised by immunostaining and Western blotting to validate deletion of SAFB1 and SAFB2. Furthermore, iPSCs could be differentiated into neurons using standard protocols established by Professor Allen's research group, and characterised for expression of SAFB1 and SAFB2 protein. As SAFB1 is critical for neuronal development and important for neuron function, it is quite possible that deletion of the dual promoter could confer toxic effects. Indeed, during the CRIPSR process, it was observed that iPSC colonies with SAFB1/2 knockout often did not grow and thrive as well as their wildtype counterparts. If this was the case, it may be preferable in future to delete SAFB1 or SAFB2 alone using modified gRNAs targeting the respective gene sequences. Cell lines edited using CRISPR/Cas9 should be screened for off-target effects (Zhang et al. 2015).

There is great potential to further utilise the SAFB dual promoter knockout cells. The HD iPSC Consortium (2012) published a landmark characterisation of iPSC lines from HD patients with various CAG repeat lengths, and from control donors. Professor Nick Allen's laboratory at Cardiff University were involved with this work and have since utilised the HD109.1 cells to create an isogenic corrected control line expressing 2 CAG repeats. Applying the CRISPR procedure detailed in this chapter to both the HD109 and corrected control iPSCs would establish a neuronal model of polyQ disease with SAFB1/2 dual promoter deletion.

In further association with the consortium, CAG repeat disease phenotyping in HD iPSCs was carried out by Mattis et al. (2015). This study established protocols for assaying disease phenotype in iPSC-derived striatal neuronal cultures, for example by inducing cell stress by growth factor withdrawal and

by glutamate-induced toxicity. In future, HD 109 and HD 2 CAG lines on both a wildtype and SAFB1/2 deletion background could be assayed to assess the effect of SAFB protein deletion on CAG-expansion dependent disease phenotypes.

4.5.5 Conclusions

This chapter built upon the results of Chapter 3 to further investigate SAFB1 in polyQ disease by developing an RNA IP protocol to quantify the association of *ATXN1* RNA with SAFB1 protein. Using this technique, it was confirmed that SAFB1 interacts with *ATXN1* RNA with a physiological CAG repeat tract, supporting the results of iCLIP experiments carried out previously by our research group. Furthermore, it was demonstrated that pathological CAG expansion modulates the interaction of SAFB1 with *ATXN1*, increasing the level of RNA associated with SAFB1. It should be noted that, despite the large effect size, further experimental replicates may be required for the current data to reach statistical significance.

This result offers a new insight into the potential mechanism which may underpin the role of SAFB1 in polyQ disease. It is possible that the long stable hairpin loop formed by the expanded CAG tract in *ATXN1* confers increased interaction with SAFB1 protein. This in turn could induce mislocalised expression of SAFB1, and consequent loss of nuclear function and/or gain of cytoplasmic function in polyQ disease patient neurons. Overall, the findings presented here (and taken together with Chapter 3) support an increasing body of evidence which shows that RBP dysregulation contributes to the aetiology of human neurodegenerative disease.

5. Chapter 5

In-vitro screening identifies kenpaullone as a novel pharmacological modulator of mitochondrial health and function

5.1 Overview

5.1.1 Chapter overview and introduction

Mitochondrial dysfunction contributes to the pathogenesis of PD and other neurodegenerative disorders. This is caused by increased mitochondrial damage, combined with dysregulation of mitochondrial quality control mechanisms including fission and fusion events which regulate the health and morphology of mitochondria, and mitophagy to remove irreparably damaged organelles (section 1.7.2). Retaining or restoring the health and normal function of mitochondria in the brain therefore represents a targetable mechanism for therapeutic intervention. The recruitment of parkin to mitochondria is an essential early step in mitophagy signalling. This study therefore used a high-content assay of parkin recruitment to identify neuroactive compounds that modulated this process. This primary screen found that kenpaullone (a glycogen synthase kinase-3 beta (GSK-3 beta) and cyclin-dependent kinase (CDK) inhibitor) negatively modulated parkin recruitment.

Secondary screening assays were also carried out using *in-vitro* mitochondrial assays, and these confirmed kenpaullone as a novel pharmacological modulator of both the morphology of the mitochondrial network and mitochondrial function. Studies in mixed human neuronal and glial cultures differentiated from foetal neuroprogenitors showed that kenpaullone modulated the appearance of the mitochondrial network. Kenpaullone or its mechanisms of action could represent a novel therapeutic approach to ameliorating mitochondrial dysfunction in neurodegenerative pathologies such as PD.

5.1.2 *Graphical abstract*

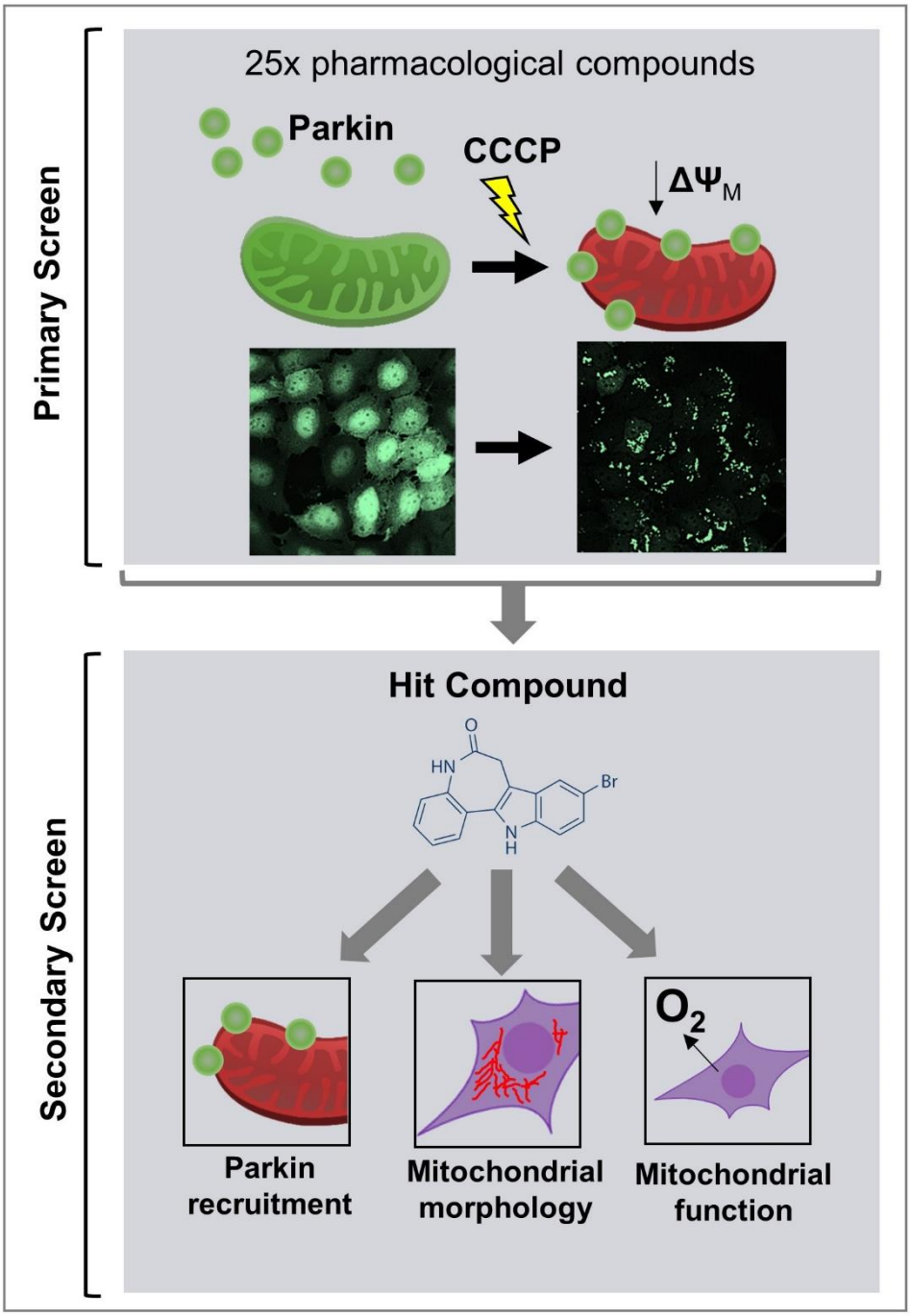

Figure 5.1 Graphical abstract for Chapter 5

5.2 Methods

5.2.1 Cell culture

Two human cell lines (H4 and SH-SY5Y) stably expressing eGFP-parkin were used for primary and secondary screening of drug compounds. Human foetal neuroprogenitor cells (hfNPCs) were utilised with the technical assistance of Ms. Andriana Gialeli for validation experiments. Cell culture methods for human cell lines are detailed in section 2.3.1 and for hfNPCs (including ethics approval details) in section 2.3.5. In all experiments, cells treated with drug compounds were directly compared to a control group treated at the same time with an equal volume of the drug solvent DMSO.

5.2.2 Induction of parkin recruitment

For experimental assays, parkin recruitment was induced in H4 eGFP-parkin cells by treatment with 15µM CCCP for 2 hours. Dose-response optimisation of CCCP-induced parkin recruitment in SH-SY5Y eGFP-parkin cells was previously carried out by Dr. Helen Scott and Mr. Gongyu Shi. This work concluded that to induce levels of parkin recruitment equivalent to that seen in H4 eGFP-parkin cells with no cell toxicity required exposure to 15µM of CCCP for 4 hours. SH-SY5Y eGFP-parkin dose-response experiments are not shown here.

5.2.3 Compound library primary screening

A small library of neuroactive drug compounds was sourced as a kind gift from Takeda, U.K. (Table 5.1). Compounds which crossed the BBB and modulated pathways and mechanisms relevant to neurodegeneration were selected by Takeda scientists. The compounds have evidence in the literature to support their potential as neuroprotective compounds, and some are in clinical trials. All compounds were sourced from Tocris except Cu-ASTM which was sourced from Sigma. Compounds were quality controlled for purity and 1µl of 5mM compound stamped onto daughter plates. Upon receipt from Takeda, daughter plates were stored at -80^{o}C, and prepared immediately before use by adding 99µl of culture media to

each well to give a 50µM stock solution. 25µl of stock compound was added to 100µl of media in cell culture plates to give a final concentration of 10µM in 0.2% DMSO. Compounds were incubated with H4 eGFP-parkin cells for 24 hours then tested for their ability to modulate parkin recruitment to mitochondria. Details of high-content image acquisition and analysis protocols can be found in section 2.4.

5.2.4 Secondary screening (parkin recruitment and mitochondrial morphology)

Parkin recruitment and mitochondrial morphology analysis in both H4 eGFP-parkin and SH-SY5Y eGFP-parkin cells was used to assay the effect of compounds in secondary screening. Details of high-content image acquisition and analysis protocols can be found in section 2.4, and details of mitochondrial assays in section 2.5. Kenpaullone was sourced from Sigma (K3888) and diluted in fresh, sterile DMSO to a stock concentration of 5mM before aliquoting and storing at -20^{o}C until use. Aliquots were thawed immediately before use and diluted to final working concentration in cell culture media before adding to cells for 24 hours prior to carrying out assays.

5.2.5 Secondary screening (MPP+ assay)

To assess whether kenpaullone is protective against mitochondrial toxins, its effect on mitochondrial MitoTracker Red staining and cell number was measured in H4 eGFP-parkin cells challenged with MPP+. Details of the MPP+ toxicity assay procedure can be found in section 2.5.3.

5.2.6 Secondary screening (live cell mitochondrial function assays)

The effect of kenpaullone on mitochondrial respiration was assessed in live H4 eGFP-parkin cells using the Seahorse XFp analyser (Agilent) (section 2.5.4).

Drug compounds (library screening)	Description
AR-A 014418	Selective GSK-3 inhibitor
Azoramide	Unfolded protein response (UPR) modulator
B2	Promotes inclusion formation in HD and PD
BIX	BiP (Hsp70-5) ER chaperone inducer
Cu-ASTM	Antioxidant, acts on peroxynitrite
Dantrolene	Ca^{2+} release inhibitor
Dimethylfumarate	Neuroprotective Nrf2 pathway activator
Edaravone	Anti-ischaemic and antioxidant
GSK2606414	Potent and selective PERK inhibitor
Kenpaullone	CDK and GSK-3beta inhibitor
LOE 908 hydrochloride	Neuroprotective broad spectrum cation channel blocker
Memantine	NMDA antagonist
N-Acetylcysteine amide	Cell permeable antioxidant
Olesoxime	Binds VDAC
PD-150606	Calpain inhibitor
Rapamycin	mTOR inhibitor, immunosuppresant
Resveratrol	Cyclooxygenase inhibitor
Riluzole	Glutamate release inhibitor, GABA uptake inhibitor
SKF 85536	Potent and selective D1-like dopamine receptor antagonist
Sodium 4-Phenylbutyrate	HDAC inhibitor, ER stress blocker
SP600125	Selective JNK inhibitor
trans-ISRIB	Integrated stress response inhibitor
TRC 051384	Inducer of heat shock protein Hsp70
Z-VAD-FMK	Cell-permeable, irreversible caspase inhibitor
Drug compounds (mechanistic testing)	**Description**
AT7519	CDK and GSK-3beta inhibitor
AZD5438	CDK and GSK-3beta inhibitor
Dexpramipexole	Weak dopamine agonist, reduces mitochondrial ROS production
Olesoxime (TRO19622)	Modulates mitochondrial permeability transition pore opening, binds outer mitochondrial membrane proteins (TSPO and VDAC)

Table 5.1 Description of pharmacological compounds tested in Chapter 5

5.2.7 Validation study in differentiated foetal neuronal/glial cells

The effect of kenpaullone on the mitochondria of differentiated foetal neuroprogenitor cells was assessed to validate the results of the primary and secondary screen. hfNPCs were grown as neurospheres in non-adherent culture. One or two individual neurospheres were picked and plated into each chamber of an 8-well chamber slide (NuncTM, Invitrogen). Chamber slides were pre-coated with sterile poly-D-lysine overnight at 37ºC, washed in sterile distilled water, then coated in sterile laminin for 1 hour at 37ºC. Neurospheres were cultured in hfNPC differentiation media for 7 days to allow them to adhere and differentiate into mixed neuronal/glial cultures.

For compound validation, foetal cultures which had grown in differentiation media for 6 days were pre-treated with 5µM of kenpaullone or DMSO for 24 hours. To visualise mitochondria, cultures were either incubated with 100nM MitoTracker Red for 1 hour at 37ºC prior to fixation, or immunolabelled using an antibody raised against TOMM20 (Table 2.3). CCCP treatment was carried out after MitoTracker Red staining. Immunofluorescent staining of foetal cells was carried out inside chamber slides. Culture media was removed and the cells gently washed with PBS. Cells were fixed in 4% PFA for 20 minutes at room temperature, washed in PBS then permeabilised in ice-cold methanol for 20 minutes at -20ºC. After washing in PBS, cells were incubated in 10% normal goat serum in PBS for 2 hours at room temperature to block non-specific binding of primary antibodies. Neurons were immunolabelled using an anti-TUBB3 antibody (Table 2.3) diluted in blocking solution overnight at 4ºC. Cells were washed and incubated in Alexa Fluor conjugated secondary antibody(ies) diluted in blocking solution for 90 minutes at room temperature (Table 2.4). Nuclei were counterstained using 1µg/ml DAPI, before mounting the cells beneath a glass coverslip in mowiol mounting medium. Slides were stored in the dark at 4ºC and imaged within 1 week using a Nikon C1 confocal microscope with EZ viewer software.

5.3.1 Parkin recruitment assay optimisation

The results of this section detail the process of optimising the induction, visualisation, segmentation and quantification of parkin recruitment to mitochondria by pharmacological insult using the ionophore CCCP. A summary of the optimisation and screening experiments of this chapter can be found in **Error! Reference source not found.**.

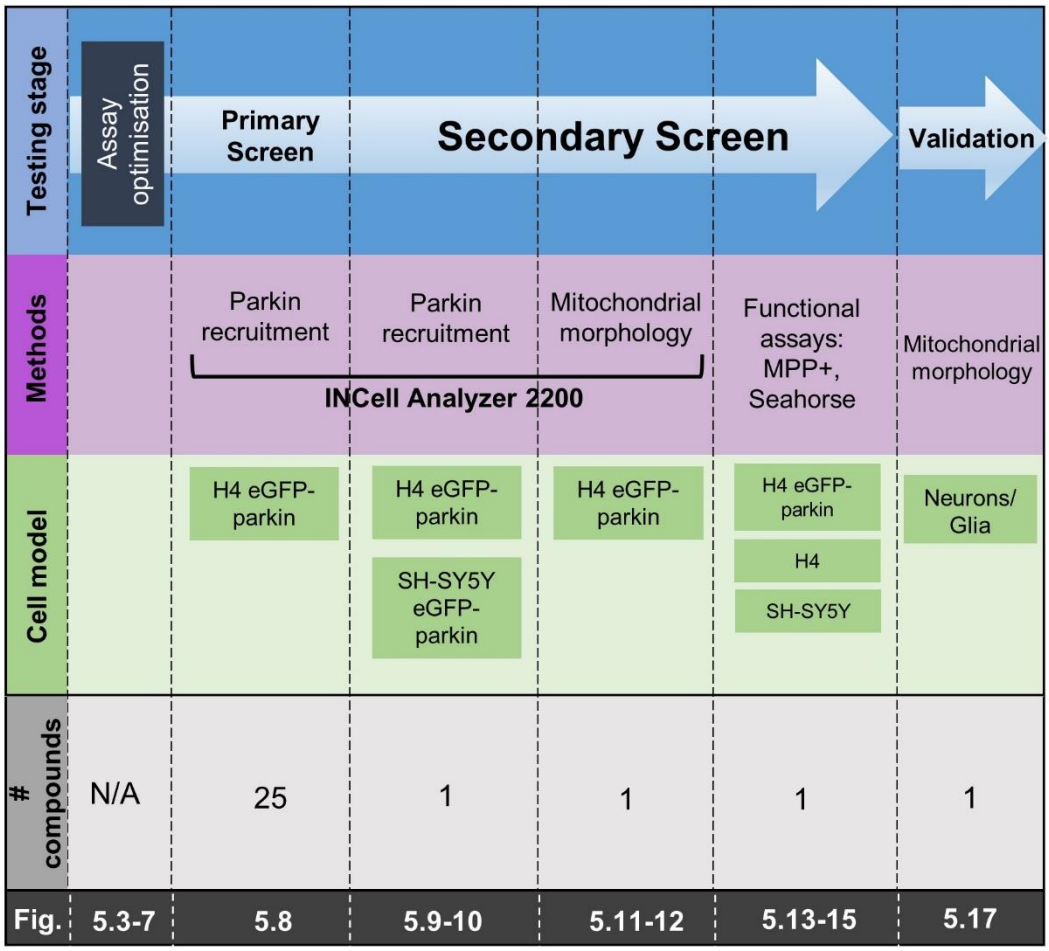

Figure 5.2 Overview of experiments carried out in Chapter 5. Assay optimisation was followed by screening and then validation of drug effects on the cellular mitochondrial network. The figure numbers relating to each experimental stage are referenced at the bottom of the diagram.

5.3.1.1 High-content imaging of parkin recruitment to mitochondria

A human neuroglioma (H4) cell line stably expressing eGFP-tagged parkin was previously created by Dr. Helen Scott (University of Bristol). The ionophore CCCP induces parkin recruitment to mitochondria by disrupting the proton gradient across the inner mitochondrial membrane, leading to organelle depolarisation and subsequent induction of mitophagy signalling cascades. CCCP-mediated induction of parkin recruitment in H4 eGFP-parkin cells has previously been used to screen siRNA libraries to identify modulators of mitochondrial function (Hasson et al. 2013, Scott et al. 2020). Prior to carrying out the drug compound screen in this study, the assay was optimised to ensure that parkin recruitment could be reliably visualised, induced and measured *in-vitro*.

Based on the protocol presented by Scott et al. (2020), H4 eGFP-parkin cells were incubated with MitoTracker Red to visualise mitochondria, then treated with either DMSO (vehicle control) or CCCP to depolarise mitochondria and induce parkin recruitment. Fluorescence microscopy showed that under baseline conditions parkin is expressed diffusely throughout the cell and upon CCCP challenge parkin forms small puncta which co-localise with mitochondria (Figure 5.3). H4 eGFP-parkin cells transfected with an siRNA directed against PINK1 and challenged with CCCP retained diffuse parkin expression, indicating that CCCP-induced parkin recruitment to mitochondria is PINK1 dependent.

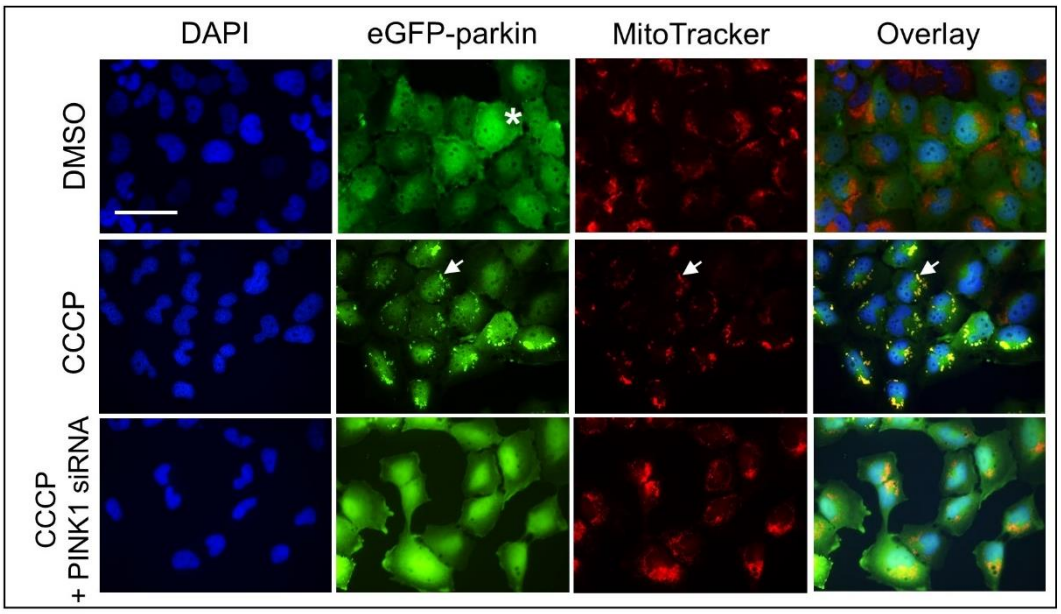

Figure 5.3 Parkin recruitment to mitochondria in H4 eGFP-parkin cells. Fluorescence images showing H4 eGFP-parkin cells stained with MitoTracker Red and treated with either DMSO or 15µM CCCP for 2 hours, with and without addition of PINK1 siRNA. Parkin was diffuse throughout the cell at baseline (asterisk), then formed small puncta co-localised with mitochondria upon CCCP challenge (arrows). Parkin puncta formation was reduced when PINK1 expression was knocked down using siRNA. Scale bar is 50µm.

After confirming that PINK1-dependent parkin recruitment is inducible in H4 eGFP-parkin cells, optimisation of high-content imaging was carried out. Parkin puncta were successfully imaged using the INCell Analyzer 2200, demonstrating a clear difference in parkin phenotype when H4 eGFP-parkin cells were challenged with CCCP compared to vehicle treated cells (Figure 5.4A). Figure 5.4B shows a representative example of cell nuclei, cell outline, parkin puncta and mitochondria segmented within H4 eGFP-parkin cells using INCell Workstation software. Parkin puncta were rare in control-treated cells, proving that the analysis protocol was able to specifically identify CCCP-induced parkin puncta with a low false-positive rate (Figure 5.4C).

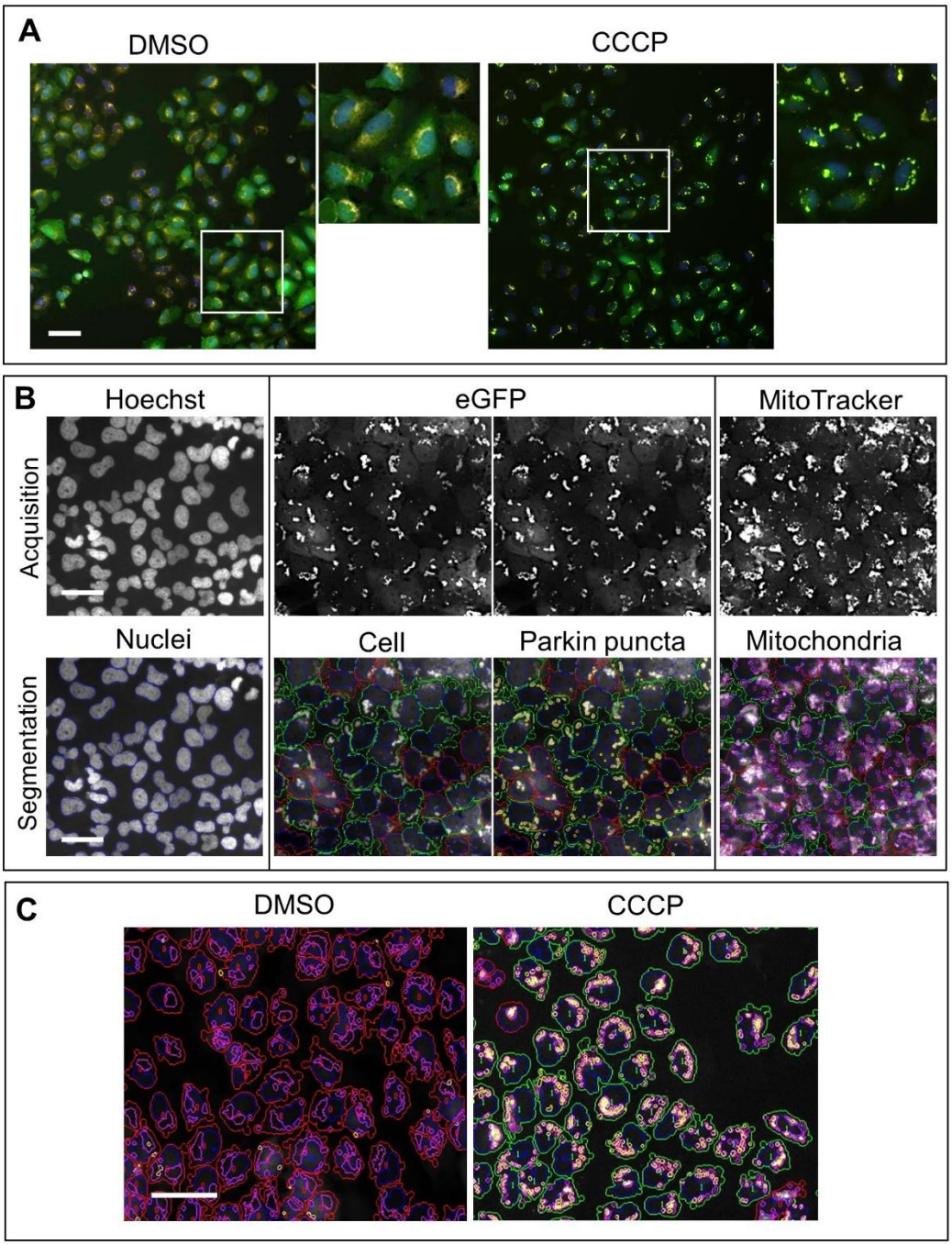

Figure 5.4 Parkin recruitment to mitochondria visualised and segmented using the INCell Analyzer 2200 high-content imaging and analysis system. **A**) Parkin puncta are clearly visible in H4 eGFP-parkin cells treated with 15µM CCCP for 2 hours (blue=Hoechst (nuclei), green=eGFP (parkin), orange=MitoTracker Red (mitochondria)). Inset squares indicate magnified regions. **B**) Image segmentation using INCell Investigator Workstation software (nuclei (blue), cell outline (red/green) and parkin puncta (yellow)). Cells containing more than 3 parkin puncta are delineated in green, cells with 3 or fewer parkin puncta are delineated in red. **C**) Segmentation of H4 eGFP-parkin cells treated with either DMSO or 15µM CCCP for 2 hours. Scale bars are 50µm.

To optimise the assay window in preparation for drug compound screening, H4 eGFP-parkin cells were treated with a range (0-20μM) of CCCP concentrations for 2 or 3 hours and the percentage of cells containing at least 3 parkin puncta quantified using the INCell Analyzer 2200 and INCell Investigator Workstation software (Figure 5.5, Table 2.10). Cell count (the mean number of cells in each imaged field identified by Hoechst stained nuclei) was used as a measure to indicate whether experimental conditions were affecting cell number. Treatment with 15-20μM CCCP for 2-3 hours did not reduce cell number (Figure 5.5A) and induced greater than 3 parkin puncta to form in approximately 80% of H4 eGFP-parkin cells (Figure 5.5B). A low proportion of vehicle control treated cells (less than 10%) were classified as containing greater than 3 puncta, demonstrating a good signal to noise ratio and a suitable assay window for screening the effect of drug compounds (Figure 5.5B). Two hours exposure to 15μM CCCP was selected as the protocol to induce parkin recruitment for further experiments, as this was the lowest dose and earliest time point to induce a high level of parkin recruitment in both experimental replicates. Although not statistically significant, there was an enrichment of eGFP fluorescence intensity within segmented mitochondria when cells were treated with 15μM CCCP compared to vehicle, indicating that segmented parkin puncta localise to mitochondria (Figure 5.5C). Co-localisation of parkin puncta with MitoTracker Red signal was clearly observed under fluorescence microscopy (Figure 5.3). siRNA knockdown of PINK1 significantly reduced parkin recruitment in H4 eGFP-parkin cells treated with CCCP compared to non-targeting control siRNA (NTC) (Figure 5.5D). This demonstrates that CCCP-induced parkin recruitment is dependent on PINK1 mediated mitophagy signalling.

Taken together these results confirm that CCCP can reliably induce PINK1-dependent parkin recruitment to mitochondria in H4 eGFP-parkin cells, which can be imaged and quantified using a high-content assay system. With this in mind, a protocol for screening test compounds was devised in preparation for carrying out the primary screening (Figure 5.6).

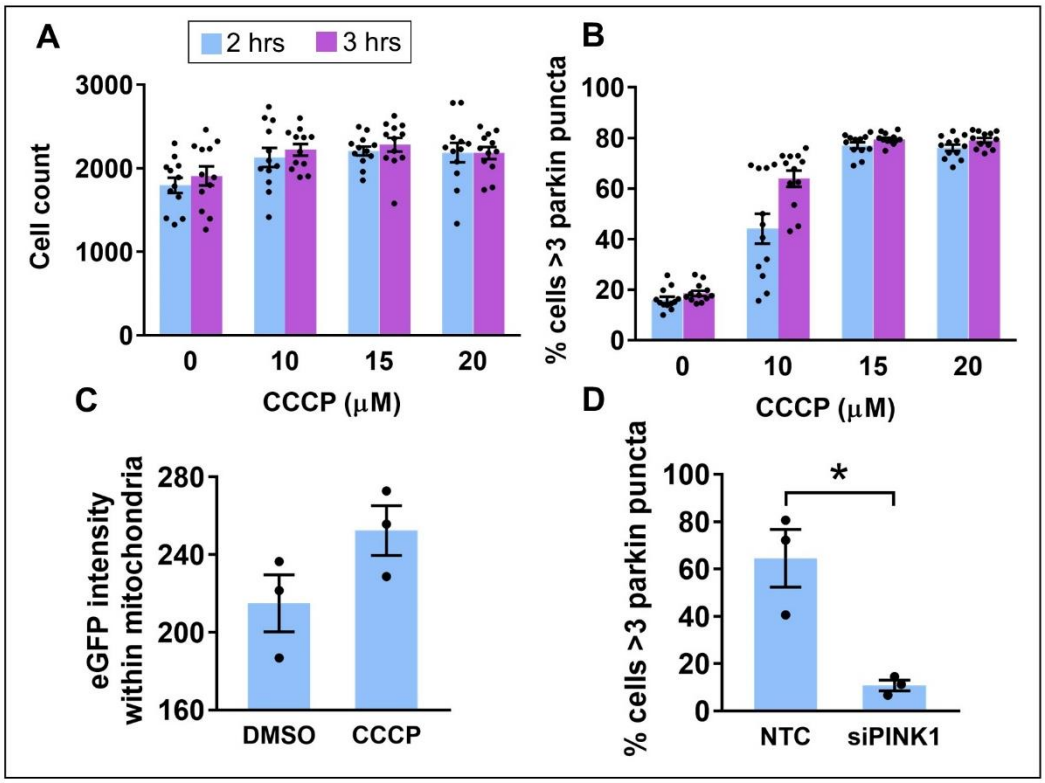

Figure 5.5 Quantification of parkin recruitment in H4 eGFP-parkin cells using INCell Workstation software. Cell count (**A**) and parkin recruitment response as percentage of cells with more than 3 parkin puncta (**B**) in H4 eGFP-parkin cells treated with 0, 10, 15 and 20μM CCCP for 2-3 hours. The data represents technical replicates of one experiment, therefore no statistical analysis was carried out. **C**) Fluorescence intensity (in arbitrary units) of eGFP-parkin signal within segmented mitochondria was increased in CCCP treated H4 eGFP-parkin cells compared to control, indicating formation of parkin puncta within mitochondria. **D**) Cells transfected with PINK1 siRNA (siPINK1) demonstrated significantly reduced parkin recruitment when compared to cells treated with non-targeting control (NTC) siRNA ($t(4)=4.34$, $p=0.013$, student's unpaired t-test). Data is displayed as mean ± SEM, For A-B n=1 independent plate with 12 technical replicates per condition, for C-D n=3 independent plates. * $p<0.05$.

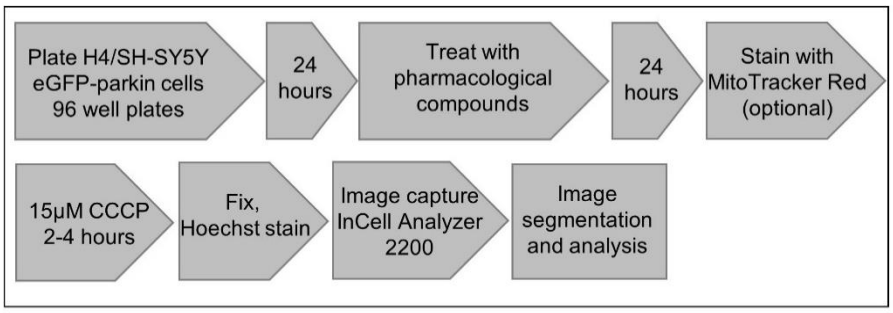

Figure 5.6 Flow diagram summarising the protocol for drug compound screening using the INCell Analyzer 2200 high-content imaging system.

5.3.1.2 Parkin recruitment phenotyping

A second cell line, SH-SY5Y (human neuroblastoma) stably expressing eGFP-parkin was created by Dr. Fella Hammachi (University of Bristol). This cell line, in addition to H4 eGFP-parkin, was used in the secondary screening stage of this chapter. To achieve a level of parkin recruitment equivalent to that observed in H4 eGFP-parkin cells (i.e. visualisation of multiple parkin puncta in 70-80% of cells with no cell death) (as in Figure 5.5A and B), it was determined that SH-SY5Y eGFP-parkin cells require exposure to 15µM CCCP for 4 hours (work carried out by Dr. Helen Scott and Mr. Gongyu Shi, data not shown here).

The spatial distribution of parkin recruitment within SH-SY5Y eGFP-parkin cells was different to that observed in H4 eGFP-parkin cells (Figure 5.7A). H4 eGFP-parkin cells challenged with CCCP expressed almost twice as many puncta per cell compared to SH-SY5Y eGFP-parkin cells, and these puncta were on average approximately 5 times smaller than those formed within SH-SY5Y eGFP-parkin cells (Figure 5.7B). Based on these differences in parkin translocation phenotype, parameters measuring a change in the number of parkin puncta per cell were not considered to be sensitive output measures for assays of parkin recruitment in SH-SY5Y eGFP-parkin cells. Instead, the area of parkin puncta per cell and intensity of parkin puncta (normalised to cell intensity) were used as measures in the secondary screening experiments in this chapter. These measures were selected based on previous validation studies carried out by Scott et al. (2020).

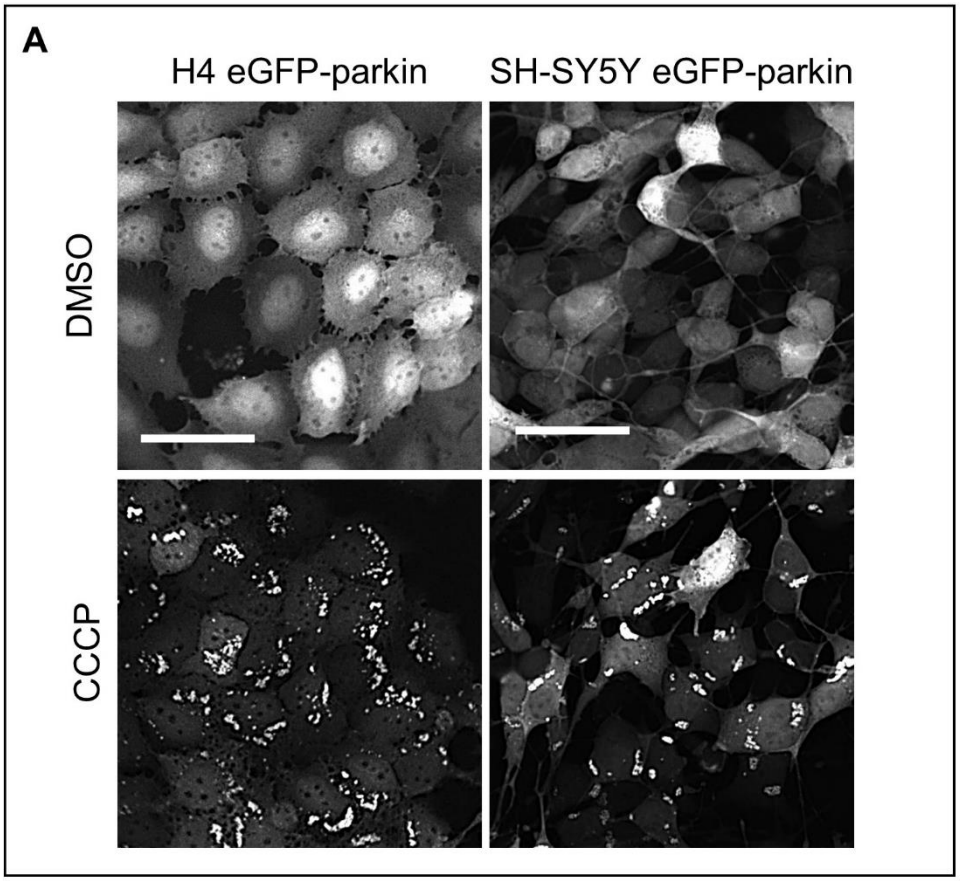

B

	H4 eGFP-parkin	SH-SY5Y eGFP-parkin
CCCP	15µM (2 hours)	15µM (4 hours)
Number of parkin puncta per cell	4.3 ± 0.2	2.4 ± 0.2
Area of each puncta	3.0 ± 0.1	15.9 ± 0.1

Figure 5.7 H4 eGFP-parkin and SH-SY5Y eGFP-parkin cells challenged with CCCP exhibit different parkin translocation phenotypes. Previously optimised protocols which induced optimal parkin recruitment levels for each cell line were used (2 hours (H4) and 4 hours (SH-SY5Y) of 15µM CCCP). **A**) Fluorescent images of eGFP-parkin captured using the INCell Analyzer 2200. Scale bars are 50µm. **B**) Table summarising the mean number and mean area of parkin puncta in H4 eGFP-parkin and SH-SY5Y eGFP-parkin cells, according to analysis using the INCell Workstation software. n=3 experimental plates per cell type, data is presented as mean ± SEM.

5.3.2 Primary screening of a drug compound library identifies kenpaullone as a novel negative modulator of parkin recruitment

To identify drug compounds and signalling pathways which could modulate mitochondrial health, a library of 25 pharmacological molecules which target cellular mechanisms associated with neurodegenerative disease (Table 5.1) was screened for modulation of parkin recruitment. This focussed drug compound library was provided by and quality controlled at Takeda, UK. Compounds were selected based on their neuroactivity and evidence for potentially neuroprotective functions. H4 eGFP-parkin cells were treated with 10µM of drug compound for 24 hours (a standard recommended concentration used in drug screening studies) then challenged with 15µM CCCP for 2 hours to induce mitochondrial depolarisation and parkin recruitment (Figure 5.8). Based on independent advice from statisticians at the University of Bristol School of Mathematics and precedent within the literature (e.g. McKenzie et al. (2015), Castell et al. (2018)) a threshold cut-off of 30% increase or decrease in parkin recruitment or cell count compared to vehicle control was employed in this screen.

GSK 2606414, BIX, Cu-ASTM and TRC 051384 reduced cell count by >30% and were therefore excluded as hit compounds in this screen (Figure 5.8A). Treatment with the kinase inhibitor kenpaullone reduced parkin puncta formation in H4 eGFP-parkin cells by 75% compared to vehicle control and was therefore classified as a hit compound for secondary screening (Figure 5.8B). Rapamycin, a drug previously established as a positive modulator of mitophagy (Li et al. 2014), was identified as a positive modulator of parkin recruitment in the screen (Figure 5.8B). However, the primary screen did not detect any novel drug compound which induced at least a 30% increase in parkin recruitment compared to control.

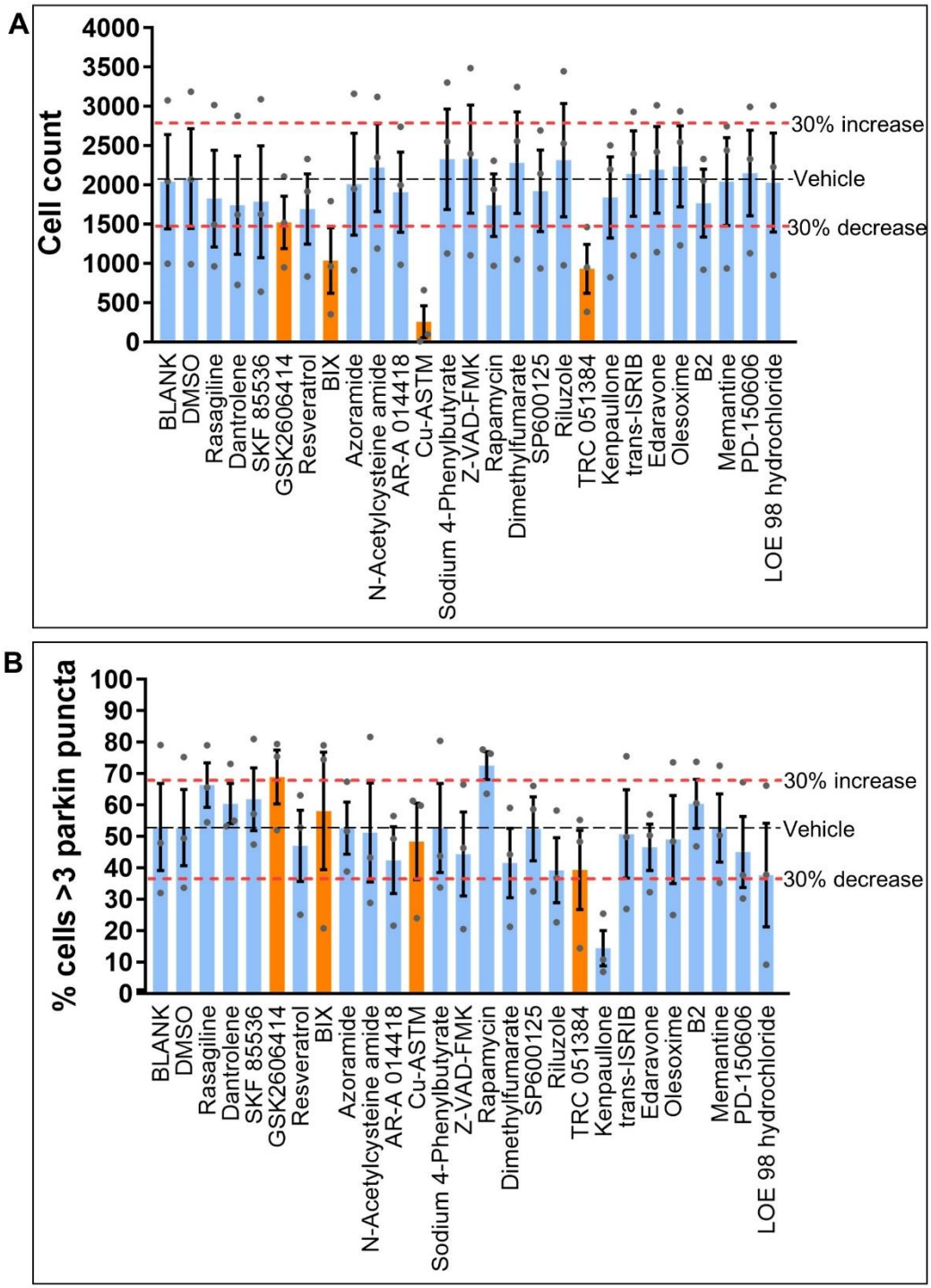

Figure 5.8 Primary screening of pharmacological compound library using parkin recruitment assay. H4 eGFP-parkin cells were pre-treated for 24 hours with 10µM compound, then challenged with 15µM CCCP for 2 hours. **A**) Cell count data. Orange bars indicate compounds which induced at least a 30% reduction in cell number. These were considered as potentially cytotoxic and therefore excluded from consideration in parkin puncta analysis. **B**) Parkin puncta formation. Rapamycin was confirmed as a positive modulator of parkin recruitment. Kenpaullone, a novel hit, induced a 75% decrease in parkin puncta formation in comparison to control and was therefore further tested in secondary screening assays. All data is displayed as mean ± SEM, n=3 plates.

5.3.3 Secondary screening

5.3.3.1 Kenpaullone negatively modulates parkin recruitment in H4- and SH-SY5Y eGFP-parkin cells

Following the drug compound primary screen, kenpaullone was sourced from Sigma (K3888) to verify its effect on parkin recruitment in both H4 eGFP-parkin (Figure 5.9) and SH-SY5Y eGFP-parkin cells (Figure 5.10) in a secondary screen. There was no change in cell count when H4 eGFP-parkin cells were treated with up to 10µM kenpaullone for 24 hours, either with or without CCCP challenge (Figure 5.9A and B). In the absence of CCCP, treatment with kenpaullone did not change the percentage of cells containing at least 3 parkin puncta compared to vehicle treated cells (Figure 5.9A and C). When cells were challenged with CCCP to induce parkin puncta formation, the percentage of cells containing at least 3 puncta was significantly reduced by both 5µM and 10µM kenpaullone treatment compared to control (Figure 5.9A and C).

In SH-SY5Y eGFP-parkin cells, visualisation of eGFP fluorescence showed that CCCP induced recruitment of parkin in a large proportion of cells, which was ameliorated by treatment with 10µM kenpaullone (Figure 5.10A). There was no significant change in cell count with treatment of up to 10µM kenpaullone, either with or without CCCP challenge (Figure 5.10B). Kenpaullone treatment did not induce a significant change in the percentage of cells containing at least 3 parkin puncta, either with or without CCCP (Figure 5.10C). This was not unexpected considering SH-SY5Y eGFP-parkin cell phenotyping which showed that these cells typically feature low numbers of large puncta (Figure 5.7). Less than 3% of cells contained at least 3 puncta upon CCCP treatment compared to an induction of around 60% in the equivalent experiment in H4 eGFP-parkin cells. Quantification of actual number of parkin puncta (as opposed to using a percentage threshold) was not considered as a solution because the typically low number of individual puncta would not provide a large enough assay window to observe the effect of drug compounds. When cells were challenged with CCCP, treatment with 10µM kenpaullone significantly reduced parkin

puncta total area compared to vehicle control treated cells (Figure 5.10D). With CCCP challenge, kenpaullone treatment at 1, 5 and 10µM induced a significant reduction in parkin puncta intensity compared to CCCP-challenged vehicle control treated cells (Figure 5.10E). There was no effect of kenpaullone on parkin puncta total area or intensity without CCCP challenge. Taken together, these results confirm that kenpaullone negatively modulates the formation of parkin recruitment to mitochondria in two human cell lines.

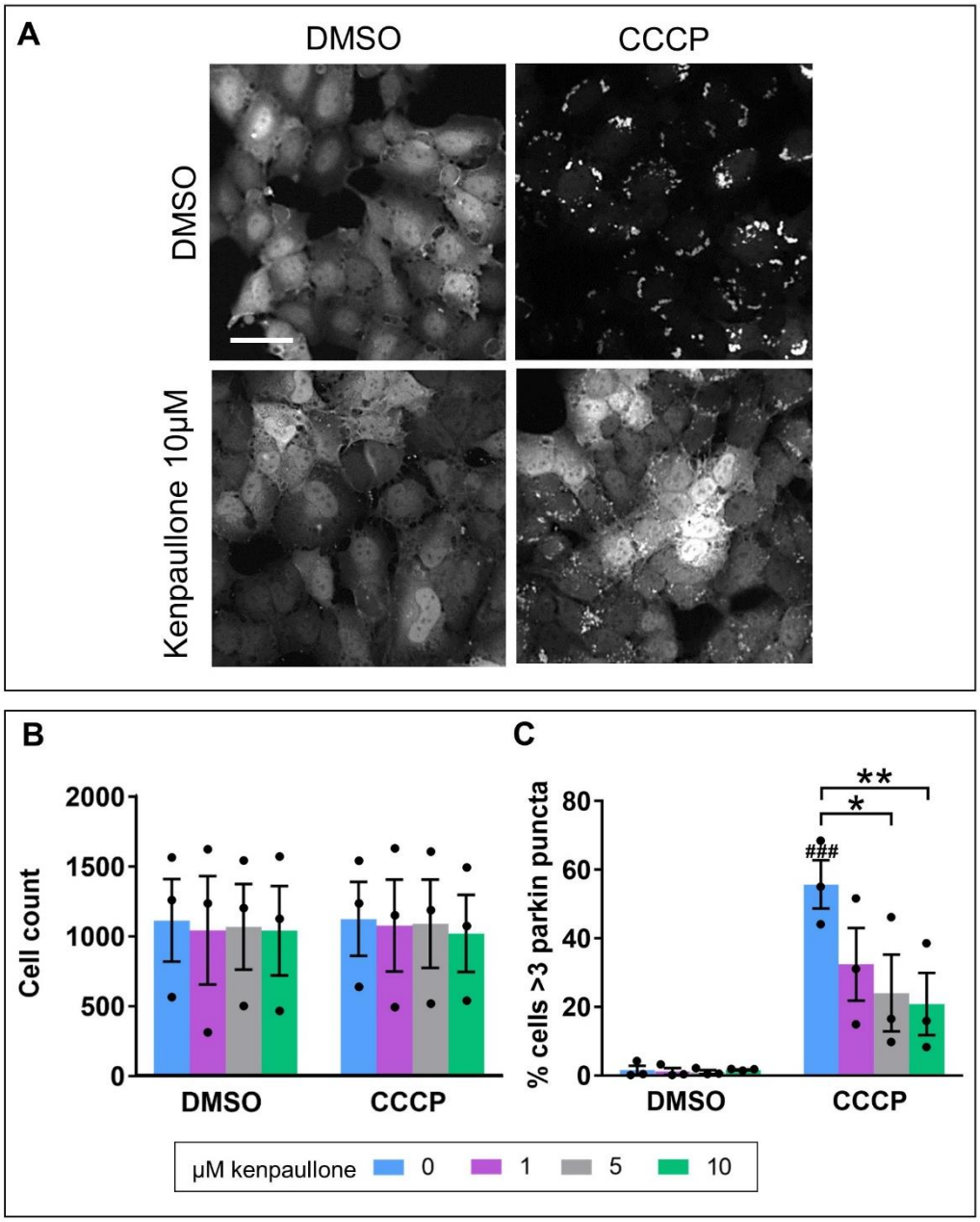

Figure 5.9 Validation of negative modulation of CCCP-induced parkin recruitment by kenpaullone in H4 eGFP-parkin cells. **A**) Representative images of eGFP fluorescence showing H4 eGFP-parkin cells treated with either DMSO or kenpaullone for 24 hours, then challenged with 15µM CCCP or DMSO for 2 hours. Scale bar is 50µm. **B**) There was no significant change in cell count when cells were treated with up to 10µM kenpaullone compared to vehicle control, either with or without the presence of CCCP. **C**) Parkin puncta formation was significantly reduced when cells were treated for 24 hours with 5µM or 10µM kenpaullone compared with DMSO vehicle control in the presence of CCCP (vehicle vs 5µM p=0.027, vehicle vs 10µM p=0.009). In cells treated with 0µM kenpaullone, CCCP induced a significant increase in parkin recruitment (p=0.0008). Kenpaullone did not alter parkin recruitment in the absence of CCCP challenge. Statistical analysis carried out by two-way ANOVA with Tukey's post-hoc test. n=3 plates, data is displayed as mean ± SEM. *p<0.05, ** p<0.01. Asterisks denote comparisons within DMSO or CCCP treated groups, hashes denote comparisons between DMSO and CCCP treated groups.

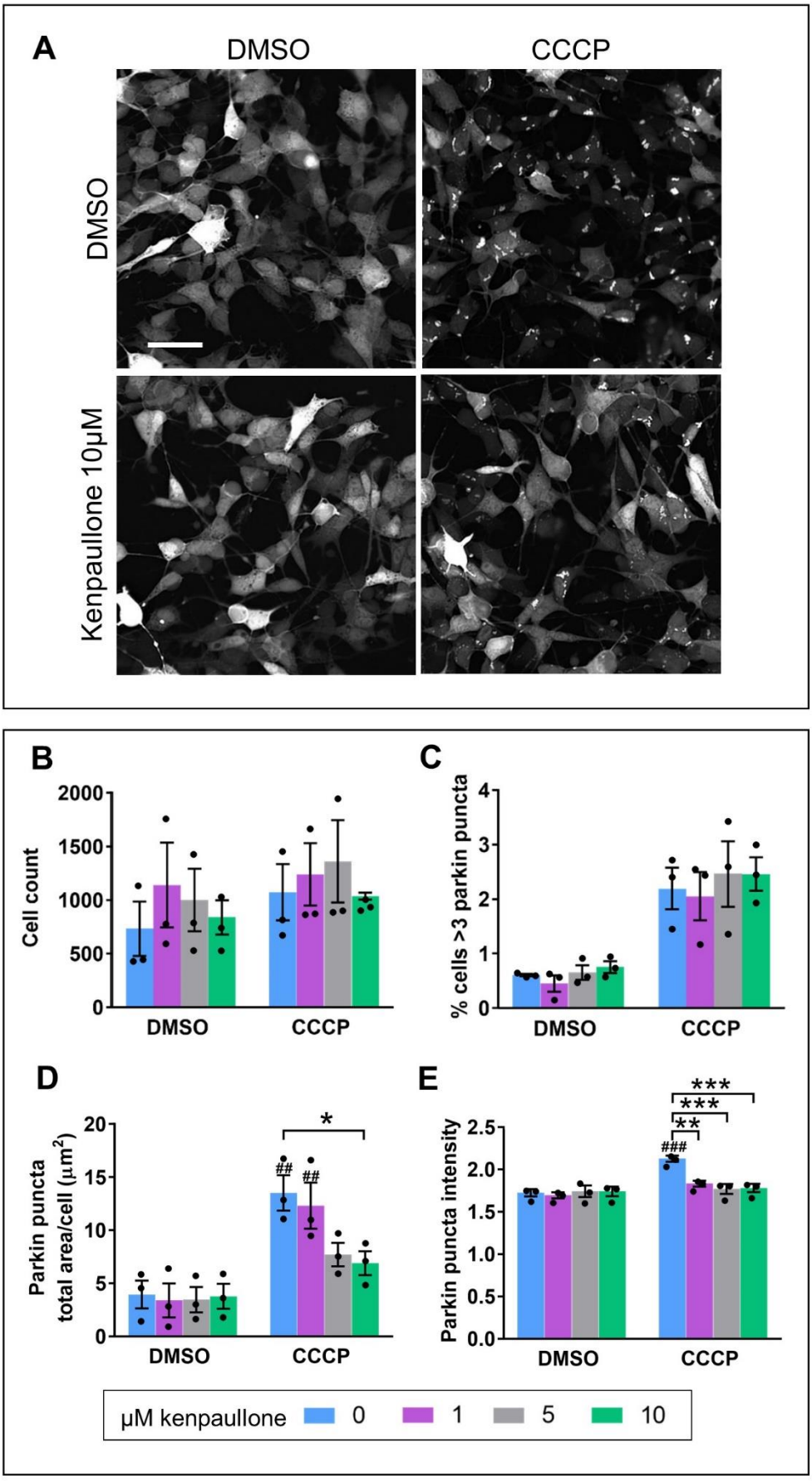

Figure 5.10 Figure legend on next page

Figure 5.10 (Previous page) Validation of negative modulation of CCCP-induced parkin recruitment by kenpaullone in SH-SY5Y eGFP-parkin cells. **A**) Representative images of eGFP fluorescence showing SH-SY5Y eGFP-parkin cells treated with either DMSO or kenpaullone for 24 hours, then challenged with 15µM CCCP or DMSO for 4 hours. Scale bar is 50µm. **B**) There was no significant change in cell count when cells were treated with up to 10µM kenpaullone compared to vehicle control, either with or without the presence of CCCP. **C**) There was no significant difference in percentage of cells containing more than 3 parkin puncta with CCCP or kenpaullone treatment. **D**) The total area of parkin puncta per cell was significantly reduced when cells were treated with 10µM kenpaullone compared with DMSO vehicle control in the presence of CCCP ($p=0.03$). In cells treated with 0µM and 1µM kenpaullone, CCCP induced a significant increase in parkin puncta total area ($p=0.005$ and $p=0.009$, respectively). Kenpaullone did not alter parkin puncta area in the absence of CCCP challenge. **E**) There was a significant decrease in parkin puncta intensity when cells were treated for 24 hours with 1µM, 5µM or 10µM kenpaullone compared with DMSO vehicle control in the presence of CCCP (vehicle vs 1µM $p=0.004$, vehicle vs 5µM $p=0.0006$, vehicle vs. 10µM $p=0.0008$). There were no significant differences in parkin puncta intensity detected in the absence of CCCP. In cells treated with 0µM kenpaullone, CCCP induced a significant increase in parkin puncta intensity ($p=0.0006$). Kenpaullone did not alter parkin puncta area in the absence of CCCP challenge. Statistical analysis carried out by two-way ANOVA with Tukey's post-hoc test. n=3 plates, data is displayed as mean ± SEM. *$p<0.05$, ** $p<0.01$, *** $p<0.001$. Asterisks denote comparisons within DMSO or CCCP treated groups, hashes denote comparisons between DMSO and CCCP treated groups.

5.3.3.2 Development of a high-content imaging protocol to analyse the 2D shape of the cellular mitochondrial network

To analyse mitochondria *in-vitro*, a method to quantify changes in the 2D cross-sectional structure of the mitochondrial network was developed. A literature review was carried out to ensure that the method developed for this study would be aligned with the standards of recent peer-reviewed publications. Table 5.2 summarises a selection of key research articles which represent current techniques. Mitochondria were frequently visualised using fluorescent MitoTracker dyes and there was a trend towards more advanced software and machine learning scripts being utilised in the more recent publications. Amongst the most frequently reported measures of the mitochondrial network were the 2D area of mitochondria within the cell and the shape (elongation or circularity) of mitochondrial organelles.

In this study, analysis of the 2D morphology (shape and size) of the mitochondrial network was carried out in H4 eGFP-parkin cells, due to their flattened cell shape and consistent size which makes them amenable to accurate segmentation of organelles using high-content imaging. MitoTracker Red was used to visualise mitochondria because it is specific for mitochondria, it is suitable for fixation, and although its initial uptake into mitochondria is dependent on an intact mitochondrial membrane potential, the dye forms covalent bonds within the organelles and therefore remains within mitochondria irrespective of future changes in membrane potential.

Mitochondria stained with MitoTracker Red could be clearly imaged using the INCell Analyzer 2200 (Figure 5.11A). An analysis protocol was developed using INCell Workstation software to segment the areas of the cell stained with MitoTracker Red (Tables 2.9 and 2.11). Visual inspection confirmed that the software was able to accurately delineate mitochondria (Figure 5.11A). To verify the ability of the analysis protocol to quantify a change in the morphology of the mitochondria, H4 eGFP-parkin cells challenged with 15µM CCCP for 2 hours as a positive control were compared against DMSO treated cells (Figure 5.11B and C). Visual

inspection of images showed that CCCP challenge reduced the area of mitochondria in each cell. The organelles also appear more rounded and condensed towards the nucleus compared to control cells (Figure 5.11B). Based on the parameters described in the literature, four output measures were chosen: total mitochondrial area per cell, mitochondrial count (the number of individually segmented objects per cell), mitochondrial elongation and mitochondrial distance to the cell nucleus.

Cells challenged with CCCP had significantly decreased total mitochondrial area per cell compared to vehicle control treated cells (Figure 5.11C). The mitochondria in CCCP challenged cells were also significantly less elongated (more circular) in comparison to control (Figure 5.11C). CCCP did not result in a significant change in mitochondrial count per cell, or alteration in the distance of mitochondrial organelles to the cell nucleus (Figure 5.11C). Based on these results, mitochondrial area and elongation were used as measures to test the effect of kenpaullone on mitochondria within H4 eGFP-parkin cells.

Ref.	Visualisation method	Imaging method	Analysis tool	Parameters to measure mitochondria
Lutz et al. (2009)	MitoTracker Red	Widefield	Ordinal scoring	Classified as tubular, fragmented or highly connected
Dagda et al. (2009)	MitoTracker Red	Confocal	ImageJ	Interconnectivity (mean area/perimeter ratio), elongation (inverse circularity)
Cribbs and Strack (2009)	MitoTracker Red, cytochrome oxidase immunostaining	Widefield and confocal	Image J	Area, perimeter, form factor (inverse circularity)
Narendra et al. (2010)	TOMM20 immunostaining	Confocal	ImageJ	Classified cells by mitochondrial phenotype: Normal, few dispersed, aggregated, no mitochondria
Mitra and Lippincott-Schwartz (2010)	Mitochondrial fluorescent dyes, fluorescent tagging, FRAP	Confocal	Volocity, Metamorph, Image J	Classified as fragmented, intermediate or tubular
Li et al. (2011)	Mitochondrial fluorescent tag	Confocal	ImageJ	Average area, interconnectivity
Peng et al. (2011)	MitoTracker Orange	Widefield	Custom software to segment image	Defined 6 subtypes: small globules, swollen globules, loops, straight tubules, twisted tubules, branched tubules
Xie and Chung (2012)	Mitochondrial fluorescent tag	Confocal	Image J	Interconnectivity (area/perimeter), circularity
Aboud et al. (2015)	MitoTracker Red	Confocal	ImageJ	Circularity, particle number, total area
Leonard et al. (2015)	MitoTracker Deep Red	INCell Analyzer 2200	GE INCell Developer Toolbox with machine learning	Defined 4 subtypes: puncta, rod, networked, large & round
McClatchey et al. (2016)	TOMM20 immunostaining	Confocal	Automated Matlab analysis	width, length, mass, subcellular localisation
Wiemerslage and Lee (2016)	MitoTracker Orange	Widefield	Image J	Number of mitochondria, size, interconnectivity, elongation

Table 5.2 Literature summary providing an overview of methods used to image and measure mitochondrial networks within the cell using fluorescence. Literature review was carried out between Oct-Dec 2016

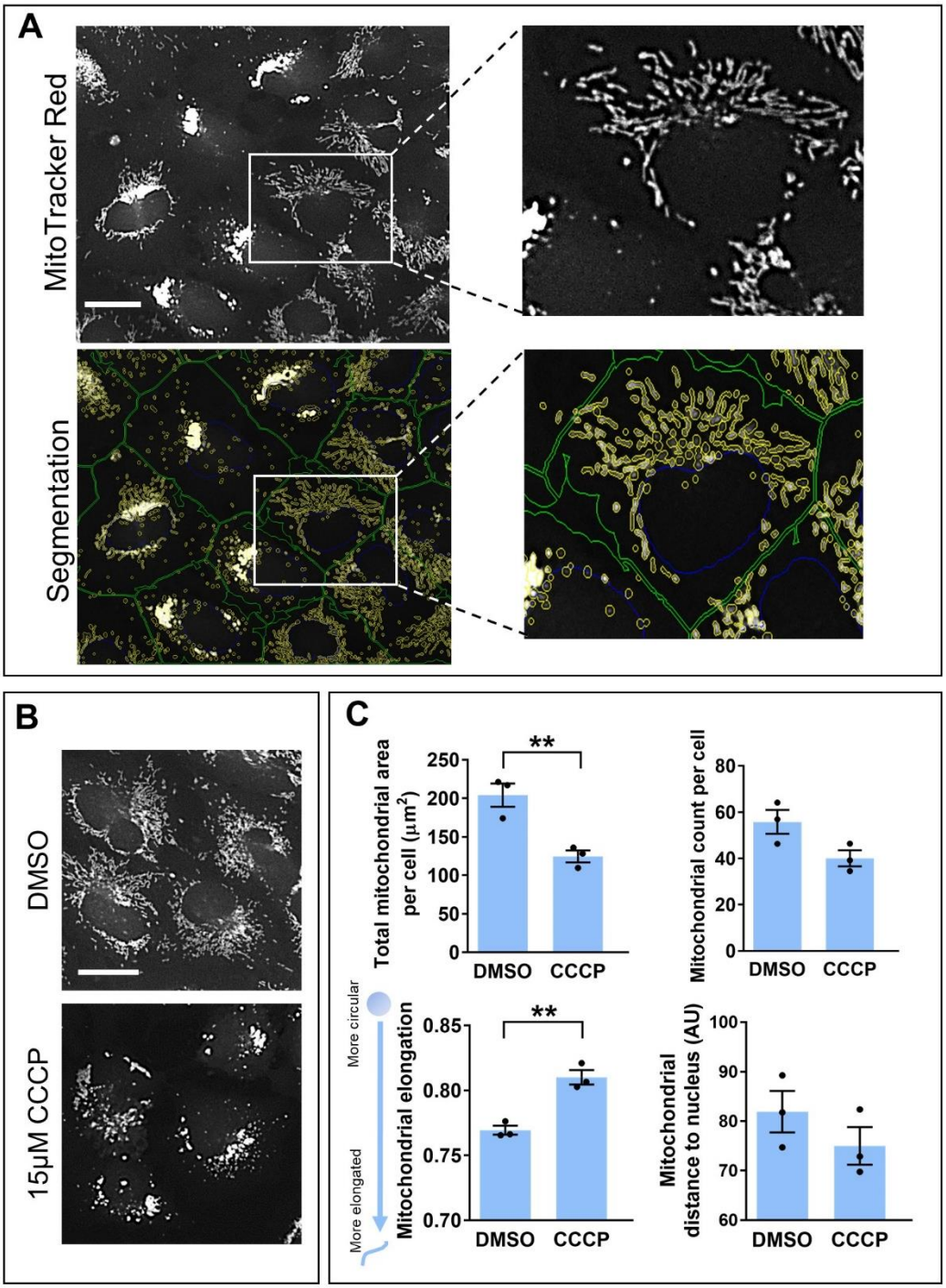

Figure 5.11 Figure legend on next page

Figure 5.11 (Previous page) Analysis of mitochondria visualised with MitoTracker Red using INCell Analyzer 2200 high-content imaging system. **A**) H4 eGFP-parkin cells under baseline conditions stained with MitoTracker Red, imaged using the INCell Analyzer 2200 2D deconvolution setting. In the segmented image, cell nuclei (blue), cell outline (green) and mitochondria (yellow) were successfully delineated using INCell Workstation software. **B**) Representative image of the mitochondrial network in H4 eGFP-parkin cells in the presence of DMSO (vehicle) or 15µM CCCP for 2 hours. Scale bars are 25µm. **C**) Output measures from the INCell Workstation software based on those observed most frequently in the published literature. Of the selected measures, CCCP treated cells had a significant decrease in total mitochondrial area per cell ($t(4)=4.68$, $p=0.0095$) and were also significantly less elongated ($t(4)=6.23$, $p=0.0034$) compared to vehicle control (unpaired, two-tailed t-tests). There was no significant difference in mitochondrial count or distance to nuclei (in arbitrary units, AU) with CCCP treatment compared to vehicle control. n=3 plates, data was analysed by unpaired, two-tailed t-tests. Data is displayed as mean ± SEM. ** $p<0.01$.

5.3.3.3 Kenpaullone rescues mitochondria from morphological changes induced by CCCP challenge

H4 eGFP-parkin cells were pre-treated with up to 10µM kenpaullone for 24 hours, stained with MitoTracker Red, then challenged with 15µM CCCP or vehicle control for 2 hours (Figure 5.12A). The mitochondrial network within the cells was analysed using the newly developed protocol (section 5.3.3.2). Under baseline conditions (in the absence of CCCP challenge), H4 eGFP-parkin cells treated with up to 10µM kenpaullone for 24 hours had no significant change in either mitochondrial total area per cell (Figure 5.12B) or mitochondrial elongation (Figure 5.12C). In the presence of CCCP, mitochondria within H4 eGFP-parkin cells pre-treated with 10µM kenpaullone had significantly increased total area of mitochondria (Figure 5.12B) and significantly more elongated mitochondria compared to control cells pre-treated with vehicle (Figure 5.12C). These results demonstrate that kenpaullone ameliorates the effects of the mitochondrial toxin CCCP on the shape and size of the mitochondrial network as visualised with high-content imaging *in-vitro*.

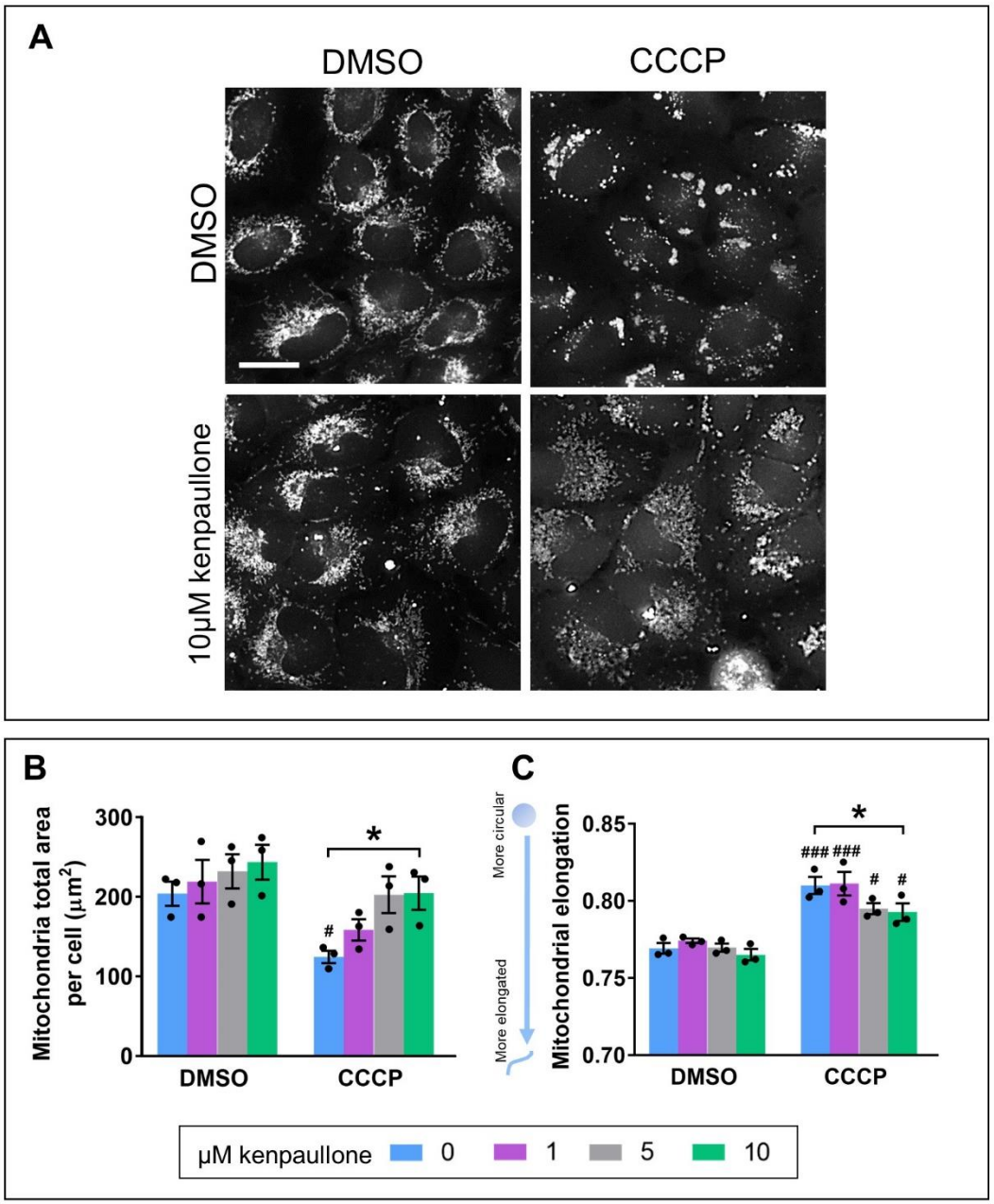

Figure 5.12 Kenpaullone modulates mitochondrial morphology in H4 eGFP-parkin cells challenged with CCCP. Mitochondria were quantified by staining cells with MitoTracker Red, and imaging them using an INCell Analyzer 2200. Measurements refer to mitochondria segmented using Workstation analysis software. **A**) Representative images of MitoTracker Red fluorescence showing H4 eGFP-parkin cells treated with either DMSO or kenpaullone for 24 hours, then challenged with 15µM CCCP or DMSO for 2 hours. Scale bar is 25µm. **B**) The total area of mitochondria per cell was significantly increased when cells were treated with 10µM kenpaullone compared with DMSO vehicle control in the presence of CCCP (p=0.04). CCCP treatment with no kenpaullone significantly reduced mitochondrial total area (p=0.02), and this effect was ameliorated with kenpaullone treatment.

(Figure legend continued next page)

Figure 5.12 (continued from previous page) **C**) Mitochondria became significantly more elongated and less circular when cells were treated with 10µM kenpaullone compared with DMSO vehicle control in the presence of CCCP (p=0.04). CCCP treatment significantly reduced mitochondrial elongation in the presence of 0, 1, 5 and 10µM of kenpaullone (p=0.0002, p=0.0007, p=0.02, p=0.01 respectively). Statistical analysis carried out by two-way ANOVA with Tukey's post-hoc test. n=3 plates, data is displayed as mean ± SEM. *p<0.05, ** p<0.01, *** p<0.001. Asterisks denote comparisons within DMSO or CCCP treated groups, hashes denote comparisons between DMSO and CCCP treated groups.

5.3.3.4 Kenpaullone rescues mitochondria from MPP+ insult

To further explore the findings that kenpaullone affects parkin recruitment and the shape and size of the mitochondrial network, a series of experiments to test the effect of kenpaullone on mitochondrial function were carried out. The first of these experiments utilised 1-methyl-4-phenylpyridinium (MPP+), the active metabolite of the complex I inhibitor MPTP. MPP+ is a mitochondrial toxin which disrupts mitochondrial membrane potential and generates reactive oxygen species to ultimately cause cytotoxicity and cell death.

H4 eGFP-parkin cells were challenged with MPP+ with or without the presence of kenpaullone for 24 hours before staining the mitochondrial network with MitoTracker Red. As the uptake of MitoTracker Red is dependent on mitochondrial membrane potential, the amount of dye taken up into the network reduces under conditions which induce mitochondrial depolarisation. This effect was observed when cells were exposed to either vehicle (DMSO) or 500µM MPP+ for 24 hours (with no kenpaullone). MPP+ challenged cells had significantly decreased MitoTracker Red intensity within the cell cytoplasm (Figure 5.13A and B). MPP+ challenge also significantly reduced cell number compared to vehicle treated cells (Figure 5.13C). Treatment with 10µM kenpaullone rescued the depletion of MitoTracker Red staining as indicated by a significant increase in fluorescence intensity compared to vehicle control in cells challenged with MPP+ (Figure 5.13B). There was no significant difference in cell number when MPP+ challenged cells were treated with kenpaullone up to 10µM (Figure 5.13C), indicating that kenpaullone was unable to rescue cell loss

in this assay. The increase in MitoTracker Red staining observed when MPP+ challenged cells were treated with kenpaullone could be attributable to either the existing mitochondria better maintaining a healthy membrane potential (and therefore taking up more MitoTracker dye), or an increase in the size or number of mitochondria. Taken together these results show that kenpaullone protects mitochondria against changes induced by the mitochondrial toxin MPP+ but was unable to rescue MPP+ induced cell loss.

5.3.4 The effect of kenpaullone on mitochondria in live cells

The effect of kenpaullone on mitochondrial function was next tested in live cells using the Seahorse Bioanalyzer XFp system (Agilent). At this stage in the study, it was observed that when kenpaullone was applied to cells at 10µM, the compound began precipitating out of solution. This effect was attributed to difference in the batch of kenpaullone, as this effect was not observed in previous assays. With this in mind, live cell assays were carried out using 5µM kenpaullone, a concentration previously shown to be effective at reducing parkin recruitment, and for which there was no evidence of compound precipitation.

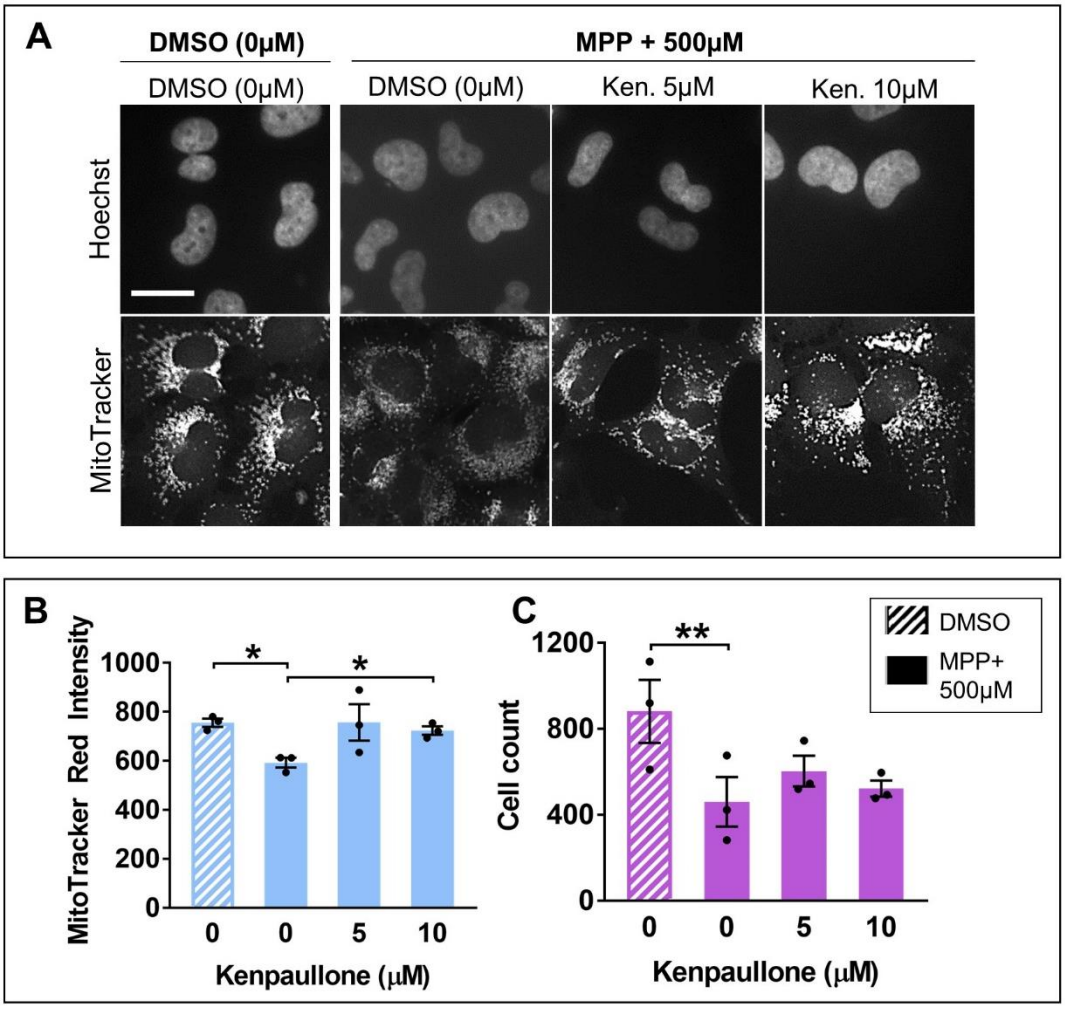

Figure 5.13 Kenpaullone ameliorates MPP+ induced loss of cytoplasmic MitoTracker Red staining, but does not rescue cell loss. H4 eGFP-parkin cells were treated with MPP+ or vehicle plus kenpaullone or vehicle for 24 hours. **A**) Representative images from each experimental condition showing Hoechst (nuclear) and MitoTracker Red (mitochondrial) staining. Scale bar is 25μm. **B**-**C**) The mitochondrially toxic effect of MPP+ was verified by treating cells with or without 500μM MPP+ (no kenpaullone). MPP+ induced a significant reduction in MitoTracker Red intensity ($p=0.037$) and cell count ($p=0.0031$). In the presence of MPP+, cells treated with 10μM kenpaullone had significantly higher MitoTracker Red intensity compared to vehicle treated cells ($p=0.037$). There was no significant difference in cell count when MPP+ challenged cells were treated with kenpaullone compared to vehicle control. Statistical analysis carried out by one-way ANOVAs within each dataset with Tukey's post-hoc test. Image capture and fluorescence intensity analysis were carried out using the INCell Analyzer 2200 and INCell Analyzer Workstation software. n=3 plates, data is displayed as mean ± SEM. * $p<0.05$, ** $p<0.01$.

5.3.4.1 Kenpaullone reduces mitochondrial maximum respiratory capacity in live cells

The Seahorse Bioanalyzer XFp (Agilent) was utilised to investigate the effect of kenpaullone on mitochondrial function in live cells (Figure 5.14 and Figure 5.15). The Mitochondrial Stress Test protocol analyses oxidative phosphorylation by measuring oxygen consumption rate (OCR) and glycolysis by measuring extracellular acidification rate (ECAR). Functions of the electron transport chain (ETC) are isolated by sequentially injecting cell culture media with drugs to disrupt specific ETC complexes (Figure 5.14A). Oligomycin inhibits ATP production, FCCP (a derivative of the ionophore CCCP) acutely disrupts the proton gradient across the inner mitochondrial membrane, stimulating maximum OCR, and antimycin A/rotenone inhibits ETC function (Figure 5.14B). H4 eGFP-parkin and SH-SY5Y eGFP-parkin cells were used in Seahorse experiments to maintain continuity with the majority of previous screening assays. Prior to use of these cell lines, a technical support scientist at Agilent was consulted to confirm that the eGFP tag expressed within the cells would not interfere with the proprietary fluorophore system used in the Seahorse probes which detects oxygen and proton flux.

The dose of FCCP which induces peak OCR was titrated in H4 eGFP-parkin and SH-SY5Y eGFP-parkin cells (Figure 5.14C and D). In H4 eGFP-parkin cells, maximal OCR was observed with 2µM FCCP, with OCR decreasing at doses above 2µM (Figure 5.14C). Doses of FCCP up to 2µM were unable to induce OCR above baseline levels in SH-SY5Y eGFP-parkin cells following oligomycin treatment (Figure 5.14D). FCCP dose-response curves for both cell lines are plotted in Figure 5.14E. H4 eGFP-parkin cells were chosen as the cell line to test the effect of kenpaullone on mitochondrial function in live cells because their higher maximal OCR in comparison to SH-SY5Y eGFP-parkin cells provides a better assay window.

H4 eGFP-parkin cells were treated with kenpaullone and challenged with CCCP according to the experimental protocol summarised in Figure 5.15A. Oxygen consumption rate was normalised to total protein after each

experiment. There was no significant difference in the mean protein yield between experimental groups (Figure 5.15B). This, alongside visual inspection of the cells before and after each assay, confirms that treatment with 5μM kenpaullone for 24 hours does not affect cell number compared to control. There was however a trend towards an increase in protein yield in cells treated with kenpaullone compared to vehicle control (Figure 5.15B). In the context of the previous results of this chapter, it is reasonable to speculate that this increase in protein in the absence of a change in cell number may be attributable to increased number or size of organelles within the mitochondrial network.

Cells exposed to kenpaullone alone, CCCP challenge alone, or kenpaullone with CCCP challenge had a reduced OCR over time (both at baseline and in response to ETC inhibitors) in comparison to control treated cells, as indicated by the trend lines in Figure 5.15C. Changes in OCR over time were used to quantify specific mitochondrial functions (Figure 5.15D). In cells challenged with CCCP, cellular maximal respiration and spare capacity was significantly reduced in comparison to vehicle control (Figure 5.15D). Pre-treatment with kenpaullone for 24 hours also induced a significant reduction in both spare capacity and maximal respiration, both with and without CCCP challenge (Figure 5.15D). There was no significant difference in any OCR measure when CCCP-challenged cells were treated with kenpaullone, compared to vehicle control (Figure 5.15D).

Plotting OCR against ECAR allows the overall metabolic state of the cells to be assessed at a given timepoint. Metabolic profiles were plotted at baseline respiration (Figure 5.15E) and maximal respiration (Figure 5.15F). Overall, regardless of experimental condition, treatment with FCCP to induce maximal OCR caused a shift towards a more energetic energy phenotype. When comparing the different experimental conditions at each timepoint, cells treated with kenpaullone and/or CCCP displayed a less energetic phenotype. At both timepoints, ECAR data indicate that cells under all conditions express a relatively glycolytic and quiescent energy phenotype, typical of cancer cell metabolism, which should be taken into

account when interpreting the results of this experiment. Overall these results show that kenpaullone modulates/decreases mitochondrial function in live cells under baseline conditions.

Figure 5.14 (next page) Optimisation of conditions for Mitochondrial Stress Test using Agilent Seahorse Bioanalyzer. **A**) Diagram of the electron transport chain indicating the pharmacological mechanisms of action of oligomycin, FCCP, antimycin A and rotenone. **B**) Illustrative graph depicting a model example of oxygen consumption rate (OCR) over time during the Mitochondrial Stress Test protocol. Coloured blocks represent the various respiratory measures. FCCP titration tests were carried out in H4 eGFP-parkin (**C**) and SH-SY5Y eGFP-parkin cells (**D**) to ascertain optimal FCCP concentration for the Mitochondrial Stress Test (see table for details of FCCP concentrations). H4 eGFP-parkin cells exhibited a maximal OCR in the presence of 2µM FCCP. FCCP did not induce maximal OCR above baseline levels in SH-SY5Y eGFP-parkin cells. **E**) FCCP dose-response plot for H4 and SH-SY5Y eGFP-parkin cells. Data is displayed as mean ± SEM.

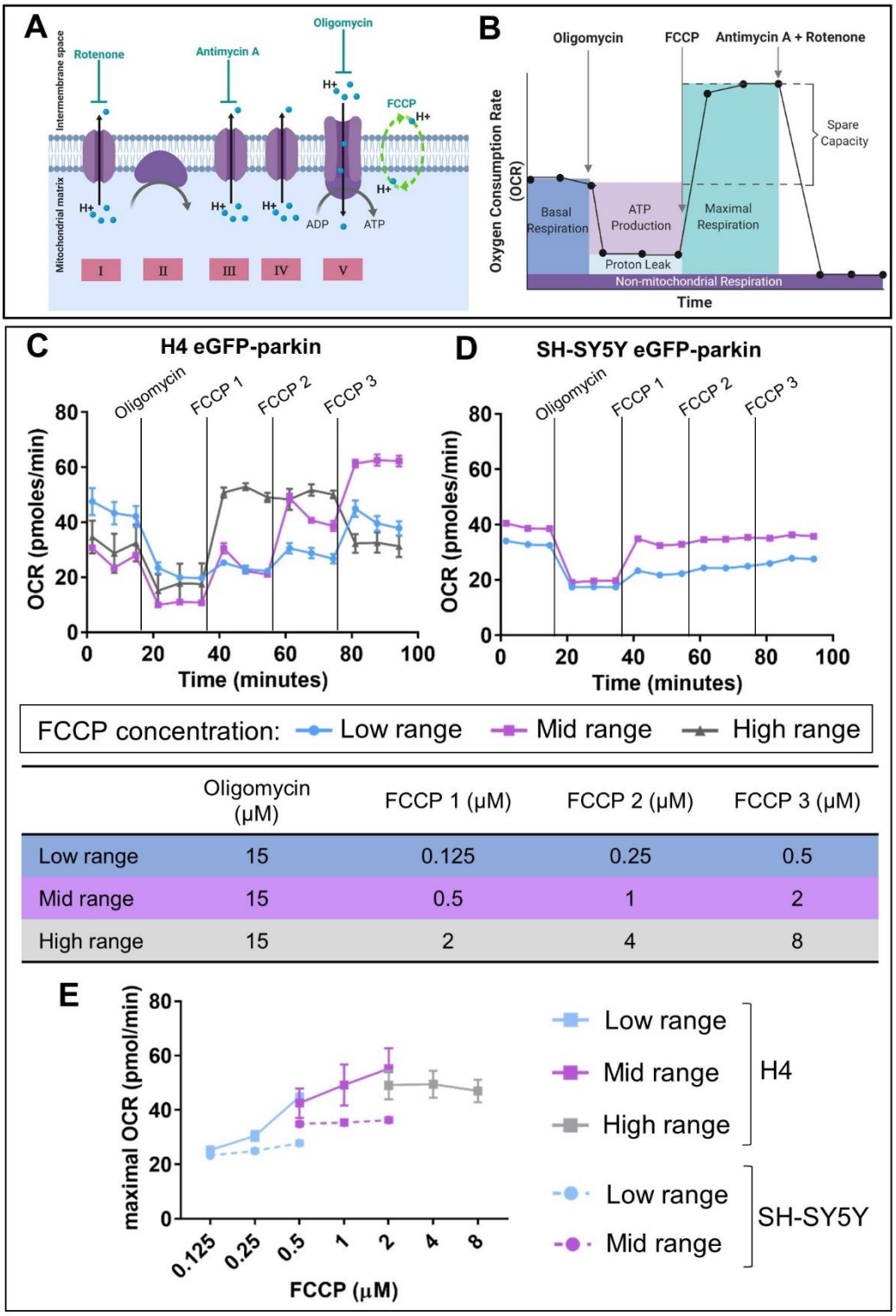

	Oligomycin (µM)	FCCP 1 (µM)	FCCP 2 (µM)	FCCP 3 (µM)
Low range	15	0.125	0.25	0.5
Mid range	15	0.5	1	2
High range	15	2	4	8

Figure 5.14 Figure legend on previous page

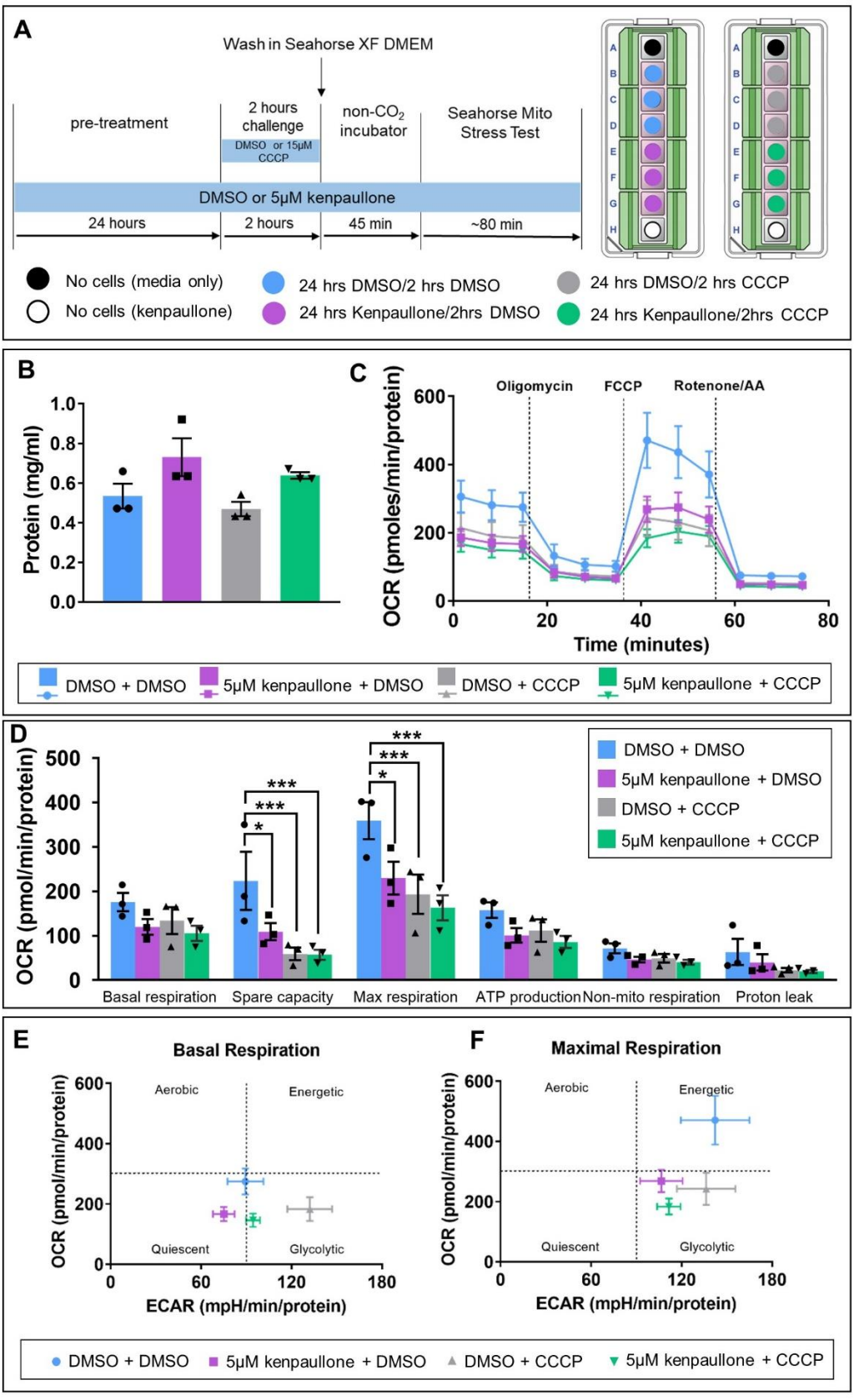

Figure 5.15 Figure legend on next page

Figure 5.15 (previous page) The effect of 5μM kenpaullone treatment for 24 hours on live cell mitochondrial function in H4 eGFP-parkin cells. **A**) Experimental protocol and plate layout for testing the effect of kenpaullone in H4 eGFP-parkin cells using the Seahorse XFp Bioanalyzer (Agilent). **B**) Protein yields per well for each experimental condition. There was no significant difference in total protein per well between experimental groups (one-way ANOVA). **C**) Oxygen Consumption Rate (OCR) (normalised to protein) over time. **D**) OCR (normalised to protein) for respiratory functional measurements. Treatment of H4 eGFP-parkin cells for 2 hours with CCCP significantly reduced spare capacity (p=0.0002) and maximal respiration rate (p=0.0002) compared to vehicle treated cells (two-way ANOVA with Tukey's post-hoc test). Kenpaullone significantly reduced spare capacity (p=0.014) and maximal respiration rate (p=0.0043) of cells without CCCP challenge, but did not have a significant effect on respiration in comparison to vehicle control on any parameters in the presence of CCCP challenge. Metabolic profiles at baseline (**E**) and at maximal respiration (**F**) provide a snapshot at individual timepoints throughout the Mitochondrial Stress Test protocol. OCR is plotted against ECAR (extracellular acidification rate, a measure of proton flux into cell culture media). n=3 plates, data is displayed as mean ± SEM. * p<0.05, *** p<0.001.

5.3.5 The effect of kenpaullone on parkin recruitment and mitochondrial morphology is replicated using two kinase inhibitor compounds

To further investigate the mechanisms underlying the modulation of mitochondria by kenpaullone, parkin recruitment and mitochondrial morphology were measured in H4 eGFP-parkin cells treated with a small panel of additional compounds (Figure 5.16, Table 5.1). AT7519 and AZD5438 were chosen because they are kinase inhibitors which act as substrates against which kenpaullone is most potent (GSK3-beta, CDK1, CDK2 and CDK5). Both drugs have also been evaluated clinically to treat solid tumours and in pre-clinical research were found to protect cells from damage in a screen for ototoxicity therapeutics (Boss et al. 2010, Hazlitt et al. 2018). There is currently no published evidence suggesting a direct effect on the mitochondrial network for either compound.

In contrast, the effect of these compounds was compared against dexpramipexole and olesoxime (TRO19622) which have been previously characterised as modulators of mitochondrial function (Bordet et al. 2010, Alavian et al. 2012). Dexpramipexole has been evaluated in clinical trials for the treatment of ALS and AD (Bozik et al. 2014, Bennett et al. 2016). Olesoxime has been investigated clinically for the treatment of ALS and spinal muscular atrophy (Lenglet et al. 2014, Bertini et al. 2017). Neither

drug is a kinase inhibitor; dexpramipexole is a weak dopamine agonist which also interacts with and increases activity of ATP-synthase (Muzzi et al. 2018), whilst olesoxime modulates mPTP opening (Bordet et al. 2010).

Results from two independent experiments evaluating the effect of these four compounds in comparison to kenpaullone on parkin recruitment and mitochondrial morphology are summarised in Figure 5.16. Both AT7519 and AZD5438 reduced cell number compared to control treated cells, but dexpramipexole and olesoxime had no effect on cell number. As AT7519 and AZD5438 are both potent inhibitors of CDKs with IC_{50} values in the low micromolar range (Table 5.3), it is likely that treatment of cells with 5µM of the drug for 24 hours could interrupt cell cycle and slow cell division. It is also not possible to rule out a cytotoxic effect of the drugs which could have reduced cell number by inducing apoptosis.

Dexpramipexole and olesoxime did not have an effect on parkin recruitment in cells challenged with CCCP, nor did they modify the total area of the mitochondrial network or elongation of mitochondrial organelles (Figure 5.16B and C). In contrast, the CDK and GSK-3 beta inhibitors AT7519 and AZD5438 replicated the effects of kenpaullone, negatively modulating parkin recruitment (Figure 5.16A) and protecting mitochondria against morphological changes induced by CCCP challenge (Figure 5.16B).

	IC_{50} (µM)			
Drug	**GSK3-beta**	**CDK1**	**CDK2**	**CDK5**
AT7519	0.089	0.21	0.047	0.013
AZD5438	0.017	0.016	0.006	0.014
Dexpramipexole	N/A	N/A	N/A	N/A
Olesoxime (TRO19622)	N/A	N/A	N/A	N/A
Kenpaullone	0.23	0.4	0.68	0.85

Table 5.3 IC_{50} values of drug compounds at selected kinases. Values were obtained by conducting a search of two NIH information portals (National Centre for Advancing Translational Sciences (NCATS): Drugs and PubChem), accessed on 25/01/20. N/A indicates no effect.

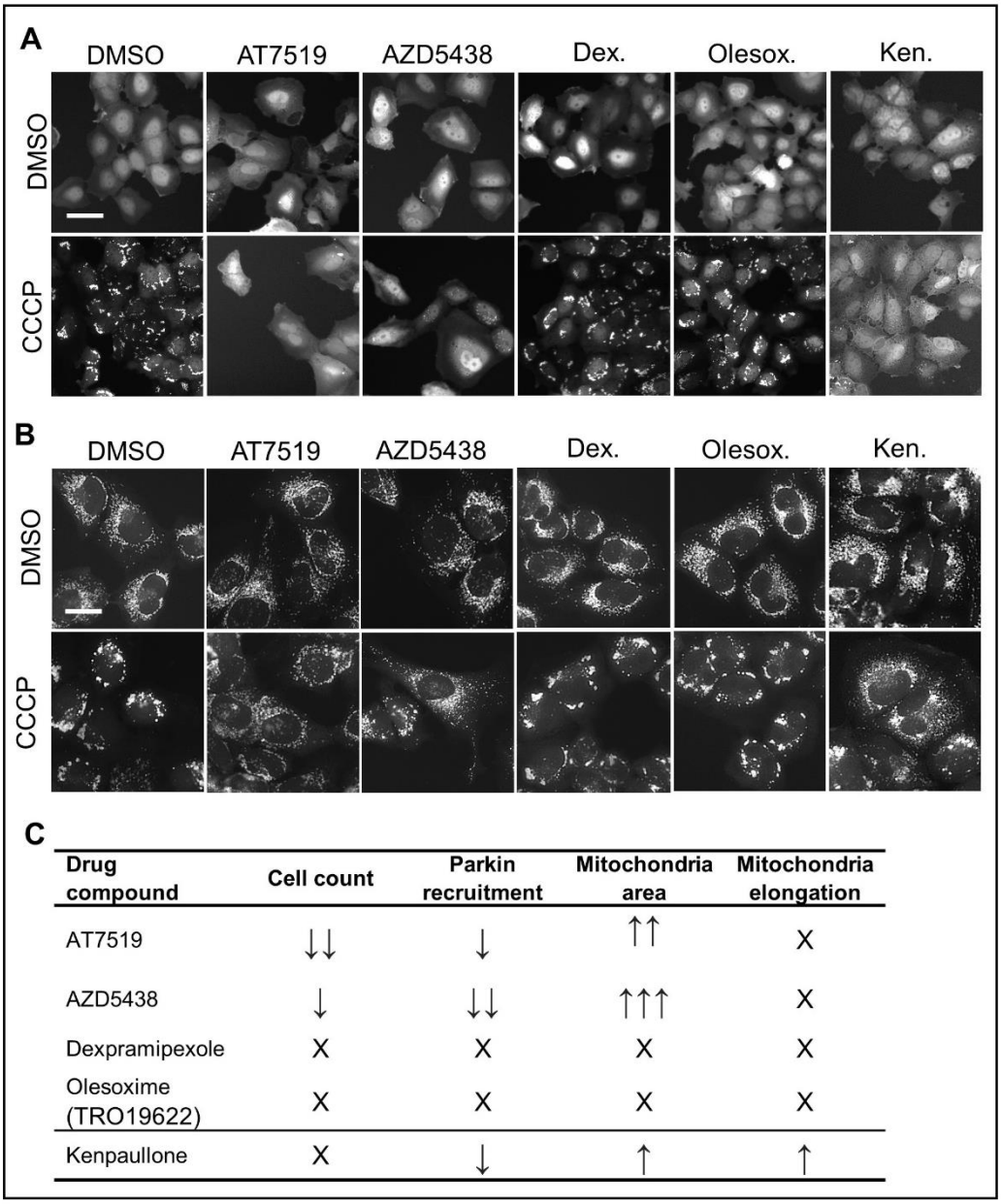

C

Drug compound	Cell count	Parkin recruitment	Mitochondria area	Mitochondria elongation
AT7519	↓↓	↓	↑↑	X
AZD5438	↓	↓↓	↑↑↑	X
Dexpramipexole	X	X	X	X
Olesoxime (TRO19622)	X	X	X	X
Kenpaullone	X	↓	↑	↑

Figure 5.16 The effect of drug compounds on parkin recruitment and mitochondrial morphology in H4 eGFP-parkin cells. Representative images of parkin recruitment (**A**) and MitoTracker Red staining (**B**) in H4 eGFP-parkin cells treated with 5μM drug compound for 24 hours, with or without CCCP challenge (15μM for 2 hours). Scale bar for (**A**) is 50μm, for (**B**) is 25 μm. **C**) Summary of the effect of drug compounds on cell count, parkin recruitment and mitochondrial morphology relative to the effect of kenpaullone. Arrows indicate the direction of change, and the number of arrows indicates strength of the effect relative to kenpaullone. An X indicates no effect. Data was summarised from two independent experiments (n=2) carried out in collaboration with Mr. Gongyu Shi.

5.3.6 Validation: Kenpaullone changes morphology of the mitochondrial network in human neurons and glia

To test the effect of kenpaullone in human neurons, human foetal neuroprogenitor cells (a kind gift from Dr. Oscar Cordero-Llana, University of Bristol) were differentiated into human neurons and glia. Differentiated cells were treated with CCCP or vehicle control, fixed, and the mitochondria visualised using fluorescence microscopy (Figure 5.17). These experiments were not quantified, nor were enough independent replicates carried out to allow certainty of the result. However, the preliminary work shown provides important initial data to describe the effect of kenpaullone in differentiated human neurons and glial cells.

In the absence of CCCP, mitochondria could be clearly visualised within foetal neurons and glial cells by immunostaining with an antibody against TOMM20 (a mitochondria-specific protein of the OMM) (Figure 5.17A). Treatment with CCCP depleted TOMM20 fluorescence signal, indicating that challenging these cells with the ionophore reduces mitochondrial area and number in a similar way to human neuroglioma and neuroblastoma cells (Figure 5.17A). There appeared to be a greater loss of mitochondria with increasing concentration and time of CCCP treatment. Differentiated foetal cells were more sensitive to CCCP treatment in comparison to the neuroglioma and neuroblastoma cell lines, as treatment with 10µM CCCP for up to an hour induced significant cell death (image not shown).

The effect of kenpaullone on mitochondria within human foetal cells was tested under baseline conditions (with no CCCP treatment). Representative images show that treatment with 5µM kenpaullone appeared to increase the size, number and staining intensity of mitochondria within human foetal neuronal and glial cells (Figure 5.17B). This effect was visualised in two separate experiments, once using MitoTracker Red and once using TOMM20 immunostaining. These results demonstrate that CCCP can be used as a mitochondrial toxin in human foetal neuronal/glial cultures, and that mitochondria can be clearly visualised by both MitoTracker dye and immunofluorescence staining in these cells. Furthermore, the preliminary

images indicate that kenpaullone could increase mitochondrial staining in differentiated human cells when compared to control treated cells. It is possible that the effect of kenpaullone on the mitochondrial network in human neuroglioma and neuroblastoma cell lines could therefore be replicated in human neuronal and glial cells. This result also shows that initial screening of compounds using cancerous human cell lines can successfully detect hit compounds which may have effects in human neurons and glia, demonstrating potential for translational capability of the screen.

Overall, kenpaullone modulates parkin recruitment and protects mitochondria against insult with CCCP and MPP+ in human cancerous cell lines and modulates mitochondrial staining in human differentiated foetal neuronal and glial cultures. Kenpaullone, or the mechanism of action underlying its effect, warrants further investigation as a potential therapeutic candidate for correcting mitochondrial dysfunction which underpins neuronal injury in neurodegenerative disease.

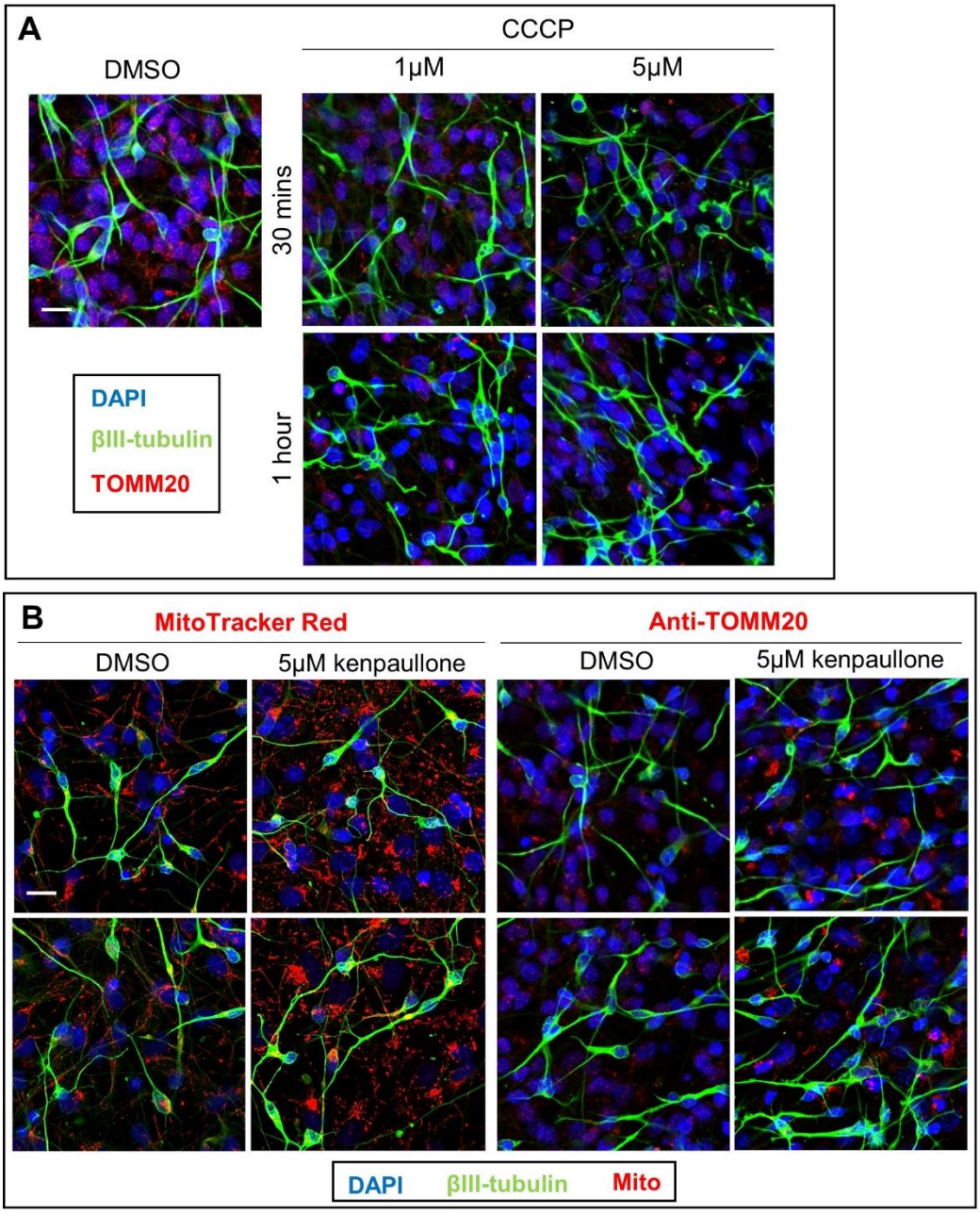

Figure 5.17 Visualisation of mitochondria and the effect of kenpaullone on human foetal neuroprogenitor cells (hfNPCs) differentiated in DMEM with N2 supplement for 7 days, immunostained for DAPI (nuclei) and beta-III-tubulin (neurons). Mitochondria were visualised either by immunolabelling with anti-TOMM20 antibody or by treating live cells with MitoTracker Red dye prior to fixation. **A**) Differentiated hfNPCs were treated with either DMSO (vehicle control), 1μM or 5μM of CCCP for either 30 minutes or 1 hour. CCCP treatment reduced mitochondrial staining with TOMM20, indicating that this protocol could be used as a model to induce mitochondrial damage by depolarisation and subsequent reduction in mitochondrial mass. **B**) Cells pre-treated with 5μM kenpaullone or DMSO for 24 hours. Treatment with kenpaullone appeared to increase the intensity and area of red mitochondrial staining with both immunodetection and dye-based visualisation. Two representative images are shown for each condition. A) n=1. B) n=1 experiment for MitoTracker staining and n=1 experiment for TOMM20 immunostaining. Scale bar is 50μm.

5.4 Discussion

5.4.1 Key findings

Mitochondrial dysfunction contributes to pathological loss of neurons in human neurodegenerative diseases such as PD. This chapter aimed to identify pharmacological compounds and druggable cell signalling pathways as novel mitochondrial modulators. A phenotypic *in-vitro* assay of PINK1-dependent parkin recruitment was successfully utilised as a tool to screen a small compound library, which identified the kinase inhibitor kenpaullone as a novel negative modulator of parkin recruitment. Validation experiments demonstrated that kenpaullone negatively modulates parkin recruitment in two neurological human cell lines. Furthermore, kenpaullone was protective against detrimental morphological changes to mitochondria induced by the ionophore CCCP, and protected against loss of MitoTracker Red dye uptake in the presence of the complex I inhibitor MPP+. Neuronal and glial cells differentiated from human foetal tissue treated with kenpaullone appeared to exhibit a morphologically enhanced mitochondrial network, as visualised with both MitoTracker Red and immunostaining. Establishment of a negative modulator of parkin recruitment as a potentially therapeutically useful tool gives reason to draw into consideration previously established understanding whereby primary consideration has been given to positive modulators of mitophagy.

5.4.2 Evaluation of the in-vitro *parkin recruitment assay as a drug screening tool*

Cells expressing fluorescently tagged parkin have been used widely and successfully in assays to screen libraries of drug compounds (Villace et al. 2016), siRNA (Lefebvre et al. 2013, Scott et al. 2020) and shRNA constructs (McCoy et al. 2014). Here, an *in-vitro* phenotypic screen of PINK1-dependent parkin recruitment was successfully optimised as a primary screening tool and used to screen a small library of 25 repurposed, neuroactive pharmacological compounds to identify novel modulators of parkin recruitment with future potential for neuro-therapeutic application. As

this screen measured only parkin recruitment, other forms of mitophagy such as receptor-mediated or lipid-mediated (Villa et al. 2018) would not be detected. It is therefore possible that compounds which primarily modulate mitophagy through non-parkin dependent mechanisms would not be identified using the current screening method.

H4 cells are derived from the brain tissue of a neuroglioma patient. They are an appropriate choice of cell line for use in this screen because they are readily grown under standard cell culture conditions, easily transfected and have an epithelial morphology conducive to high-content imaging. SH-SY5Y cells are derived from a metastatic bone tumour biopsy from a neuroblastoma patient and exist as both an adherent and a floating population. SH-SY5Y cells can be differentiated using retinoic acid to a more neuronal-like phenotype with some dopaminergic features (Kovalevich and Langford 2013). In this study the adherent, undifferentiated cell population was used because they are morphologically the most suitable for use in high-content fluorescence imaging. Both H4 and SH-SY5Y cells are cancerous lines with abnormal karyotypes (H4 cells are near-triploid, whilst SH-SY5Y cells carry a chromosome 1q duplication). These genetic alterations confer phenotypes which differ to normal human cells *in-vivo*, particularly non-dividing neurons. Expression of key cell signalling molecules including GSK-3 beta are dysregulated in glioma cells (Zhao et al. 2015), a finding which should be taken into account when assessing compounds which act on this target. Despite this, the neurological origin of these human cells means they are widely accepted as an appropriate model system for screening and first-line investigation into the cellular signalling pathways related to neurodegenerative disease.

The primary screen was developed with an assay window capable of detecting both positive and negative modulators of parkin recruitment. Rapamycin is a widely prescribed immunosuppressant and enhancer of autophagy which inhibits mTOR, a PI3-kinase family member involved in mitochondrial metabolism (Schapira 2012). Rapamycin positively modulates mitophagy in experimental models of neuronal injury (Li et al.

2014, Wang et al. 2017), and reduces mitochondrial dysfunction in a neuroprotective manner in a *Drosophila* model of PD (Tain 2009). Rapamycin was included as a positive control compound in the parkin recruitment screen, and was identified as a positive modulator of parkin recruitment using this assay.

Parkin recruitment to mitochondria is an indirect measurement of mitochondrial quality control by mitophagy. Methods to directly quantify mitophagy by measuring mitochondrial localisation to autophagosomes and lysosomal degradation have previously been utilised in high-content screening studies (Chandrachud et al. 2015, Diot et al. 2015). Although PINK1/parkin dependent mitophagy has been demonstrated to occur *in-vivo* (Vandenberghe et al. 2018), the scarcity of such evidence is recognised as a limitation within the research field (Chu 2018). There is particularly limited evidence of PINK1/parkin mediated mitophagy in neuronal tissue. These considerations highlight the importance of validating the current results in neuronal cells. The fact that the Hit compound from primary screening may modulate mitochondria in a preliminary validation experiment using human neuronal and glial cells differentiated from foetal neuroprogenitors indicates that use of H4 and SH-SY5Y cells in screening studies is translational to primary human neurons.

5.4.3 Previous evidence for the effects of kenpaullone

This chapter identified kenpaullone as a novel negative modulator of parkin recruitment. Kenpaullone also ameliorated damage-induced changes to the 2D morphology of the mitochondrial network in H4 eGFP-parkin cells by rescuing CCCP-induced fragmentation of mitochondria and attenuating reduction in mitochondrial area. Furthermore, kenpaullone rescued loss of MitoTracker Red dye uptake in cells challenged with MPP+, and affected mitochondrial metabolism by reducing the effect of FCCP on maximally-induced mitochondrial respiration.

Kenpaullone is a small molecule kinase inhibitor which was originally discovered as one of a class of cyclin-dependent kinase (CDK) inhibitors

(Zaharevitz et al. 1999). It acts as a potent inhibitor of both GSK-3 beta and various CDKs including CDK5 (Leost et al. 2000). As both GSK3-beta and CDK5 are implicated in neurodegenerative disease (see 5.4.8 and 5.4.9.1), many studies have further investigated the neuronal effects of kenpaullone.

Petit-Paitel et al. (2009) demonstrated that kenpaullone is protective against MPP+ induced neurotoxicity in mouse primary neurons and immortalised cell lines. Kenpaullone also enhanced neurogenesis (increased the number of beta-tubulin positive cells) in differentiating human neuroprogenitor cells with no effects on cell cycle or cell survival (Lange et al. 2011). There is also evidence to show that kenpaullone exerts protective actions. Pre-treatment with kenpaullone reduced ROS and downregulated autophagy markers and expression of apoptosis-activating genes in cardiomyocytes exposed to experimental oxidative stress (Joo et al. 2018). The actions of kenpaullone also translate into other terminally differentiated cell types, as it was recently demonstrated to protect podocytes (the highly specialised cells responsible for filtration at the kidney glomerulus) against puromycin-induced injury *in-vitro* (Lee et al. 2017). Kenpaullone has also been demonstrated as neuroprotective in a human model of neurodegenerative disease. It promoted survival of human induced motor neurons from ALS patients, and furthermore rescued disease cells from neurodegenerative functional deficits (increased cell survival, ameliorated electrophysiological deficits and restored normal synaptic function) (Yang et al. 2013, Liu et al. 2016).

A small number of studies have investigated the protective effect of kenpaullone *in-vivo*. Trans-tympanic kenpaullone was reported to protect mice and rats against cisplatin- and noise-induced hearing loss (Teitz et al. 2018). This efficacy in post-mitotic cochlear cells *in-vivo* is a promising insight suggestive that kenpaullone may also be efficacious and potentially neuroprotective in the brain. Indeed, Kitabayashi et al. (2019) demonstrated that kenpaullone contributes to suppression of glioblastoma in mice, further indicating efficacy of kenpaullone in the mouse CNS.

Taken together, these studies indicate that kenpaullone is efficacious in neurons *in-vitro* and *in-vivo* and may exert neuroprotective effects. Until now, the mechanisms underlying these effects have not been elucidated. The current study describes for the first time the mitochondrial actions of kenpaullone which may contribute to its previously described neuroprotective functions.

5.4.4 Effect of kenpaullone on mitochondrial morphology

A high-content protocol for analysing the 2D shape and size of the mitochondrial network visualised using MitoTracker Red was successfully developed. MitoTracker Red was chosen because it is specific for mitochondria, it is suitable for fixation, and although its initial uptake into mitochondria is dependent on an intact mitochondrial membrane potential, the dye forms covalent bonds within the organelles so remains within mitochondria irrespective of future changes in membrane potential.

The INCell Analyzer 2200 is a suitable screening tool because it allows rapid analysis of numerous experimental conditions. This chapter demonstrated that the INCell system was able to accurately segment and quantify mitochondria. A lower throughput but more detailed analysis of the mitochondrial network would be possible utilising more recently described techniques. For example, use of Image J plugins to quantify 3D changes in mitochondria imaged using confocal microscopy could be used in future validation studies in neuronal cultures (Chaudhry et al. 2019).

The elongation of the cross-sectional area of segmented mitochondria was used to indicate organelle shape. In the presence of CCCP, the mitochondria of cells treated with kenpaullone were more elongated than those treated with vehicle and became morphologically more similar to cells at baseline (those not challenged with CCCP). Although not a direct measurement of mitochondrial fission or fusion, this result is an indirect indication that kenpaullone may be influencing mitochondrial dynamics to induce a fusion-rich phenotype. Mitochondrial fusion can be considered a rescue event against mitochondrial damage (Seo et al. 2010), therefore

these results suggest that kenpaullone could be exerting a protective effect over mitochondrial network dynamics. As kenpaullone negatively modulates parkin recruitment to mitochondria, this result is in line with previous findings which demonstrate that PINK1/parkin signalling promotes mitochondrial fission (Poole et al. 2008).

Kenpaullone was also found to increase the total cross-sectional area of the mitochondrial network in CCCP-challenged cells. This increase in the size of the mitochondrial network supports the finding that kenpaullone reduces parkin recruitment and is therefore a negative modulator of mitophagy. Furthermore, this increase in size of the network could be considered a protective mechanism against the loss of mitochondria which occurs in the presence of CCCP. Baseline effects of kenpaullone (in the absence of CCCP) were observed in the preliminary validation study in neuronal/glial cells derived from human foetal neuroprogenitors. Using this model, kenpaullone treatment appeared to increase the size of the mitochondrial network in neuronal and glial cells. It was observed that the most noticeable change appears to be in glial (βIII-tubulin negative) cells. This may be because the majority of cells in the cultures were non-neuronal. The involvement of glial cell mitochondrial dysfunction in neurodegenerative diseases is now being increasingly well-understood, as recently reviewed by McAvoy and Kawamata (2019).

No experiments were performed to directly analyse the effect on kenpaullone on mitochondrial biogenesis. Indirect evidence from protein quantification analysis identified a trend towards increased protein content in kenpaullone-treated H4 eGFP-parkin cells in the absence of changes in cell number, potentially indicating an increase in mitochondrial protein. This could be confirmed by carrying out specific assays to look at mitochondrial biogenesis (see 5.4.10).

5.4.5 Effect of kenpaullone on mitochondrial membrane potential

In the MPP+ assay, MitoTracker Red was employed to indirectly assay mitochondrial membrane potential. In mitochondrial morphology assays,

cells were stained with the dye before mitochondrial challenge with CCCP, where it binds covalently to the organelles irrespective of future changes to mitochondrial membrane potential. In contrast, in the MPP+ assay, cells were stained with MitoTracker Red after applying the mitochondrial insult (MPP+).

Kenpaullone is protective against MPP+ induced neurotoxicity *in-vitro* (Petit-Paitel et al. 2009), and this effect has been partially replicated in human immortalised cells in the present study. Treatment of cells with kenpaullone for 24 hours protected against MPP+-induced loss of MitoTracker Red uptake, providing indirect evidence that the compound is attenuating loss of mitochondrial membrane potential induced by MPP+ challenge. Although kenpaullone did not rescue MPP+ induced cell death, this assay used a relatively harsh treatment protocol (inducing 50% cell death) and furthermore kenpaullone was administered at the same time as MPP+. Pre-treatment of cells with kenpaullone prior to a milder MPP+ challenge may reveal a cytoprotective effect of kenpaullone.

It is important to consider that, the increase in MitoTracker Red staining observed when MPP+ challenged cells were treated with kenpaullone could be attributable to either the existing mitochondria better maintaining a healthy membrane potential (and therefore taking up more MitoTracker dye), or an increase in the size or number of mitochondria. As MitoTracker Red dye was administered after 24 hours of kenpaullone treatment, uptake would also be reduced if there was a kenpaullone-mediated reduction in mitochondrial number. However, in the context of other experiments of this chapter which evidence the opposite effect, on balance it is unlikely that loss of mitochondrial number is responsible for the decreased uptake of MitoTracker Red. This hypothesis is supported by the results presented in Figure 5.12 and Figure 5.17 which demonstrate that kenpaullone treatment may increase the area of the mitochondrial network in both neuroglioma cells and foetal-derived neuronal/glial cultures.

Because depolarised mitochondria with low uptake of MitoTracker Red were below the sensitivity threshold of the INCell mitochondrial organelle segmentation protocol, the MitoTracker Red fluorescence staining intensity was assessed in the whole cytoplasm to measure the effect of MPP+ on mitochondrial membrane potential. This means that the area and shape of the mitochondrial network was not measurable in this experiment. Complementing this study with a repeat experiment using mitochondrial immunostaining or MitoTracker Green (a membrane potential-independent dye) would clarify the current results.

5.4.6 Effect of kenpaullone on mitochondrial respiration in live cells

The Seahorse Bioanalyzer XFp system is a gold-standard assay for quantifying mitochondrial respiratory function in intact cells (Brand and Nicholls 2011). Kenpaullone reduced maximal respiration (maximal oxygen uptake into mitochondria stimulated by acute FCCP treatment) both with and without the presence of CCCP challenge. Kenpaullone had no effect on basal respiration or ATP production. It is important to distinguish the difference between use of CCCP and FCCP in this experiment. Acute and low-dose administration of FCCP is used to stimulate maximal oxygen uptake into mitochondria. In contrast, higher dose exposure to CCCP for a number of hours is used to induce mitochondrial stress via global mitochondrial depolarisation.

It is generally accepted that compounds which enhance mitochondrial function induce an increase in either basal or FCCP-stimulated oxygen consumption and ATP production. Kenpaullone did not achieve this effect. In contrast, kenpaullone attenuated FCCP-induced oxygen consumption. This finding does not necessarily preclude its actions as an overall enhancer of mitochondrial function. Although it does not affect mitochondrial respiration at baseline, it is possible that temporary kenpaullone-induced dampening of mitochondrial oxygen uptake in damaged cells could induce a subsequent protective shift in the balance of mitochondrial biogenesis, fission and fusion events.

It has been previously established that bioenergetic differences between cultured cell lines and neurons can substantially impact the effect of experimental modulation of mitochondrial quality control pathways (Van Laar et al. 2011). Neurons are highly dependent on oxidative phosphorylation to generate energy. In contrast, cancerous cells (including H4 and SH-SY5Y) are adapted through the Warburg effect to primarily generate energy through glycolysis (cytoplasmic conversion of glucose into pyruvate to make ATP) (Aminzadeh et al. 2015). This difference should be taken into account when evaluating the current results. Culturing of H4 or SH-SY5Y cells in high-glucose media allows the cells to respirate primarily through glycolysis, explaining the relatively small increase in OCR in response to acute FCCP induced in both cell lines. Culturing of cells in glucose-free or glucose-reduced media could induce an energy phenotype more dependent on oxidative phosphorylation. Furthermore, differentiation of SH-SY5Y cells may alter their cellular metabolism to become more dependent on oxidative phosphorylation compared to undifferentiated cells, therefore more closely replicating neuronal bioenergetics (Schneider et al. 2011).

5.4.7 Pharmacological mechanisms underlying the effects of kenpaullone on mitochondria

The IC_{50} values of kenpaullone at its main targets are summarised in Table 5.4. Although the pharmacological promiscuity of kenpaullone could draw into question its direct applicability as a potentially therapeutic agent, it is possible that synergistic mechanisms relating to its effect at multiple substrates are responsible for its novel and potentially therapeutic effects on the mitochondrial network.

Kenpaullone acts with highest potency at GSK3-beta, and CDK1, 2 and 5. AT7519 and AZD5438 are potent inhibitors of these kinases (Table 5.3) and were demonstrated to mimic the effects of kenpaullone on both parkin recruitment and mitochondrial area in H4 eGFP-parkin cells challenged with CCCP. The strength of these effects appears to correlate to the compounds' potency of action at GSK3-beta, CDK1, CDK2 and CDK5 (compare Table

5.3 and Figure 5.16C). The following sections describe the potential pharmacological mechanisms underlying the action of kenpaullone on mitochondria at GSK3-beta, and CDK1, 2 and 5.

Target	IC_{50} (μM)
GSK-3 beta	0.23
CDK1/cyclin B	0.4
CDK2/cyclin A	0.68
CDK5/p35	0.85
ERK2	9
c-Src	15
Casein kinase 2	20
ERK1	20
MAP4K4	not established (effect described by (Yang et al. 2013))

Table 5.4 IC_{50} values of kenpaullone in cell-free assay conditions (Zaharevitz et al. 1999).

5.4.8 Inhibition of GSK-3 beta

Kenpaullone acts as an inhibitor of GSK-3 beta at low micromolar potency. GSK-3 beta is a serine-threonine kinase with over 100 substrates, implicated in many diseases including cancer, inflammatory conditions and neurological disorders (Beurel et al. 2015). GSK-3 beta has been established as a mediator of neuronal oxidative stress and apoptosis (Lee et al. 2007), and dysregulated GSK-3 beta signalling is known to contribute to the cellular pathology of neurodegenerative diseases such as PD (Golpich et al. 2015). GSK-3 beta is partially localised to mitochondria in both SH-SY5Y cells (Bijur and Jope 2003) and in mouse primary and immortalised neurons (Petit-Paitel et al. 2009). This mitochondrial population of GSK-3 beta is more active under apoptotic stimuli in comparison to that within the cytosolic compartment (Bijur and Jope 2003). As a signalling protein which can mediate neuronal death by mitochondrial dysfunction, GSK-3 beta inhibition has previously been hypothesised as protective against mitochondrial induced neuronal stress, and evidence suggests that GSK-3 inhibition can ameliorate pathological signalling which causes dopaminergic neuronal death (Golpich et al. 2015).

Pharmacological inhibition of GSK-3 reduces mitochondrial biogenesis in SH-SY5Y cells under metabolic stress induced by 2-deoxyglucose treatment, but not under baseline conditions (Ngamsiri et al. 2014). This implies that the increase in mitochondrial area induced by kenpaullone treatment during experimentally induced mitochondrial stress observed in the present study may not be mediated by enhanced biogenesis. Mitochondrial-E.R. interaction via mitochondria-associated membranes (MAMs) is an important aspect of regulation of mitophagy signalling in health and disease (Rodriguez-Arribas et al. 2017). Activation of GSK-3 beta destabilises MAM tethering proteins, leading to disrupted ER-mitochondrial signalling and consequent disruption to mitophagy (Stoica et al. 2016). Kenpaullone-induced inhibition of GSK-3 beta could reduce disruption of MAM tethering, thereby contributing towards re-balanced mitophagy signalling and healthy mitochondrial quality control. Previous research demonstrated that kenpaullone promotes neurogenesis in differentiating neuroprogenitor cells without influencing cell cycle or cell survival, and this action is dependent on stimulation of Wnt/beta-catenin signalling which is antagonised by GSK-3 beta (Lange et al. 2011).

The data from this chapter combined with that in the published literature demonstrates that the action of kenpaullone on GSK-3 beta could contribute to the mitochondrial effects observed in the present study. However, further indications of kenpaullone's mechanism of action on parkin recruitment can be inferred from the effect of other compounds tested in the primary screen. AR-A 014418 is a kinase inhibitor highly specific for GSK-3 (IC_{50}=0.10μM) which does not inhibit CDK2 or CDK5 (Bhat et al. 2003). Despite the fact that the reported IC_{50} value of AR-A 014418 on GSK-3 beta is approximately half that of kenpaullone, AR-A 014418 induced only a modest reduction in parkin recruitment in the primary screen. Furthermore, the neuroprotective effect of kenpaullone on motor neuron survival was previously demonstrated to be dependent on pharmacological inhibition of CDK2 and MAP4K4, as opposed to an isolated effect of GSK-3 beta inhibition (Yang et al. 2013, Liu et al. 2016). Taken together this evidence indicates that the

effect of kenpaullone on mitophagy signalling is unlikely to be attributable to its action on GSK-3 beta alone.

5.4.9 Inhibition of cyclin-dependent kinases

5.4.9.1 CDK5

Cyclin-dependent kinases (CDKs) are serine/threonine kinases which interact with particular cyclin subunits to regulate cell cycle. Activation of CDK5 requires association with p35 or p39, and kenpaullone inhibits CDK5 with an IC_{50} of 0.85. Unlike its homologous family members, CDK5 does not regulate cell cycle in proliferating cells and is unique in that it is critical to the function of post-mitotic neurons (Cortes et al. 2019). CDK5 is dysregulated in a number of human neurodegenerative conditions including AD, HD and PD (Shah and Lahiri 2014, Mushtaq et al. 2016, Gupta and Singh 2019) and is therefore considered as a drug target for many neurological disorders. In this chapter, the potent CDK5 inhibitors AT7519 and AZD5438 were found to mimic the effect of kenpaullone on CCCP-induced parkin recruitment and mitochondrial morphology.

There are a number of signalling pathways downstream of CDK5 which could mediate the mitochondrial actions of kenpaullone. CDK5 regulates the activity of parkin through serine phosphorylation (Avraham et al. 2007), therefore the modulation of parkin recruitment by kenpaullone could be mediated by its inhibition of CDK5. CDK5 is upregulated in MPTP-treated mice (Smith et al. 2003) and neurotoxic insults activate CDK5, mediating activation of Bcl-2 family proteins and inducing mitochondrial dysfunction (Nikhil and Shah 2017). Kenpaullone-induced inhibition of CDK5 may therefore attenuate this pathway and promote healthy mitochondrial function. Indeed, Smith et al. (2003) demonstrated that pharmacological inhibition of CDK5 attenuated loss of dopaminergic neurons and rescued motor deficits in MPTP treated mice. CDK5 phosphorylates and promotes the degradation of E3 ubiquitin ligases including glycoprotein 78 (GP78), an enzyme which has been identified as protective in models of PD (Wang et

al. 2018). Kenpaullone treatment may therefore upregulate levels of neuroprotective molecules such as GP78.

Using a novel lysosomal trafficking probe, Ishii et al. (2019) showed that kenpaullone upregulated lysosomal biogenesis in HeLa cells. This effect was proven to occur independently of cell cycle arrest, and to be dependent on the action of kenpaullone as a CDK5 inhibitor (Ishii et al. 2019). As lysosomal trafficking is integral to mitochondrial quality control by induced mitophagy (section 1.8), this study supports the hypothesis that kenpaullone may enhance mitochondrial quality control. The ability of kenpaullone to upregulate lysosomal biogenesis also raises the question of whether the compound can also regulate mitochondrial biogenesis, a hypothesis which requires further experimental investigation (section 5.4.10).

Kenpaullone-mediated CDK5 inhibition could also directly modulate mitochondrial dynamics. Wong et al. (2011) demonstrated that CDK5 mediated phosphorylation of endophilin B1 is necessary for neuronal autophagy, and dysregulation of this pathway was shown to contribute to the pathophysiology of PD. Endophilin B1 is an important modulator of mitochondrial morphology (Karbowski et al. 2004), implicating that kenpaullone-mediated CDK5 inhibition could directly contribute to the effect of kenpaullone on mitochondrial dynamics. Utilising MPTP to model PD in non-human primates, Park et al. (2019) demonstrated that excessive mitochondrial fission associated with parkinsonian neurodegeneration was driven by CDK5-induced phosphorylation of Drp1. Although the ethics of using non-human primates here should be questioned, the results do provide insight into mitochondrial dynamics in the primate brain. By inhibiting neuronal CDK-5, kenpaullone could counteract excessive disease-associated mitochondrial fission and rebalance mitochondrial dynamics towards a healthier, fusion-associated phenotype. Indeed, the current results support this hypothesis, as kenpaullone was demonstrated to counteract CCCP-induced fragmentation of mitochondria in H4 cells.

5.4.9.2 CDK1 and CDK2

Although there is evidence to indicate that kenpaullone may be acting on the non-mitotically associated CDK5, its pharmacodynamics imply that its effect could be partially exerted by inhibition of CDKs associated with cell cycle progression. Kenpaullone inhibits both CDK1 and CDK2 with IC_{50} values in the low micromolar range (Table 5.4). CDK1 acts at mitochondria to modulate respiration (Qin et al. 2015, Xie et al. 2019), whilst CDK2 is required for mPTP-mediated control of apoptosis (Park and Jin 2004, Choi et al. 2007).

The potent inhibitors of CDK1 and 2, AT7519 and AZD5438, were found to mimic the effect of kenpaullone on parkin recruitment and mitochondrial area, but also dramatically reduced cell number. Although loss of cell number due to cytotoxicity (for example through induction of apoptosis) cannot be ruled out at this stage, it is reasonable to assume that the loss in cell number following 24 hours of treatment is attributable to cell cycle arrest via CDK1 and CDK2 inhibition.

Compared to AT7519 and AZD5438, kenpaullone acts with much lower efficacy at CDKs 1 and 2. Pre-treatment with kenpaullone for 24 hours at the same concentration (5µM) does not alter cell number yet still induces significant modulation of parkin recruitment and mitochondrial area. This indicates that the cell-cycle modulatory effects of these kinase inhibitors are dispensable for their actions at the mitochondria. This hypothesis is further supported by the preliminary findings in human differentiated neuronal/glial cultures, which featured enhanced mitochondrial networks when treated with kenpaullone.

5.4.10 Recommendations for future work

As kenpaullone was demonstrated to affect the shape and size of the mitochondrial network, it is recommended that future and ongoing work should seek to gain further mechanistic insight into the effect of kenpaullone on mitochondrial dynamics. Firstly, it would be important to understand

whether the compound is directly affecting mitochondrial biogenesis. ELISAs to quantify inhibitors and activators of biogenesis would give an overall indication of whether kenpaullone modulates generation of new mitochondria. Alternatively, detection of mtDNA-encoded genes such as MTCO1 by qPCR and expressing this as a ratio to a nuclear encoded gene would give a quantitative measure of biogenesis, whilst mtDNA expression levels alone would represent the relative quantity of total mitochondria in cells treated with kenpaullone compared to control. Immunostaining of mtDNA-encoded proteins and fluorescent imaging (especially using confocal microscopy) would act as a validation experiment to complement the results of the current study which describe kenpaullone-induced changes to the mitochondrial network using MitoTracker Red. These assays could be readily implemented into a modified battery of screening tests for use with various drug compound libraries in the future.

Although requiring more intensive optimisation and a heavier investment of time, it would be possible to assay the effect of kenpaullone specifically on mitochondrial fusion. Jourdain and Martinou (2010) describe a fusion assay whereby different domains of Renilla luciferase are expressed within mitochondrial matrix of two different cell lines, and after mixing of the two isolated mitochondrial populations, functional luciferase is produced upon mitochondrial fusion. This assay only permits assessment of fusion in cell-free conditions. The Youle research group previously described use of a mitochondrial matrix targeted photoactivatable-GFP, imaged using time-lapse confocal microscopy to assess fusion events in whole cells (Karbowski et al. 2004). The effect of kenpaullone on mitochondrial fission could potentially be measured by assessing expression and/or localisation of Drp1 by immunofluorescence, Western blotting or qPCR. Alternatively, immunofluorescent labelling of mitochondria after kenpaullone treatment could be readily combined with 3D confocal microscopy to gain a more detailed insight into the shape of the organelles in a variety of cell types, as a surrogate measure of fission and fusion events.

It would be useful to determine whether kenpaullone directly affects mitochondrial membrane potential. Mitochondrial probes such as JC-1 can be used to assay mitochondrial membrane potential, although as a single excitation/dual emission probe, would not be suitable for use with the INCell Analyzer. Alternative membrane-potential dependent dyes such as TMRM may be preferable for use in plate-based assays (Nicholls 2012, Lefebvre et al. 2013).

In addition to clarifying the specific effects of kenpaullone on mitochondrial dynamics, it is recommended that ongoing work should focus on understanding which pharmacological targets of kenpaullone are important in mediating its mitochondrial effects. The use of cell lines carrying a knockout of specific kenpaullone targets would contribute to our understanding of the relative importance of the various substrates. Bristol Renal research group at Bristol Medical School, University of Bristol, have developed GSK-3 knockout podocyte lines and have agreed to a collaborative project to assess the effect of kenpaullone on mitochondrial health and function in these cells. This would be especially interesting considering recent evidence which reports that kenpaullone protects podocytes (Lee et al. 2017).

As kenpaullone acts with low micromolar efficacy on cell-cycle mediating CDKs (CDK1 and CDK2), it is important to investigate whether kenpaullone treatment modulates cell cycle progression and how this may relate to its mitochondrial effects. Although CDK1 and CDK2 may not have significant functional importance in the cell cycle of post-mitotic neurons, they are likely to play an important role in the phenotype of human cancerous cell lines such as H4 and SH-SY5Y.

In a future experiment, the effect of kenpaullone should be compared against that of a cell-cycle modulator which works via mechanisms unrelated to CDK inhibition and which are not candidate drugs for mitochondrial modulation. Suitable examples include either ABT 751 or epothilones which exert anti-mitotic effects by inhibiting microtubule

polymerisation or CFM4 which induces cell cycle arrest by preventing function of cell cycle and apoptosis regulator-1 (CARP-1). Preference could be given to drugs which do not target microtubules, as mitochondrial dynamics (movement, fission and fusion) are in part mediated by mitochondrial association with microtubules. Importantly, the evidence presented in this chapter suggests that kenpaullone induces modulation of the mitochondrial network in post-mitotic human neurons and glia differentiated from foetal cells. This indicates that kenpaullone is not entirely dependent on cell-cycle modulation to exert its effects on mitochondria.

Further validation experiments must be carried out to confirm and quantify the effect of kenpaullone in foetal-derived neuronal/glial cultures. Capture of mitochondrial immunofluorescence should be carried out using confocal microscopy under blinded conditions, and images quantified using software such as ImageJ. Further study into the effect of kenpaullone in neurons could be executed by culturing primary neurons from rodents and measuring the effect on kenpaullone on mitochondria visualised by immunostaining or MitoTracker Red uptake. This could be taken further by utilising cells from rodent models of PD. Likewise, neurons derived from human iPSCs derived from either control patients, or patients diagnosed with neurodegenerative conditions such as PD could be used to test the potentially therapeutic potential of kenpaullone.

There have been very few *in-vivo* studies of kenpaullone carried out to date. Ultimately, it will be unknown whether kenpaullone is capable of exerting potentially neuroprotective effects until testing is carried out in a mouse model of neurodegenerative disease. Animal testing should only be carried out after *in-vitro* studies (as recommended above) have taken place and indicated therapeutic promise and should be initially restricted to using mice. Kenpaullone has a relatively low molecular weight (327.2 g/mol) and is lipophilic and therefore likely to pass the blood-brain barrier (Kitabayashi et al. 2019). The same study reported intraperitoneal administration of kenpaullone for 9 weeks with no obvious adverse effects. As previously described, kenpaullone was also demonstrated to be effective *in-vivo* in

mouse models of glioblastoma and hearing-loss (Teitz et al. 2018, Kitabayashi et al. 2019), setting a precedent for its efficacy at terminally differentiated cells *in-vivo* including within the CNS.

It should also be noted that other drugs in the paullone family, such as alsterpaullone and 1-azakenpaullone, are also potent inhibitors of GSK-3 beta and CDK5 (Leost et al. 2000, Kunick et al. 2004) which have been previously demonstrated as cytoprotective (Lee et al. 2017)). Further investigation into these closely related chemical compounds should be considered, as they may confer pharmacological properties more suitable for *in-vivo* application.

5.4.11 Conclusions

In summary, this chapter reports the development and implementation of *in-vitro* assays to screen the effects of drug compounds on parkin recruitment, mitochondrial morphology and mitochondrial respiratory function. Kenpaullone was identified as a novel negative modulator of parkin recruitment to mitochondria. Further analysis revealed that kenpaullone modulated the 2D morphology of the mitochondrial network, and protected mitochondria against the mitochondrial toxin MPP+. Initial experiments suggest that kenpaullone could alter the morphology of the mitochondrial network in human foetal-derived neurons and glial cells, enhancing the size and number of organelles which could be bioenergetically favourable and increase resilience to pathogenic change. This finding implies that negative modulators of parkin recruitment may exert beneficial effects on the mitochondrial network. This in turn indicates that modulators of mitochondrial health and function with potentially therapeutic applications need not push the balance of mitophagy in one particular direction.

Overall this chapter identifies kenpaullone as a novel modulator of mitochondria which could ameliorate bioenergetic failure and cellular stress caused by mitochondrial dysfunction, perhaps through enhanced mitochondrial quality control and healthy mitochondrial dynamics. This

action could be mediated by inhibitory actions on important neuronal kinases with mitochondrial modulatory functions including GSK-3 beta and CDK5.

6. Chapter 6

General Discussion

6.1 Thesis results and wider context

Neurodegenerative disease represents a critical area of unmet clinical need. This complex and usually fatal group of disorders results in economical and medical impact at both the societal and individual patient level. There are currently no curative or disease-modifying therapies approved for the treatment of any neurodegenerative condition, whilst prevalence of neurodegenerative diagnoses is predicted to continue to increase alongside an ageing population.

In addition to improvement of clinical trial design and development of biomarkers to facilitate early diagnoses, further developing knowledge of the molecular pathology of neurodegenerative disease is considered a high-priority research area (The Royal Society). As neurons have highly active and complex transcriptomes, they are especially vulnerable to alterations in RNA processing which occurs as a result of altered RBP expression and function. Neuronal function necessitates high energy expenditure, and neurons are therefore also highly susceptible to imbalances in energy homeostasis which occur as a result of impaired mitochondrial health and function. Abnormal RBP function and mitochondrial dysfunction are both linked to genetically inherited neurodegenerative conditions, and are also associated with idiopathic disease. This thesis aimed to investigate both RBP dysfunction and mitochondrial dysfunction as two important molecular hallmarks of neurodegenerative disease with future therapeutic promise.

6.1.1 Chapters 3 and 4: Investigating the RNA binding protein SAFB1

SAFB1 is an RBP of increasing importance to human disease pathology. The structure and diverse functions of SAFB1 have been previously established using *in-vitro* cell models and transgenic animals (reviewed by Norman et al. (2016)). Previous research demonstrated a role for SAFB1 in

cancer (Oesterreich et al. 2001, Hong et al. 2012, Allahyani 2020) and indicated that it could be associated with the pathology of neurodegenerative disease ((Rivers et al. 2015, Norman et al. 2016). Although it was previously shown that SAFB1 is highly expressed in the rodent and human brain (section 1.5, Figures 1.12 and 1.13), characterisation of its expression pattern in either aged or degenerating human brain had not been previously characterised.

Chapter 3 presents a detailed immunohistochemical analysis of SAFB1 in human brain areas affected by neurodegenerative disease. In patients with no history of neurological illness, immunohistological staining showed that SAFB1 was highly expressed in the cerebellum, in the nuclei of granule cells, molecular layer cells, and Purkinje cells. There was low expression of SAFB1 in the large principle neurons of the cerebellar DN. SAFB1 was highly expressed in the nuclei of both glial and neuronal cells in control patient striatum. In contrast, there was low expression of SAFB1 in the substantia nigra. The nuclear expression pattern of SAFB1 was unaltered in the cerebellum of patients with MS, and in the substantia nigra of patients with PD. However, the expression pattern of SAFB1 was markedly different in the brains of patients with polyQ disease. In SCA cerebellum, SAFB1 was expressed throughout the cytoplasm of Purkinje cell soma and dendrites, alongside expression in the nuclei. There was also a dramatic increase in the nuclear expression of SAFB1 in DN neurons of SCA patients, alongside cytoplasmic immunopositivity. In the striatum of patients with HD, nuclear SAFB1 expression was accompanied by abnormal cytoplasmic staining in neurons which morphologically resembled degenerating MSNs.

SAFB1 has structural and functional similarities to RBPs implicated in neurodegenerative disease (e.g. TDP-43 and FUS). These RBPs have been shown to bind expanded polyQ peptides (Doi et al. 2008, Schwab et al. 2008, Kino et al. 2016, Coudert et al. 2019), associate with other proteins altered in polyQ disorders (Becker et al. 2017), and have altered nucleocytoplasmic transport (Fahrenkrog and Harel 2018). Because SAFB1 was previously demonstrated to interact strongly with *ATXN1* RNA and it

did not associate with ataxin1 protein (Rivers et al. (2015), sections 3.2 and 4.2), the RNA binding functions of SAFB1 were further investigated.

Chapter 4 interrogated the interaction of SAFB1 with *ATXN1* RNA with varying polyCAG tract lengths, to model the interaction of SAFB1 with expanded CAG RNA in polyQ disease. RNA IP experiments demonstrated that SAFB1 binds to *ATXN1* RNA with varying CAG repeat tract lengths. Pathological expansion resulted in increased levels of *ATXN1* RNA associated with SAFB1. This may be mediated by the altered secondary structure of the 85 CAG tract, which is predicted to form a highly stable long hairpin loop.

Consequences of the altered RNA binding function of SAFB1 are currently uncertain. It is possible that increased binding of SAFB1 to polyCAG xtrRNA facilitates the aberrant export of SAFB1 into the cytoplasm, in turn inducing a cytoplasmic gain of function or nuclear loss of function. Alternatively, newly translated SAFB1 could be sequestered in the cytoplasm by polyCAG mRNA transcripts which cause it to be pathologically retained in the neuronal cytoplasmic compartment. Previous proteomic evidence (Zhang et al. 2018, Allahyani 2020), combined with the current immunostaining data, do not support a direct protein-protein interaction of SAFB1 and expanded polyQ peptides. However, as expanded CAG tracts are associated with dysregulated translation, it is possible that pathological RAN peptides of the *ATXN1* or *HTT* gene could be interacting with SAFB1 in the nucleus or cytoplasm of polyQ neurons. These hypotheses pose unanswered questions which could inform the basis for future research into the role and mechanism of SAFB1 in polyQ disease pathogenesis.

Wider reaching questions are also raised by this work. For example, could furthering our understanding of the mechanisms behind SAFB1 expression in polyQ disease provide clues to help explain the elusive selective vulnerability of neurons in polyQ disease? Furthermore, is abnormal SAFB1 expression a cause or consequence of neuronal pathology? The hypotheses posed here to explain the causes and consequences of altered

SAFB1 expression are based on previous research which postulates that altered RBP expression is detrimental to cells and induces toxic loss or gain of function contributing to neuronal damage. However, it cannot currently be disproved that the altered expression of SAFB1 may in fact be protective. In human polyQ patient brains, the surviving neurons at end stage disease are indeed the ones which abnormally express SAFB1.

6.1.2 Chapter 5: identification of kenpaullone as a novel mitochondrial modulator

Mitochondrial dysfunction and impaired mitochondrial quality control have been well-established as mechanisms associated with several neurodegenerative diseases including PD (section 1.9). This knowledge has been used to drive the development of disease-modifying therapies, some of which have been tested in clinical trials (section 1.9.2). In Chapter 5, an *in-vitro* screen of parkin recruitment was used to test pharmacological compounds from a repurposed drug library. Kenpaullone was identified as a negative modulator of parkin recruitment, which also increased the size and elongation of the mitochondrial network in human cell lines. Kenpaullone protected against the mitochondrial toxin MPP+ and altered mitochondrial respiratory function. In neuronal and glial cells derived from foetal neuroprogenitors, kenpaullone dramatically increased the size of the mitochondrial network. Of note, the most apparent change to the mitochondrial network appeared to be within the non-neuronal (glial) cells. As previously described, non-neuronal cells make up half of the cells in the human brain, and their role in neurodegenerative pathology is becoming increasingly well understood.

Previously published research established that kenpaullone downregulates autophagy and apoptosis (Joo et al. 2018), promotes neurogenesis (Lange et al. 2011), protects podocytes (Lee et al. 2017) and promotes survival of motor neurons from ALS patients (Liu et al. 2016). Kenpaullone also ameliorated *in-vivo* pathology in mice (Teitz et al. 2018, Kitabayashi et al. 2019). The current findings present a novel, mitochondrial role for

kenpaullone, which may underpin its previously established cyto- and neuro-protective effects.

However, there are still outstanding research questions to be considered. The most important of these relate to a) confirming the mechanism of action which mediates the mitochondrial effects of kenpaullone and/or its related compounds, and b) further validating the effect of kenpaullone in neurons and *in-vivo*, with the ultimate aim of studying the compound in a model of neurodegeneration to test its neuroprotective potential.

The current model of parkin function in PD relates primarily to its role as a critical component for stress-induced mitophagy signalling and therefore the removal of damaged mitochondria. The fact that PINK1 or parkin mutations directly cause familial PD leave little doubt that mitophagy and/or quality control signalling is critical for dopaminergic neuron survival in the SNpc. However, it is important to contextualise this against the current mechanistic knowledge regarding mitophagy in neurons *in-vivo* (section 1.8.3). To date, studies have generated mixed and sometimes apparently contradictory results which suggest that both parkin function and control of mitophagy in neurons *in-vivo* is rather more complex than originally hypothesised. Indeed, parkin is known to have diverse functions in addition to its established role in mitophagy signalling. Its ubiquitin ligase activity regulates apoptosis, cell cycle control and neuroinflammation, in addition to other mitochondria related functions such as biogenesis, transport and morphological regulation of the mitochondrial network (reviewed by Shires et al. (2017) and Montava-Garriga and Ganley (2020)).

In addition to the role of kenpaullone as a modulator of parkin recruitment, its ability to increase the elongation and number of mitochondria hint towards a function in modulating mitochondrial dynamics and possibly biogenesis. This may be especially important when considering the inconsistent evidence for parkin-mediated mitophagy signalling in neurons; it is possible that alternative mitochondrial quality control mechanisms may be more important in neurons than in dividing cells including experimental

cell lines. Even when analysing mitochondrial quality control in mammalian *in-vivo* systems, this could differ greatly to the situation in the aged human brain, where individual neurons survive and function for many decades and therefore may require species-specific mitochondrial quality control systems. This in turn highlights the importance of a) developing pre-clinical models of mitochondrial dysfunction which are relevant to the mechanisms underpinning human disease, and b) the need for good experimental design in clinical trials, such as patient stratification using biomarkers of mitochondrial dysfunction.

If future work were to confirm kenpaullone as a neuroprotective or disease-modifying compound, this would highlight a wider consideration for research into mitochondrial targeted therapeutics. Consensus within the field has previously established that mitochondrial quality control is impaired in PD, and that mitophagy is downregulated, resulting in impaired ability of neurons to clear damaged and dysfunctional mitochondria (section 1.9). This has naturally led to research efforts biased towards the discovery of interventions which upregulate mitophagy signalling. However, it is possible that downregulation of mitophagy, or of a specific mitophagy signalling pathway, could also be therapeutically beneficial. Downregulation of mitophagy could result in increased overall number of mitochondria in the cell, either through reduced clearance and/or a feed-forward effect which upregulates mitochondrial biogenesis and/or fusion. In the presence of this increased mitochondrial number, dysfunctional organelles may then be primed to undergo increased fusion with healthy ones, increasing the overall health of the mitochondrial network. This may be a direct result of increased organelle number or could occur as a result of downstream signalling events initiated by the action of compounds such as kenpaullone.

6.2 Crosstalk between RBPs and mitochondria

The mechanisms which underpin the molecular pathology of neurodegenerative disease are often considered in isolation to facilitate experimental design. It is likely that there is complex crosstalk between

different pathological mechanisms which converge to result in neuronal loss *in-vivo*. The combination of mechanisms is likely to vary with disease type, disease stage, and between individual patients.

RBPs are important modulators of mitochondrial function (Koc and Spremulli 2003, Schatton and Rugarli 2018, Gopalakrishna et al. 2019) and mitochondrial damage is known to be an aspect of RBP proteinopathy. This mitochondrial crosstalk has been most well-studied in the “prototypical” RBPs associated with neurodegenerative disease, FUS and TDP-43, which both interact with mitochondria and induce the mitochondrial unfolded protein response (Deng et al. 2018, Wang et al. 2019). TDP-43 was shown to interact with proteins required for mitochondrial dynamics and with mitophagy associated proteins (Davis et al. 2018), whilst inhibiting mitochondrial localisation of TDP-43 in ALS neurons abolished mitochondrial dysfunction and neuronal loss (Wang et al. 2016). PINK1 or parkin downregulation rescued locomotor deficits in *Drosophila* expressing mutant FUS (Chen et al. 2016), demonstrating that genes involved in mitochondrial quality control act as modifiers of RBP pathology. This finding further supports the argument established in Chapter 5, that downregulation of parkin function may be a potentially therapeutically useful mechanism, and that modulation of mitophagy signalling in either direction may result in correction of pathological mitochondrial imbalances in neurons.

Several other RBPs have also been implicated in mitochondrial dysfunction. Mitochondrial impairment is a feature of SCA1 (Stucki et al. 2016), and mutant forms of the DRBP ataxin1 impair the function of DNA damage response proteins responsible for mtDNA repair (Ito et al. 2015). The RBP ataxin2 modifies PINK1 expression levels and modifies its signalling (Sen et al. 2016, Sen et al. 2017). TIA-1, an RBP implicated in AD, ALS and FTD, regulates mitochondrial dynamics by enhancing the expression of genes which control mitochondrial fission (Tak et al. 2017) and downregulates expression of OPA1 (Carrascoso et al. 2017).

It is also important to consider the communication between mitochondria and other organelle systems within degenerating neurons. Mitochondria are physically associated with the E.R. through mitochondria-associated membranes (MAMs). Disruption to E.R.-mitochondrial signalling is implicated in the pathology of FTD and ALS (Lau et al. 2018). The E.R.-mitochondrial tethering protein complex VAPB-PTPIP51 is important in regulation of autophagy (Gomez-Suaga et al. 2017) and its function is disrupted by both TDP-43 (Stoica et al. 2014) and FUS (Stoica et al. 2016). Interestingly, this is dependent on GSK-3 beta activation by both FUS and TDP-43, which disrupt binding of the protein complex through an unknown mechanism. Inhibiting GSK-3 beta was shown to correct FUS-induced disruptions to E.R.-mitochondrial signalling (Stoica et al. 2014, Stoica et al. 2016). This holds further implications for kenpaullone and its related compounds, which are potent inhibitors of GSK-3 beta.

6.3 Translational and therapeutic potential of the current findings

Further research to elucidate the mechanisms of abnormal SAFB1 expression and its role in polyQ disease may identify new therapeutic approaches. If SAFB1 expression level is pathologically altered in polyQ disease, restoration of normal expression could be clinically beneficial. This could be achieved using antisense oligonucleotides (ASOs) which target and bind mRNA transcripts to prevent translation. This therapeutic approach has already been used clinically in the case of spinal muscular atrophy to correct pathological splicing and expression of the SMN2 gene (Mercuri et al. 2018). If it was demonstrated that SAFB1 in the cytoplasm of degenerating neurons was aggregation prone, it may be therapeutic to prevent or reverse this. ASOs have also been previously utilised for this purpose, for example, targeting ataxin2 with ASOs reduced aggregation of mutant TDP-43 and improved survival in mice (Becker et al. 2017). Modulation of RBP chaperone proteins may also reduce RBP aggregation and associated neuronal toxicity (Crippa et al. 2016).

As SAFB1 was shown to sequester pathological expansion repeat RNA, interventions to downregulate this interaction may be therapeutically useful. Both ASOs and small molecules have previously been utilised for this purpose. Oligonucleotides which bind xtrRNA repeats or alter their secondary structure attenuate RBP binding (Wheeler et al. 2009). Small molecules designed to either bind RNA trinucleotide repeat sequences or disrupt mRNA structural motifs have also been shown to reduce RBP binding (Childs-Disney et al. 2013, Coonrod et al. 2013).

The novel findings presented in Chapter 5 are highly translational. Kenpaullone crosses the BBB, and a precedent for clinical trials for mitochondrial modifying drugs for PD and other neurodegenerative conditions has already been well-established (section 1.9.2). Mitochondrial dysfunction is implicated in many neurodegenerative disease (PD, HD, AD, ALS, FTD) and is also involved in the pathogenesis of ageing, cancer, heart and liver disease, alongside specific mitochondrial disorders such as mitochondrial myopathy. This implies that compounds which restore mitochondrial quality control and function may have wider clinical applications.

6.4 Final summary and conclusions

In summary, this thesis has contributed to the knowledge that RBPs play a role in the pathology of polyQ disease. SAFB1 was found to be abnormally expressed in the degenerating neurons of patients with polyQ disorders. It was then confirmed that SAFB1 interacts differentially with physiological and pathologically expanded *ATXN1* RNA, offering a novel mechanistic insight into the RNA binding properties of SAFB1 in polyQ disease. This also implicates that RBP dysfunction may lead to neurodegenerative pathology. The second part of this thesis identified the kinase inhibitor kenpaullone as a novel modulator of mitochondrial health and function which increased mitochondrial area in human neuronal and glial cells. It is hypothesised that these effects may be attributable to its inhibition of GSK-3 beta and/or CDK5. It is hoped that this work can be further built upon to

explore kenpaullone and/or its related compounds as potentially neuroprotective in diseases including PD, and to further understand the emerging role of SAFB proteins in polyQ neuropathology.

References

Aboud, A. A. et al. (2015). PARK2 patient neuroprogenitors show increased mitochondrial sensitivity to copper. Neurobiol Dis **73**: 204-212.

Abou-Sleiman, P. M. et al. (2006). Expanding insights of mitochondrial dysfunction in Parkinson's disease. Nat Rev Neurosci **7**(3): 207-219.

Alavian, K. N. et al. (2012). Effects of dexpramipexole on brain mitochondrial conductances and cellular bioenergetic efficiency. Brain Res **1446**: 1-11.

Alexander, C. et al. (2000). OPA1, encoding a dynamin-related GTPase, is mutated in autosomal dominant optic atrophy linked to chromosome 3q28. Nat Genet **26**(2): 211-215.

Allahyani, M. (2020). Investigating the roles SAFB proteins play in controlling haemopoiesis and in acute lymphobastic leukaemia. Faculty of Health Sciences, Univeristy of Bristol. **Ph.D**.

Altmeyer, M. et al. (2013). The chromatin scaffold protein SAFB1 renders chromatin permissive for DNA damage signaling. Mol Cell **52**(2): 206-220.

Alzheimer's Research UK. Retrieved December 2019, from https://www.dementiastatistics.org/statistics-about-dementia/prevalence/.

Alzheimer's Society. Retrieved December 2019, from https://www.alzheimers.org.uk/about-us/policy-and-influencing/what-we-think/demography.

Aminzadeh, S. et al. (2015). Energy metabolism in neuroblastoma and Wilms tumor. Transl Pediatr **4**(1): 20-32.

Anderson, K. E. et al. (2018). Clinical Management of Neuropsychiatric Symptoms of Huntington Disease: Expert-Based Consensus Guidelines on Agitation, Anxiety, Apathy, Psychosis and Sleep Disorders. J Huntingtons Dis **7**(3): 355-366.

Andreassi, C. et al. (2018). Post-transcriptional Processing of mRNA in Neurons: The Vestiges of the RNA World Drive Transcriptome Diversity. Front Mol Neurosci **11**: 304.

Angelova, P. R. et al. (2018). Mitochondrial dysfunction in Parkinsonian mesenchymal stem cells impairs differentiation. Redox Biol **14**: 474-484.

Apicco, D. J. et al. (2018). Reducing the RNA binding protein TIA1 protects against tau-mediated neurodegeneration in vivo. Nat Neurosci **21**(1): 72-80.

Arai, T. et al. (2006). TDP-43 is a component of ubiquitin-positive tau-negative inclusions in frontotemporal lobar degeneration and amyotrophic lateral sclerosis. Biochem Biophys Res Commun **351**(3): 602-611.

Arai, T. et al. (2009). Phosphorylated TDP-43 in Alzheimer's disease and dementia with Lewy bodies. Acta Neuropathol **117**(2): 125-136.

Arao, Y. et al. (2000). A nuclear matrix-associated factor, SAF-B, interacts with specific isoforms of AUF1/hnRNP D. Arch Biochem Biophys **380**(2): 228-236.

Arrasate, M. and S. Finkbeiner (2012). Protein aggregates in Huntington's disease. Exp Neurol **238**(1): 1-11.

Ash, P. E. et al. (2013). Unconventional translation of C9ORF72 GGGGCC expansion generates insoluble polypeptides specific to c9FTD/ALS. Neuron **77**(4): 639-646.

Ashizawa, T. et al. (2018). Spinocerebellar ataxias: prospects and challenges for therapy development. Nat Rev Neurol **14**(10): 590-605.

Ashrafi, G. et al. (2014). Mitophagy of damaged mitochondria occurs locally in distal neuronal axons and requires PINK1 and Parkin. J Cell Biol **206**(5): 655-670.

Ataxia UK. Retrieved December 2019, from https://www.ataxia.org.uk/what-is-ataxia.

Athauda, D. and T. Foltynie (2015). The ongoing pursuit of neuroprotective therapies in Parkinson disease. Nat Rev Neurol **11**(1): 25-40.

Audano, M. et al. (2018). Mitochondria, lysosomes, and dysfunction: their meaning in neurodegeneration. J Neurochem **147**(3): 291-309.

Avraham, E. et al. (2007). Phosphorylation of Parkin by the cyclin-dependent kinase 5 at the linker region modulates its ubiquitin-ligase activity and aggregation. J Biol Chem **282**(17): 12842-12850.

Azevedo, F. A. et al. (2009). Equal numbers of neuronal and nonneuronal cells make the human brain an isometrically scaled-up primate brain. J Comp Neurol **513**(5): 532-541.

Babij, R. et al. (2013). Purkinje cell axonal anatomy: quantifying morphometric changes in essential tremor versus control brains. Brain **136**(Pt 10): 3051-3061.

Baines, C. P. and M. Gutierrez-Aguilar (2018). The still uncertain identity of the channel-forming unit(s) of the mitochondrial permeability transition pore. Cell Calcium **73**: 121-130.

Ballard, P. A. et al. (1985). Permanent human parkinsonism due to 1-methyl-4-phenyl-1,2,3,6-tetrahydropyridine (MPTP): seven cases. Neurology **35**(7): 949-956.

Baltz, A. G. et al. (2012). The mRNA-bound proteome and its global occupancy profile on protein-coding transcripts. Mol Cell **46**(5): 674-690.

Banez-Coronel, M. et al. (2015). RAN Translation in Huntington Disease. Neuron **88**(4): 667-677.

Banfi, S. et al. (1994). Identification and characterization of the gene causing type 1 spinocerebellar ataxia. Nat Genet **7**(4): 513-520.

Baradaran-Heravi, Y. et al. (2019). Stress granule mediated protein aggregation and underlying gene defects in the FTD-ALS spectrum. Neurobiol Dis **134**: 104639.

Barsoum, M. J. et al. (2006). Nitric oxide-induced mitochondrial fission is regulated by dynamin-related GTPases in neurons. Embo j **25**(16): 3900-3911.

Baxter, R. V. et al. (2002). Ganglioside-induced differentiation-associated protein-1 is mutant in Charcot-Marie-Tooth disease type 4A/8q21. Nat Genet **30**(1): 21-22.

Becker, L. A. et al. (2017). Therapeutic reduction of ataxin-2 extends lifespan and reduces pathology in TDP-43 mice. Nature **544**(7650): 367-371.

Beckmann, B. M. et al. (2015). The RNA-binding proteomes from yeast to man harbour conserved enigmRBPs. Nat Commun **6**: 10127.

Bender, A. et al. (2006). High levels of mitochondrial DNA deletions in substantia nigra neurons in aging and Parkinson disease. Nat Genet **38**(5): 515-517.

Bennett, J. et al. (2016). Safety and Tolerability of R(+) Pramipexole in Mild-to-Moderate Alzheimer's Disease. J Alzheimers Dis **49**(4): 1179-1187.

Benvegnu, S. (2019). Nucleus-cytoplasm cross-talk in the aging brain. J Neurosci Res.

Bernard-Marissal, N. et al. (2018). Endoplasmic reticulum and mitochondria in diseases of motor and sensory neurons: a broken relationship? Cell Death Dis **9**(3): 333.

Bertini, E. et al. (2017). Safety and efficacy of olesoxime in patients with type 2 or non-ambulatory type 3 spinal muscular atrophy: a randomised, double-blind, placebo-controlled phase 2 trial. Lancet Neurol **16**(7): 513-522.

Beurel, E. et al. (2015). Glycogen synthase kinase-3 (GSK3): regulation, actions, and diseases. Pharmacol Ther **148**: 114-131.

Bhat, R. et al. (2003). Structural insights and biological effects of glycogen synthase kinase 3-specific inhibitor AR-A014418. J Biol Chem **278**(46): 45937-45945.

Bijur, G. N. and R. S. Jope (2003). Glycogen synthase kinase-3 beta is highly activated in nuclei and mitochondria. Neuroreport **14**(18): 2415-2419.

Billingsley, K. J. et al. (2019). Mitochondria function associated genes contribute to Parkinson's Disease risk and later age at onset. NPJ Parkinsons Dis **5**: 8.

Binda F. et al. (2020). Cerebellar Development and Circuit Maturation: A Common Framework for Spinocerebellar Ataxias. Front. Neurosci **14**(293).

Bingol, B. et al. (2014). The mitochondrial deubiquitinase USP30 opposes parkin-mediated mitophagy. Nature **510**(7505): 370-375.

Birsa, N. et al. (2019). Cytoplasmic functions of TDP-43 and FUS and their role in ALS. Semin Cell Dev Biol.

Blair, J. A. et al. (2016). Individual Case Analysis of Postmortem Interval Time on Brain Tissue Preservation. PLoS One **11**(3): e0151615.

Blanco, F. J. and G. Montoya (2011). Transient DNA / RNA-protein interactions. Febs j **278**(10): 1643-1650.

Bordeaux, J. et al. (2010). Antibody validation. Biotechniques **48**(3): 197-209.

Bordet, T. et al. (2010). Olesoxime (TRO19622): A Novel Mitochondrial-Targeted Neuroprotective Compound. Pharmaceuticals (Basel) **3**(2): 345-368.

Boss, D. S. et al. (2010). Safety, tolerability, pharmacokinetics and pharmacodynamics of the oral cyclin-dependent kinase inhibitor AZD5438 when administered at intermittent and continuous dosing schedules in patients with advanced solid tumours. Ann Oncol **21**(4): 884-894.

Bozik, M. E. et al. (2014). A post hoc analysis of subgroup outcomes and creatinine in the phase III clinical trial (EMPOWER) of dexpramipexole in ALS. Amyotroph Lateral Scler Frontotemporal Degener **15**(5-6): 406-413.

Braga Neto, P. et al. (2016). Current concepts in the treatment of hereditary ataxias. Arq Neuropsiquiatr **74**(3): 244-252.

Brand, M. D. and D. G. Nicholls (2011). Assessing mitochondrial dysfunction in cells. Biochem J **435**(2): 297-312.

Bras, J. et al. (2015). SnapShot: Genetics of Parkinson's disease. Cell **160**(3): 570-570.e571.

Buijsen, R. A. M. et al. (2018). Generation of 3 spinocerebellar ataxia type 1 (SCA1) patient-derived induced pluripotent stem cell lines LUMCi002-A, B, and C and 2 unaffected sibling control induced pluripotent stem cell lines LUMCi003-A and B. Stem Cell Res **29**: 125-128.

Buijsen, R. A. M. et al. (2019). Genetics, Mechanisms and Therapeutic Progress in Polyglutamine Spinocerebellar Ataxias. Neurotherapeutics **16**(2): 263-286.

Buratti, E. (2015). Functional Significance of TDP-43 Mutations in Disease. Adv Genet **91**: 1-53.

Caga, J. et al. (2019). The Impact of Cognitive and Behavioral Symptoms on ALS Patients and Their Caregivers. Front Neurol **10**: 192.

Caggiu, E. et al. (2019). Inflammation, Infectious Triggers, and Parkinson's Disease. Front Neurol **10**: 122.

Cai, Q. et al. (2012). Spatial parkin translocation and degradation of damaged mitochondria via mitophagy in live cortical neurons. Curr Biol **22**(6): 545-552.

Carrascoso, I. et al. (2017). T-Cell Intracellular Antigens and Hu Antigen R Antagonistically Modulate Mitochondrial Activity and Dynamics by Regulating Optic Atrophy 1 Gene Expression. Mol Cell Biol **37**(17).

Castell, A. et al. (2018). A selective high affinity MYC-binding compound inhibits MYC:MAX interaction and MYC-dependent tumor cell proliferation. Sci Rep **8**(1): 10064.

Castello, A. et al. (2012). Insights into RNA biology from an atlas of mammalian mRNA-binding proteins. Cell **149**(6): 1393-1406.

Chan, C. W. et al. (2007). A novel member of the SAF (scaffold attachment factor)-box protein family inhibits gene expression and induces apoptosis. Biochem J **407**(3): 355-362.

Chan, W. M. et al. (2011). Expanded polyglutamine domain possesses nuclear export activity which modulates subcellular localization and toxicity of polyQ disease protein via exportin-1. Hum Mol Genet **20**(9): 1738-1750.

Chandrachud, U. et al. (2015). Unbiased Cell-based Screening in a Neuronal Cell Model of Batten Disease Highlights an Interaction between Ca2+ Homeostasis, Autophagy, and CLN3 Protein Function. J Biol Chem **290**(23): 14361-14380.

Charvin D. et al. (2018). Therapeutic Strategies for Parkinson disease: Beyond Dopaminergic Drugs. Nat Rev Drug Discovery **17**(11): 804-822

Chaudhry, A. et al. (2019). A pipeline for multidimensional confocal analysis of mitochondrial morphology, function and dynamics in pancreatic beta-cells. Am J Physiol Endocrinol Metab.

Chen, H. et al. (2007). Mitochondrial fusion protects against neurodegeneration in the cerebellum. Cell **130**(3): 548-562.

Chen, H. J. et al. (2019). RRM adjacent TARDBP mutations disrupt RNA binding and enhance TDP-43 proteinopathy. Brain **142**(12): 3753-3770.

Chen, L. and B. Liu (2017). Relationships between Stress Granules, Oxidative Stress, and Neurodegenerative Diseases. Oxid Med Cell Longev **2017**: 1809592.

Chen, Y. et al. (2016). PINK1 and Parkin are genetic modifiers for FUS-induced neurodegeneration. Hum Mol Genet **25**(23): 5059-5068.

Cheng, H. C. et al. (2010). Clinical progression in Parkinson disease and the neurobiology of axons. Ann Neurol **67**(6): 715-725.

Childs-Disney, J. L. et al. (2013). Induction and reversal of myotonic dystrophy type 1 pre-mRNA splicing defects by small molecules. Nat Commun **4**: 2044.

Chiu, C. C. et al. (2019). PARK14 (D331Y) PLA2G6 Causes Early-Onset Degeneration of Substantia Nigra Dopaminergic Neurons by Inducing Mitochondrial Dysfunction, ER Stress, Mitophagy Impairment and Transcriptional Dysregulation in a Knockin Mouse Model. Mol Neurobiol **56**(6): 3835-3853.

Choi, J. S. et al. (2007). Cyclin-dependent protein kinase 2 activity is required for mitochondrial translocation of Bax and disruption of mitochondrial transmembrane potential during etoposide-induced apoptosis. Apoptosis **12**(7): 1229-1241.

Chu, C. T. (2018). Multiple pathways for mitophagy: A neurodegenerative conundrum for Parkinson's disease. Neurosci Lett.

Chuang, Y. C. et al. (2019). Sirtuin 1 Regulates Mitochondrial Biogenesis and Provides an Endogenous Neuroprotective Mechanism Against Seizure-Induced Neuronal Cell Death in the Hippocampus Following Status Epilepticus. Int J Mol Sci **20**(14).

Ciesiolka, A. et al. (2017). Structural Characteristics of Simple RNA Repeats Associated with Disease and their Deleterious Protein Interactions. Front Cell Neurosci **11**: 97.

Clery A. and Allain F. H.-T. (2011). From structure to function of RNA binding proteins. Austin (TX), Landes Bioscience.

Colley, S. M. et al. (2002). MET, a novel stimulator of estrogen-induced transcription isolated from mouse bone marrow.

Conlon, E. G. and J. L. Manley (2017). RNA-binding proteins in neurodegeneration: mechanisms in aggregate. Genes Dev **31**(15): 1509-1528.

Cookson, M. R. (2017). RNA-binding proteins implicated in neurodegenerative diseases. Wiley Interdiscip Rev RNA **8**(1).

Coonrod, L. A. et al. (2013). Reducing levels of toxic RNA with small molecules. ACS Chem Biol **8**(11): 2528-2537.

Cooper-Knock, J. et al. (2015). Antisense RNA foci in the motor neurons of C9ORF72-ALS patients are associated with TDP-43 proteinopathy. Acta Neuropathol **130**(1): 63-75.

Cornelissen, T. et al. (2018). Deficiency of parkin and PINK1 impairs age-dependent mitophagy in Drosophila. Elife **7**.

Cortes, N. et al. (2019). CDK5: A Unique CDK and Its Multiple Roles in the Nervous System. J Alzheimers Dis **68**(3): 843-855.

Corti, O. (2019). Neuronal Mitophagy: Lessons from a Pathway Linked to Parkinson's Disease. Neurotox Res **36**(2): 292-305.

Coudert, L. et al. (2019). Phosphorylated and aggregated TDP-43 with seeding properties are induced upon mutant Huntingtin (mHtt) polyglutamine expression in human cellular models. Cell Mol Life Sci **76**(13): 2615-2632.

Couthouis, J. et al. (2012). Evaluating the role of the FUS/TLS-related gene EWSR1 in amyotrophic lateral sclerosis. Hum Mol Genet **21**(13): 2899-2911.

Cribbs, J. T. and S. Strack (2009). Functional characterization of phosphorylation sites in dynamin-related protein 1. Methods Enzymol **457**: 231-253.

Crippa, V. et al. (2016). The chaperone HSPB8 reduces the accumulation of truncated TDP-43 species in cells and protects against TDP-43-mediated toxicity. Hum Mol Genet **25**(18): 3908-3924.

Cummings, J. (2017). Disease modification and Neuroprotection in neurodegenerative disorders. Transl Neurodegener **6**: 25.

Dagda, R. K. et al. (2009). Loss of PINK1 function promotes mitophagy through effects on oxidative stress and mitochondrial fission. J Biol Chem **284**(20): 13843-13855.

Daubner, G. M. et al. (2013). RRM-RNA recognition: NMR or crystallography...and new findings. Curr Opin Struct Biol **23**(1): 100-108.

Dauer, W. and S. Przedborski (2003). Parkinson's disease: mechanisms and models. Neuron **39**(6): 889-909.

Dave, K. D. et al. (2014). Phenotypic characterization of recessive gene knockout rat models of Parkinson's disease. Neurobiol Dis **70**: 190-203.

Davidson, Y. S. et al. (2017). Heterogeneous ribonuclear protein A3 (hnRNP A3) is present in dipeptide repeat protein containing inclusions in Frontotemporal Lobar Degeneration and Motor Neurone disease associated with expansions in C9orf72 gene. Acta Neuropathol Commun **5**(1): 31.

Davis, S. A. et al. (2018). TDP-43 interacts with mitochondrial proteins critical for mitophagy and mitochondrial dynamics. Neurosci Lett **678**: 8-15.

De Conti, L. et al. (2017). Neurodegeneration and RNA-binding proteins. Wiley Interdiscip Rev RNA **8**(2).

de Mezer, M. et al. (2011). Mutant CAG repeats of Huntingtin transcript fold into hairpins, form nuclear foci and are targets for RNA interference. Nucleic Acids Res **39**(9): 3852-3863.

DeJesus-Hernandez, M. et al. (2011). Expanded GGGGCC hexanucleotide repeat in noncoding region of C9ORF72 causes chromosome 9p-linked FTD and ALS. Neuron **72**(2): 245-256.

den Dunnen, W. F. (2013). Neuropathological diagnostic considerations in hyperkinetic movement disorders. Front Neurol **4**: 7.

Denegri, M. et al. (2002). Human chromosomes 9, 12, and 15 contain the nucleation sites of stress-induced nuclear bodies. Mol Biol Cell **13**(6): 2069-2079.

Deng, J. et al. (2018). FUS interacts with ATP synthase beta subunit and induces mitochondrial unfolded protein response in cellular and animal models. Proc Natl Acad Sci U S A **115**(41): E9678-e9686.

Denison, S. R. et al. (2003). Alterations in the common fragile site gene Parkin in ovarian and other cancers. Oncogene **22**(51): 8370-8378.

Deshaies, J. E. et al. (2018). TDP-43 regulates the alternative splicing of hnRNP A1 to yield an aggregation-prone variant in amyotrophic lateral sclerosis. Brain **141**(5): 1320-1333.

Devi, L. et al. (2008). Mitochondrial import and accumulation of alpha-synuclein impair complex I in human dopaminergic neuronal cultures and Parkinson disease brain. J Biol Chem **283**(14): 9089-9100.

Dickey, A. S. and A. R. La Spada (2018). Therapy development in Huntington disease: From current strategies to emerging opportunities. Am J Med Genet A **176**(4): 842-861.

Dickson D. W. et al. (2009). Neuropathology of Non-Motor Features of Parkinson Disease. Parkinsonism Relat Disord **15**(Suppl 3):S1-5

Dickson, D. W. (2012). Parkinson's disease and parkinsonism: neuropathology. Cold Spring Harb Perspect Med **2**(8).

Diedrich, M. et al. (2011). Brain region specific mitophagy capacity could contribute to selective neuronal vulnerability in Parkinson's disease. Proteome Sci **9**: 59.

Diot, A. et al. (2015). A novel quantitative assay of mitophagy: Combining high content fluorescence microscopy and mitochondrial DNA load to quantify mitophagy and identify novel pharmacological tools against pathogenic heteroplasmic mtDNA. Pharmacol Res **100**: 24-35.

Doi, H. et al. (2008). RNA-binding protein TLS is a major nuclear aggregate-interacting protein in huntingtin exon 1 with expanded polyglutamine-expressing cells. J Biol Chem **283**(10): 6489-6500.

Dolle, C. et al. (2016). Defective mitochondrial DNA homeostasis in the substantia nigra in Parkinson disease. Nat Commun **7**: 13548.

Dominguez, D. et al. (2018). Sequence, Structure, and Context Preferences of Human RNA Binding Proteins. Mol Cell **70**(5): 854-867.e859.

Dormann, D. and C. Haass (2011). TDP-43 and FUS: a nuclear affair. Trends Neurosci **34**(7): 339-348.

Dormann, D. et al. (2010). ALS-associated fused in sarcoma (FUS) mutations disrupt Transportin-mediated nuclear import. Embo j **29**(16): 2841-2857.

Drakouli, S. et al. (2017). Enhancer of rudimentary homologue interacts with scaffold attachment factor B at the nuclear matrix to regulate SR protein phosphorylation. Febs j **284**(15): 2482-2500.

Dziewulska, D. and J. Rafalowska (2005). Proteinaceous intracellular inclusions in neurodegenerative disorders. Folia Neuropathol **43**(2): 51-63.

Ederle, H. and D. Dormann (2017). TDP-43 and FUS en route from the nucleus to the cytoplasm. FEBS Lett **591**(11): 1489-1507.

Eiyama, A. and K. Okamoto (2015). PINK1/Parkin-mediated mitophagy in mammalian cells. Curr Opin Cell Biol **33**: 95-101.

Elden, A. C. et al. (2010). Ataxin-2 intermediate-length polyglutamine expansions are associated with increased risk for ALS. Nature **466**(7310): 1069-1075.

Emamzadeh, F. N. and A. Surguchov (2018). Parkinson's Disease: Biomarkers, Treatment, and Risk Factors. Front Neurosci **12**: 612.

Erickson-Davis, C. R. et al. (2010). "Hairy baskets" associated with degenerative Purkinje cell changes in essential tremor. J Neuropathol Exp Neurol **69**(3): 262-271.

Fahrenkrog, B. and A. Harel (2018). Perturbations in Traffic: Aberrant Nucleocytoplasmic Transport at the Heart of Neurodegeneration. Cells **7**(12).

Farley M. M. and T. A. Watkins (2018). Intrinsic Neuronal Stress Response Pathways in Injury and Disease. Annu Rev Pathol (**24**)13: 93-116.

Fecher, C. et al. (2019). Cell-type-specific profiling of brain mitochondria reveals functional and molecular diversity. Nat Neurosci **22**(10): 1731-1742.

Ferrer, I. (2015). Selection of controls in the study of human neurodegenerative diseases in old age. J Neural Transm (Vienna) **122**(7): 941-947.

Fiesel, F. C. et al. (2015). (Patho-)physiological relevance of PINK1-dependent ubiquitin phosphorylation. EMBO Rep **16**(9): 1114-1130.

Filosto, M. et al. (2011). The role of mitochondria in neurodegenerative diseases. J Neurol **258**(10): 1763-1774.

Fischer, F. et al. (2012). Mitochondrial quality control: an integrated network of pathways. Trends Biochem Sci **37**(7): 284-292.

Fryer, J. D. et al. (2011). Exercise and genetic rescue of SCA1 via the transcriptional repressor Capicua. Science **334**(6056): 690-693.

Gao, F. et al. (2017). Mitophagy in Parkinson's Disease: Pathogenic and Therapeutic Implications. Front Neurol **8**: 527.

Gao, J. et al. (2018). Pathomechanisms of TDP-43 in neurodegeneration. J Neurochem.

Gasset-Rosa, F. et al. (2017). Polyglutamine-Expanded Huntingtin Exacerbates Age-Related Disruption of Nuclear Integrity and Nucleocytoplasmic Transport. Neuron **94**(1): 48-57.e44.

Gegg, M. E. and A. H. Schapira (2016). Mitochondrial dysfunction associated with glucocerebrosidase deficiency. Neurobiol Dis **90**: 43-50.

Gerfen C. R. (2004). Basal Ganglia in the Rat Nervous System, Third Edition, G. Paxios, ed. (Academic Press), 455-508.

Ghosh R. and Tabrizi S. (2018). Polyglutamine Disorders, Springer.

Gibson-Corley, K. N. et al. (2013). Principles for valid histopathologic scoring in research. Vet Pathol **50**(6): 1007-1015.

Giguere, N. et al. (2018). Comparative analysis of Parkinson's disease-associated genes in mice reveals altered survival and bioenergetics of Parkin-deficient dopamine neurons. J Biol Chem **293**(25): 9580-9593.

Gispert, S. et al. (2009). Parkinson phenotype in aged PINK1-deficient mice is accompanied by progressive mitochondrial dysfunction in absence of neurodegeneration. PLoS One **4**(6): e5777.

Gladkova, C. et al. (2018). Mechanism of parkin activation by PINK1. Nature **559**(7714): 410-414.

Goldberg, M. S. et al. (2003). Parkin-deficient mice exhibit nigrostriatal deficits but not loss of dopaminergic neurons. J Biol Chem **278**(44): 43628-43635.

Golebiowski, F. et al. (2009). System-wide changes to SUMO modifications in response to heat shock. Sci Signal **2**(72): ra24.

Golpich, M. et al. (2015). Glycogen synthase kinase-3 beta (GSK-3beta) signaling: Implications for Parkinson's disease. Pharmacol Res **97**: 16-26.

Gomes, L. C. et al. (2011). During autophagy mitochondria elongate, are spared from degradation and sustain cell viability. Nat Cell Biol **13**(5): 589-598.

Gomez-Pastor, R. et al. (2017). Abnormal degradation of the neuronal stress-protective transcription factor HSF1 in Huntington's disease. Nat Commun **8**: 14405.

Gomez-Suaga, P. et al. (2017). The ER-Mitochondria Tethering Complex VAPB-PTPIP51 Regulates Autophagy. Curr Biol **27**(3): 371-385.

Gopalakrishna, S. et al. (2019). C6orf203 is an RNA-binding protein involved in mitochondrial protein synthesis. Nucleic Acids Res **47**(17): 9386-9399.

Gray, M. A. et al. (2013). Prefrontal activity in Huntington's disease reflects cognitive and neuropsychiatric disturbances: the IMAGE-HD study. Exp Neurol **239**: 218-228.

Grunewald, A. et al. (2016). Mitochondrial DNA Depletion in Respiratory Chain-Deficient Parkinson Disease Neurons. Ann Neurol **79**(3): 366-378.

Gupta, K. K. and S. K. Singh (2019). Cdk5: A main culprit in neurodegeneration. Int J Neurosci **129**(12): 1192-1197.

Gusella, J. F. and M. E. MacDonald (2000). Molecular genetics: unmasking polyglutamine triggers in neurodegenerative disease. Nat Rev Neurosci **1**(2): 109-115.

Gustafsson, A. B. and G. W. Dorn, 2nd (2019). Evolving and Expanding the Roles of Mitophagy as a Homeostatic and Pathogenic Process. Physiol Rev **99**(1): 853-892.

Hammerich-Hille, S. et al. (2010). SAFB1 mediates repression of immune regulators and apoptotic genes in breast cancer cells. J Biol Chem **285**(6): 3608-3616.

Han, S. P. et al. (2010). Functional diversity of the hnRNPs: past, present and perspectives. Biochem J **430**(3): 379-392.

Harris, J. J. et al. (2012). Synaptic energy use and supply. Neuron **75**(5): 762-777.

Hashimoto, T. et al. (2020). Scaffold attachment factor B: distribution and interaction with ERalpha in the rat brain. Histochem Cell Biol.

Hasson, S. A. et al. (2013). High-content genome-wide RNAi screens identify regulators of parkin upstream of mitophagy. Nature **504**(7479): 291-295.

Hattingen, E. et al. (2009). Phosphorus and proton magnetic resonance spectroscopy demonstrates mitochondrial dysfunction in early and advanced Parkinson's disease. Brain **132**(Pt 12): 3285-3297.

Hautbergue, G. M. et al. (2017). SRSF1-dependent nuclear export inhibition of C9ORF72 repeat transcripts prevents neurodegeneration and associated motor deficits. Nat Commun **8**: 16063.

Hayashi, T. et al. (2009). DJ-1 binds to mitochondrial complex I and maintains its activity. Biochem Biophys Res Commun **390**(3): 667-672.

Hazlitt, R. A. et al. (2018). Development of Second-Generation CDK2 Inhibitors for the Prevention of Cisplatin-Induced Hearing Loss. J Med Chem **61**(17): 7700-7709.

Head, B. et al. (2009). Inducible proteolytic inactivation of OPA1 mediated by the OMA1 protease in mammalian cells. J Cell Biol **187**(7): 959-966.

Hegele, A. et al. (2012). Dynamic protein-protein interaction wiring of the human spliceosome. Mol Cell **45**(4): 567-580.

Hentze, M. W. et al. (2018). A brave new world of RNA-binding proteins. Nat Rev Mol Cell Biol **19**(5): 327-341.

Heo, J. Y. et al. (2012). DJ-1 null dopaminergic neuronal cells exhibit defects in mitochondrial function and structure: involvement of mitochondrial complex I assembly. PLoS One **7**(3): e32629.

Herndon, E. S. et al. (2009). Neuroanatomic profile of polyglutamine immunoreactivity in Huntington disease brains. J Neuropathol Exp Neurol **68**(3): 250-261.

Herrera, A. et al. (2017). Are Dopamine Oxidation Metabolites Involved in the Loss of Dopaminergic Neurons in the Nigrostriatal System in Parkinson's Disease? ACS Chem Neurosci **8**(4): 702-711.

Ho, D. H. et al. (2019). G2019s LRRK2 promotes mitochondrial fission and increases TNFalpha-mediated neuroinflammation responses. Anim Cells Syst (Seoul) **23**(2): 106-111.

Holmans, P. A. et al. (2017). Genetic modifiers of Mendelian disease: Huntington's disease and the trinucleotide repeat disorders. Hum Mol Genet **26**(R2): R83-r90.

Holmes S. E. Et al. (1999). Expansion of a Novel CAG Trinucleotide Repeat in the 5' Region of PPP2R2B Is Associated With SCA12. Nat. Genet **23**(4): 391-2

Hong, E. A. et al. (2012). SAFB1- and SAFB2-mediated transcriptional repression: relevance to cancer. Biochem Soc Trans **40**(4): 826-830.

Hong, E. et al. (2015). Unravelling the RNA-Binding Properties of SAFB Proteins in Breast Cancer Cells. Biomed Res Int **2015**: 395816.

Hou, X. et al. (2018). Age- and disease-dependent increase of the mitophagy marker phospho-ubiquitin in normal aging and Lewy body disease. Autophagy.

Hou, Y. et al. (2019). Ageing as a risk factor for neurodegenerative disease. Nat Rev Neurol **15**(10): 565-581.

Houlden, H. et al. (2007). Mutations in TTBK2, encoding a kinase implicated in tau phosphorylation, segregate with spinocerebellar ataxia type 11. Nat Genet **39**(12): 1434-1436.

Hsieh, C. H. et al. (2016). Functional Impairment in Miro Degradation and Mitophagy Is a Shared Feature in Familial and Sporadic Parkinson's Disease. Cell Stem Cell **19**(6): 709-724.

Hudson, W. H. and E. A. Ortlund (2014). The structure, function and evolution of proteins that bind DNA and RNA. Nat Rev Mol Cell Biol **15**(11): 749-760.

Huntington's Disease Association. Retrieved January 2020, from www.hda.org.uk.

Huo, X. et al. (2019). The Nuclear Matrix Protein SAFB Cooperates with Major Satellite RNAs to Stabilize Heterochromatin Architecture Partially through Phase Separation. Mol Cell.

Hutten, S. and D. Dormann (2019). Nucleocytoplasmic transport defects in neurodegeneration - Cause or consequence? Semin Cell Dev Biol.

Ihara, R. et al. (2013). RNA binding mediates neurotoxicity in the transgenic Drosophila model of TDP-43 proteinopathy. Hum Mol Genet **22**(22): 4474-4484.

Imbert, G. et al. (1996). Cloning of the gene for spinocerebellar ataxia 2 reveals a locus with high sensitivity to expanded CAG/glutamine repeats. Nat Genet **14**(3): 285-291.

Irrcher, I. et al. (2010). Loss of the Parkinson's disease-linked gene DJ-1 perturbs mitochondrial dynamics. Hum Mol Genet **19**(19): 3734-3746.

Irwin, S. et al. (2005). RNA association and nucleocytoplasmic shuttling by ataxin-1. J Cell Sci **118**(Pt 1): 233-242.

Ishii S. et al. (2019). Identification of a factor controlling lysosomal homeostasis using a novel lysosomal trafficking probe. Sci Rep **9**(11): 11635

Ito, H. et al. (2015). HMGB1 facilitates repair of mitochondrial DNA damage and extends the lifespan of mutant ataxin-1 knock-in mice. EMBO Mol Med **7**(1): 78-101.

Ivanova, M. et al. (2005). Scaffold attachment factor B1 functions in development, growth, and reproduction. Mol Cell Biol **25**(8): 2995-3006.

Izumikawa, K. et al. (2017). TDP-43 stabilises the processing intermediates of mitochondrial transcripts. Sci Rep **7**(1): 7709.

Jansen, I. E. et al. (2019). Genome-wide meta-analysis identifies new loci and functional pathways influencing Alzheimer's disease risk. Nat Genet **51**(3): 404-413.

Jiang, S. et al. (2015). Scaffold attachment factor B2 (SAFB2)-null mice reveal non-redundant functions of SAFB2 compared with its paralog, SAFB1. Dis Model Mech **8**(9): 1121-1127.

Jin, S. M. et al. (2010). Mitochondrial membrane potential regulates PINK1 import and proteolytic destabilization by PARL. J Cell Biol **191**(5): 933-942.

Johnson, J. O. et al. (2014). Mutations in the Matrin 3 gene cause familial amyotrophic lateral sclerosis. Nat Neurosci **17**(5): 664-666.

Jolly, C. et al. (2004). Stress-induced transcription of satellite III repeats. J Cell Biol **164**(1): 25-33.

Joo, H. C. et al. (2018). Protective effects of kenpaullone on cardiomyocytes following H2O2-induced oxidative stress are attributed to inhibition of connexin 43 degradation by SGSM3. Biochem Biophys Res Commun **499**(2): 368-373.

Joselin, A. P. et al. (2012). ROS-dependent regulation of Parkin and DJ-1 localization during oxidative stress in neurons. Hum Mol Genet **21**(22): 4888-4903.

Jourdain, A. and J. C. Martinou (2010). Mitochondrial dynamics: quantifying mitochondrial fusion in vitro. BMC Biol **8**: 99.

Kabashi, E. et al. (2008). TARDBP mutations in individuals with sporadic and familial amyotrophic lateral sclerosis. Nat Genet **40**(5): 572-574.

Kabeya, Y. et al. (2000). LC3, a mammalian homologue of yeast Apg8p, is localized in autophagosome membranes after processing. Embo j **19**(21): 5720-5728.

Kalani, K. et al. (2018). Mitochondrial permeability transition pore: a potential drug target for neurodegeneration. Drug Discov Today **23**(12): 1983-1989.

Kandel E. R. et al. (2013) Principles of Neural Science, Fifth Edition. McGraw-Hill Companies. Part VI:43.

Kane, L. A. et al. (2014). PINK1 phosphorylates ubiquitin to activate Parkin E3 ubiquitin ligase activity. J Cell Biol **205**(2): 143-153.

Karbowski, M. et al. (2004). Endophilin B1 is required for the maintenance of mitochondrial morphology. J Cell Biol **166**(7): 1027-1039.

Keeney, P. M. et al. (2006). Parkinson's disease brain mitochondrial complex I has oxidatively damaged subunits and is functionally impaired and misassembled. J Neurosci **26**(19): 5256-5264.

Kemp, K. C. et al. (2016). Purkinje cell injury, structural plasticity and fusion in patients with Friedreich's ataxia. Acta Neuropathol Commun **4**(1): 53.

Kharel, P. et al. (2020). The role of RNA G-quadruplexes in human diseases and therapeutic strategies. Wiley Interdiscip Rev RNA **11**(1): e1568.

Kiledjian, M. and G. Dreyfuss (1992). Primary structure and binding activity of the hnRNP U protein: binding RNA through RGG box. Embo j **11**(7): 2655-2664.

Kim, Y. Y. et al. (2019). Assessment of mitophagy in mt-Keima Drosophila revealed an essential role of the PINK1-Parkin pathway in mitophagy induction in vivo. Faseb j **33**(9): 9742-9751.

Kino, Y. et al. (2016). FUS/TLS acts as an aggregation-dependent modifier of polyglutamine disease model mice. Sci Rep **6**: 35236.

Kipp, M. et al. (2000). SAF-Box, a conserved protein domain that specifically recognizes scaffold attachment region DNA. Mol Cell Biol **20**(20): 7480-7489.

Kitabayashi, T. et al. (2019). Identification of GSK3beta inhibitor kenpaullone as a temozolomide enhancer against glioblastoma. Sci Rep **9**(1): 10049.

Kitada, T. et al. (1998). Mutations in the parkin gene cause autosomal recessive juvenile parkinsonism. Nature **392**(6676): 605-608.

Klement, I. A. et al. (1998). Ataxin-1 nuclear localization and aggregation: role in polyglutamine-induced disease in SCA1 transgenic mice. Cell **95**(1): 41-53.

Koc, E. C. and L. L. Spremulli (2003). RNA-binding proteins of mammalian mitochondria. Mitochondrion **2**(4): 277-291.

Koeppen, A. H. (2005). The pathogenesis of spinocerebellar ataxia. Cerebellum **4**(1): 62-73.

Koeppen, A. H. (2018). The neuropathology of the adult cerebellum. Handb Clin Neurol **154**: 129-149.

Koeppen, A. H. et al. (2013). The reciprocal cerebellar circuitry in human hereditary ataxia. Cerebellum **12**(4): 493-503.

Konig, J. et al. (2011). iCLIP--transcriptome-wide mapping of protein-RNA interactions with individual nucleotide resolution. J Vis Exp(50).

Konovalova, E. V. et al. (2015). Mutations in the Parkinson's Disease-Associated PARK2 Gene Are Accompanied by Imbalance in Programmed Cell Death Systems. Acta Naturae **7**(4): 146-149.

Kovalevich, J. and D. Langford (2013). Considerations for the use of SH-SY5Y neuroblastoma cells in neurobiology. Methods Mol Biol **1078**: 9-21.

Koyano, F. et al. (2019). Parkin recruitment to impaired mitochondria for nonselective ubiquitylation is facilitated by MITOL. J Biol Chem **294**(26): 10300-10314.

Koyano, S. et al. (2002). Paradoxical absence of nuclear inclusion in cerebellar Purkinje cells of hereditary ataxias linked to CAG expansion. J Neurol Neurosurg Psychiatry **73**(4): 450-452.

Kraemer, B. C. et al. (2010). Loss of murine TDP-43 disrupts motor function and plays an essential role in embryogenesis. Acta Neuropathol **119**(4): 409-419.

Kraus-Perrotta, C. and S. Lagalwar (2016). Expansion, mosaicism and interruption: mechanisms of the CAG repeat mutation in spinocerebellar ataxia type 1. Cerebellum Ataxias **3**: 20.

Krauss, S. et al. (2013). Translation of HTT mRNA with expanded CAG repeats is regulated by the MID1-PP2A protein complex. Nat Commun **4**: 1511.

Krol, H. A. et al. (2008). Polyglutamine expansion accelerates the dynamics of ataxin-1 and does not result in aggregate formation. PLoS One **3**(1): e1503.

Kumar, S. et al. (2019). Lifespan Extension in C. elegans Caused by Bacterial Colonization of the Intestine and Subsequent Activation of an Innate Immune Response. Dev Cell **49**(1): 100-117.e106.

Kunick, C. et al. (2004). 1-Azakenpaullone is a selective inhibitor of glycogen synthase kinase-3 beta. Bioorg Med Chem Lett **14**(2): 413-416.

Kwiatkowski, T. J., Jr. et al. (2009). Mutations in the FUS/TLS gene on chromosome 16 cause familial amyotrophic lateral sclerosis. Science **323**(5918): 1205-1208.

Labbadia, J. and R. I. Morimoto (2013). Huntington's disease: underlying molecular mechanisms and emerging concepts. Trends Biochem Sci **38**(8): 378-385.

Labbe, K. et al. (2014). Determinants and functions of mitochondrial behavior. Annu Rev Cell Dev Biol **30**: 357-391.

Lam, Y. C. et al. (2006). ATAXIN-1 interacts with the repressor Capicua in its native complex to cause SCA1 neuropathology. Cell **127**(7): 1335-1347.

Lange, C. et al. (2011). Small molecule GSK-3 inhibitors increase neurogenesis of human neural progenitor cells. Neurosci Lett **488**(1): 36-40.

Lapointe, C. P. et al. (2015). Protein-RNA networks revealed through covalent RNA marks. Nat Methods **12**(12): 1163-1170.

Lau, D. H. W. et al. (2018). Disruption of ER-mitochondria signalling in fronto-temporal dementia and related amyotrophic lateral sclerosis. Cell Death Dis **9**(3): 327.

Law, M. J. et al. (2006). The role of RNA structure in the interaction of U1A protein with U1 hairpin II RNA. Rna **12**(7): 1168-1178.

Lee J. M. et al. (2019). CAG Repeat Not Polyglutamine Length Determines Timing of Huntington's Disease Onset. Cell **178**(4): 887-900.e814.

Lee, H. W. et al. (2017). High content screening assay based discovery of paullones as novel podocyte protective agents. Am J Physiol Renal Physiol: ajprenal.00338.02017.

Lee, J. (2016). Mitochondrial drug targets in neurodegenerative diseases. Bioorg Med Chem Lett **26**(3): 714-720.

Lee, J.-M. et al. (2015). Identification of Genetic Factors that Modify Clinical Onset of Huntington's Disease. Cell **162**(3): 516-526.

Lee, J.-M. et al. (2019). CAG Repeat Not Polyglutamine Length Determines Timing of Huntington's Disease Onset. Cell **178**(4): 887-900.e814.

Lee, K. Y. et al. (2007). Glycogen synthase kinase-3beta activity plays very important roles in determining the fate of oxidative stress-inflicted neuronal cells. Brain Res **1129**(1): 89-99.

Lee, S. B. et al. (2019a). Neuroprotective effect of anodal transcranial direct current stimulation on 1-methyl-4-phenyl-1,2,3,6-tetrahydropyridine (MPTP)-induced neurotoxicity in mice through modulating mitochondrial dynamics. Neurochem Int **129**: 104491.

Lee, Y. B. et al. (2007). SAFB re-distribution marks steps of the apoptotic process. Exp Cell Res **313**(18): 3914-3923.

Lefebvre, V. et al. (2013). Genome-wide RNAi screen identifies ATPase inhibitory factor 1 (ATPIF1) as essential for PARK2 recruitment and mitophagy. Autophagy **9**(11): 1770-1779.

Leidal, A. M. et al. (2020). The LC3-conjugation machinery specifies the loading of RNA-binding proteins into extracellular vesicles. Nat Cell Biol.

Lemasters, J. J. (2014). Variants of mitochondrial autophagy: Types 1 and 2 mitophagy and micromitophagy (Type 3). Redox Biol **2**: 749-754.

Lenglet, T. et al. (2014). A phase II-III trial of olesoxime in subjects with amyotrophic lateral sclerosis. Eur J Neurol **21**(3): 529-536.

Leonard, A. P. et al. (2015). Quantitative analysis of mitochondrial morphology and membrane potential in living cells using high-content imaging, machine learning, and morphological binning. Biochim Biophys Acta **1853**(2): 348-360.

Leost, M. et al. (2000). Paullones are potent inhibitors of glycogen synthase kinase-3beta and cyclin-dependent kinase 5/p25. Eur J Biochem **267**(19): 5983-5994.

Li, L. B. et al. (2008). RNA toxicity is a component of ataxin-3 degeneration in Drosophila. Nature **453**(7198): 1107-1111.

Li, Q. et al. (2014). Rapamycin attenuates mitochondrial dysfunction via activation of mitophagy in experimental ischemic stroke. Biochem Biophys Res Commun **444**(2): 182-188.

Li, Y. et al. (2011). p32 regulates mitochondrial morphology and dynamics through parkin. Neuroscience **199**: 346-358.

Li, Y. R. et al. (2013). Stress granules as crucibles of ALS pathogenesis. J Cell Biol **201**(3): 361-372.

Licatalosi, D. D. and R. B. Darnell (2010). RNA processing and its regulation: global insights into biological networks. Nat Rev Genet **11**(1): 75-87.

Lieberman, A. P. et al. (2019). Polyglutamine Repeats in Neurodegenerative Diseases. Annu Rev Pathol **14**: 1-27.

Lim, J. et al. (2008). Opposing effects of polyglutamine expansion on native protein complexes contribute to SCA1. Nature **452**(7188): 713-718.

Lin, M. Y. et al. (2017). Releasing Syntaphilin Removes Stressed Mitochondria from Axons Independent of Mitophagy under Pathophysiological Conditions. Neuron **94**(3): 595-610.e596.

Lindholm, C. K. et al. (2000). Shf, a Shb-like adapter protein, is involved in PDGF-alpha-receptor regulation of apoptosis. Biochem Biophys Res Commun **278**(3): 537-543.

Liu, M. L. et al. (2016). Direct Lineage Reprogramming Reveals Disease-Specific Phenotypes of Motor Neurons from Human ALS Patients. Cell Rep **14**(1): 115-128.

Louis, E. D. et al. (2014). Torpedo formation and Purkinje cell loss: modeling their relationship in cerebellar disease. Cerebellum **13**(4): 433-439.

Luca, A. et al. (2018). Molecular Bases of Alzheimer's Disease and Neurodegeneration: The Role of Neuroglia. Aging Dis **9**(6): 1134-1152.

Ludtmann, M. H. R. et al. (2018). alpha-synuclein oligomers interact with ATP synthase and open the permeability transition pore in Parkinson's disease. Nat Commun **9**(1): 2293.

Lunde, B. M. et al. (2007). RNA-binding proteins: modular design for efficient function. Nat Rev Mol Cell Biol **8**(6): 479-490.

Lutz, A. K. et al. (2009). Loss of parkin or PINK1 function increases Drp1-dependent mitochondrial fragmentation. J Biol Chem **284**(34): 22938-22951.

MacAskill, A. F. et al. (2010). Mitochondrial trafficking and the provision of energy and calcium buffering at excitatory synapses. Eur J Neurosci **32**(2): 231-240.

MacDonald, M. E. et al. (1993). A novel gene containing a trinucleotide repeat that is expanded and unstable on Huntington's disease chromosomes. Cell **72**(6): 971-983.

Mackenzie, I. R. et al. (2010). TDP-43 and FUS in amyotrophic lateral sclerosis and frontotemporal dementia. Lancet Neurol **9**(10): 995-1007.

Mackenzie, I. R. et al. (2017). TIA1 Mutations in Amyotrophic Lateral Sclerosis and Frontotemporal Dementia Promote Phase Separation and Alter Stress Granule Dynamics. Neuron **95**(4): 808-816.e809.

Malik, A. M. et al. (2018). Matrin 3-dependent neurotoxicity is modified by nucleic acid binding and nucleocytoplasmic localization. Elife **7**.

Mandal, A. and C. M. Drerup (2019). Axonal Transport and Mitochondrial Function in Neurons. Front Cell Neurosci **13**: 373.

Maris, C. et al. (2005). The RNA recognition motif, a plastic RNA-binding platform to regulate post-transcriptional gene expression. Febs j **272**(9): 2118-2131.

Marti, E. (2016). RNA toxicity induced by expanded CAG repeats in Huntington's disease. Brain Pathol **26**(6): 779-786.

Martinez-Martin, P. et al. (2007). Prevalence of nonmotor symptoms in Parkinson's disease in an international setting; study using nonmotor symptoms questionnaire in 545 patients. Mov Disord **22**(11): 1623-1629.

Martinez-Vicente, M. (2017). Neuronal Mitophagy in Neurodegenerative Diseases. Front Mol Neurosci **10**.

Matsuda, K. I. et al. (2018). Intranuclear Mobility of Estrogen Receptor: Implication for Transcriptional Regulation. Acta Histochem Cytochem **51**(4): 129-136.

Matsuyama, Z. et al. (1999). The effect of CAT trinucleotide interruptions on the age at onset of spinocerebellar ataxia type 1 (SCA1). J Med Genet **36**(7): 546-548.

Mattis, V. B. et al. (2015). HD iPSC-derived neural progenitors accumulate in culture and are susceptible to BDNF withdrawal due to glutamate toxicity. Hum Mol Genet **24**(11): 3257-3271.

Maziuk, B. et al. (2017). Dysregulation of RNA Binding Protein Aggregation in Neurodegenerative Disorders. Front Mol Neurosci **10**: 89.

McAvoy, K. and H. Kawamata (2019). Glial mitochondrial function and dysfunction in health and neurodegeneration. Mol Cell Neurosci **101**: 103417.

McClatchey, P. M. et al. (2016). Fully automated software for quantitative measurements of mitochondrial morphology. Mitochondrion **26**: 58-71.

McColgan, P. and S. J. Tabrizi (2017). Huntington's disease: a clinical review. Eur J Neurol.

McCoy, M. K. et al. (2014). Hexokinase activity is required for recruitment of parkin to depolarized mitochondria. Hum Mol Genet **23**(1): 145-156.

McKenzie, B. A. et al. (2015). In vitro screen of a small molecule inhibitor drug library identifies multiple compounds that synergize with oncolytic myxoma virus against human brain tumor-initiating cells. Neuro Oncol **17**(8): 1086-1094.

McLaughlin, B. A. et al. (1996). CAG trinucleotide RNA repeats interact with RNA-binding proteins. Am J Hum Genet **59**(3): 561-569.

McMahon, A. C. et al. (2016). TRIBE: Hijacking an RNA-Editing Enzyme to Identify Cell-Specific Targets of RNA-Binding Proteins. Cell **165**(3): 742-753.

McWilliams, T. G. and I. G. Ganley (2016). Life in lights: Tracking mitochondrial delivery to lysosomes in vivo. Autophagy **12**(12): 2506-2507.

McWilliams, T. G. et al. (2016). mito-QC illuminates mitophagy and mitochondrial architecture in vivo. J Cell Biol **214**(3): 333-345.

McWilliams, T. G. et al. (2018). Phosphorylation of Parkin at serine 65 is essential for its activation in vivo. Open Biol **8**(11).

McWilliams, T. G. et al. (2018a). Basal Mitophagy Occurs Independently of PINK1 in Mouse Tissues of High Metabolic Demand. Cell Metab **27**(2): 439-449.e435.

Menon, R. P. et al. (2013). The role of interruptions in polyQ in the pathology of SCA1. PLoS Genet **9**(7): e1003648.

Mercuri, E. et al. (2018). Nusinersen versus Sham Control in Later-Onset Spinal Muscular Atrophy. N Engl J Med **378**(7): 625-635.

Mishra, P. and D. C. Chan (2014). Mitochondrial dynamics and inheritance during cell division, development and disease. Nat Rev Mol Cell Biol **15**(10): 634-646.

Mitra, K. and J. Lippincott-Schwartz (2010). Analysis of mitochondrial dynamics and functions using imaging approaches. Curr Protoc Cell Biol **Chapter 4**: Unit 4.25.21-21.

Moffitt, H. et al. (2009). Formation of polyglutamine inclusions in a wide range of non-CNS tissues in the HdhQ150 knock-in mouse model of Huntington's disease. PLoS One **4**(11): e8025.

Montava-Garriga, L. and I. G. Ganley (2020). Outstanding Questions in Mitophagy: What We Do and Do Not Know. J Mol Biol **432**(1): 206-230.

Moren, C. et al. (2019). GBA mutation promotes early mitochondrial dysfunction in 3D neurosphere models. Aging (Albany NY) **11**(22): 10338-10355.

Moreno-García, A. et al. (2018). An Overview of the Role of Lipofuscin in Age-Related Neurodegeneration. Front Neurosci **12**: 464.

Morozova, N. et al. (2006). Protein-RNA interactions: exploring binding patterns with a three-dimensional superposition analysis of high resolution structures. Bioinformatics **22**(22): 2746-2752.

Mortiboys, H. et al. (2010). Mitochondrial impairment in patients with Parkinson disease with the G2019S mutation in LRRK2. Neurology **75**(22): 2017-2020.

Mortiboys, H. et al. (2018). Translational approaches to restoring mitochondrial function in Parkinson's disease. FEBS Lett **592**(5): 776-792.

Motor Neuron Disease Association. Retrieved December 2019, from https://static.mndassociation.org/app/uploads/2019/02/14093255/mnd-association-key-messages-infographic.pdf.

MS Society. Retrieved December 2019, from https://www.mssociety.org.uk/care-and-support/resources-and-publications/publications-search/ms-in-the-uk.

Mushtaq, G. et al. (2016). Neuroprotective Mechanisms Mediated by CDK5 Inhibition. Curr Pharm Des **22**(5): 527-534.

Muzzi, M. et al. (2018). Dexpramipexole improves bioenergetics and outcome in experimental stroke. Br J Pharmacol **175**(2): 272-283.

Nadeau, J. H. and D. Sankoff (1997). Comparable rates of gene loss and functional divergence after genome duplications early in vertebrate evolution. Genetics **147**(3): 1259-1266.

Nalavade, R. et al. (2013). Mechanisms of RNA-induced toxicity in CAG repeat disorders. Cell Death Dis **4**(8): e752.

Nalls, M. A. et al. (2019). Identification of novel risk loci, causal insights, and heritable risk for Parkinson's disease: a meta-analysis of genome-wide association studies. Lancet Neurol **18**(12): 1091-1102.

Narendra, D. et al. (2008). Parkin is recruited selectively to impaired mitochondria and promotes their autophagy. J Cell Biol **183**(5): 795-803.

Narendra, D. et al. (2010). p62/SQSTM1 is required for Parkin-induced mitochondrial clustering but not mitophagy; VDAC1 is dispensable for both. Autophagy **6**(8): 1090-1106.

Narita, M. et al. (1998). Bax interacts with the permeability transition pore to induce permeability transition and cytochrome c release in isolated mitochondria. Proc Natl Acad Sci U S A **95**(25): 14681-14686.

Nasir, J. et al. (1995). Targeted disruption of the Huntington's disease gene results in embryonic lethality and behavioral and morphological changes in heterozygotes. Cell **81**(5): 811-823.

Naumann, M. et al. (2018). Impaired DNA damage response signaling by FUS-NLS mutations leads to neurodegeneration and FUS aggregate formation. Nat Commun **9**(1): 335.

Nayler, O. et al. (1998). SAF-B protein couples transcription and pre-mRNA splicing to SAR/MAR elements. Nucleic Acids Res **26**(15): 3542-3549.

Neelagandan, N. et al. (2019). TDP-43 enhances translation of specific mRNAs linked to neurodegenerative disease. Nucleic Acids Res **47**(1): 341-361.

Nestor, C. E. and D. G. Monckton (2011). Correlation of inter-locus polyglutamine toxicity with CAG*CTG triplet repeat expandability and flanking genomic DNA GC content. PLoS One **6**(12): e28260.

Neumann, M. et al. (2006). Ubiquitinated TDP-43 in frontotemporal lobar degeneration and amyotrophic lateral sclerosis. Science **314**(5796): 130-133.

Neumann, M. et al. (2011). FET proteins TAF15 and EWS are selective markers that distinguish FTLD with FUS pathology from amyotrophic lateral sclerosis with FUS mutations. Brain **134**(Pt 9): 2595-2609.

Newton, K. et al. (2008). Ubiquitin chain editing revealed by polyubiquitin linkage-specific antibodies. Cell **134**(4): 668-678.

Ngamsiri, P. et al. (2014). Glycogen synthase kinase-3 (GSK3) controls deoxyglucose-induced mitochondrial biogenesis in human neuroblastoma SH-SY5Y cells. Mitochondrion **14**(1): 54-63.

NHS England (Neurological Conditions). Retrieved 16.10.19, from https://www.england.nhs.uk/ourwork/clinical-policy/ltc/our-work-on-long-term-conditions/neurological/.

Nicholls, D. G. (2012). Fluorescence measurement of mitochondrial membrane potential changes in cultured cells. Methods Mol Biol **810**: 119-133.

Nikhil, K. and K. Shah (2017). The Cdk5-Mcl-1 axis promotes mitochondrial dysfunction and neurodegeneration in a model of Alzheimer's disease. J Cell Sci **130**(18): 3023-3039.

Norman, M. et al. (2016). The increasing diversity of functions attributed to the SAFB family of RNA-/DNA-binding proteins. Biochem J **473**(23): 4271-4288.

Nussbacher, J. K. et al. (2019). Disruption of RNA Metabolism in Neurological Diseases and Emerging Therapeutic Interventions. Neuron **102**(2): 294-320.

Oesterreich, S. et al. (1997). Novel nuclear matrix protein HET binds to and influences activity of the HSP27 promoter in human breast cancer cells. J Cell Biochem **67**(2): 275-286.

Oesterreich, S. et al. (2001). High rates of loss of heterozygosity on chromosome 19p13 in human breast cancer. Br J Cancer **84**(4): 493-498.

Oh, C. K. et al. (2017). S-Nitrosylation of PINK1 Attenuates PINK1/Parkin-Dependent Mitophagy in hiPSC-Based Parkinson's Disease Models. Cell Rep **21**(8): 2171-2182.

Opal, P. (2017). Spinocerebellar Ataxia Type 1. GeneReviews, University of Washington, Seattle.

Orr, H. T. et al. (1993). Expansion of an unstable trinucleotide CAG repeat in spinocerebellar ataxia type 1. Nat Genet **4**(3): 221-226.

Osborne, R. J. and C. A. Thornton (2006). RNA-dominant diseases. Hum Mol Genet **15 Spec No 2**: R162-169.

Ostrowski, L. A. et al. (2017). Ataxin-2: From RNA Control to Human Health and Disease. Genes (Basel) **8**(6).

Pacelli, C. et al. (2015). Elevated Mitochondrial Bioenergetics and Axonal Arborization Size Are Key Contributors to the Vulnerability of Dopamine Neurons. Curr Biol **25**(18): 2349-2360.

Palikaras, K. et al. (2015). Coordination of mitophagy and mitochondrial biogenesis during ageing in C. elegans. Nature **521**(7553): 525-528.

Pan, F. et al. (2018). Structure and Dynamics of DNA and RNA Double Helices Obtained from the CCG and GGC Trinucleotide Repeats. J Phys Chem B **122**(16): 4491-4512.

Pankiv, S. et al. (2007). p62/SQSTM1 binds directly to Atg8/LC3 to facilitate degradation of ubiquitinated protein aggregates by autophagy. J Biol Chem **282**(33): 24131-24145.

Papkovskaia, T. D. et al. (2012). G2019S leucine-rich repeat kinase 2 causes uncoupling protein-mediated mitochondrial depolarization. Hum Mol Genet **21**(19): 4201-4213.

Park, B.-D. and Y. H. Jin (2004). Activation of Cdk2 and Cdc2 is required for the mitochondrial permeability transition during apoptosis. Cancer Res **64**(7 Supplement): 1006-1006.

Park, J. et al. (2019). Abnormal Mitochondria in a Non-human Primate Model of MPTP-induced Parkinson's Disease: Drp1 and CDK5/p25 Signaling. Exp Neurobiol **28**(3): 414-424.

Park, J. S. et al. (2015). The role of ATP13A2 in Parkinson's disease: Clinical phenotypes and molecular mechanisms. Mov Disord **30**(6): 770-779.

Park, J. S. et al. (2018). Mitochondrial Dysfunction in Parkinson's Disease: New Mechanistic Insights and Therapeutic Perspectives. Curr Neurol Neurosci Rep **18**(5): 21.

Parkinson's UK. Retrieved December 2019, from https://www.parkinsons.org.uk/sites/default/files/2018-01/Prevalence%20%20Incidence%20Report%20Latest_Public_2.pdf.

Paulson, H. L. et al. (2017). Polyglutamine spinocerebellar ataxias - from genes to potential treatments. Nat Rev Neurosci **18**(10): 613-626.

Pearson, C. E. (2011). Repeat associated non-ATG translation initiation: one DNA, two transcripts, seven reading frames, potentially nine toxic entities! PLoS Genet **7**(3): e1002018.

Peng, J. Y. et al. (2011). Automatic morphological subtyping reveals new roles of caspases in mitochondrial dynamics. PLoS Comput Biol **7**(10): e1002212.

Perez, F. A. and R. D. Palmiter (2005). Parkin-deficient mice are not a robust model of parkinsonism. Proc Natl Acad Sci U S A **102**(6): 2174-2179.

Peteri, U. K. et al. (2019). Astrocytes in Neuropathologies Affecting the Frontal Cortex. Front Cell Neurosci **13**: 44.

Petit-Paitel, A. et al. (2009). Involvment of cytosolic and mitochondrial GSK-3beta in mitochondrial dysfunction and neuronal cell death of MPTP/MPP-treated neurons. PLoS One **4**(5): e5491.

Pickrell, A. M. and R. J. Youle (2015). The roles of PINK1, parkin, and mitochondrial fidelity in Parkinson's disease. Neuron **85**(2): 257-273.

Pickrell, A. M. et al. (2015). Endogenous Parkin Preserves Dopaminergic Substantia Nigral Neurons following Mitochondrial DNA Mutagenic Stress. Neuron **87**(2): 371-381.

Plotkin, J. L. and D. J. Surmeier (2015). Corticostriatal synaptic adaptations in Huntington's disease. Curr Opin Neurobiol **33**: 53-62.

Poole, A. C. et al. (2008). The PINK1/Parkin pathway regulates mitochondrial morphology. Proc Natl Acad Sci U S A **105**(5): 1638-1643.

Poon, L. H. et al. (2010). Role of tetrabenazine for Huntington's disease-associated chorea. Ann Pharmacother **44**(6): 1080-1089.

Popov, V. et al. (2005). Mitochondria form a filamentous reticular network in hippocampal dendrites but are present as discrete bodies in axons: a three-dimensional ultrastructural study. J Comp Neurol **492**(1): 50-65.

Postuma, R. B. et al. (2015). MDS clinical diagnostic criteria for Parkinson's disease. Mov Disord **30**(12): 1591-1601.

Prudencio, M. et al. (2015). Distinct brain transcriptome profiles in C9orf72-associated and sporadic ALS. Nat Neurosci **18**(8): 1175-1182.

Qin, L. et al. (2015). CDK1 Enhances Mitochondrial Bioenergetics for Radiation-Induced DNA Repair. Cell Rep **13**(10): 2056-2063.

Raca, G. et al. (2000). Expansion of the (CTG)(n) repeat in the 5'-UTR of a reporter gene impedes translation. Nucleic Acids Res **28**(20): 3943-3949.

Raele, R. (2020). Title TBC. Faculty of Health Sciences, University of Bristol. **PhD**.

Ramanathan, M. et al. (2019). Methods to study RNA-protein interactions. Nat Methods **16**(3): 225-234.

Rangaraju, V. et al. (2014). Activity-driven local ATP synthesis is required for synaptic function. Cell **156**(4): 825-835.

Ratovitski, T. et al. (2012). Huntingtin protein interactions altered by polyglutamine expansion as determined by quantitative proteomic analysis. Cell Cycle **11**(10): 2006-2021.

Redondo, J. et al. (2015). Purkinje Cell Pathology and Loss in Multiple Sclerosis Cerebellum. Brain Pathol **25**(6): 692-700.

Reeve, A. K. et al. (2015). Aggregated alpha-synuclein and complex I deficiency: exploration of their relationship in differentiated neurons. Cell Death Dis **6**: e1820.

Reeve, A. K. et al. (2018). Mitochondrial dysfunction within the synapses of substantia nigra neurons in Parkinson's disease. NPJ Parkinsons Dis **4**: 9.

Renz, A. and F. O. Fackelmayer (1996). Purification and molecular cloning of the scaffold attachment factor B (SAF-B), a novel human nuclear protein that specifically binds to S/MAR-DNA. Nucleic Acids Res **24**(5): 843-849.

Repici, M. and F. Giorgini (2019). DJ-1 in Parkinson's Disease: Clinical Insights and Therapeutic Perspectives. J Clin Med **8**(9).

Rivers, C. et al. (2015). iCLIP identifies novel roles for SAFB1 in regulating RNA processing and neuronal function. BMC Biol **13**: 111.

Roberts, R. F. et al. (2016). Defending the mitochondria: The pathways of mitophagy and mitochondrial-derived vesicles. Int J Biochem Cell Biol **79**: 427-436.

Robinson, A. C. et al. (2016). Extended post-mortem delay times should not be viewed as a deterrent to the scientific investigation of human brain tissue: a study from the Brains for Dementia Research Network Neuropathology Study Group, UK. Acta Neuropathol **132**(5): 753-755.

Rodger, C. E. et al. (2018). Mammalian mitophagy - from in vitro molecules to in vivo models. Febs j **285**(7): 1185-1202.

Rodriguez-Arribas, M. et al. (2017). Mitochondria-Associated Membranes (MAMs): Overview and Its Role in Parkinson's Disease. Mol Neurobiol **54**(8): 6287-6303.

Rodriguez-Enriquez, S. et al. (2006). Tracker dyes to probe mitochondrial autophagy (mitophagy) in rat hepatocytes. Autophagy **2**(1): 39-46.

Rohilla, K. J. and K. T. Gagnon (2017). RNA biology of disease-associated microsatellite repeat expansions. Acta Neuropathol Commun **5**(1): 63.

Rolfe, D. F. and G. C. Brown (1997). Cellular energy utilization and molecular origin of standard metabolic rate in mammals. Physiol Rev **77**(3): 731-758.

Rolfs, A. et al. (2003). Clinical features and neuropathology of autosomal dominant spinocerebellar ataxia (SCA17). Ann Neurol **54**(3): 367-375.

Rousseaux, M. W. C. et al. (2018). ATXN1-CIC Complex Is the Primary Driver of Cerebellar Pathology in Spinocerebellar Ataxia Type 1 through a Gain-of-Function Mechanism. Neuron.

Ruano, L. et al. (2014). The global epidemiology of hereditary ataxia and spastic paraplegia: a systematic review of prevalence studies. Neuroepidemiology **42**(3): 174-183.

Rub, U. et al. (2016). Huntington's disease (HD): the neuropathology of a multisystem neurodegenerative disorder of the human brain. Brain Pathol **26**(6): 726-740.

Rue, L. et al. (2016). Targeting CAG repeat RNAs reduces Huntington's disease phenotype independently of huntingtin levels. J Clin Invest **126**(11): 4319-4330.

Rugarli, E. I. and T. Langer (2012). Mitochondrial quality control: a matter of life and death for neurons. Embo j **31**(6): 1336-1349.

Salapa, H. E. et al. (2018). Dysfunctional RNA binding proteins and stress granules in multiple sclerosis. J Neuroimmunol **324**: 149-156.

San Gil, R. et al. (2017). The heat shock response in neurons and astroglia and its role in neurodegenerative diseases. Mol Neurodegener **12**.

Sanchez de Groot, N. et al. (2019). RNA structure drives interaction with proteins. Nat Commun **10**(1): 3246.

Santos, D. et al. (2015). The Impact of Mitochondrial Fusion and Fission Modulation in Sporadic Parkinson's Disease. Mol Neurobiol **52**(1): 573-586.

Schapira, A. H. (2012). Mitochondrial diseases. Lancet **379**(9828): 1825-1834.

Schapira, A. H. et al. (1989). Mitochondrial complex I deficiency in Parkinson's disease. Lancet **1**(8649): 1269.

Schapira, A. H. et al. (2014). Slowing of neurodegeneration in Parkinson's disease and Huntington's disease: future therapeutic perspectives. Lancet **384**(9942): 545-555.

Schatton, D. and E. I. Rugarli (2018). A concert of RNA-binding proteins coordinates mitochondrial function. Crit Rev Biochem Mol Biol **53**(6): 652-666.

Schilling, J. et al. (2019). Deregulated Splicing Is a Major Mechanism of RNA-Induced Toxicity in Huntington's Disease. J Mol Biol **431**(9): 1869-1877.

Schwab, C. et al. (2008). Colocalization of transactivation-responsive DNA-binding protein 43 and huntingtin in inclusions of Huntington disease. J Neuropathol Exp Neurol **67**(12): 1159-1165.

Schwab, L. C. et al. (2015). Dopamine and Huntington's disease. Expert Rev Neurother **15**(4): 445-458.

Schwaber, J. et al. (2019). Shedding light: The importance of reverse transcription efficiency standards in data interpretation. Biomol Detect Quantif **17**: 100077.

Schwake, M. et al. (2013). Lysosomal membrane proteins and their central role in physiology. Traffic **14**(7): 739-748.

Scott, H. L. et al. (2020). A dual druggable genome-wide siRNA and compound library screening approach identifies modulators of parkin recruitment to mitochondria. J Biol Chem **295**(10): 3285-3300.

Scott, I. and R. J. Youle (2010). Mitochondrial fission and fusion. Essays Biochem **47**: 85-98.

Scrivo, A. et al. (2018). Selective autophagy as a potential therapeutic target for neurodegenerative disorders. Lancet Neurol **17**(9): 802-815.

Scudamore, C. L. et al. (2011). The effect of post-mortem delay on immunohistochemical labelling—a short review. Comparative Clinical Pathology **20**(2): 95-101.

Seibler, P. et al. (2011). Mitochondrial Parkin recruitment is impaired in neurons derived from mutant PINK1 induced pluripotent stem cells. J Neurosci **31**(16): 5970-5976.

Seidel, K. et al. (2012). Brain pathology of spinocerebellar ataxias. Acta Neuropathol **124**(1): 1-21.

Sellier, C. et al. (2010). Sam68 sequestration and partial loss of function are associated with splicing alterations in FXTAS patients. Embo j **29**(7): 1248-1261.

Sen, N. E. et al. (2016). Search for SCA2 blood RNA biomarkers highlights Ataxin-2 as strong modifier of the mitochondrial factor PINK1 levels. Neurobiol Dis **96**: 115-126.

Sen, N. E. et al. (2017). PINK1 and Ataxin-2 as modifiers of growth. Oncotarget **8**(20): 32382-32383.

Seo, A. Y. et al. (2010). New insights into the role of mitochondria in aging: mitochondrial dynamics and more. J Cell Sci **123**(Pt 15): 2533-2542.

Sephton, C. F. and G. Yu (2015). The function of RNA-binding proteins at the synapse: implications for neurodegeneration. Cell Mol Life Sci **72**(19): 3621-3635.

Sephton, C. F. et al. (2011). Identification of neuronal RNA targets of TDP-43-containing ribonucleoprotein complexes. J Biol Chem **286**(2): 1204-1215.

Sergeant, K. A. et al. (2007). Alternative RNA splicing complexes containing the scaffold attachment factor SAFB2. J Cell Sci **120**(Pt 2): 309-319.

Shah, K. and D. K. Lahiri (2014). Cdk5 activity in the brain - multiple paths of regulation. J Cell Sci **127**(Pt 11): 2391-2400.

Shaltouki, A. et al. (2018). Alpha-synuclein delays mitophagy and targeting Miro rescues neuron loss in Parkinson's models. Acta Neuropathol.

Shiba-Fukushima, K. et al. (2017). Evidence that phosphorylated ubiquitin signaling is involved in the etiology of Parkinson's disease. Hum Mol Genet **26**(16): 3172-3185.

Shires, S. E. et al. (2017). Beyond Mitophagy: The Diversity and Complexity of Parkin Function. Circ Res **120**(8): 1234-1236.

Sidransky, E. et al. (2009). Multicenter analysis of glucocerebrosidase mutations in Parkinson's disease. N Engl J Med **361**(17): 1651-1661.

Singh, A. et al. (2019). LRRK2 and mitochondria: Recent advances and current views. Brain Res **1702**: 96-104.

Singh, S. and N. Joshi (2017). Astrocytes: inexplicable cells in neurodegeneration. Int J Neurosci **127**(3): 204-209.

Singleton, A. and J. Hardy (2019). Progress in the genetic analysis of Parkinson's disease. Hum Mol Genet **28**(R2): R215-r218.

Skinner, P. J. et al. (1997). Ataxin-1 with an expanded glutamine tract alters nuclear matrix-associated structures. Nature **389**(6654): 971-974.

Sliter, D. A. et al. (2018). Parkin and PINK1 mitigate STING-induced inflammation. Nature **561**(7722): 258-262.

Smith, P. D. et al. (2003). Cyclin-dependent kinase 5 is a mediator of dopaminergic neuron loss in a mouse model of Parkinson's disease. Proc Natl Acad Sci U S A **100**(23): 13650-13655.

Sobczak, K. and W. J. Krzyzosiak (2004). Imperfect CAG repeats form diverse structures in SCA1 transcripts. J Biol Chem **279**(40): 41563-41572.

Sobczak, K. and W. J. Krzyzosiak (2005). CAG repeats containing CAA interruptions form branched hairpin structures in spinocerebellar ataxia type 2 transcripts. J Biol Chem **280**(5): 3898-3910.

Sobczak, K. et al. (2010). Structural diversity of triplet repeat RNAs. J Biol Chem **285**(17): 12755-12764.

Spinazzi, M. and B. De Strooper (2016). PARL: The mitochondrial rhomboid protease. Semin Cell Dev Biol.

Srinageshwar, B. et al. (2020). Prion-like mechanisms in neurodegenerative disease: Implications for Huntington's disease therapy. Stem Cells Transl Med.

St-Amour, I. et al. (2018). Co-occurrence of mixed proteinopathies in late-stage Huntington's disease. Acta Neuropathol **135**(2): 249-265.

Stan, A. D. et al. (2006). Human postmortem tissue: what quality markers matter? Brain Res **1123**(1): 1-11.

Sterky, F. H. et al. (2011). Impaired mitochondrial transport and Parkin-independent degeneration of respiratory chain-deficient dopamine neurons in vivo. Proc Natl Acad Sci U S A **108**(31): 12937-12942.

Stoica, R. et al. (2014). ER-mitochondria associations are regulated by the VAPB-PTPIP51 interaction and are disrupted by ALS/FTD-associated TDP-43. Nat Commun **5**: 3996.

Stoica, R. et al. (2016). ALS/FTD-associated FUS activates GSK-3beta to disrupt the VAPB-PTPIP51 interaction and ER-mitochondria associations. EMBO Rep **17**(9): 1326-1342.

Stoss, O. et al. (2004). p59(fyn)-mediated phosphorylation regulates the activity of the tissue-specific splicing factor rSLM-1. Mol Cell Neurosci **27**(1): 8-21.

Stucki, D. M. et al. (2016). Mitochondrial impairments contribute to Spinocerebellar ataxia type 1 progression and can be ameliorated by the mitochondria-targeted antioxidant MitoQ. Free Radic Biol Med **97**: 427-440.

Sturm, D. et al. (2019). Easing Burden and Stress: Intervention Needs of Family Members of Patients with Parkinson's Disease. J Parkinsons Dis **9**(1): 221-227.

Sugiura, A. et al. (2014). A new pathway for mitochondrial quality control: mitochondrial-derived vesicles. Embo j **33**(19): 2142-2156.

Sullivan R. et al. (2019). Spinocerebellar Ataxia: An Update. J Neurol **266**(2): 533-544

Sun, N. et al. (2015). Measuring In Vivo Mitophagy. Mol Cell **60**(4): 685-696.

Surmeier, D. J. et al. (2017). Selective neuronal vulnerability in Parkinson disease. Nat Rev Neurosci **18**(2): 101-113.

Suzuki, S. et al. (2017). Efficient induction of dopaminergic neuron differentiation from induced pluripotent stem cells reveals impaired mitophagy in PARK2 neurons. Biochem Biophys Res Commun **483**(1): 88-93.

SysMed PD. Retrieved January 2020, from https://clinicaltrials.gov/ct2/show/NCT03421899.

Tada, M. et al. (2018). Matrin 3 Is a Component of Neuronal Cytoplasmic Inclusions of Motor Neurons in Sporadic Amyotrophic Lateral Sclerosis. Am J Pathol **188**(2): 507-514.

Tain, L. S. (2009). Rapamycin activation of 4E-BP prevents parkinsonian dopaminergic neuron loss. **12**(9): 1129-1135.

Tak, H. et al. (2017). T-cell-restricted intracellular antigen 1 facilitates mitochondrial fragmentation by enhancing the expression of mitochondrial fission factor. Cell Death Differ **24**(1): 49-58.

Takahashi, N. et al. (1992). Focal appearance of cerebellar torpedoes associated with discrete lesions in the cerebellar white matter. Acta Neuropathol **84**(2): 153-156.

Takeuchi, T. and Y. Nagai (2017). Protein Misfolding and Aggregation as a Therapeutic Target for Polyglutamine Diseases. Brain Sci **7**(10).

Tang, B. L. (2018). Unconventional Secretion and Intercellular Transfer of Mutant Huntingtin. Cells **7**(6).

Tauffenberger, A. et al. (2013). Reduction of polyglutamine toxicity by TDP-43, FUS and progranulin in Huntington's disease models. Hum Mol Genet **22**(4): 782-794.

Teitz, T. et al. (2018). CDK2 inhibitors as candidate therapeutics for cisplatin- and noise-induced hearing loss. J Exp Med **215**(4): 1187-1203.

Tezenas du Montcel, S. et al. (2014). Prediction of the age at onset in spinocerebellar ataxia type 1, 2, 3 and 6. J Med Genet **51**(7): 479-486.

Thandapani, P. et al. (2013). Defining the RGG/RG motif. Mol Cell **50**(5): 613-623.

The Human Protein Atlas (SAFB). Retrieved February 2020, from https://www.proteinatlas.org/ENSG00000160633-SAFB/tissue.

The Neurological Alliance Retrieved January 2019, from https://www.neural.org.uk/assets/pdfs/neuro-numbers-2019.pdf.

The Royal Society. Retrieved February 2020, from https://royalsociety.org/~/media/about-us/international/g-science-statements/2017-may-aging-population.pdf?la=en-GB.

The HD iPSC Consortium (2012). Induced Pluripotent Stem Cells from Patients with Huntington's Disease Show CAG-Repeat-Expansion-Associated Phenotypes. Cell Stem Cell **11**(2): 264-278.

Thomas, K. J. et al. (2011). DJ-1 acts in parallel to the PINK1/parkin pathway to control mitochondrial function and autophagy. Hum Mol Genet **20**(1): 40-50.

Todd, P. K. et al. (2013). CGG repeat-associated translation mediates neurodegeneration in fragile X tremor ataxia syndrome. Neuron **78**(3): 440-455.

Tofaris, G. K. and N. J. Buckley (2018). Convergent molecular defects underpin diverse neurodegenerative diseases. J Neurol Neurosurg Psychiatry **89**(9): 962-969.

Townson, S. M. et al. (2003). SAFB2, a new scaffold attachment factor homolog and estrogen receptor corepressor. J Biol Chem **278**(22): 20059-20068.

Tsai, C. C. et al. (2004). Ataxin 1, a SCA1 neurodegenerative disorder protein, is functionally linked to the silencing mediator of retinoid and thyroid hormone receptors. Proc Natl Acad Sci U S A **101**(12): 4047-4052.

Tsoi, H. et al. (2011). Perturbation of U2AF65/NXF1-mediated RNA nuclear export enhances RNA toxicity in polyQ diseases. Hum Mol Genet **20**(19): 3787-3797.

Tsoi, H. et al. (2012). CAG expansion induces nucleolar stress in polyglutamine diseases. Proc Natl Acad Sci U S A **109**(33): 13428-13433.

Twig, G. et al. (2008). Fission and selective fusion govern mitochondrial segregation and elimination by autophagy. Embo j **27**(2): 433-446.

Uittenbogaard, M. and A. Chiaramello (2014). Mitochondrial biogenesis: a therapeutic target for neurodevelopmental disorders and neurodegenerative diseases. Curr Pharm Des **20**(35): 5574-5593.

United Nations, World Population Ageing accessed February 2020. Retrieved 18.02.20, from https://www.un.org/en/development/desa/population/publications/pdf/ageing/WPA2017_Highlights.pdf.

Valente, E. M. et al. (2004). Hereditary early-onset Parkinson's disease caused by mutations in PINK1. Science **304**(5674): 1158-1160.

Van Laar, V. S. et al. (2011). Bioenergetics of neurons inhibit the translocation response of Parkin following rapid mitochondrial depolarization. Hum Mol Genet **20**(5): 927-940.

Vance, C. et al. (2009). Mutations in FUS, an RNA processing protein, cause familial amyotrophic lateral sclerosis type 6. Science **323**(5918): 1208-1211.

Vandenberghe, W. et al. (2018). Imaging Mitophagy in the Fruit Fly. Autophagy **14**(9): 1656-1657.

Varadi, M. et al. (2015). Functional Advantages of Conserved Intrinsic Disorder in RNA-Binding Proteins. PLoS One **10**(10): e0139731.

Velichko, A. K. et al. (2013). Mechanisms of heat shock response in mammals. Cell Mol Life Sci **70**(22): 4229-4241.

Villa, E. et al. (2018). No Parkin Zone: Mitophagy without Parkin. Trends Cell Biol.

Villace, P. et al. (2016). Fluorescent Parkin Cell-Based Assay Development for the Screening of Drugs against Parkinson Disease. J Biomol Screen.

Vincow, E. S. et al. (2013). The PINK1-Parkin pathway promotes both mitophagy and selective respiratory chain turnover in vivo. Proc Natl Acad Sci U S A **110**(16): 6400-6405.

Voigt, A. et al. (2010). TDP-43-mediated neuron loss in vivo requires RNA-binding activity. PLoS One **5**(8): e12247.

Volkening, K. et al. (2018). RNA and Protein Interactors with TDP-43 in Human Spinal-Cord Lysates in Amyotrophic Lateral Sclerosis. J Proteome Res **17**(4): 1712-1729.

Vonsattel, J. P. (2008). Huntington disease models and human neuropathology: similarities and differences. Acta Neuropathol **115**(1): 55-69.

Vonsattel, J. P. et al. (1985). Neuropathological classification of Huntington's disease. J Neuropathol Exp Neurol **44**(6): 559-577.

Waldvogel, H. J. et al. (2015). The Neuropathology of Huntington's Disease. Curr Top Behav Neurosci **22**: 33-80.

Walter, J. et al. (2019). Neural Stem Cells of Parkinson's Disease Patients Exhibit Aberrant Mitochondrial Morphology and Functionality. Stem Cell Reports.

Wang, C. and R. J. Youle (2009). The role of mitochondria in apoptosis*. Annu Rev Genet **43**: 95-118.

Wang, C. et al. (2017). The post-therapeutic effect of rapamycin in mild traumatic brain-injured rats ensuing in the upregulation of autophagy and mitophagy. Cell Biol Int **41**(9): 1039-1047.

Wang, P. et al. (2019). TDP-43 induces mitochondrial damage and activates the mitochondrial unfolded protein response. PLoS Genet **15**(5): e1007947.

Wang, Q. et al. (2018). CDK5-Mediated Phosphorylation-Dependent Ubiquitination and Degradation of E3 Ubiquitin Ligases GP78 Accelerates Neuronal Death in Parkinson's Disease. Mol Neurobiol **55**(5): 3709-3717.

Wang, W. et al. (2016). The inhibition of TDP-43 mitochondrial localization blocks its neuronal toxicity. Nat Med **22**(8): 869-878.

Wang, X. et al. (2011). PINK1 and Parkin target Miro for phosphorylation and degradation to arrest mitochondrial motility. Cell **147**(4): 893-906.

Weighardt, F. et al. (1999). A novel hnRNP protein (HAP/SAF-B) enters a subset of hnRNP complexes and relocates in nuclear granules in response to heat shock. J Cell Sci **112 (Pt 10)**: 1465-1476.

Welinder, C. and L. Ekblad (2011). Coomassie staining as loading control in Western blot analysis. J Proteome Res **10**(3): 1416-1419.

Weng, G. et al. (2019). Sitagliptin promotes mitochondrial biogenesis in human SH-SY5Y cells by increasing the expression of PGC-1alpha/NRF1/TFAM. IUBMB Life **71**(10): 1515-1521.

Wheeler, T. M. et al. (2009). Reversal of RNA dominance by displacement of protein sequestered on triplet repeat RNA. Science **325**(5938): 336-339.

White, M. C. et al. (2010). Inactivation of hnRNP K by expanded intronic AUUCU repeat induces apoptosis via translocation of PKCdelta to mitochondria in spinocerebellar ataxia 10. PLoS Genet **6**(6): e1000984.

Wiemerslage, L. and D. Lee (2016). Quantification of mitochondrial morphology in neurites of dopaminergic neurons using multiple parameters. J Neurosci Methods **262**: 56-65.

Wilkins, A. (2017). Cerebellar Dysfunction in Multiple Sclerosis. Front Neurol **8**: 312.

Williams, D. C. et al. (2013). Rapid and permanent neuronal inactivation in vivo via subcellular generation of reactive oxygen with the use of KillerRed. Cell Rep **5**(2): 553-563.

Wolozin, B. (2012). Regulated protein aggregation: stress granules and neurodegeneration. Mol Neurodegener **7**: 56.

Wong, A. S. et al. (2011). Cdk5-mediated phosphorylation of endophilin B1 is required for induced autophagy in models of Parkinson's disease. Nat Cell Biol **13**(5): 568-579.

Wong, Y. C. et al. (2019). Neuronal vulnerability in Parkinson disease: Should the focus be on axons and synaptic terminals? Mov Disord.

World Health Organisation, accessed Feb 2020. Retrieved February 2020, from https://www.who.int/news-room/detail/19-05-2016-life-expectancy-increased-by-5-years-since-2000-but-health-inequalities-persist.

World Health Organisation, accessed March 2019. Retrieved 28.03.19, 2019, from https://www.who.int/en/news-room/fact-sheets/detail/dementia.

Wu, S. et al. (2011). Mitochondrial oxidative stress causes mitochondrial fragmentation via differential modulation of mitochondrial fission-fusion proteins. Febs j **278**(6): 941-954.

Xie, B. et al. (2019). Cyclin B1/CDK1-regulated mitochondrial bioenergetics in cell cycle progression and tumor resistance. Cancer Lett **443**: 56-66.

Xie, W. and K. K. Chung (2012). Alpha-synuclein impairs normal dynamics of mitochondria in cell and animal models of Parkinson's disease. J Neurochem **122**(2): 404-414.

Yamaguchi, A. and K. Takanashi (2016). FUS interacts with nuclear matrix-associated protein SAFB1 as well as Matrin3 to regulate splicing and ligand-mediated transcription. Sci Rep **6**: 35195.

Yamano, K. et al. (2016). The ubiquitin signal and autophagy: an orchestrated dance leading to mitochondrial degradation. EMBO Rep **17**(3): 300-316.

Yang, Y. M. et al. (2013). A small molecule screen in stem-cell-derived motor neurons identifies a kinase inhibitor as a candidate therapeutic for ALS. Cell Stem Cell **12**(6): 713-726.

Yoon, Y. et al. (2018). Genetic Ablation of EWS RNA Binding Protein 1 (EWSR1) Leads to Neuroanatomical Changes and Motor Dysfunction in Mice. Exp Neurobiol **27**(2): 103-111.

Youle, R. J. and D. P. Narendra (2011). Mechanisms of mitophagy. Nat Rev Mol Cell Biol **12**(1): 9-14.

Yu, M. et al. (2019). Assessment of Caregiver Burden in Huntington's Disease. J Huntingtons Dis **8**(1): 111-114.

Yue, S. et al. (2001). The spinocerebellar ataxia type 1 protein, ataxin-1, has RNA-binding activity that is inversely affected by the length of its polyglutamine tract. Hum Mol Genet **10**(1): 25-30.

Zaharevitz, D. W. et al. (1999). Discovery and initial characterization of the paullones, a novel class of small-molecule inhibitors of cyclin-dependent kinases. Cancer Res **59**(11): 2566-2569.

Zhang X. et al. (2015). Off-target effects in CRISPR/Cas9-mediated genome engineering. Mol Ther Nucleic Acids **4**(11): e264

Zhang, S. et al. (2018). Complementary proteomics strategies capture an ataxin-1 interactome in Neuro-2a cells. Sci Data **5**: 180262.

Zhang, S. et al. (2018a). The ataxin-1 interactome reveals direct connection with multiple disrupted nuclear transport pathways. bioRxiv: 438523.

Zhao, P. et al. (2015). GSK-3β regulates tumor growth and angiogenesis in human glioma cells. Oncotarget **6**(31): 31901-31915.

Zheng, Q. et al. (2016). Dysregulation of Ubiquitin-Proteasome System in Neurodegenerative Diseases. Front Aging Neurosci **8**: 303.

Zoghbi, H. Y. et al. (1988). Spinocerebellar ataxia: variable age of onset and linkage to human leukocyte antigen in a large kindred. Ann Neurol **23**(6): 580-584.

Zu, T. et al. (2011). Non-ATG-initiated translation directed by microsatellite expansions. Proc Natl Acad Sci U S A **108**(1): 260-265.

Zu, T. et al. (2013). RAN proteins and RNA foci from antisense transcripts in C9ORF72 ALS and frontotemporal dementia. Proc Natl Acad Sci U S A **110**(51): E4968-4977.